UNIVERSITY OF OKLAHOMA

GRADUATE COLLEGE

STRATEGIES OF GEOLOGICAL MODELING AND SCALE-UP IN RESERVOIR SIMULATION

A Dissertation

SUBMITTED TO THE GRADUATE FACULTY

in partial fulfillment of the requirements for the

degree of

Doctor Of Philosophy

BY

WEI WANG

Norman, Oklahoma

1998

UMI Number: 9911863

STRATEGIES OF GEOLOGICAL MODELING AND SCALE-UP IN RESERVOIR SIMULATION

A Dissertation

APPROVED FOR THE SCHOOL OF PETROLEUM AND GEOLOGICAL ENGINEERING

BY

D E Menzie

ACKNOWLEDGEMENTS

The help, support, and encouragement from the following people throughout the accomplishment of my dissertation is acknowledged as follows:

I would like to express my sincere thanks to Dr. Anuj Gupta, my dissertation advisor, for his understanding, guidance, and recommendations during my study towards Ph.D.

Special appreciation is due to Dr. Roy Knapp for his understanding, encouragement, support, and valuable technical suggestions.

I would like to thank Dr. Daniel J. O'Meara Jr. for the financial support, including the computer and software used during this study.

I also want to thank Dr. Donald E. Menzie, Dr. Samuel Osisanya, and Dr. Anant R. Kukreti, for serving on my advisory committee and providing advice and support.

Finally, I want to express my deep gratitude and respect to my husband, Xianhong Yang, and my lovely son, John Yang, for their love, understanding, and support during the accomplishment of this dissertation. Deep gratitude is also given to my father, Huachang Wang, my mother, Yuzhi Wang, my aunt, Yufeng Wang, and all the people in my family, for their love, sincere hope and support.

In these last few years, special people and friends have come into my life. Their friendship and sincere hope to my success are also greatly appreciated.

I would like to dedicate this dissertation to all of you. I would never forget you, ever.

TABLE OF CONTENTS

LIST OF TABLES

LIST OF FIGURES

ABSTRACT

The objective of this study was to study the improved vertical layering method for scale-up, to develop an effective scale-up methodology, and to investigate the effects of geological modeling strategies, well locations, and reservoir boundary conditions on the scale-up of petrophysical properties. The Gypsy formation was used as the experimental site in this study.

Three Gypsy models, channel model, lithofacies model, and flow unit model, were generated in this study. A methodology for scale-up was developed, in which transmissibility, instead of permeability, was scaled up. After a linear scale-up was conducted between the grid blocks, a scale-up on productivity index, or PI scale-up, was performed to consider the radial flow around the wellbore. Special considerations were given to the pinch-out grid blocks in the system in order to obtain a representative flow simulation. Two hypothetical models, a layer-cake model and a pinch-out model were used to illustrate the application of the methodology. Successful scale-up results were obtained after a PI scale-up technique around the wellbore was applied.

The scale-up method developed in this study was applied for three Gypsy models. It was observed that the transmissibility scale-up is only suitable for linear flow. A scale-up on productivity index must be conducted to consider the effects of radial flow around wellbore in order to obtain a satisfactory scale-up result. Significant improvements were obtained after conducting a PI scale-up. Contrary to our expectation, channel model and lithofacies model resulted in similar scale-up results, but

flow unit model resulted in large errors. Comparing the scale-up results for three different production scenarios and three different boundary conditions, it was observed that the proposed scaling process provided better results in scenario involving line-drive compared to the nine-spot and five-spot scenarios. The method also produced better scale-up results for system with no-flow boundary condition compared to bottom-water drive and edge-water drive.

CHAPTER I

INTRODUCTION

Detailed reservoir descriptions are now possible with the development of geological and engineering reservoir characterization techniques that both honor and integrate information from core analysis, well logs, well tests, geological and geophysical data. The purpose of such description is to provide an accurate quantitative physical model of the reservoir that can be used by a numerical reservoir simulator to predict oil and gas recoveries under various production scenarios.

However, the detailed reservoir description models with millions of grid blocks cannot be directly incorporated into reservoir simulators because of their intensive computational cost. Despite advances in computer technology, most commercial reservoir simulators are limited to fewer than 10,000 grid blocks, basically 100 times less than the detailed geological models. Scale-up techniques are needed to bridge the gap between fine-scale and coarse-scale models.

Scale-up techniques have been developed in recent years. One limitation of these scale-up methods is that they concentrate only on the mathematics of combining petrophysical properties of finer grid-blocks, while giving little consideration to the heterogeneity of geological and structural details. These methods choose coarse-grid cell boundaries independent of the distribution of reservoir properties, i.e., averaging reservoir properties within layers or channels without considering the effect of heterogeneity on fluid flow and scale-up. Such 'layer or channel scale-up' may average out the effects of extreme values of reservoir properties, such as thin continuous communicating layers, large flow barriers, or partially communicating faults. Therefore, in order to obtain reliable results in scale-up for reservoir simulation, not only is it very important to use a reliable mathematical method for the calculation of average value of reservoir properties for the upscaled grid blocks, but also to find an effective method to determine the boundaries of upscaled grid blocks. A successful scale-up result can be obtained with the combination of reliable mathematical scale-up methodology and detailed description of formation heterogeneity.

1.1 Objectives of the Study

Reservoir properties, such as permeability and porosity, are heterogeneous and their values can change in three dimensions of space. Based on the processes of deposition and diagenesis of formation, the variation of these properties in the vertical direction is more abrupt compared to the variation in the horizontal direction. The purpose of this study is to evaluate the issues surrounding scale up in the vertical direction of the reservoir and to develop new methodologies for scale up modeling.

The objectives of this study are:

(1) To develop an improved vertical layering method for scale-up in reservoir simulation using information typically available from well logging and core analysis.

(2) To develop an effective scale-up methodology that can be used in reservoir simulation.

(3) To investigate the effects of geological modeling, well location, production-injection scenario, and boundary condition on scale-up.

1.2 Contents of the Study

Seven chapters are included in this study. Chapter II contains a brief literature review on the classification of reservoir heterogeneity and scale, development of reservoir description techniques as well as scale-up techniques.

Chapter III includes the development of three different models for Gypsy formation and the analysis of the heterogeneity of these three models.

Chapter IV discusses the strategies of transmissibility scale-up developed and used in this study. Two different hypothetical models are used to illustrate the methodology. Further improvement in scale-up is accomplished by considering the scale-up around wellbore area using PI scale-up method. Successful scale-up results are obtained and displayed in this Chapter.

Chapter V presents the application of the scale-up methodology developed in Chapter IV to three Gypsy models. Scale-up results demonstrated that strategies of geological modeling have significant effects on scale-up.

Chapter VI studies the effects of well location, production-injection scenario, and boundary condition of reservoir on scale-up. Relative error is used as criterion to evaluate the effects of various strategies on scale-up.

Chapter VII presents the conclusions of this study and the recommendations for the study in future.

CHAPTER II

RESERVOIR DESCRIPTION AND SCALE-UP

To obtain successful scale-up results, three concepts are very important. They are: (1) reservoir scale and heterogeneity; (2) reservoir description; and (3) scale-up techniques. The following is a review of each of these concepts.

2.1 Reservoir Scale and Heterogeneity

Reservoir heterogeneity can be characterized at different scales from microscopic to gigascopic scale. Flow phenomena observed at a given scale of heterogeneity exhibit different features compared to those observed at other scales. During reservoir characterization, all available measurements are used, including laboratory measurements at core-scale, well test data at interwell scale, and seismic and production data at reservoir scale. Reservoir description is a combined effort of dividing the reservoir into units, such as layers which are further divided into grid blocks, and assigning values to all pertinent physical properties for these blocks. For this purpose, data from several scales and sources are available. Information at each scale results in different level of accuracy and involves measurement averaging over a different volume of rock (Haldorsen, 1986).

Four conceptual scales of averaging volumes can be classified that exhibit various types of reservoir heterogeneity. They are: (1) microscopic; (2) macroscopic;

(3) megascopic; (4) and gigascopic. Fig. 2-1 is an illustration of these four scales (Haldorsen, 1986).

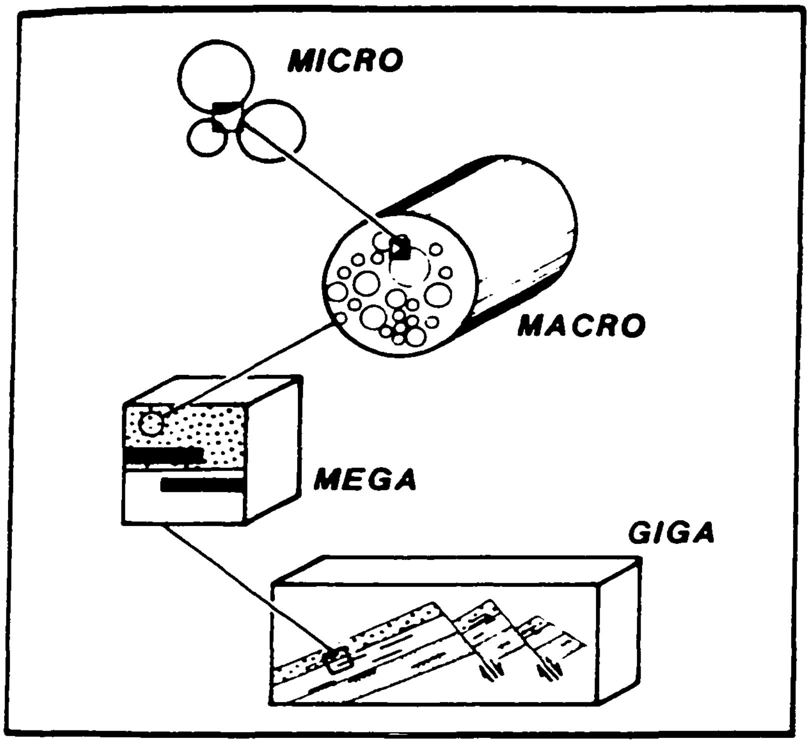

Fig. 2-1 Illustration of Four Conceptual Scales (Haldorsen, 1986)

Microscopic is the scale at which pore throats and grain sizes are described. Variability at this scale produces microscopic scale heterogeneity which governs the distribution of fluid saturation in reservoir. The data for this scale can be obtained from Scanning Electron Miscroscope (SEM) analysis, Pore Image Analysis (PIA), and conventional thin section analysis. The study on this scale is often conducted using a network modeling approach, which assumes that the pore throats of porous media possess different shapes and explicitly incorporates pore wettability effects into a network model in order to quantify flow parameters, to fit experimental data, and to examine the sensitivities of a given process to a variety of phenomena.

Macroscopic is the scale at which core analysis is conducted using core plugs to obtain the properties of the reservoir, such as porosity, permeability, water saturation, capillary pressure, relative permeability, and wettability. From a mechanistic point of view, macroscopic scale corresponds to the viscous-capillary flow regime where gravity forces are considered negligible (Lasseter *et al.*, 1986). This is the most important scale in reservoir study because the continuity equations describing the fluid transport phenomena in porous media are derived based on this scale. The properties of rock within this scale are usually considered to be constant. The data obtained from this scale are used to calibrate the data from well logs and well testing, and used as the input in reservoir simulation. However, the data obtained from this scale are not accurate enough to represent the conditions of reservoir because many factors can affect the measurements, such as pressure, temperature, orientation, and boundary conditions.

Megascopic is the scale at which well logs and well tests are conducted. This scale corresponds to the viscous-capillary-gravity dominated flow regime, in which all three forces play significant roles in determining the dynamic multiphase behavior (Lasseter *et al.*, 1986). Reservoir simulation and scale-up are conducted on this scale, in which reservoir formation is divided into many grid blocks where the variations of rock and fluid properties are averaged or upscaled from macroscopic scale to be assigned as single values to the whole grid block. Because of the limitation of time and computer memory, only thousands of grid blocks can be handled in reservoir simulation. This means that the grid blocks used in simulation have to be large enough to represent the whole reservoir using only several thousand gird-blocks. Each parameter value, such as permeability and porosity, that is assigned to the large grid blocks is an important consideration. Collins (1961) recommended that porosity of reservoir at megascopic scale should be calculated from core data as the volume weighted arithmetic average. The probable error in average porosity is proportional to the inverse square root of the total volume of cores analyzed. Porosity is an intrinsic property of porous medium that is independent of the boundary condition measured. In contrast, the permeability of a heterogenous medium is defined for equivalent homogeneous medium that, with different boundary conditions, would produce different flow movement. Thus, permeability of a porous medium depends on both the boundary conditions and the heterogeneity of the porous medium studied (Begg and King, 1985).

Gigascopic is the scale of total formation that consists of many depositional units and perhaps several depositional environments. The essential features of the gigascopic scale are lateral continuity and vertical communication. Seismic and production data are mostly used to obtain the information on this scale.

To realistically predict reservoir performance, reservoir heterogeneity at various scales must be modeled accurately. Reservoir engineers and geologists should combine efforts to develop a quantitative approach to define the depositional units and the depositional environments of the reservoir in which it was formed. Reservoir engineers must attain efficient means to use these detailed, quantitative, and complex descriptions of reservoirs in reservoir simulation models.

2.2 Reservoir Description

The task of reservoir description is to characterize the physical and chemical properties of porous medium and its pore fluids over a broad range of dimensions from pore throat to whole reservoir. The purpose of such descriptions is to provide an accurate quantitative physical model of the reservoir that can be translated for use in numerical reservoir simulation models to predict the performance of oil and gas reservoirs under various production scenarios (Forgotson, 1996).

In the past, reservoir description for simulation has evolved from simple to quite complex models. Past reservoir simulation studies treated the reservoir as a package of superimposed subhomogeneous layers, or layer cakes, in which reservoir properties, such as porosity and permeability, were assigned constant values based on the data obtained from core measurements. Because of the discontinuity of sand bodies of variable thickness or the occurrence of major lateral permeability contrast, this was often an over-simplification. In recent years, 3-D heterogeneous geological models were developed, in which each layer was horizontally divided into many grid blocks with different petrophysical properties.

Four major studies are included in conventional reservoir description. These are: (1) rock studies to define lithology, depositional environment of the reservoir, and correlations of rock properties; (2) framework studies that establish the structural continuity of reservoir and nonreservoir rock and gross thickness; (3) reservoir quality studies to determine the variation of rock properties (permeability, porosity); and (4) integration studies that yield maps of porosity, permeability, and formation thickness across the reservoir (Willhite, 1986).

Rock studies are used to identify the rock types for both reservoir and nonreservoir rocks that make up the reservoir intervals and to interpret the depositional origin of the intervals using information from cutting, cores, well logs, and routine core-analysis data. This information is fundamental in predicting reservoir continuity and thickness patterns and variation in pore-space properties. Typical output developed at this level of analysis are core-description graphs and porosity-permeability cross-plots (Harris and Hewitt, 1977).

Framework studies determine the geometric configuration of the trap and the vertical and lateral distribution of the rock types that were identified in rock studies. Framework studies begin by mapping the gross structure from well and seismic data to define the areal and vertical extent of the deposit. It is important to identify aquifer and estimate aquifer size in framework studies because it is a measure of the capacity of reservoir to maintain reservoir pressure under primary production. The principal activity in framework studies is the determination of areas and vertical limits and the continuity of reservoir and nonreservoir zones.

Reservoir quality studies utilize well logs, core analysis, and well test data to ascertain pore-space attributes and distributions. Special core analysis and petrophysical studies may be required to identify the pay zone and to predict fluid saturation distribution (Harris and Hewitt, 1977).

Integration studies are the epitome of the total effort, because both data and professional experience must be used to complete the description activity satisfactorily. Porosity and/or permeability maps can be combined with net-thickness maps to provide the pore-volume or transmissibility maps needed in reservoir simulation. Reservoir simulation techniques can then be used to match reservoir history and predict future performance.

In reservoir description, the tasks for geologists are to identify and describe the mineralogy, texture, grain size, bedding and flow structures, depositional sequences and the geometry of genetically related depositional units, using the information from seismic, outcrop, and cores, and finally to produce a conceptual geological model. The tasks of petrophysicists are to measure and provide the information of porosity, permeability, fluid saturation, and well logs. Finally, reservoir engineers need to combine all of the available information from exploration, drilling, reservoir engineering and production data to build up a discrete geological model used to predict the performance of the reservoir for different production scenarios.

The most common method to determine if a model is adequately describing a reservoir is to match the reservoir's performance history. Reservoir engineers, in general, have found it difficult to use a geological model developed by conventional methods to match the history of a reservoir. The geological models developed by conventional methods are too coarse and too homogeneous to match reservoir performance, because they do not reflect the vertical and lateral variations of reservoir heterogeneity. Reservoirs are so complex and heterogeneous that it is impossible to have a geological model to describe them completely. Numerous techniques for improved reservoir characterization were developed in 1980s.

Reservoir characterization is a detailed quantitative description of the physical and chemical properties of a porous medium and its contained fluids. The present emphasis on reservoir characterization is to integrate geological, geophysical, and engineering data at many scales to obtain a more comprehensive understanding of the distribution of reservoir rock and fluid properties.

Two distinct approaches to the determination of lateral reservoir properties are being developed. The first approach is based on deterministic method, and the second approach based on statistical methods is referred to as geostatistical reservoir characterization..

The deterministic method is used to determine the distribution of reservoir properties for systems with small well spacing and reasonably simple reservoir architecture. Deterministic weighting weights the data based on the distance from the well to the center of the cell being calculated. This method honors the data at the well locations. The following equation is used in the interpolation to derive the cell value (Landmark, 1995):

$$V = \frac{\sum_{i=1}^{n} W(r_i, R).Z_i}{\sum_{i=1}^{n} W(r_i, R)} \tag{2-1}$$

where:

V = final cell value,

W = the weighting function,

r = the distance from the interpolated point,

R = the search radius,

n = total number of well values used,

Z = well value.

The weighting function W in the equation is represented by the following equation:

$$W(r,R) = (1 - r/R)^2 . (R/r)^x \qquad (2\text{-}2)$$

where:

x = power factor.

Values R and x reflect the heterogeneity of a reservoir, and they need to be determined experimentally for a specific reservoir. R should be determined based on the well spacing, distance of wells from the boundary of the reservoir, and the distribution area of the layer studied.

When the well spacing is very large and reservoir architecture is very complex, a deterministic correlation may not be accurate enough to describe the heterogeneity of reservoir. In this case, a statistical approach is more appropriate to use to develop a more accurate configuration of reservoir architecture (Weber and Geuns, 1990).

The geostatistical method was developed based on the discovery that many earth-science variables present two main characteristics: there is some randomness in their behavior, but at the same time there is some continuity (Dubrule and Haldorson, 1986). This means that knowing the value at one point x gives some information about the values in the neighborhood of x (continuity), but not enough to exactly predict what these values are (randomness). Geostatistics takes into account the randomness by considering the value Z(x) at point x as the realization for a random variable Z(x). The continuity is represented by a variogram $\gamma(h)$, which is a measure of the difference between values estimated as a function of the distance of separation. For a certain reservoir, a variogram correlation for the variable studied is first generated using the available data. This correlation is then applied to represent the degree of continuity of the variable in the specific reservoir. Geostatistical method is especially useful for the estimation of reservoir properties during the development of reservoir in early stages, when limited data is available.

Variations of reservoir properties in the vertical direction can be determined by combining information from well logs and core analysis. Frequently open hole logs, gamma ray and induction/resistivity, may identify the stratigraphic sequences or depositional units that are consistent with seismic interpretations.

Several methods have been proposed and used for subdividing a sedimentary interval for reservoir description. Statistical techniques based on the variations of permeability have been used by previous investigators to zone the reservoir into layers. Testerman (1962) proposed a statistical reservoir 'zonation technique' using permeability data from a sedimentary interval to identify and describe naturally occurring zones in a reservoir. First, the interval was divided into two zones and then into three zones. The subdivision of additional zones continued until the zones had minimum internal variation in permeability and maximum variation between zones. The problem with this method is that it does not take into account the geological attributes that control reservoir zonation.

With advances in facies modeling, sedimentological studies have introduced facies-zones, and facies associations as flow units for reservoir layering. A facies is a three-dimensional body of rock having the same environment as determined from characteristics such as external and internal geometry, sedimentary structures, lithology, organic content, stratigraphic relations, and associated sedimentary facies (Finley and Tyler, 1986).

Rodriguez (1988) characterized facies units by identifying major changes in the related depositional sequences using porosity and permeability values. In their study, eight facies were first identified using the type of lithology, sedimentary structures, sedimentary textures, and amount of bioturbation. Facies were then grouped into four facies assemblages or sedimentary units, according to attributes such as, the first appearance of conglomeratic sand with erosive basal contact with the underlying Paleocene carbonate sequence, presence of a very fine-grained sand sequence with continuous shales intercalations, and the first appearance of an heterolithic sand/shale sequence with considerable thickness.

In recent years, the concept of hydraulic or flow unit was introduced as a method of subdividing a sedimentary interval for reservoir description. The term 'flow unit' has different definitions depending on its application. A flow unit is defined as a volume of reservoir rock that is continuous laterally and vertically and has similar averages of those rock properties that affect fluid flow. It represents an assemblage of facies having similar characteristics. The significance of dividing the sedimentary intervals into flow units is that each flow unit usually reflects a specific depositional environment and characteristics of fluid flow (Ti *et al.*, 1995). A compelling reason for describing reservoirs in terms of depositional units is that units formed in the same depositional environment have similar characteristics (Lasseter *et al.* 1986). Thus in reservoir simulation, each flow unit can be treated as a layer or a vertical gridblock (Weber and Geuns, 1990). Continuous flow units with similar properties can be scaled up into one layer to reduce the amount of memory and computing time needed without adversely affecting the accuracy of simulation results to obtain the optimum layering for reservoir simulation.

Scuta (1997) used injected and produced volumes of oil and water, oil-water contact map, and time-lapse injectivity profiles, to interpret flow units in a complex carbonate reservoir using sequence-stratigraphic concepts as well as the interpreted structural evolution for Vacuum Field in New Mexico. A 3-D geological model was built to understand and visualize the three-dimensional distribution of properties. This model was later upscaled for reservoir simulation by first summing and averaging porosity in each layer, and then ranking and grouping the layers with similar ranks. Various parameters were used to determine the optimal layering scheme that would maintain the structure and detail of the geological model for reservoir simulation.

Hearn *et al.* (1986) defined a flow unit as a zone that is continuous over a defined volume of the reservoir, has similar average properties that affect fluid flow, and has similar bedding characteristics. The distribution of flow unit is related to the facies distribution, but flow unit boundaries do not necessarily coincide with facies boundaries. They used the concept of flow unit in the simulation of Hartzog Draw Field. In their study, flow units were defined based on the range of porosity and permeability distribution as shown in Fig. 2-2.

Slatt and Hopkins (1988) developed a flow unit model which integrated detailed geological and petrophysical properties to provide a more comprehensive understanding of reservoir architecture and heterogeneity within Balmoral Field. Five flow units were defined using measurements of porosity, permeability, grain-size, capillary pressure curves, and various geological properties. This flow unit model is considered to be the

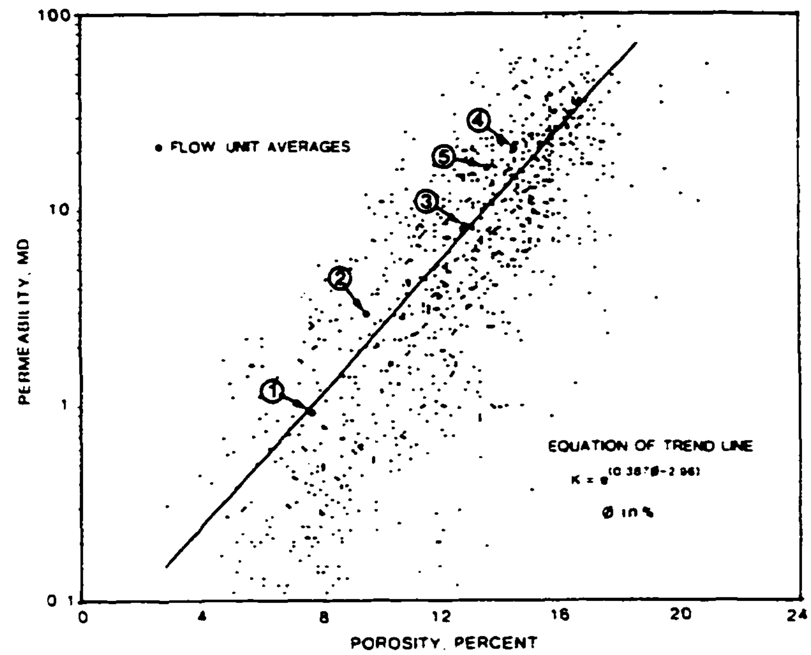

Fig. 2-2 Classification of Flow Units by Permeability and Porosity ((Hearn *et al.*, 1986)

most complex model, because it incorporates a variety of geological and petrophysical parameters and it provides the most comprehensive description for simulation studies.

Ti *et al.* (1995) developed a quantitative way to classify a reservoir into distinct flow units. Sedimentary intervals of the cored wells were divided into major zones on the basis of core description information. The major zones were further subdivided into subzones to allow less variation in geologic and petrophysical properties within each subzone and more variation between the subzones. On the basis of the transmissibility, storativity, and net-to-gross-thickness data, the subzones were classified into four distinct fluid flow units by use of the statistical method of cluster analysis.

Understanding the complex variations in pore geometry within different lithofacies is the key to improving reservoir description and subsequently, reservoir exploration (Amaefule *et al.*, 1993). The variations in pore geometrical attributes can be used to identify distinct zones or hydraulic flow units with similar fluid-flow characteristics. Amaefule *et al.* (1993) proposed a methodology to identify and characterize hydraulic flow units based on a modified Kozeny-Carmen equation using the mean hydraulic radius. A hydraulic unit is defined as the representative elementary volume of total reservoir rock within which geological and petrophysical properties that affect fluid flow are internally consistent. Hydraulic units are related to geologic facies distribution, but do not necessarily coincide with facies boundaries (Hearn *et al.*, 1984). According to their proposed method, a log-log plot of RQI versus ϕ_z, which are defined in the following equations, for the same flow unit with an ideal pore geometry should follow a straight line with a slope of 1.0.

$$\mathrm{RQI} = 0.0314\sqrt{\frac{k}{\phi}} \tag{2-3}$$

$$\phi_z = \left(\frac{\phi}{1-\phi}\right) \tag{2-4}$$

k is permeability in mD. ϕ is porosity in fraction. Fig. 2-3 illustrates a log-log plot of RQI versus ϕ_z for East Texas.

2.3 Scale-up Techniques

Two categories of scale-up techniques have been developed: single-phase scale-up and two-phase scale-up. Single-phase scale-up focuses on preserving the gross

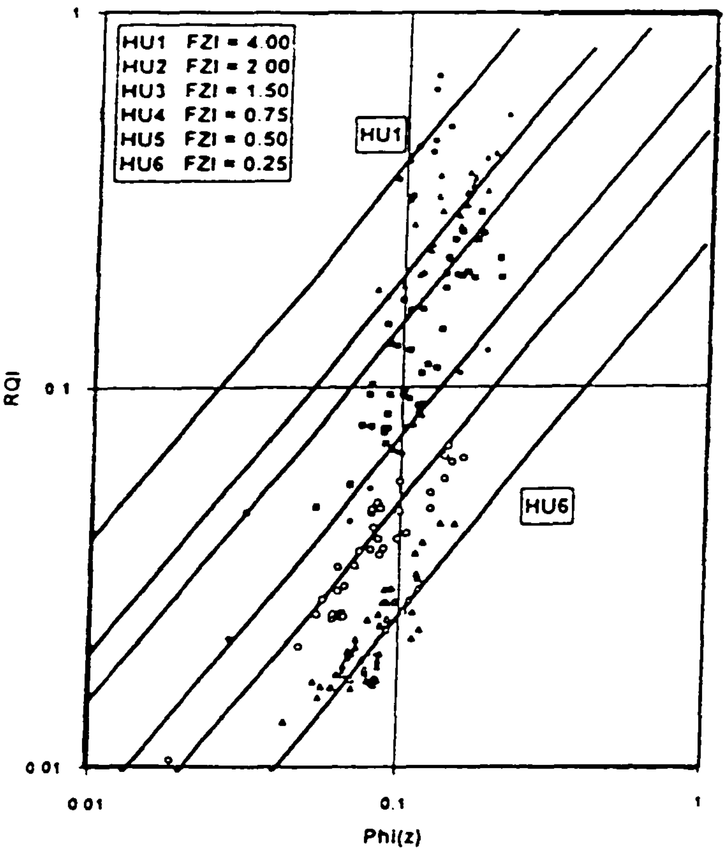

Fig. 2-3 Log-Log Plot of RQI versus ϕ_z for East Texas (Amaefule *et al.*, 1993)

feature of flow on the simulation grid and calculates an effective permeability, which can result in the same total flow rate of fluids through the coarse, homogeneous block as that obtained from the fine heterogeneous blocks. Scale-up of two phase flow is more complicated than single-phase flow since it involves not only absolute permeability but also relative permeability and capillary pressure. In this study, only one phase flow was studied. Therefore, only one phase scale up is discussed below.

2.3.1 Scale-up for Linear Flow

Numerous methods for scale-up of single phase flow have been developed. including average method (arithmetic/geometric/harmonic) (Cardwell and Parsons. 1945; Begg *et al.*. 1989), tensor method (Pickup *et al.*, 1992; Aasum *et al.* 1993; King. 1993; Pickup and Sorbie, 1994). transmissibility scale-up (White and Horne. 1987; Peaceman. 1996). renormalization technique (King, 1989; Gautier and Natinger. 1994; Christie *et al.*. 1995; King and Williams, 1994). and pressure-solver method (Begg and King. 1985; Begg *et al.*. 1989).

The simplest method for calculating average permeability of porous medium is the average method. Begg *et al.* (1989) calculated the average permeability for different rocks using three average methods and determined that harmonic and arithmetic methods gave the lowest and highest values of average permeability. Geometric method provided average values between the values from harmonic and arithmetic methods.

White and Horne (1987) present an algorithm to compute transmissibility using permeability heterogeneity and anisotropy at fine scale. In their proposed method. the transmissibility for coarse-scale grid blocks was treated as a tensor. and. for a 2-D simulation. the flux across the +x face of coarse-scale grid block was expressed as:

$$q_{i+1/2,j} = -\left[T^{xx}_{i+1/2,j}\Delta p_{x\,i+1/2,j} + T^{xy}_{i+1/2,j}\Delta p_{y\,i+1/2,j}\right] \tag{2-5}$$

Where:

$q_{i+1/2,j}$ = flux between two grid blocks.

$T^{xx}_{i+1/2,j}$ = normal transmissibility between two grid blocks.

$T^{xy}_{i+1/2,j}$ = transverse transmissibility between two grid blocks.

$\Delta p_{x,i+1/2,j}$ = pressure difference between two grid blocks in x direction.

$\Delta p_{y,i+1/2,j}$ = pressure difference between two grid blocks in y direction.

Similarly, the expression of flux in y direction can be also expressed as Eq. (2-5). The well to well-block transmissibility is determined by the following equation:

$$Q = T_b\left(p_{i,j} - p_b\right) \tag{2-6}$$

where:

Q = total flow rate of well.

T_b = transmissibility of well to wellblock.

$p_{i,j}$ = wellblock pressure.

p_b = wellbore pressure.

In order to solve for both normal and transverse transmissibilities, at least two distinct boundary conditions must be set. The pressures and fluxes for coarse-scale grid blocks were obtained by averaging and summing the pressures and fluxes from fine-scale simulations with different boundary conditions. Least-squares method was then used to estimate the transmissibilities between coarse-scale grid blocks and between well to wellblock. It was demonstrated that the general tensor scaling procedure can give accurate, efficient production estimate on a coarse grid.

Peaceman (1996) proposed a methodology in which six half-block transmissibilities for each coarse grid-block were calculated by directly solving the finite-difference equations for pressure in each of six half-blocks. Uniform pressures are applied at two opposite faces and no-flow boundary conditions are applied at the other four faces when solving the finite-difference equation.

Tensor method takes effective permeability of reservoir as a full tensor with elements k_{xx}, k_{xy}, k_{xz}, k_{yy}, k_{yx}, k_{yz}, k_{zx}, k_{zy}, and k_{zz} to represent the heterogeneity and anisotropy of reservoir formation. Aasum *et al.* (1993) developed an analytical method to calculate effective permeability tensor for a grid block by accounting for small scale heterogeneity within the grid block. The method honors both location and orientation of the small scale heterogeneity. Pickup and Sorbie (1994) developed a new scale-up method based on tensor permeabilities. The method was validated when it accurately reproduced fine grid calculations using tensors on a coarser grid. Tensor method is significantly more accurate than other scale-up methods, but it greatly increases the computation time needed for simulation. Therefore, it still cannot be directly incorporated into a commercial reservoir simulator without significantly slowing down computation time.

Renormalization Technique for effective permeability was pioneered by King (1993). The idea of the renormalization method is to replace a single scale-up step from the fine grid to the coarse grid with a series of steps which transits from fine grid to coarse grid through a series of increasingly coarse intermediate grids (Christie *et al.*, 1995). The approach works by taking a large problem and breaking it down into a hierarchy of manageable problems (Christie, 1996). In the application of the method, King *et al.* (1993) used a resistor-network analogy for the direct expression of effective permeability. The effective permeability of a small group of cells was first calculated and then put back in place of the original fine group of cells. The process can be repeated for many levels and provides a quick estimation of effective permeability. Renormalization method provided comparable results to that of simulation results. The technique is valid for situations with large permeability variation or with a finite fraction of non-reservoir rock (Christie, 1996).

Begg *et al.* (1989) described a pressure-solver method for the scale-up of single-phase flow similar to the method of Kyte and Berry (1975). The method was developed based on the principle that the effective permeability, k_e, of a heterogeneous medium is the permeability of an equivalent homogeneous medium that, for the same boundary conditions, would give the same flux. Therefore, it depends on both the boundary conditions and the distribution of heterogeneity, and the volume being considered. In this method, the effective permeability for coarse grid block was calculated to produce the same flow rate as for the fine-grid blocks. The results obtained using this method depend on the assumptions and specific boundary conditions made. Fig. 2-4 is an illustration of pressure-solver method.

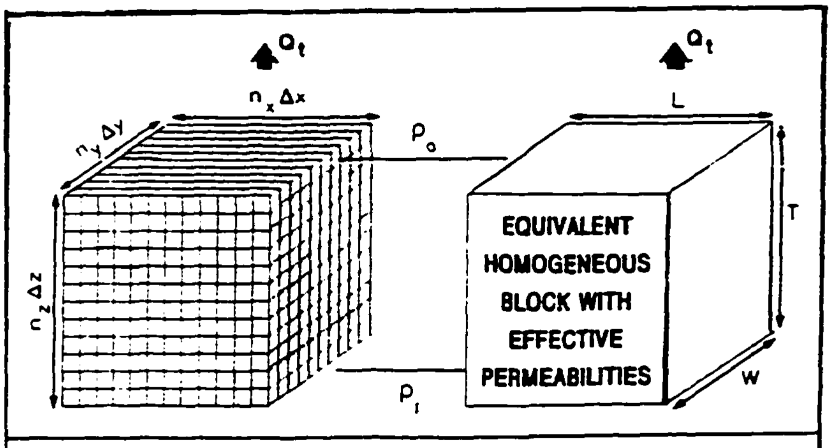

Fig. 1—Illustration of pressure-solver method.

Fig. 2-4 Illustration Of Pressure-Solver Method (Begg *et al.*, 1989)

2.3.2 Scale-up for Radial Flow Near Wellbore

As discussed earlier, the scale-up on permeability or transmissibility is only suitable for a linear flow condition when grid blocks do not contain wells. For grid blocks in which production well or injection wells are located, the method discussed previously may not be appropriate to obtain a satisfactory result in scale-up.

The flow region in a reservoir can be divided into two types: a radial flow region with a high pressure gradient and a linear flow region with a low pressure gradient. The radial flow region is usually more important in production forecasting, because it is directly related to the wells.

Several authors have proposed methods for scale-up at the wellbore or in the vicinity of wells that consider the characteristics of radial flow. Soeriawinata and Kelkar (1996) presented an analytical method to calculate effective permeability for a coarse-grid wellblock from fine-grid permeabilities. The wellblock was divided into many sectors, as shown in Fig. 2-5. Two kinds of reservoir conditions were considered: (1) no communication along the θ and z directions and (2) communication in θ direction. In the first reservoir condition, the permeability for each sector was calculated using the following equation:

$$K_{sector} = \frac{\sum_{i=1}^{nb_{sector}} ln\left(\frac{r_{f,i}}{r_{n,i}}\right)}{\sum_{i=1}^{nb_{sector}} \frac{ln\left(\frac{r_{f,i}}{r_{n,i}}\right)}{k_i}} \tag{2-7}$$

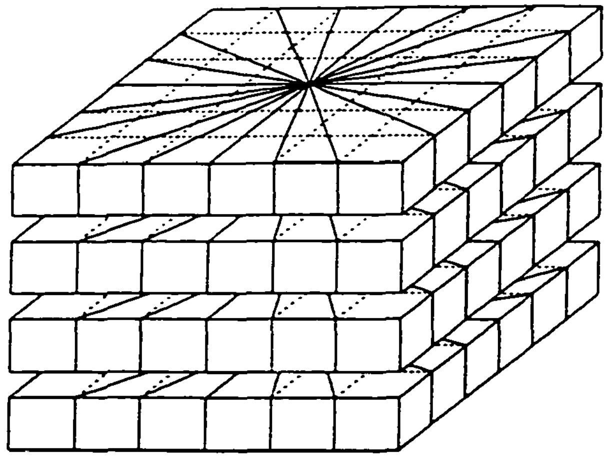

Fig. 2-5 Illustration of Wellblock Divided into Sectors (Soeriawinta and Kelkar, 1996)

The permeability for each layer was calculated as the weighted arithmetic average as follows:

$$K_{layer} = \frac{\sum_{j=1}^{n_{sector}} k_{sector,j} w_{sector,j}}{\sum_{j=1}^{n_{sector}} w_{sector,j}} \tag{2-8}$$

$$w_{sector,j} = \sum_{i=1}^{nb_{sector}} ln\left(\frac{r_{f,i}}{r_{n,i}}\right)_j \tag{2-9}$$

where:

k_{sector} =permeability for the sector (mD).

$r_{f,i}$ = farthest point from i-th block to the well (ft).

$r_{n,i}$ = nearest point from i-th block to the well (ft).

nb_{sector} = total number of blocks in a sector.

k_{layer} = permeability for the layer (mD),

n_{sector} = total number of sector,

$w_{sector,j}$ = weighting coefficient of the i-th sector.

The permeability of the wellblock was determined using a thickness averaging method. Eq. 2-7 reflects the averaging procedure for parallel beds with radial flow. The results of coarse grid simulations with the permeabilities upscaled through the new well-block approach were comparable to the results of the fine grid simulation with initial permeability distributions. This method can only be used for scale-up of permeability.

Ding (1995) proposed a scale-up procedure to calculate the equivalent coarse grid transmissibility for the linear flow region based on the results of simulation on fine grid. For radial flow in the vicinity of a well, the transmissibility was scaled-up by using an imposed well condition. A numerical productivity index (PI) for wellblocks in coarse gird was defined as follows:

$$PI_c = PI_f (P_f - P_w) / (P_c - P_w) = Q / \left(P_c - P_w\right) \tag{2-10}$$

where:

PI_c = productivity index of coarse grid (STB/day/psi),

PI_f = productivity index of fine gird (STB/day/psi),

P_f = wellblock pressure of fine grid (psi),

P_c = wellblock pressure of coarse grid (psi),

P_w = wellbore pressure (psi),

Q = flow rate (STB/day).

If well production rate, wellblock pressure, and wellbore pressure are known. the productivity index for a coarse-scale grid block can be calculated using Eq. 2-10. Ding (1995) tested single-phase incompressible flow by conducting a simulation with a fine-scale model, which was used as the reference solution. Then scale-up was conducted using a standard procedure developed by Begg *et al.* (1989). The second scale-up method used included the standard procedure for linear flow pattern and the procedure for radial flow pattern. Fig. 2-6 illustrates the flow rates obtained from three different simulations for each individual well (nine wells in total).. The errors caused by the new scale-up procedure including a radial flow region are generally lower than the error caused by standard procedure. Therefore, it was concluded that scale-up for radial flow is very important in an overall scale-up process.

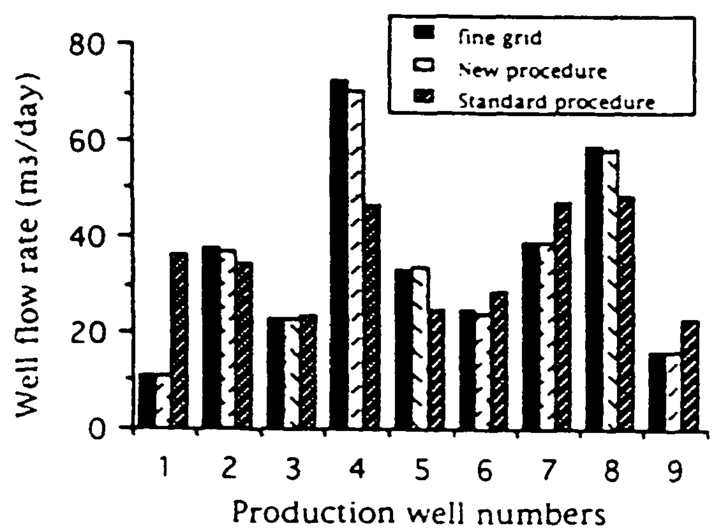

Fig. 2-6 Comparison of Well Flow Rates from Fine-Scale Simulation and Two Different Scale-up Procedures (Ding, 1995)

CHAPTER III

DEVELOPMENT OF GYPSY GEOLOGICAL MODELS

The Gypsy formation was chosen as the experimental site to develop three different geological models, which are used in later chapters to conduct the scale up and study the effects of geological modeling, boundary conditions, and well locations on scale up.

The Gypsy formation is a non-oil bearing formation located in northeastern Oklahoma near Lake Keystone, as shown in Fig. 3-1. It was chosen as the experimental site for this study because of the extensive data available from 22 wells completed in the formation. Data were collected from these 22 wells by BP Exploration between 1989 to 1992 and 1,056 core samples were acquired and studied (Doyle and Sweet, 1992). Data available include permeability, porosity, and lithofacies. These were measured and identified at one foot intervals or smaller, when there was a significant change in rock properties within one foot interval.

3.1 Geology of Gypsy Formation

Gypsy sandstone is an informal name for the lowermost interval of the upper Pennsylvanian Vamoosa Formation. Gypsy formation was deposited as a mixed load meanderbelt system and the sediment transport direction was dominantly west to northwest (Doyle and Sweet, 1992).

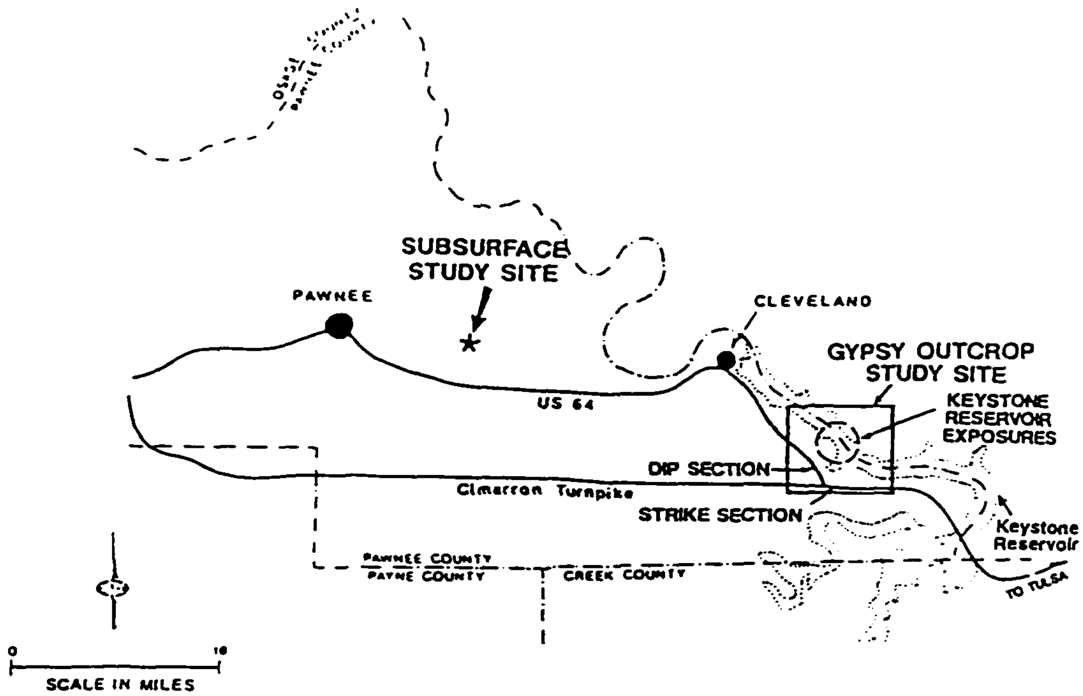

Fig. 3-1 Location of Gypsy Formation (Doyle and Sweet, 1992)

Six channels and one crevasse-splay, in total seven channels, were identified within the Gypsy Outcrop formation. Channel sandbodies are subparallel and trend north to northwest, ranging from 6 to 21 ft thick and 150 to 560 ft wide. Isopach maps of gross thickness for the seven channels present in Gypsy formation were generated as part of this study using Geographix software, are provided as Figs. 3-2 to 3-8. The well data used to generate these maps were provided by Collins (1996). The modeled area is 1181 feet wide and 1378 feet long. The lower contact of each channel sandbody is erosional, and upper contacts may be erosional with younger channels or conformable with floodplain deposits. All of the channels are surrounded or partially subdivided by floodplain deposits that are dominantly composed of impermeable mudstone and siltstone.

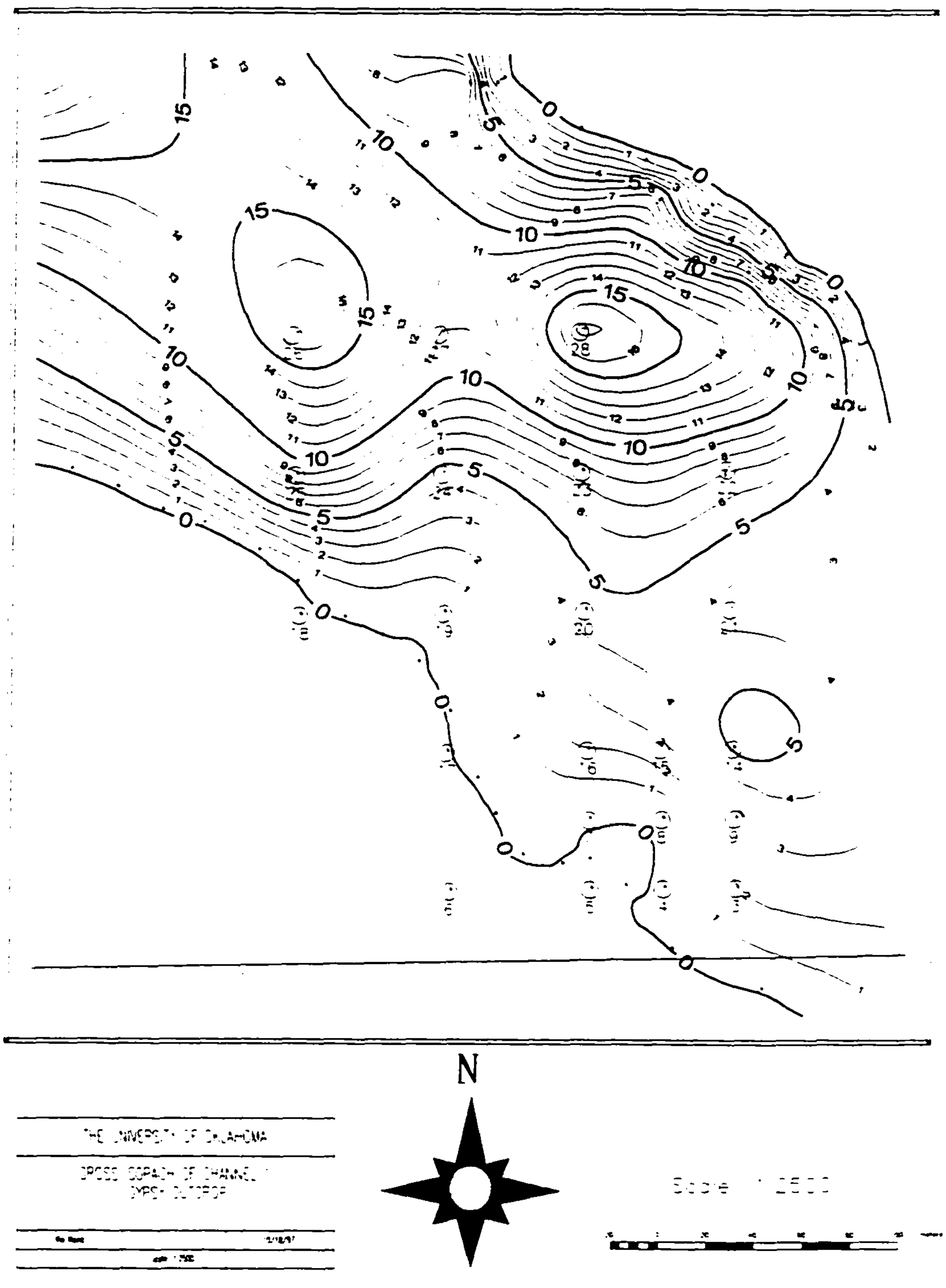

Fig. 3-2 Gross Isopach of Channel 1 In Gypsy Formation

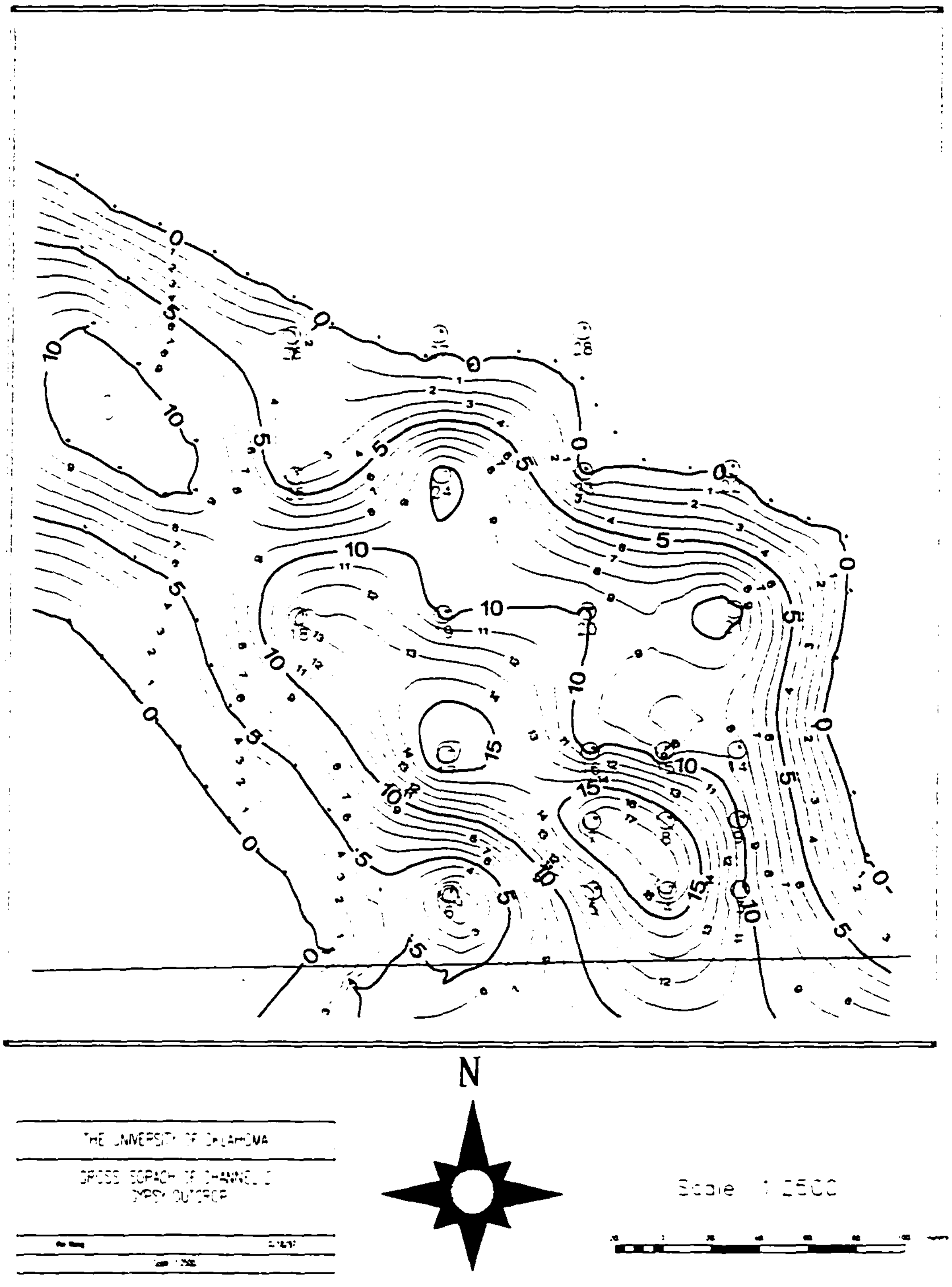

Fig. 3-3 Gross Isopach of Channel 2 In Gypsy Formation

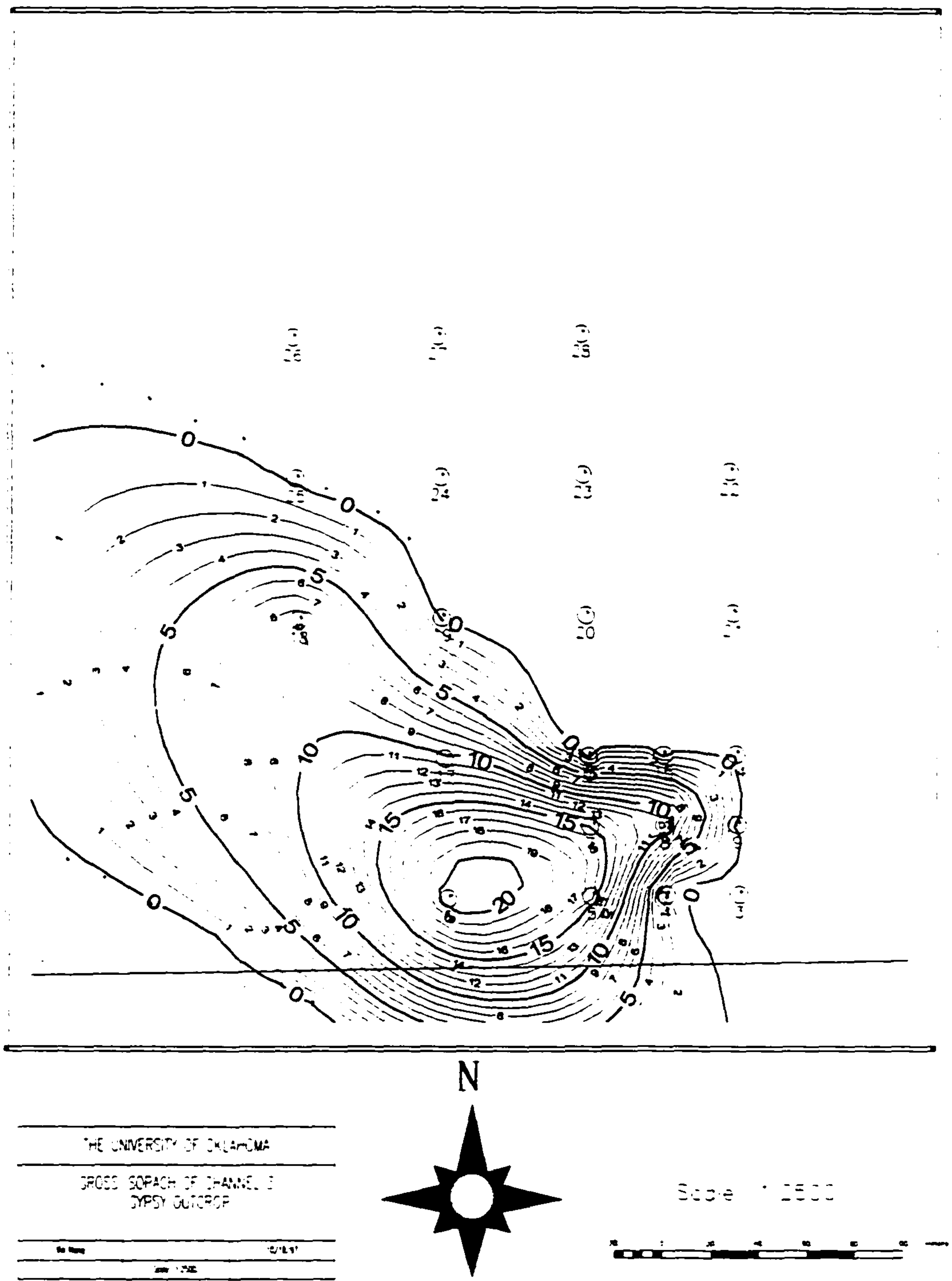

Fig. 3-4 Gross Isopach of Channel 3 In Gypsy Formation

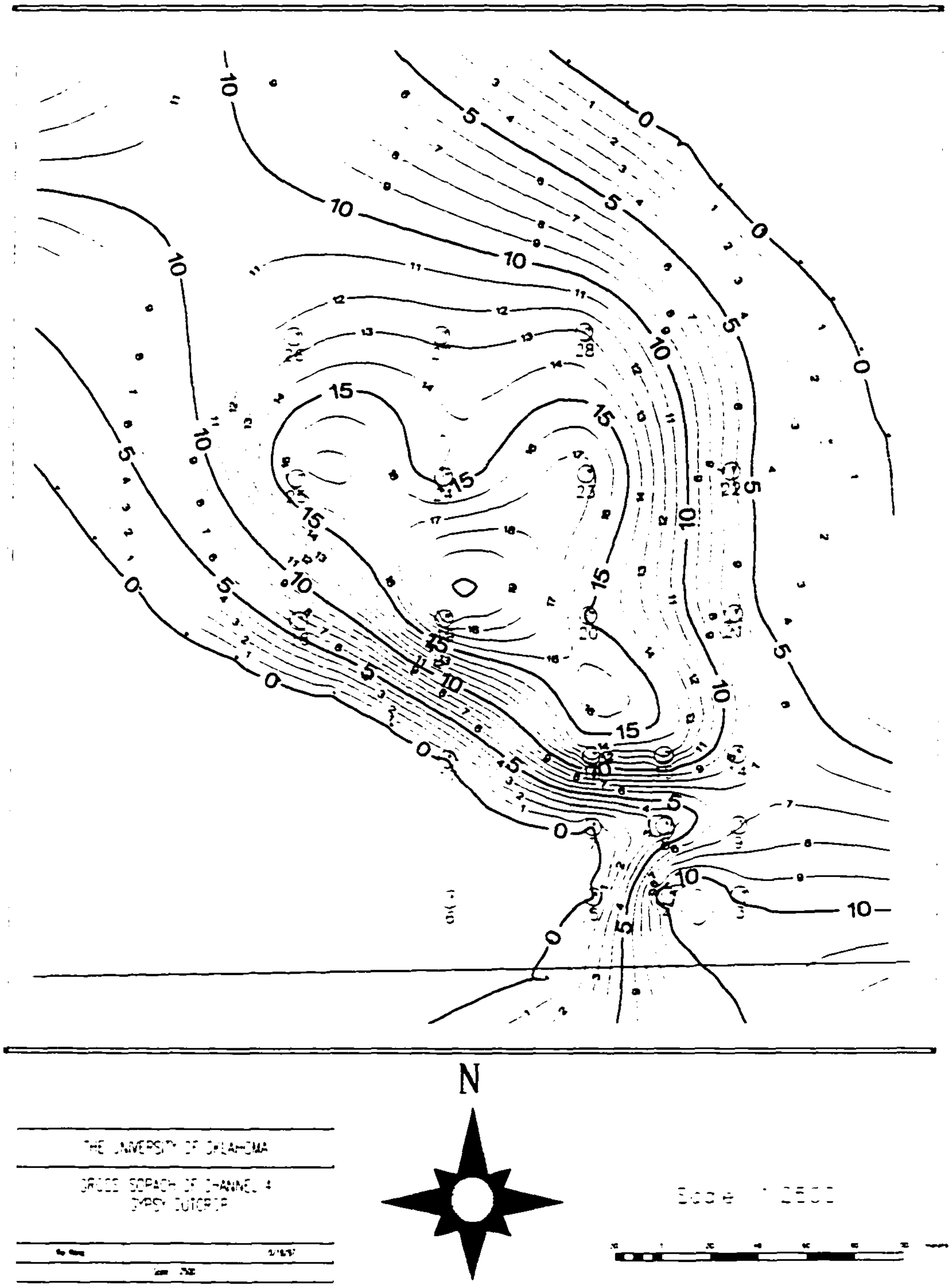

Fig. 3-5 Gross Isopach of Channel 4 In Gypsy Formation

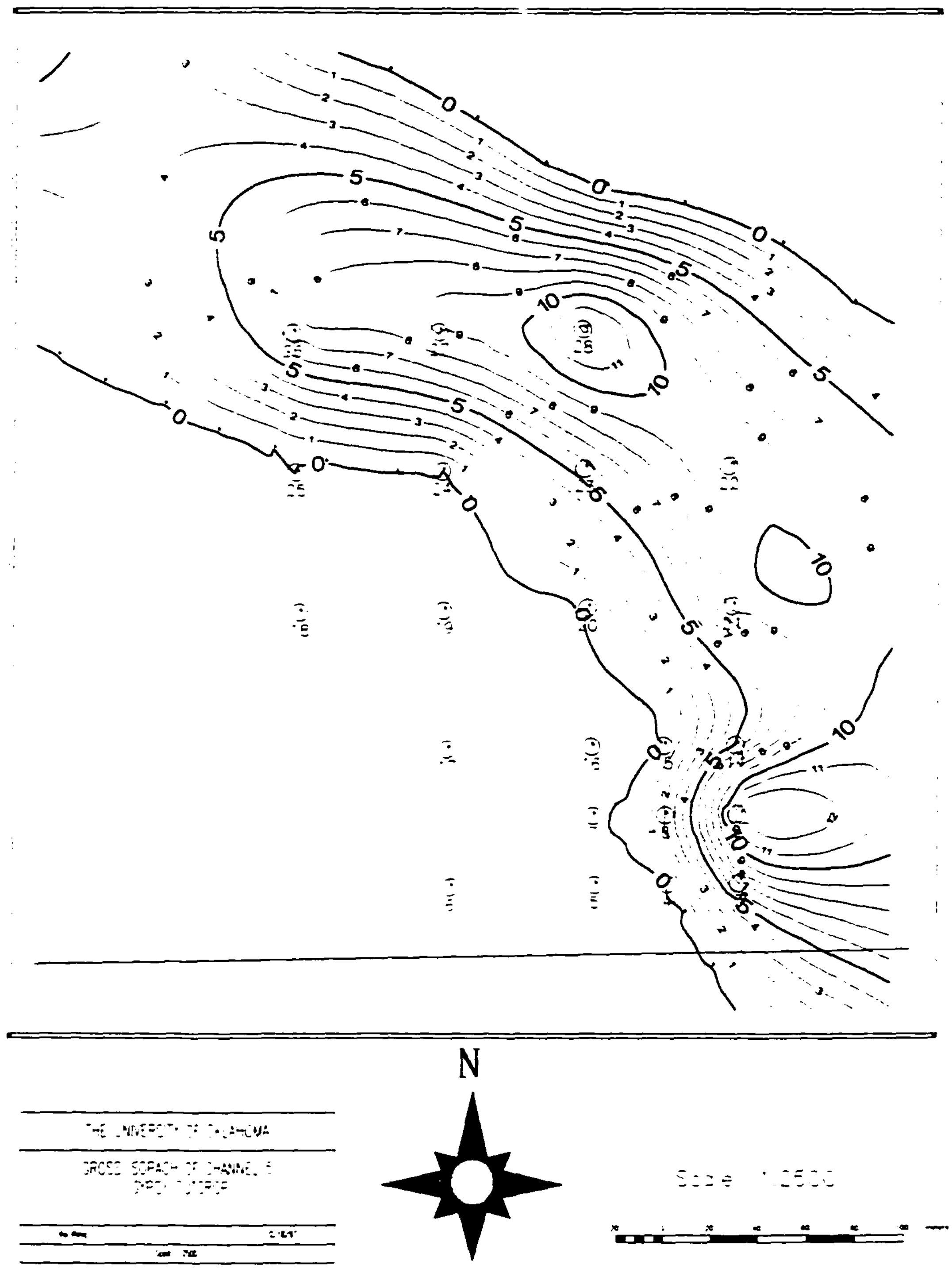

Fig. 3-6 Gross Isopach of Channel 5 In Gypsy Formation

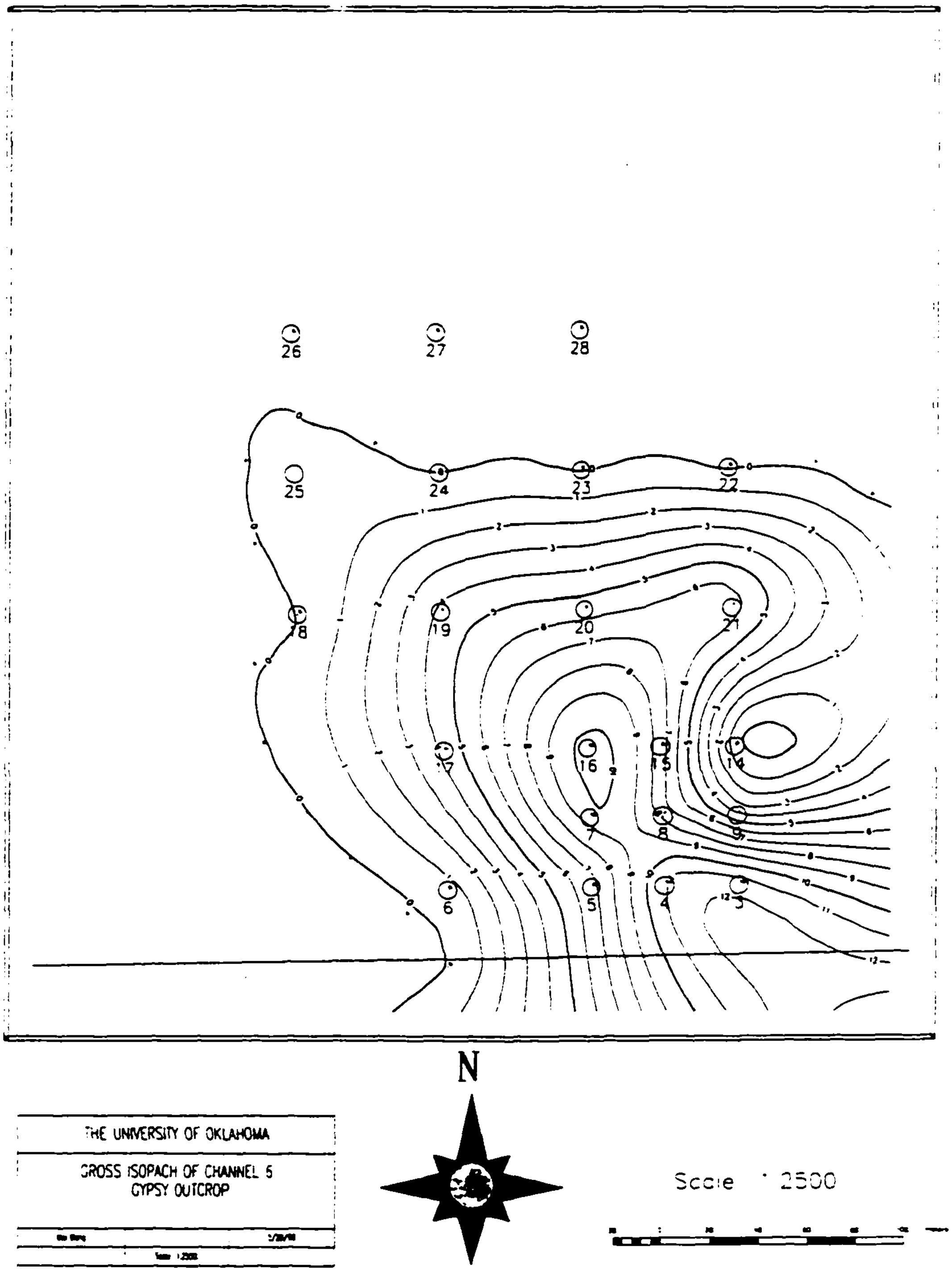

Fig. 3-7 Gross Isopach of Channel 6 (Crevasse-Spay) In Gypsy Formation

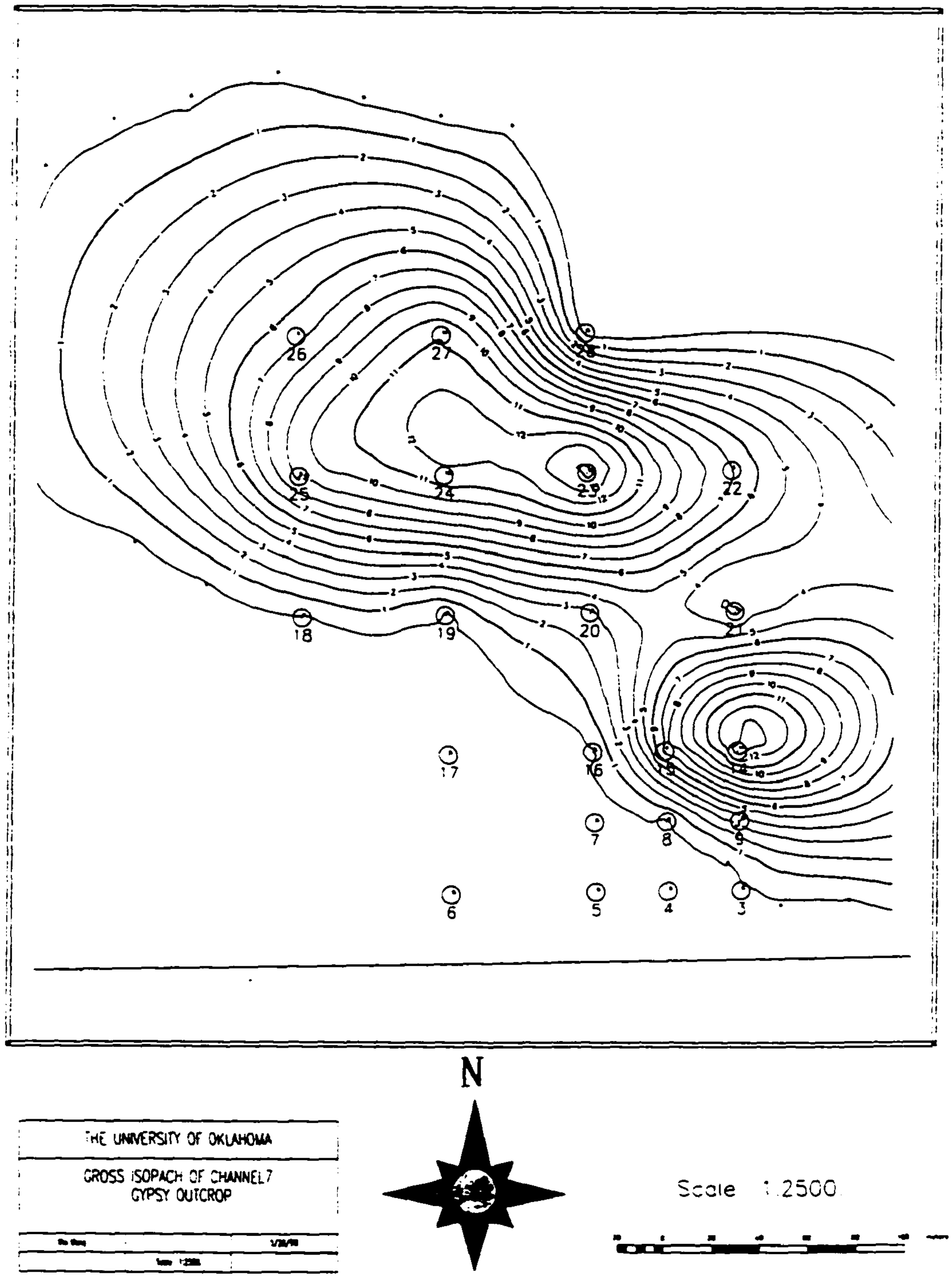

Fig. 3-8 Gross Isopach of Channel 7 In Gypsy Formation

As stated earlier, the Gypsy formation was well studied. 1,056 core samples were analyzed and described from 22 wells. Five sandstone lithofacies identified within Gypsy sandbodies, are mudclast, cross-beds, plane-beds, ripple-beds, and overbank. In addition, some core samples represent soft sediment deformation and unidentifiable sedimentary structures. The lateral extent of lithofacies has been determined to be less than 100 ft (Doyle *et al.*, 1992). A typical lithofacies sequence within an individual channel sandbody of the Gypsy sandstone is illustrated in Fig. 3-9. Most core descriptions in 22 wells follow the distribution illustrated in Fig. 3-9 in the vertical direction, except some cross-beds and plane-beds occur interchangeably within one channel.

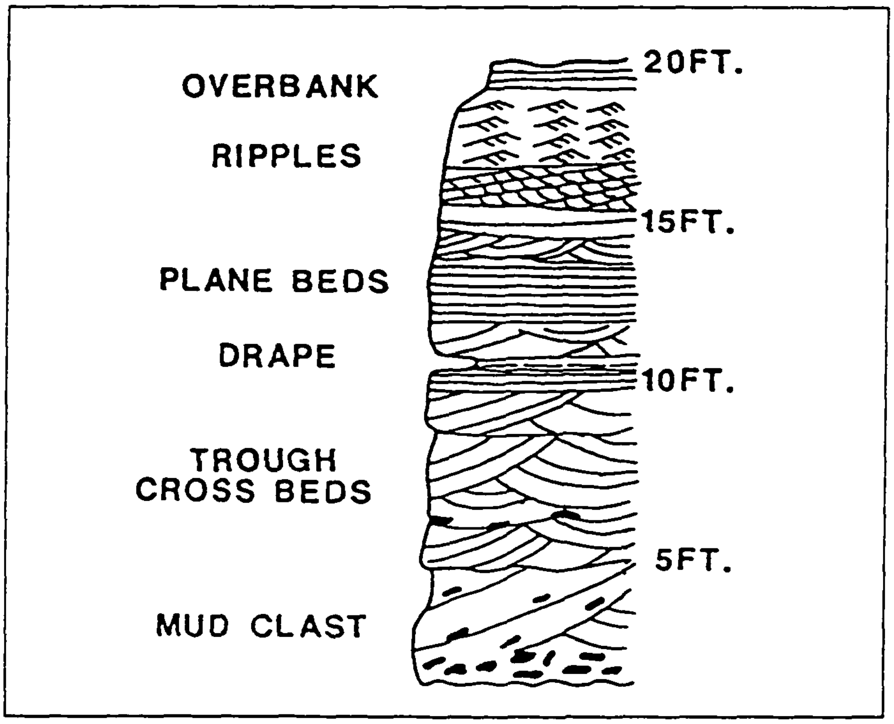

Fig. 3-9 Typical Lithofacies Sequence in Gypsy Formation ((Doyle and Sweet, 1992)

Mudclast sandstone is more extensively developed in the lower channels than in the higher ones. The characteristic grains of this facies are cobble to medium sand-size intraclasts of red, green, and/or grey mudstone. The individual facies is typically 1 to 3 ft thick. **Cross-Beds** sandstone is composed of 0.3 to 3 ft thick sets of cross-bedding. The grain size is very fine to medium sand with some coarse sand and granule-size intraclasts observed on foreset laminations. **Plane-beds** sandstone is fine to very fine grained sandstone with a planar bedding thickness ranging from 0.5 to 3 ft. **Ripple-beds** sandstone is fine to very fine sandstone and often interlaminated with mudstone and siltstone. **Overbank** is mainly composed of impermeable mudstone and siltstone ranging 4.5 to 13 ft thick (Doyle and Sweet, 1992).

Using porosity and permeability data from the 22 wells, a relationship was plotted as in Fig. 3-10. It was observed that cross-beds, plane-beds, and mudstone exhibit better correlation as compared to ripple-beds and mudclast. Cross-beds and plane-beds exhibit the best reservoir quality and also show similar trend in this plot. Overbank presents the lowest values of porosity and permeability. The properties of ripple-beds fall between cross-beds, plane-beds and overbank. Mudclast is the most heterogeneous lithofacies in the Gypsy formation and exhibits a wide distribution of properties as shown in Fig. 3-10. Table 3-1 lists the statistical characteristics for the five lithofacies in the Gypsy formation.

3.2 Channel Model

Landmark's Stratigraphic Geocellular Modeling (SGM) was used to develop the geological models in this study. SGM is used to model heterogeneous rock and fluid

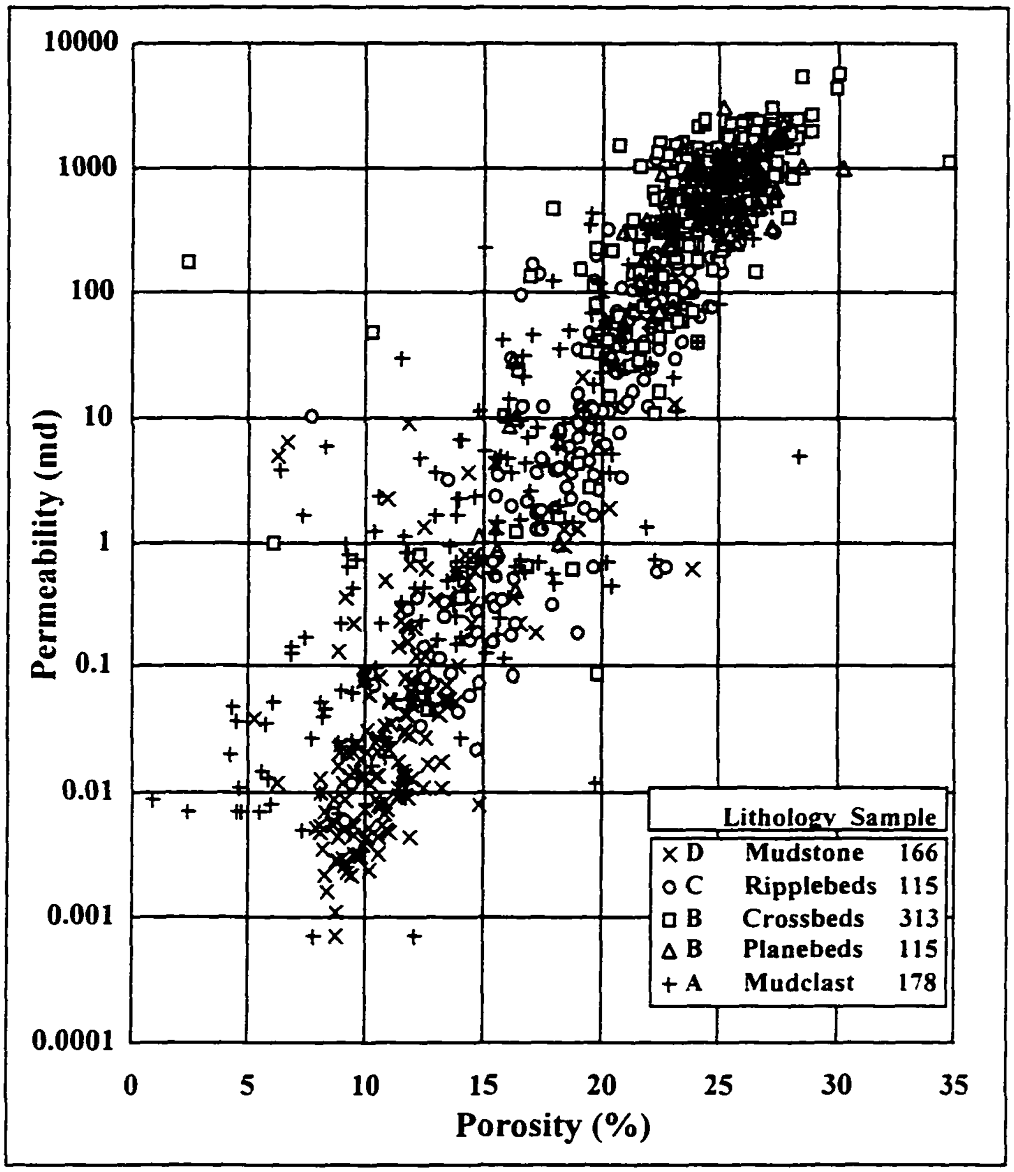

Fig. 3-10 Cross Plot of Permeability and Porosity for Gypsy Formation

Table 3-1 Statistical Characteristics of the Different Lithofacies In Gypsy Formation

Lithofacies	ϕ (%) Mean	ϕ (%) Standard Deviation	k (mD) Mean	k (mD) Standard Deviation
Mudstone	11.38	2.78	0.52	2.15
Ripple-beds	19.47	3.93	88.08	190.92
Cross-beds	24.23	3.24	871.90	779.59
Plane-beds	24.12	2.84	658.68	520.77
Musclast	15.04	5.80	60.43	170.11

properties in three dimensions for geological analysis and visualization. Incorporating grided subsurface horizons and well data from all available sources. SGM can generate a comprehensive 3-D geological model at finer resolution to better assist the petroleum engineer in understanding reservoir characteristics. SGM uses stratigraphic patterns to generate a three-dimensional framework for geological models. The surface maps representing the distribution of layers in space were generated by Geographix (1994).

The structural behavior of Gypsy sandbodies was determined in BP's Integrated Reservoir Description Project in 1989 (Doyle and Sweet, 1992) by observing and analyzing the outcrops and core samples from 22 well bores. Table 3-2 shows the top and bottom elevation of seven channels observed in 22 wells.

Fourteen surface maps. including the tops and bottoms of the seven channels. were generated using Geographix and the data in Table 3-2. The modeling grid system used was 36 by 42. with a grid size of 32.8 feet in both X and Y direction.

Table 3-2. Correlation of Channels in the Gypsy Formation

Well	S. E.	T7	B7	T6	B6	T5	B5	T4
3	885.9	.	.	878.4	866.8	866.1	857.7	857.6
4	882.1	.	.	875.5	864.3	.	.	863.9
5	878.0	.	.	872.4	866.1	.	.	.
6	866.1	.	.		865.7	.	.	.
7	887.8	.	.	875.7	865.8	.	.	.
8	893.1	.	.	876.9	869.7	869.4	867.4	866.3
9	891.1	877.9	874.6	874.6	870.8	870.8	858	858
14	887.7	879.5	865.9			864.6	859.5	859.4
15	896.7	877.5	870.2	870.2	862.6	.	.	862
16	896.0	.	.	875.6	865.2	.	.	860.7
17	879.1	.	.	876	871.8	.	.	.
18	867.8	.				.	.	863.1
19	889.5	.	.	874.8	870.5	.	.	861.7
20	900.4	875.3	872.5	872.5	867	.	.	861.8
21	878.1	878.1	875.4	875.4	868.7	868	858.7	858.6
22	871.2	870.6	863.5	.	.	863.5	853.7	853.6
23	892.4	881.3	866.9	.	.	866.9	861.3	861.3
24	897.0	879.7	868	.	.	.	.	862
25	877.5	875.4	866.1	866	864.9	.	.	861.5
26	880.5		873.9	.	.	873.9	866.2	866.1
27	896.5	883	872.1	.	.	872.1	863	862.9
28	878.7	.	.	.	.	878.7	866.6	865.4
Well	**B4**	**T3**	**B3**	**T2**	**B2**	**T1**	**B1**	**Tallant**
3	848	.	.	847.9	837.7	837.7	835.6	830.7
4	851.7	.	.	851.7	834.3	.	.	828.9
5	.	863	846.5	846.5	834.6	.	.	827
6	.	864.9	843.9			.	.	828.5
7	.	863.8	848.8	848.8	830.8	.	.	828.8
8	864.4	864.3	851.9	851.9	836.1	.	.	829.6
9	851.1	.	.	851	841.1	841.1	838.5	830.3
14	851.7	.	.	851.6	842.9	842.8	837.4	832
15	848.5	.	.	848.5	840.5	840.5	837.8	829.6
16	846.7	.	.	846.7	837.1	837	834.9	829.1
17	.	861.3	851	850.9	834.6	.	.	828.1
18	856.4	856.4	847.4	847.3	834	.	.	828.3
19	842.1	.	.	842.1	832.5	.	.	822.6
20	847	.	.	846.9	836.8	836.7	832.1	824.2
21	852.5	.	.	852.5	841.6	841.6	837.9	832.7
22	847.5	.	.	.	.	847.5	840.5	834.1
23	843.7	.	.	.	.	843.7	836.2	830.9
24	848	.	.	847.9	837	837	832.7	827.1
25	844.7	.	.	844.7	841.6	841.6	832.7	826.3
26	853.7	.	.	853.6	850.1	850	833.2	825.4
27	850.2	.	.	.	.	850.1	839.2	824.8
28	852.7	.	.	.	.	852.6	835.4	827.9

Note: S.E. - surface elevation. T7 - top of channel 7. B7 - bottom of channel 7.
Tallant - bottom of Gypsy formation

These fourteen surface maps were imported into SGM to generate a 3D geological channel model. Permeability and porosity data in 22 wells were used as control points to determine the distribution of reservoir properties.

The deterministic method, as discussed in Chapter II, was used to determine the distribution of reservoir properties, including permeability and porosity. One important parameter, which effects the heterogeneity of geological model, is the search radius, R, which determines how many wells are included when the properties of grid blocks are calculated. There exist a minimum and a maximum values of R. The minimum value of R is the smallest one that does not create null values, and the maximum value of R is the one that still provides the best characterization of reservoir heterogeneity. To determine a value of R applicable for Gypsy formation, several R values were used to generate 3-D models. The statistical characteristics of the heterogeneity of the model were then compared with the one obtained from core analysis. Statistical mean and standard deviation were used to evaluate the effects of R value on the heterogeneity of reservoir models.

Figs. 3-11 to 3-14 illustrate the statistical characteristics of the channel model when three different R values were used as compared to the statistical characteristics from core analysis. The minimum search radius for the channel model of Gypsy formation was determined to be 534 ft, because null values were observed when a value of R less than 534 ft was used. The geological models become more homogeneous as R increases, as is apparent from smaller values of the standard deviations for porosity and permeability with increasing R values. This is consistent with the principle of deterministic algorithms. Even though 534 ft is probably not

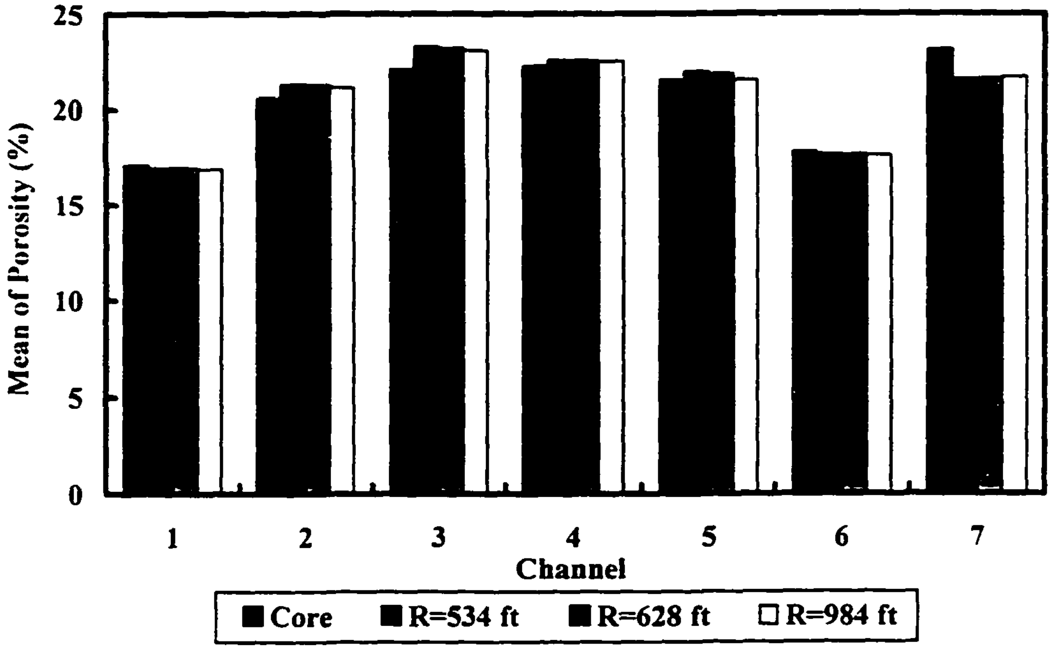

Fig. 3-11 Statistical Mean of Porosity for Channel Model

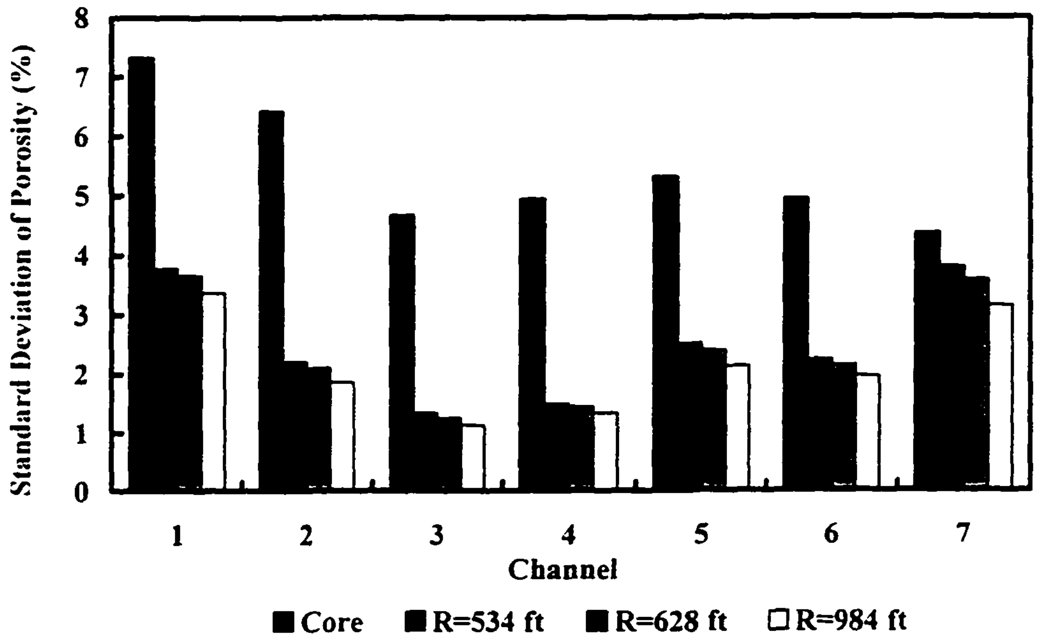

Fig. 3-12 Standard Deviation of Porosity for Channel Model

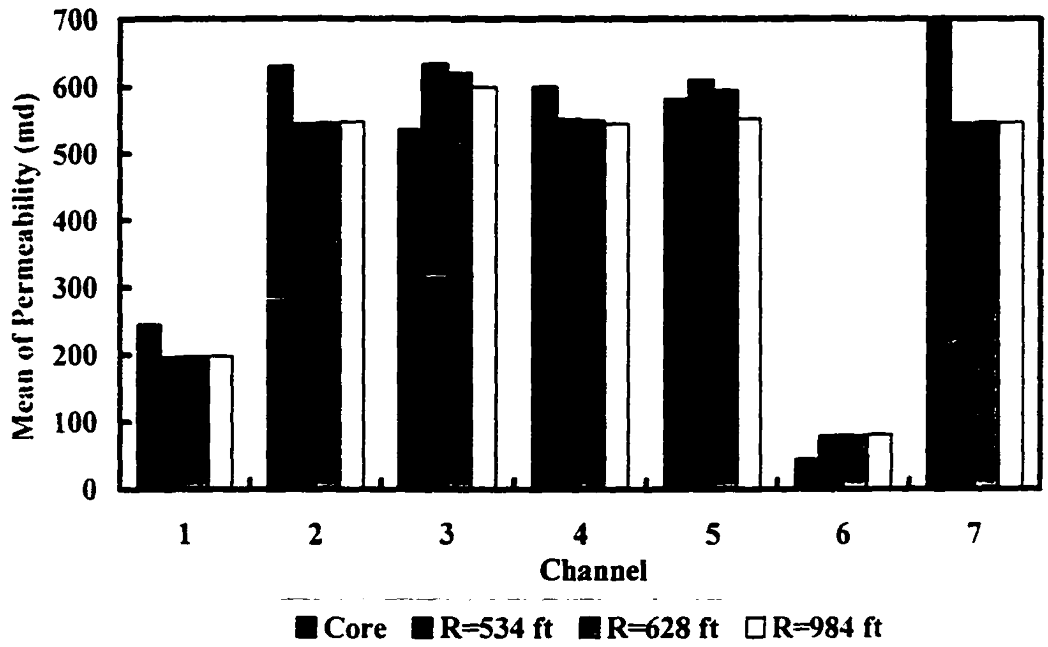

Fig. 3-13 Statistical Mean of Permeability for Channel Model

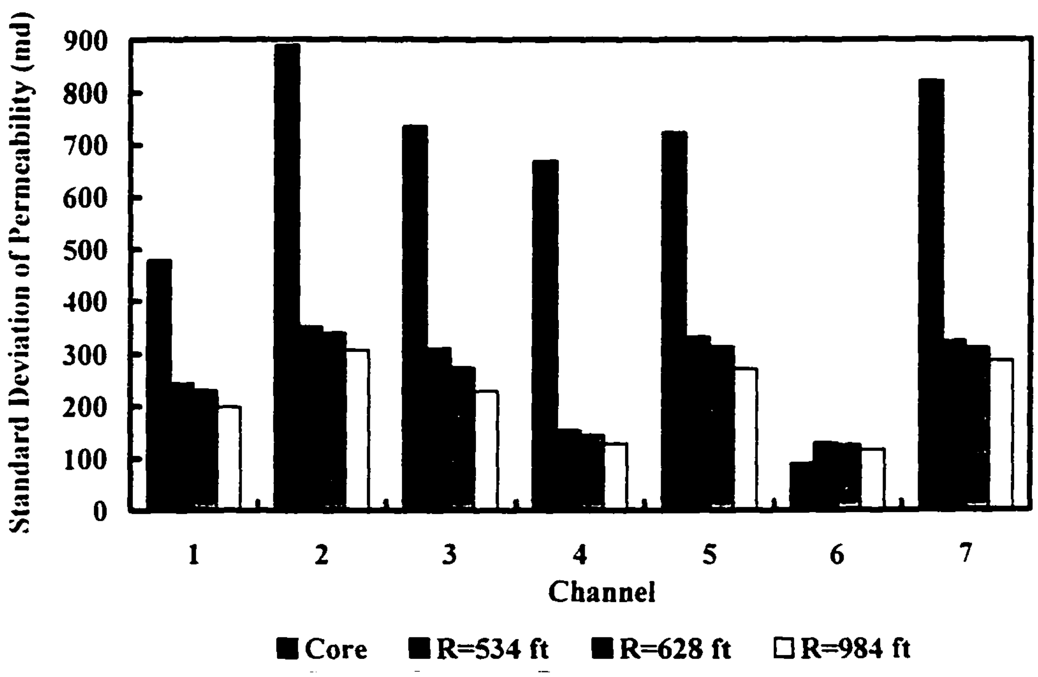

Fig. 3-14 Standard Deviation of Permeability for Channel Model

small enough to characterize the statistical variations in the properties of Gypsy formation. null value did occur when smaller R values were used. Therefore, 534 ft was determined to be the optimum R value for Gypsy channel model. It can be observed that the mean and standard deviation of porosity are not very sensitive to R values. but the mean and standard deviation of permeability are very sensitive to R values used.

Fig. 3-15 is the cross sectional view of coarse-scale Gypsy channel model. in which different colors represent different channels from channel 1 to 7. The deep blue color represents the mudstone and siltstone between channels. Pinch-outs can be obviously observed in all seven channels.

3.3 Lithofacies Model

To develop a lithofacies model. initial identification of lithofacies layers is necessary. The channel boundaries may not intersect such lithofacies layers because floodplain or mudstone layers exist that acts as a flow barrier between channels. even though they are not continuous over the whole formation area. It is very important that a lateral correlation of each lithofacies unit between wells exists and such correlation is mappable. Therefore. it was required in this study that each individual lithofacies within a channel must occur in at least two wells. If it exists in only one well and its thickness is less than one foot. it was ignored and combined with an adjacent lithofacies unit that demonstrates similar properties. Observing the distribution of lithofacies in 22 wells. it is apparent that five kinds of lithofacies are present and follow the sequence of overbank. ripple-bed. plane-beds. cross-beds. and mudclast.

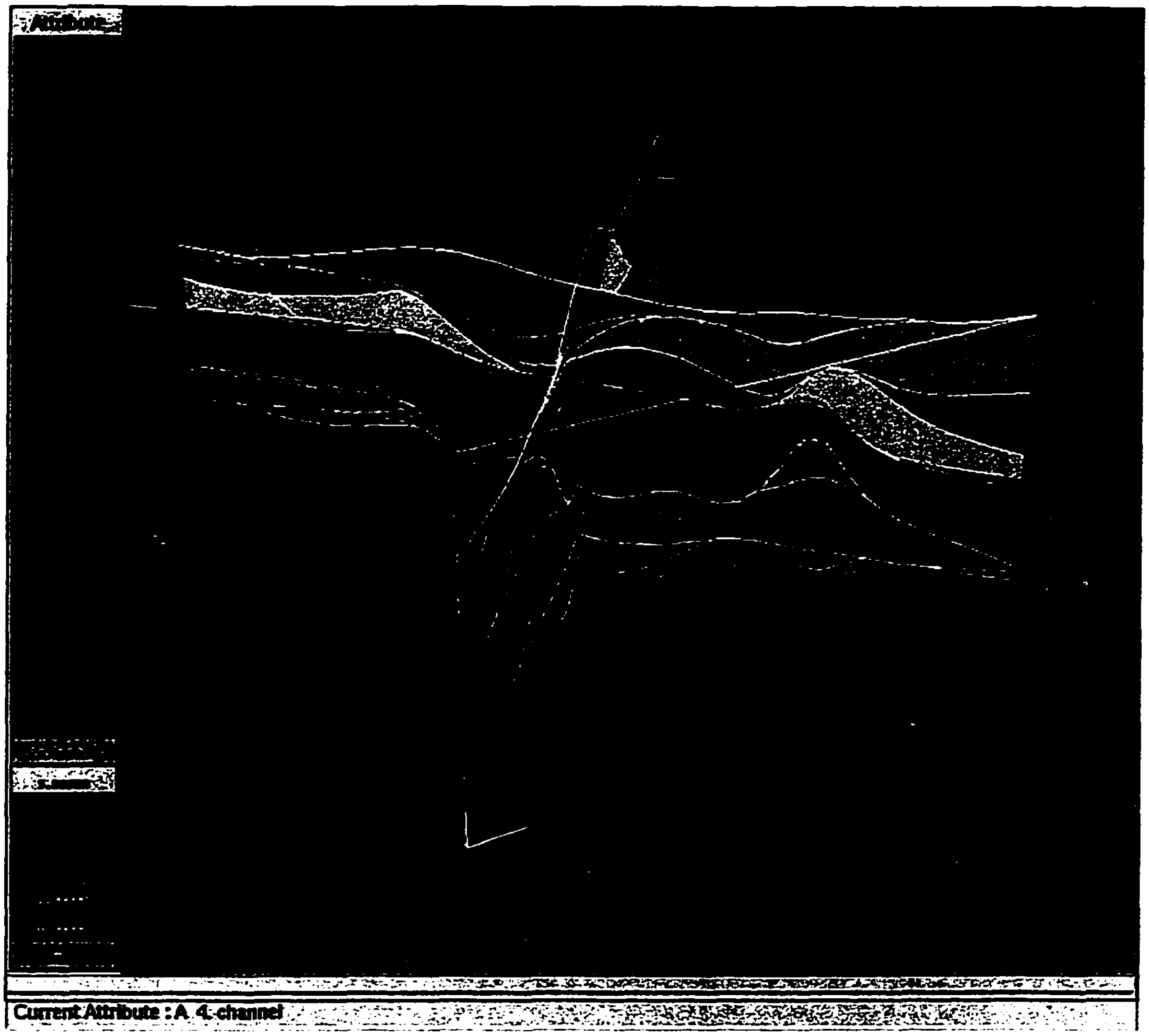

Fig. 3-15 Cross-Sectional View of Channel Model

from top to bottom, except that plane-beds and cross-beds occur interchangeably in some wells. Because cross-beds and plane-beds possess similar rock properties, as shown in Fig. 3-10, they were combined and treated as one lithofacies unit. Hence, there were only four significant lithofacies units in each individual channel in the lithofacies model. In total, 22 lithofacies units were identified in the Gypsy formation. Therefore, there are 28 layers in lithofacies model, including 22 lithofacies layers and six barriers between channels. The top and bottom positions of each lithofacies unit in the study area were determined and listed in Table 3-3.

Based on the correlation of lithofacies in Table 3-3, fifteen surface maps were generated using Geographix in addition to the fourteen surface maps generated in channel model, or a total of 29 surface maps were used to generate a 3-D lithofacies model. The search radius, R, was determined to be 890 ft for lithofacies model. Fig. 3-16 is the cross-sectional view of the lithofacies model for Gypsy formation. As for channel model, different colors represent different lithofacies units from 1 to 22 in the model. It can be observed that each channel was divided into 2 to 4 lithofacies units, which was indicated by the boundary lines in the model.

3.4 Flow Unit Model

The concept of flow unit has been discussed in Chapter II. In this study, the definition of hydraulic flow unit, which was proposed by Amaefule *et al.* (1993) was used to identify the possible flow units for Gypsy formation.

The channel model consists of only thirteen layers, including sandbodies and barriers between channels. The lithofacies model is probably the most accurate model.

Table 3-3 Correlation of Lithofacies Units in the Gypsy Formation

WELL	SURFACE	T7C	T7B	T7A	B7	T6D	T6C	B6	T5C	T5B	T5A	B5	T4D	T4C	T4B	T4A
3	885 9					878 4		866 8		864 86	858 73	857 7			857 8	
4	882 1						875 5	864 3						863 9	858.95	
5	878						872 4	866 1								
6	866 1						866 1	865 7								
7	887 8						875 7	865 8								
8	893 1					876.9	872 45	869 7	869 4			867 4		866 3		
9	891 1	877 9	876 7		874 6	874 6	874 1	870 8	870 8	865 2		858		858	855.175	
14	887 7	879 5	871 7	867 3	865 9					864 6		859 5		859 4	854 9	
15	896 7	877 5	874 2		870 2		870 2	862 6							862	
16	896						875 6	865 2							860 7	847 125
17	879 1						876	871 8								
18	867 8													863 1	862 775	
19	889 5						874 8	870 5						861 7	861.25	846.375
20	900 4		875 3		872 5	872 5		867							861.8	
21	878 1		878 1		875.4		875 4	868 7	868	861 875		858 7		858 6	855.1	
22	871 2			870 6	863 5					863.5	857.2	853 7				853 6
23	892 4		881 3	868.4	866 9				866 9	863 4		861 3	861 3	861 025	858.4	848 4
24	897		879 7		868									862	857 85	
25	877 5		875.4		866 1		866	864 9						861 5	859.5	848.5
26	880 5		880.5		873 9					873 9		866.2	866 1	865 05	883.5	855 05
27	886 5		883		872 1					872 1	864 375	863			862.9	
28	878 7									878 7		866 6		865 6	863 7	
WELL	SURFACE	B4	T3C	T3B	B3	T2D	T2C	T2B	T2A	B2	T1D	T1C	T1B	T1A	B1	TALLANT
3	885.9	848						847 9	841 4	837 7				837 7	835 6	830 7
4	882 1	851 7						851 7	840 3	834 3						828 9
5	878			863	846.5			846 5	841	834 6						827
6	866 1		864.9	859 1	843 9											828.5
7	887 8		863 8	860 55	848 8			848 8	837 8	830 8						828 8
8	893 1	864 4	864.3	860 5	851 9	851 9		851 1	843 55	836 1						829 6
9	891 1	851 1						851	843 37	841 1				841 1	838.5	830.3
14	887 7	851 7					851 6	850 55	845 05	842 9		842 8		841 45	837 4	832
15	896 7	848 5						848 5	842 7	840 5				840 5	837 8	829 6
16	896	846 7						846 7	842	837.1				837	834 9	829 1
17	879 1		861 3	859 05	851			850 9	842 95	834 1						828 1
18	867 8	856 4	856 4	855 11	847 4			847 3	839 565	834						828 3
19	889 5	842 1						842 1	838 5	832 5						822 6
20	900 4	847						846 9	840 35	836 8			836 7	834 425	832 1	824 2
21	878 1	852 5						852 5	847 45	841 6				841 6	837 9	832 7
22	871 2	847 5									847 5			844 2	840 5	834 1
23	892 4	843 7											843.7	839 4	836 2	830 9
24	897	848				847 9	844 125	842 125	840 7	837				837	832 7	827 1
25	877.5	844 7					844 7		843	841 6		841 6		837 5	832 7	826 3
26	880 5	853 7						853 6		850 1	850	847 575	838 225	835 4	833 2	825 4
27	886 5	850 2											850.1	842 5	839 2	824 8
28	878 7	852 7											852 6	842 7	835 4	827 9

- A · Mudclast B · Crossbeds and Planebeds C Ripple D Overbank
- T7C · Top of lithofacies C in channel 7 B6 · Bottom of channel 6 Surface surface of Gypsy formation Tallant bottom of Gypsy formation

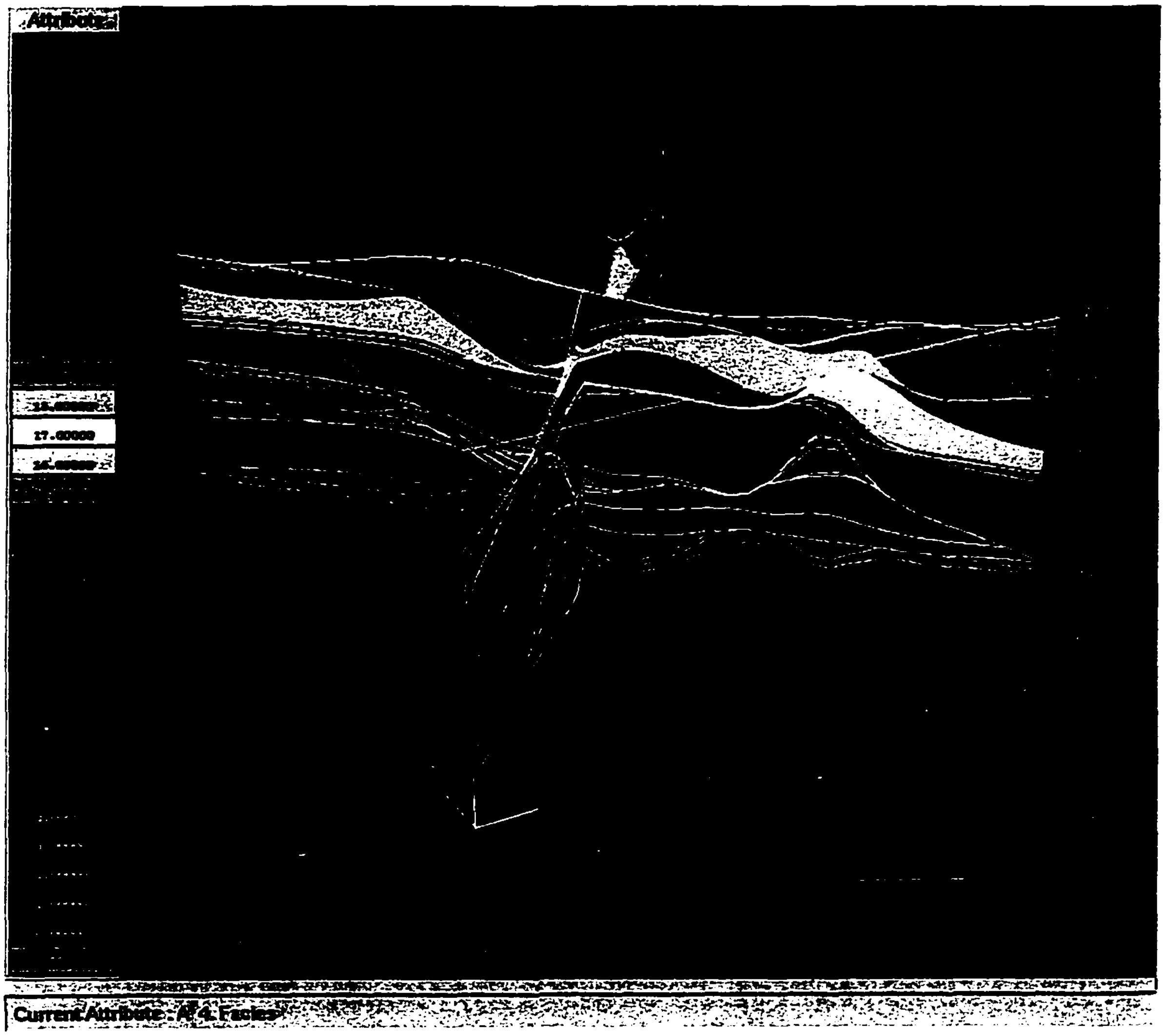

Fig. 3-16 Cross-Sectional View of Lithofacies Model

In a practical reservoir simulation study, it would be prohibitively expensive to use so many layers. Therefore, it is of significant benefit to develop a geological model that uses less layers than lithofacies model, yet provides satisfactory results in reservoir simulation and scale-up. The flow unit concept offers a possible approach that may accomplish such a geological model.

Flow units can only be obtained by combining some continuous layers or lithofacies units. As mentioned previously, lithofacies unit is probably the most homogeneous unit we can obtain based on the information available, but the boundaries of channels are not crossable, because barriers exist between channels. Therefore, this study focused on identifying the lithofacies units in the same channel that could be combined to form the same flow unit.

As stated previously, there are four lithofacies in Gypsy formation. In total, 22 lithofacies units were identified. Observing the distribution of lithofacies in 22 wells, overbank occurs on the tops of channel 1, 2, 4, and 6 only (only one well has overbank deposits in channel 5, it was combined with the adjacent lithofacies). Overbank deposits consists mainly of mudstone and siltstone which has an average permeability of 0.52 md. The rock with such low permeability offers significant resistance to fluid flowing through it and represents a flow barrier between two lithofacies in this study. Floodplain deposits that bound and partially subdivide the Gypsy sandstone are predominantly mudstone and siltstone, but include lenticular, fine-grained sandstones as well. To efficiently conduct reservoir simulation, it is reasonable to combine the overbank and floodplain between channels to reduce the number of active grid blocks in the simulation model.

After combining overbanks with floodplain deposits in channels 1, 2, 4, and 6, the number of lithofacies units considered was reduced to three. Plotting RQI versus ϕ_z for each lithofacies unit on log-log plots, it was observed that the cross-beds, plane-beds and ripple-beds combined exist very good correlation in channels 1, 2, and 7. They were, therefore, treated as one flow unit. The mudclast in channels 1, 2, and 7 exhibit more heterogeneous characteristics. They exist individually as single flow unit. Lithofacies in channels 3, 4, and 5 have similar characteristics so that they were combined to form one flow unit in these three channels. Only the ripple-bed occurs in channel 6 and it exhibits a good trend on this plot. Based on the analysis, ten flow units were identified in the seven channels, as plotted in Figs. 3-17 to 3-26. The characteristics of the ten flow units are listed in Table 3-4. Based on Amaefule *et al.* 's theory, for ideal porous media, the slopes of the plots should be 1.0. However, they are not 1.0 in these plots. This is because Amaefule *et al.* assumed that the porous medium consists of capillary tubes. For a real porous medium, this is a too simple assumption. Based on the slope and FZI (Flow Zone Indicator) listed in Table 3-4, it was observed that the ten flow units can be classified into two groups. Group one only consists of mudclast. Group two consists of plane-beds , cross-beds, and ripple-beds. In flow unit 5 and 6, mudclast was combined with group two. This means that there are mainly two flow units in Gypsy formation. However, ten flow units were numbered because the flow units in the same group, but in different channel can not be combined. The search radius for flow unit model is determined to be 928 ft. Fig. 3-27 is a cross-sectional view of the flow unit model. As in channel model and lithofacies model, different colors represent different flow units.

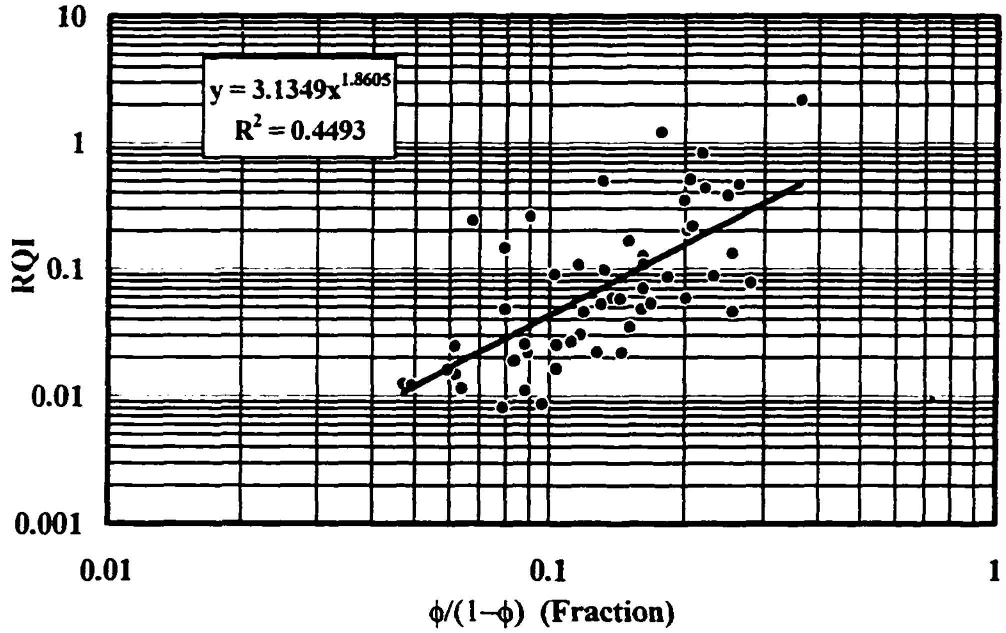

Fig. 3-17 Log-Log Plot of RQI vs ϕ_z for Flow Unit #1

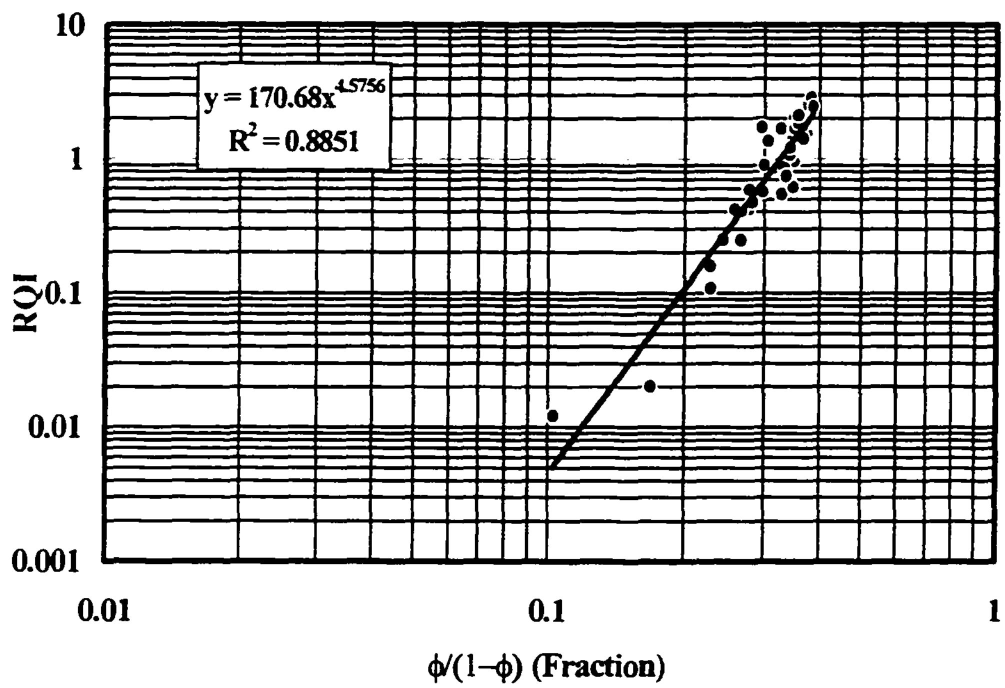

Fig. 3-18 Log-Log Plot of RQI vs ϕ_z for Flow Unit #2

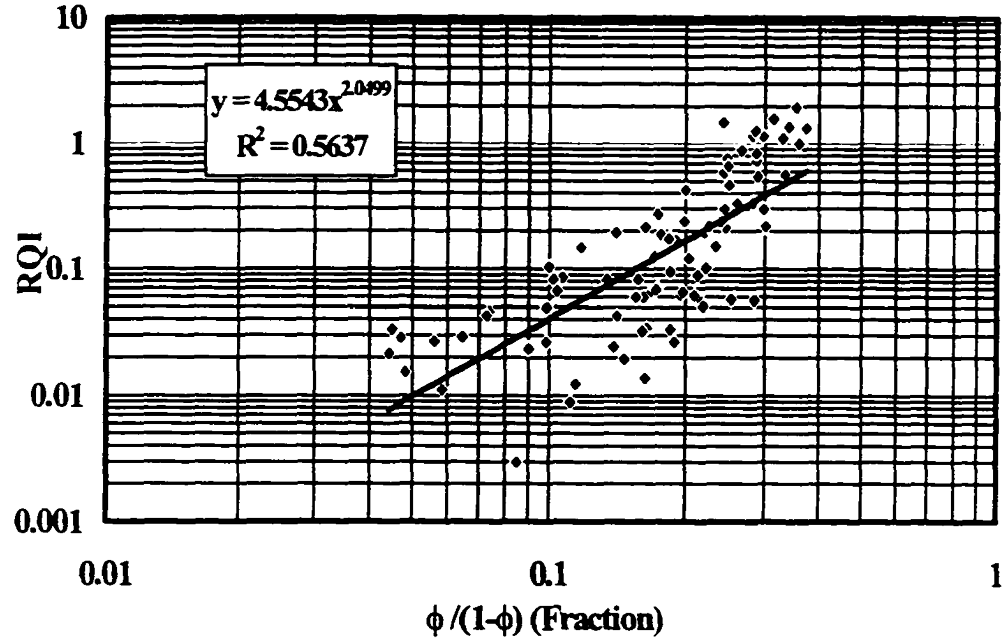

Fig. 3-19 Log-Log Plot of RQI vs ϕ_z for Flow Unit #3

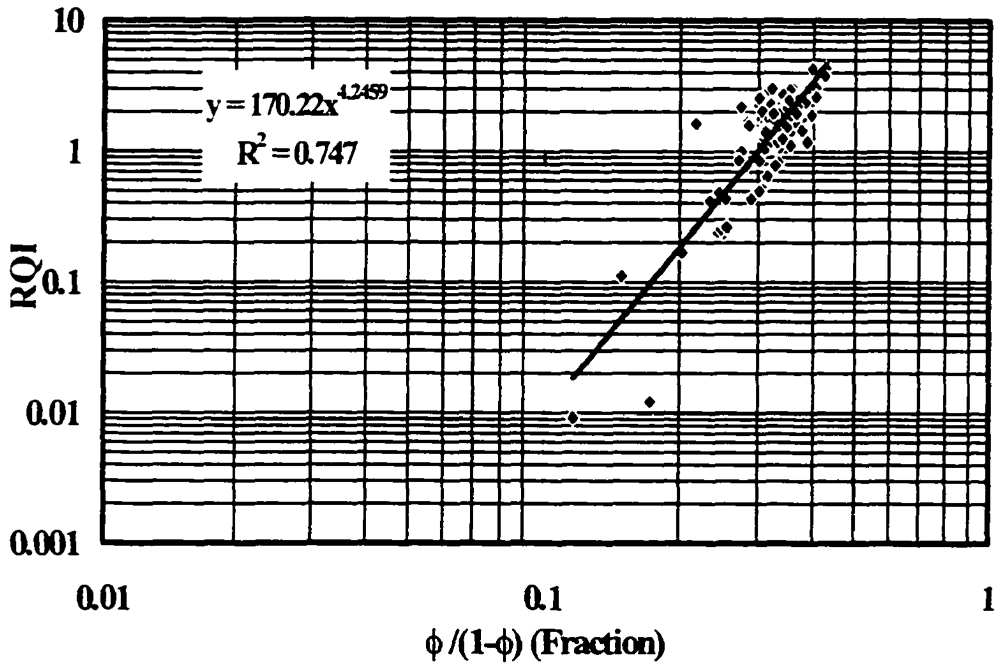

Fig. 3-20 Log-Log Plot of RQI vs ϕ_z for Flow Unit #4

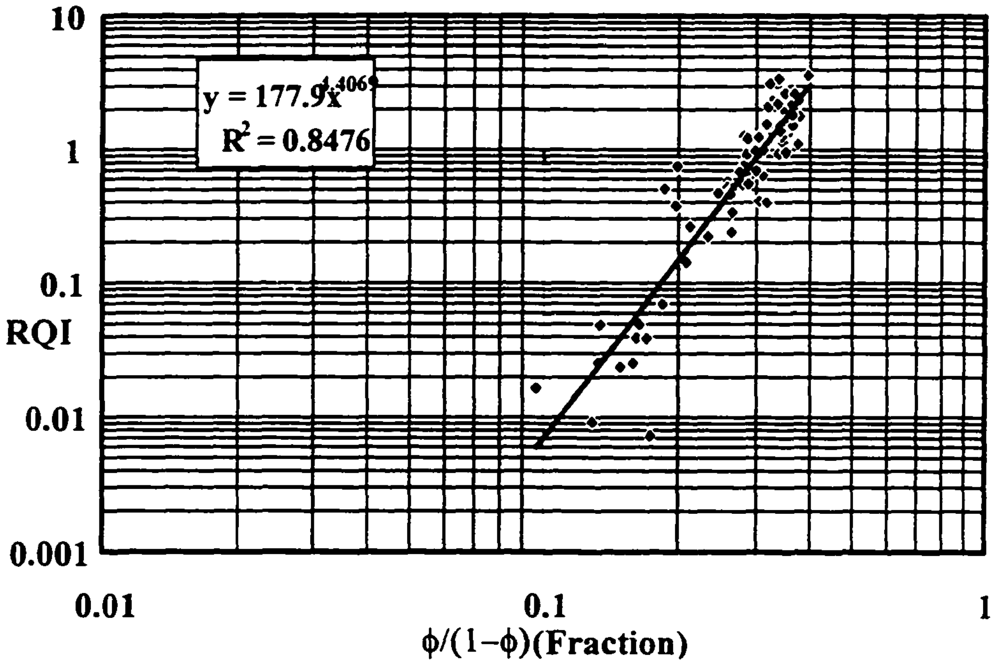

Fig. 3-21 Log-Log Plot of RQI vs ϕ_z for Flow Unit #5

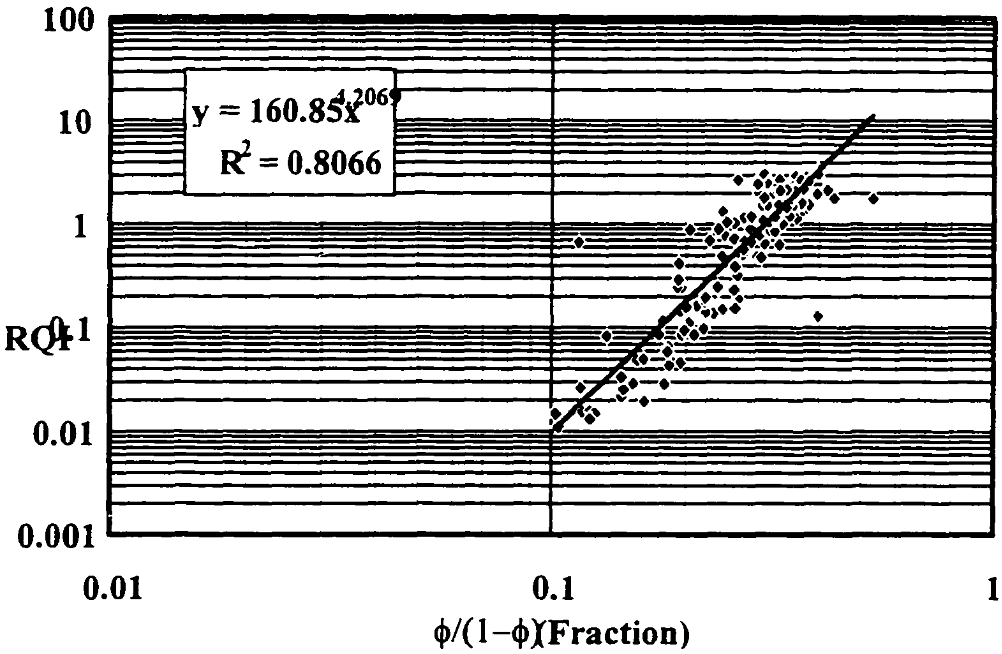

Fig. 3-22 Log-Log Plot of RQI vs ϕ_z for Flow Unit #6

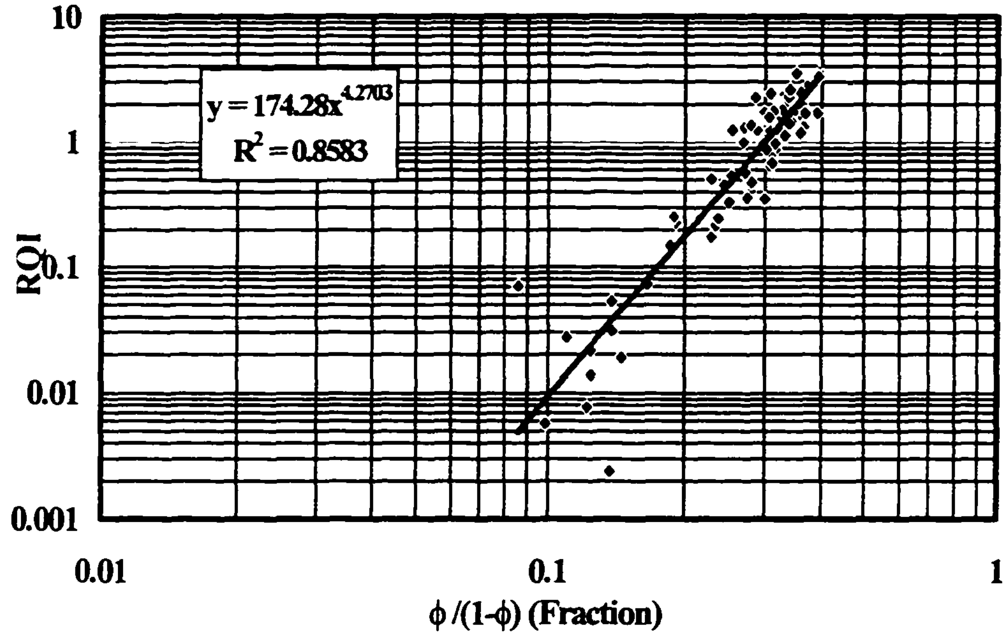

Fig. 3-23 Log-Log Plot of RQI vs ϕ_z for Flow Unit #7

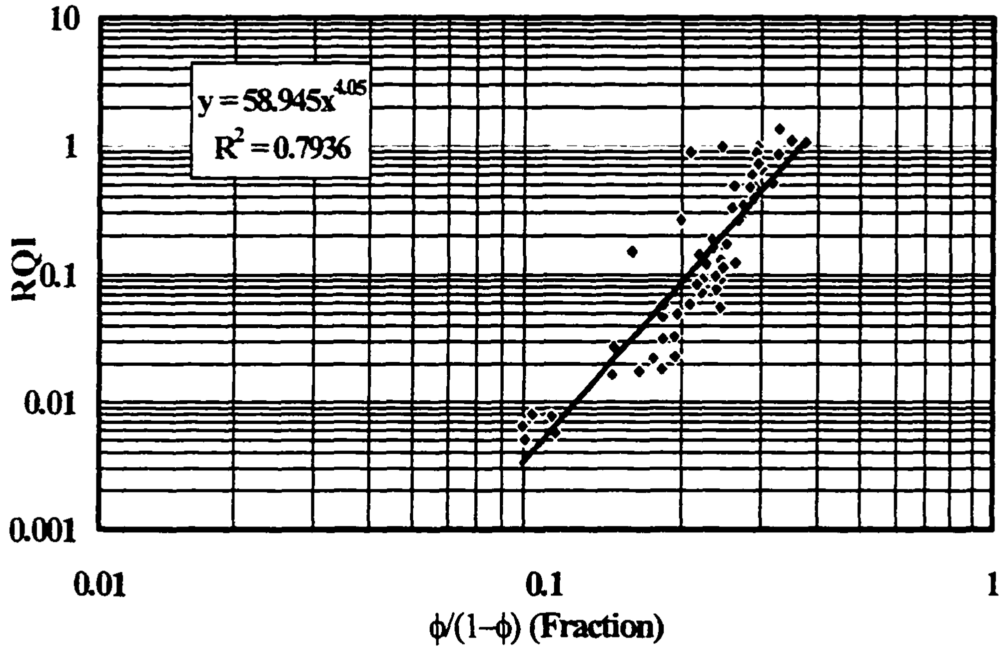

Fig. 3-24 Log-Log Plot of RQI vs ϕ_z for Flow Unit #8

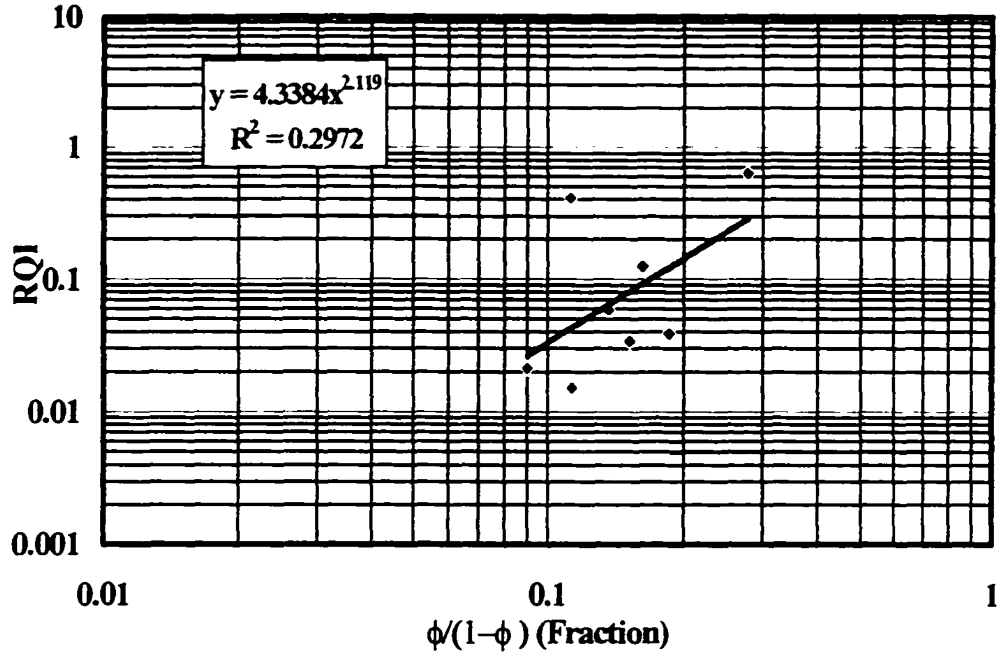

Fig. 3-25 Log-Log Plot of RQI vs ϕ_z for Flow Unit #9

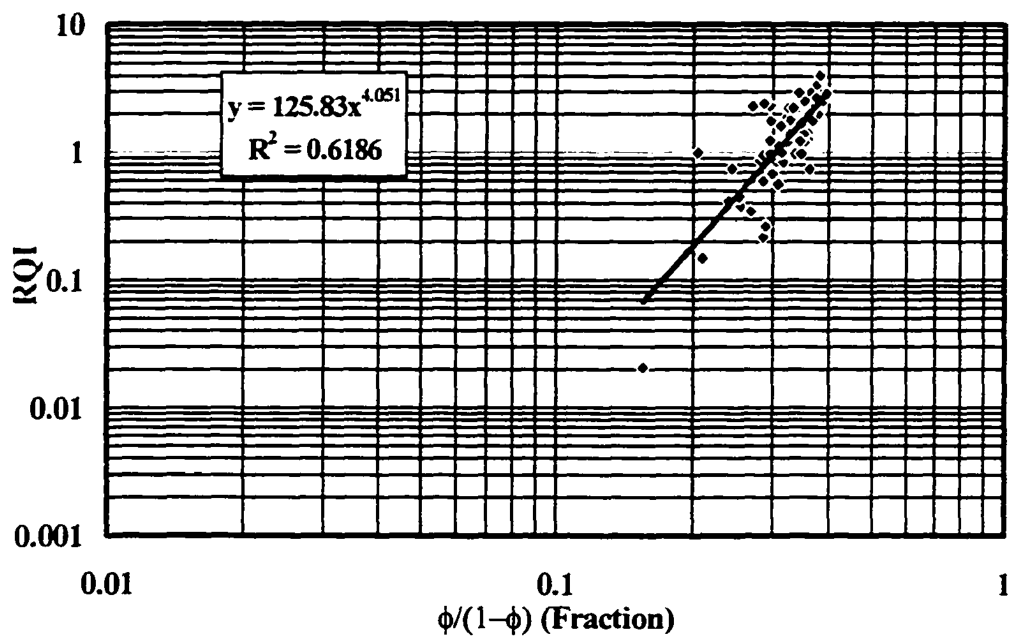

Fig. 3- 26 Log-Log Plot of RQI vs ϕ_z for Flow Unit #10

Table 3-4 Identification of Flow Units in Gypsy Formation

Channel	Facies	Flow Unit	Slope	FZI
	C			
7	B	10	4.0510	125.83
	A	9	2.1190	4.3384
6	C	8	4.0500	58.95
	C			
5	B	7	4.2703	174.28
	A			
	C			
4	B	6	4.2069	160.85
	A			
	C			
3	B	5	4.4069	177.90
	C			
2	B	4	4.2459	170.22
	A	3	2.0499	4.5543
	C			
1	B	2	4.5756	170.68
	A	1	1.8605	3.1349

3.5 Heterogeneity Analysis of Three Geological Models

Fig. 3-28 is the illustration for the three models, where each column lists the contents of the channel model, the lithofacies model and the flow unit model.

The statistical characteristics for the properties of lithofacies model and flowunit model are provided in Figs. 3-29 to 3-36. The statistical characteristics for channel model were provided earlier in Figs. 3-11 to 3-14. When comparing the statistical characteristics of porosity and permeability for the three models, it was observed that porosity was more accurately characterized than permeability. The averages of porosity determined by the models are similar to that obtained from core

Fig. 3-27 Cross-Sectional View Of Flow Unit Model

CHANNEL	LITHOFACIES	FLOW UNIT
	7C	
CHANNEL 7	7B	FLOW UNIT 10
	7A	FLOW UNIT 9
B7	B7	
	6D	B7
CHANNEL 6	6C	FLOW UNIT 8
B6	B6	B6
	5C	
CHANNEL 5	5B	FLOW UNIT 7
	5A	
B5	B5	
	4D	B5
	4C	
CHANNEL 4	4B	FLOW UNIT 6
	4A	
B4	B4	B4
	3C	
CHANNEL 3	3B	FLOW UNIT 5
B3	B3	
	2D	B3
	2C	
CHANNEL 2	2B	FLOW UNIT 4
	2A	FLOW UNIT 3
B2	B2	
	1D	B2
	1C	
CHANNEL 1	1B	FLOW UNIT 2
	1A	FLOW UNIT 1
B1	B1	B1

Fig. 3-28 Illustration of Three Geological Models for the Gypsy Formation

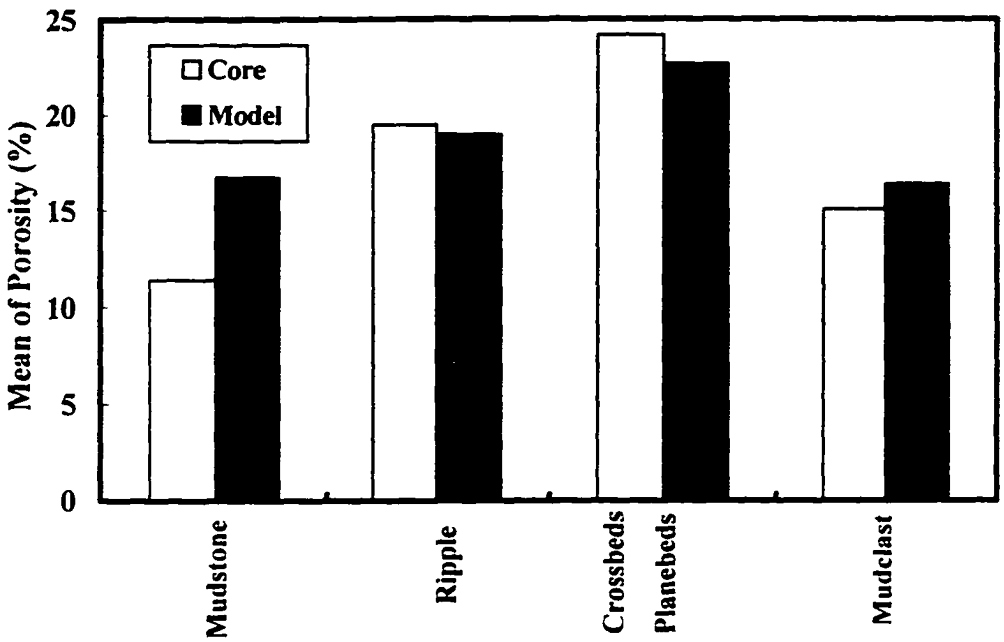

Fig. 3-29 Statistical Mean of Porosity for Lithofacies Model

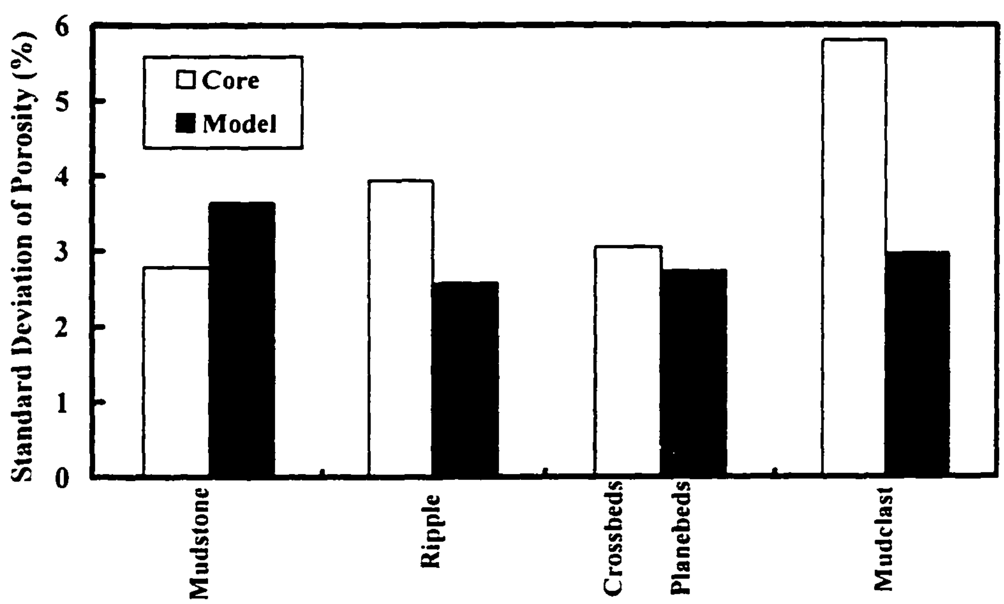

Fig. 3-30 Standard Deviation of Porosity for Lithofacies Model

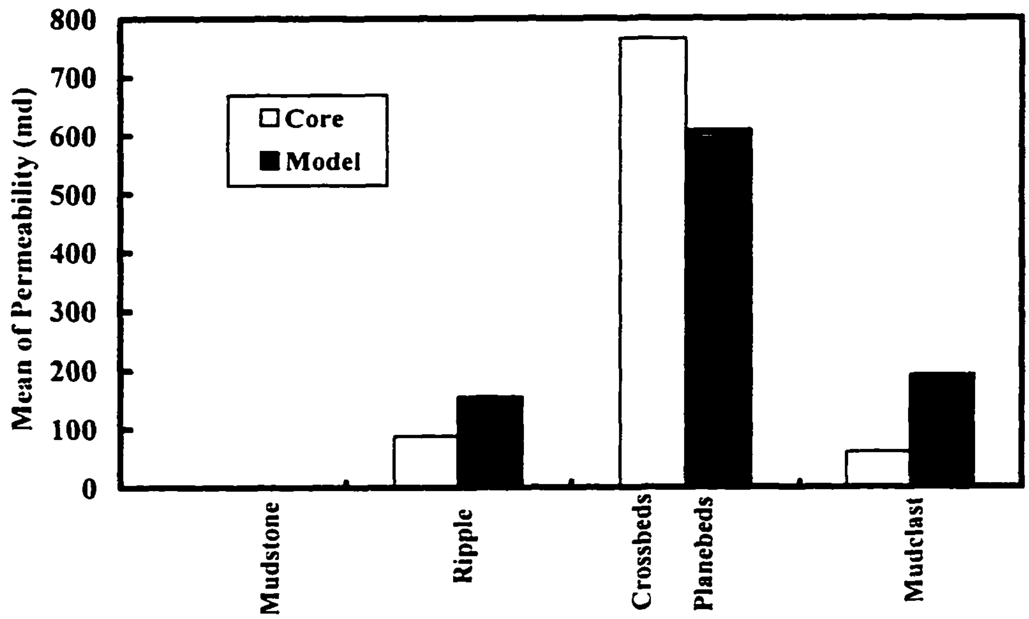

Fig. 3-31 Statistical Mean of Permeability for Lithofacies Model

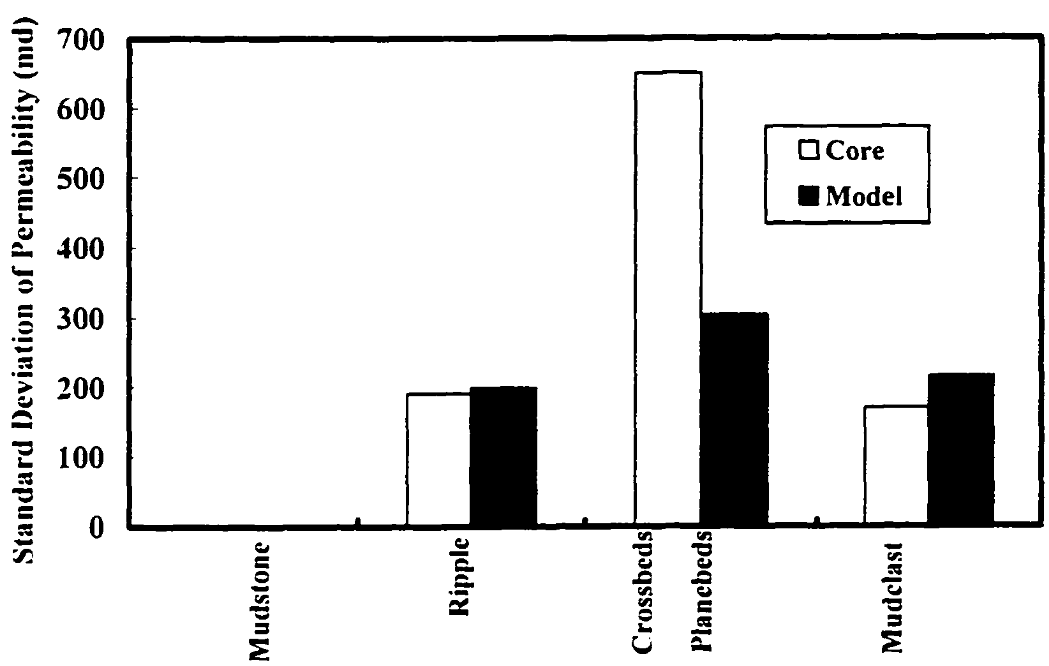

Fig. 3-32 Standard Deviation of Permeability for Lithofacies Model

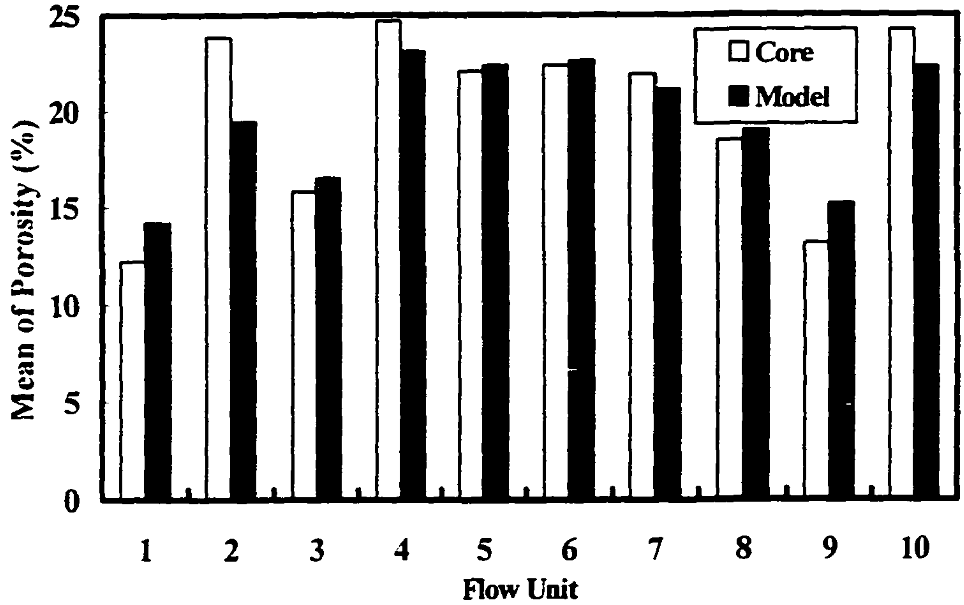

Fig. 3-33 Statistical Mean of Porosity for Flow Unit Model

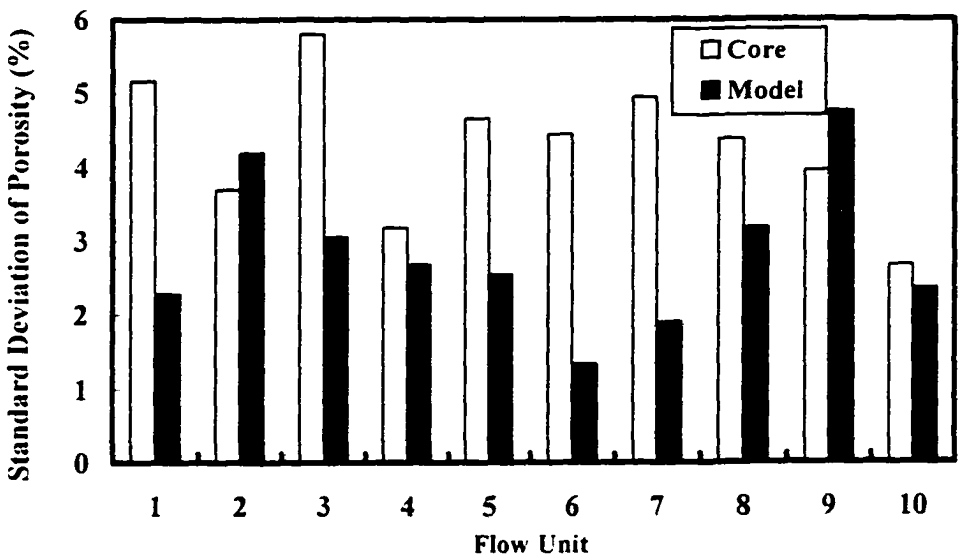

Fig. 3-34 Standard Deviation of Porosity for Flow Unit Model

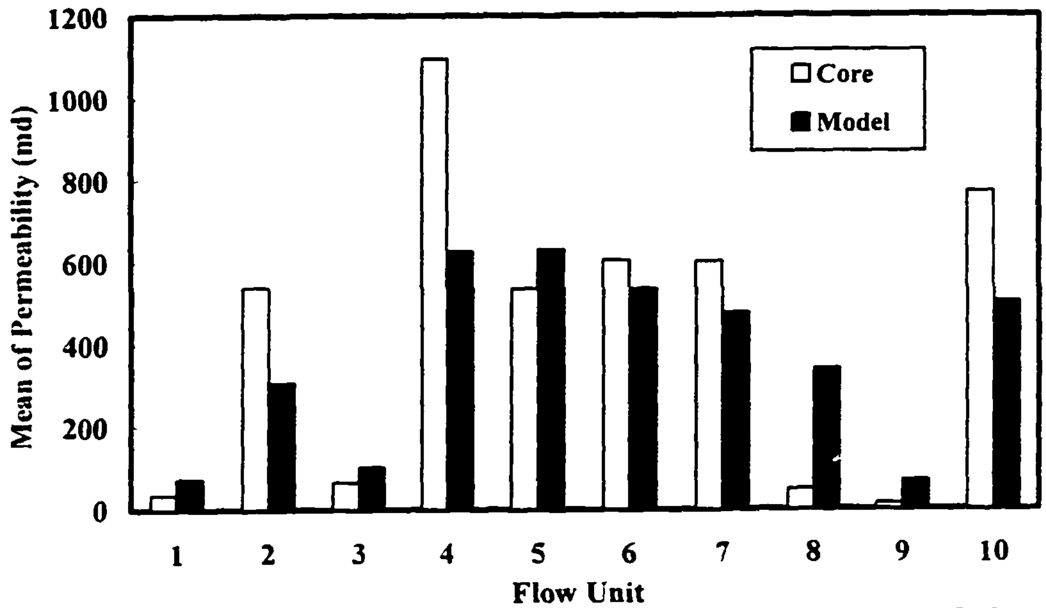

Fig. 3-35 Statistical Mean of Permeability for Flow Unit Model

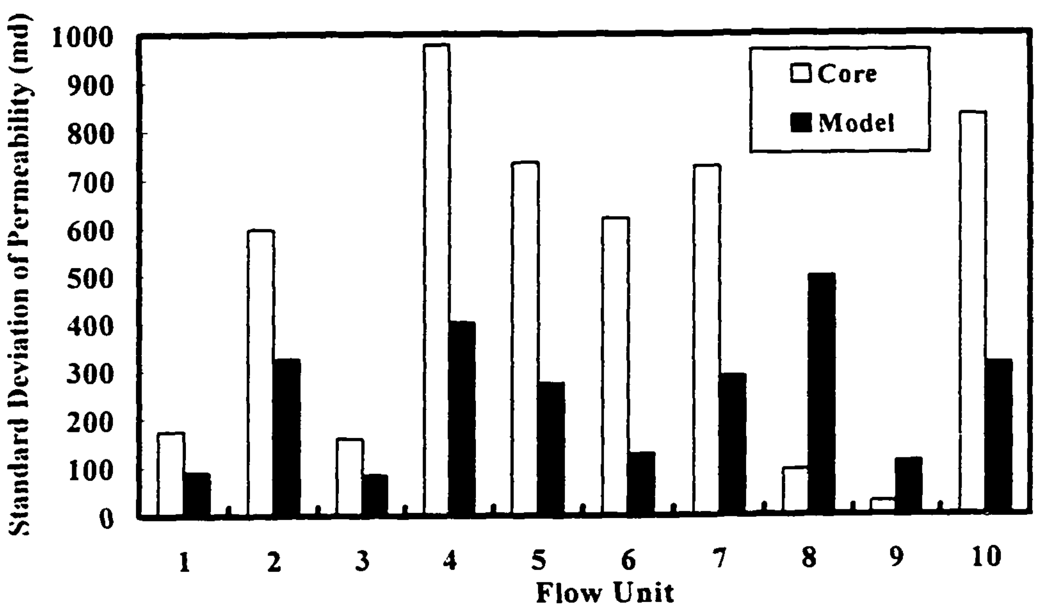

Fig. 3-36 Standard Deviation of Permeability for Flow Unit Model

measurements. The differences of standard deviations from core measurement and models for porosity are much smaller than that for permeability. This is because porosity has more homogeneous characteristics than permeability in the Gypsy formation. Comparing the three models, it was observed that the lithofacies model provided a better description than the other two models, except that the permeability of mudstone in the lithofacies model had a unreasonably large deviation in both its mean and standard deviation because of its sparse distribution. It, therefore, was not presented in the plot.

In SGM, only one search radius, R, can be used for all layers in each model. Because of the different distribution in channels, lithofacies, and flowunits, this may lead to the homogenization during the generation of the geological models. To prevent this error, it is recommended that different search radius, R, should be used for each unit in the generation of geological models if deterministic method is used.

Different strategies of geological modeling can lead to different characteristics of heterogeneity for the models. When comparing the three models generated in this study, the lithofacies model produced more accurate characterization than channel model and flowunit model. In the deterministic method, the search radius, R, has a significant effect on the heterogeneity of geological model. The extent of heterogeneity decreased with increasing values of R.

CHAPTER IV

STRATEGIES OF SCALE - UP

In this chapter. the strategies of scale-up developed in this study will be discussed. Two hypothetical geological models are used to illustrate the application of these scale-up strategies.

4.1 Scale-up of Transmissibility for Single Phase Flow

In Chapter II. scale-up methods developed in literature were reviewed. In summary. the scale-up for equivalent properties of heterogeneous porous medium can be classified into two kinds of categories. The first category consists of determining the effective permeability according to spatial distribution or correlation. It provides the average effective properties for porous medium that are independent of the flow conditions of reservoir. and this is a purely mathematical scale-up strategy. The second category consists of providing the equivalent permeabilities which produce the flow rates from coarse-scale simulation comparable to those from fine gscale. The boundary conditions imposed on the fine-scale model to determine the equivalent properties on the coarse-scale model can significantly influence the scale-up results.

In the second category of scale-up. most work has concentrated on the scale-up of effective permeability. The purpose of permeability scale-up is to preserve the gross features of flow on a coarse grid and to match them to a fine gird in reservoir simulation. The algorithm calculates an 'effective permeability' that will result in the same total flow of single-phase fluid through the coarse, homogeneous block as that obtained from fine heterogeneous block (Christie, 1996)

Even though effective permeability is used as the input in reservoir simulation, what is required in simulator to solve the partial differential equation is the transmissibility from the center of one grid block to the center of an adjacent grid block, as shown in Fig. 4-1. Many scale-up methods concentrate on keeping the heterogeneity trend in coarse-scale model the same as in fine-scale model. However, the same heterogeneity trend may not produce the same simulation results in the two different scales.

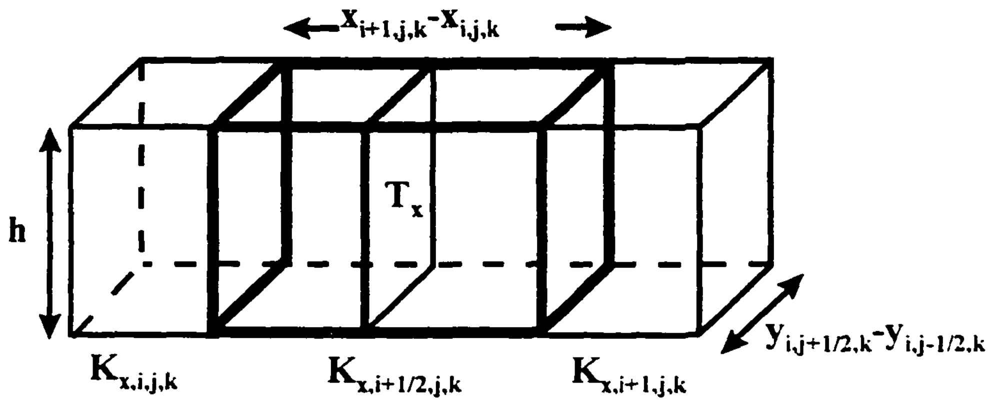

Fig. 4-1 Illustration of Transmissibility (T_x) in Reservoir Simulation

Eqs. 4-1 to 4-3 are used to define transmissibility in reservoir simulation in x, y, and z directions, respectively.

$$(T_x)_{i+1/2,j,k} = \frac{(k_x)_{i+1/2,j,k}\left(\Delta z_{i,j,k} + \Delta z_{i+1,j,k}\right)\left(\Delta y_{i,j,k} + \Delta y_{i+1,j,k}\right)}{4\left(x_{i+1,j,k} - x_{i,j,k}\right)} \tag{4-1}$$

$$(T_y)_{i,j+1/2,k} = \frac{(k_y)_{i,j+1/2,k}(\Delta x_{i,j,k} + \Delta x_{i,j+1,k})(\Delta z_{i,j,k} + \Delta z_{i,j+1,k})}{4(y_{i,j+1,k} - y_{i,j,k})} \tag{4-2}$$

$$(T_z)_{i,j,k+1/2} = \frac{(k_z)_{i,j,k+1/2}(\Delta x_{i,j,k} + \Delta x_{i,j,k+1})(\Delta y_{i,j,k} + \Delta y_{i,j,k+1})}{4(z_{i,j,k+1} - z_{i,j,k})} \tag{4-3}$$

where:

T_x, T_y, T_z = transmissibility in x, y, and z directions (ft. mD).

k_x, k_y, k_z = average permeabilities of the two-half grid blocks that are neighbors (mD).

$\Delta x, \Delta y, \Delta z$ = length of grid block in x, y, and z directions (ft),

x, y, z = dimensions of grid block (ft).

When the dimensions of the grid blocks in three dimensions are variables, the average permeability of two-half grid blocks ($(k_x)_{i+1/2,j,k}$, $(k_y)_{i,j+1/2,k}$, $(k_z)_{i,j,k-1/2}$ in Eq. 4-1 to 4-3 can be calculated by the following equations:

$$(k_x)_{i+1/2,j,k} = \frac{2(k_x)_{i,j,k}(k_x)_{i+1,j,k}(x_{i+1,j,k} - x_{i,j,k})\Delta y_{i,j,k}\Delta z_{i,j,k}\Delta y_{i+1,j,k}\Delta z_{i+1,j,k}}{\left[(k_x)_{i,j,k}\Delta x_{i+1,j,k}\Delta y_{i,j,k}\Delta z_{i,j,k} + (k_x)_{i+1,j,k}\Delta x_{i,j,k}\Delta y_{i+1,j,k}\Delta z_{i+1,j,k}\right]}$$
$$\frac{4}{\left(\Delta y_{i,j,k} + \Delta y_{i+1,j,k}\right)\left(\Delta z_{i,j,k} + \Delta z_{i+1,j,k}\right)} \tag{4-4}$$

$$(k_y)_{i,j+1/2,k} = \frac{2(k_y)_{i,j,k}(k_y)_{i,j+1,k}(y_{i,j+1,k} - y_{i,j,k})\Delta x_{i,j,k}\Delta z_{i,j,k}\Delta x_{i,j+1,k}\Delta z_{i,j+1,k}}{\left[(k_y)_{i,j,k}\Delta x_{i,j,k}\Delta y_{i,j+1,k}\Delta z_{i,j,k} + (k_y)_{i,j+1,k}\Delta x_{i,j+1,k}\Delta y_{i,j,k}\Delta z_{i,j+1,k}\right]}$$
$$\frac{4}{\left(\Delta x_{i,j,k} + \Delta x_{i,j+1,k}\right)\left(\Delta z_{i,j,k} + \Delta z_{i,j+1,k}\right)} \tag{4-5}$$

$$(k_z)_{i,j,k+1/2} = \frac{2(k_z)_{i,j,k}(k_z)_{i,j,k+1}(z_{i,j,k+1} - z_{i,j,k})\Delta x_{i,j,k}\Delta y_{i,j,k}\Delta x_{i,j,k+1}\Delta y_{i,j,k+1}}{\left[(k_z)_{i,j,k}\Delta x_{i,j,k}\Delta y_{i,j,k}\Delta z_{i,j,k+1} + (k_z)_{i,j,k+1}\Delta x_{i,j,k+1}\Delta y_{i,j,k+1}\Delta z_{i,j,k}\right]}$$
$$\frac{4}{\left(\Delta x_{i,j,k} + \Delta x_{i,j,k+1}\right)\left(\Delta y_{i,j,k} + \Delta z_{i,j,k+1}\right)} \tag{4-6}$$

In reservoir simulation, partial differential equations are solved simultaneously in 3-D. For one phase flow, there are no capillary and gravity effects. It was assumed that Darcy's Law is still valid for the flow between two grid blocks in any directions as follows:

$$Q_{x,i+1/2,j,k} = \frac{(k_x M)_{i+1/2,j,k}(\Delta y_{i,j,k} + \Delta y_{i+1,j,k})(\Delta z_{i,j,k} + \Delta z_{i+1,j,k})(\Phi_{i,j,k} - \Phi_{i+1,j,k})}{4\left(x_{i+1,j,k} - x_{i,j,k}\right)/0.001127} \tag{4-7}$$

$$Q_{y,i,j+1/2,k} = \frac{(k_y M)_{i,j+1/2,k}(\Delta x_{i,j,k} + \Delta x_{i,j+1,k})(\Delta z_{i,j,k} + \Delta z_{i,j+1,k})(\Phi_{i,j,k} - \Phi_{i,j+1,k})}{4\left(y_{i,j+1,k} - y_{i,j,k}\right)/0.001127} \tag{4-8}$$

$$Q_{z,i,j,k+1/2} = \frac{(k_z M)_{i,j,k+1/2}(\Delta x_{i,j,k} + \Delta x_{i,j,k+1})(\Delta y_{i,j,k} + y_{i,j,k+1})(\Phi_{i,j,k} - \Phi_{i,j,k+1})}{4\left(z_{i,j,k+1} - z_{i,j,k}\right)/0.001127} \tag{4-9}$$

where:

Q_x, Q_y, Q_z = flow rate in x, y, and z directions, respectively (STB/day).

M = mobility of the fluid and can be expressed as: $M = \dfrac{k_r}{B\mu}$.

k_r = relative permeability of fluid (dimensionless).

B = formation volume factor (rb/stb).

μ = viscosity (cp).

Φ = potential of grid block (psi).

Using T_x, T_y, and T_z to replace the terms in Eqs. 4-7 to 4-9, respectively, the following relationships were obtained :

$$Q_{x,i+1/2,j,k} = 0.001127(T_x M)_{i+1/2,j,k}(\Phi_{i,j,k} - \Phi_{i+1,j,k}) \tag{4-10}$$

$$Q_{y,i,j+1/2,k} = 0.001127(T_y M)_{i,j+1/2,k}(\Phi_{i,j,k} - \Phi_{i,j+1,k}) \tag{4-11}$$

$$Q_{z,i,j,k+1/2} = 0.001127(T_z M)_{i,j,k+1/2}(\Phi_{i,j,k} - \Phi_{i,j,k+1}) \tag{4-12}$$

Hence, the transimissibilities T_x, T_y, and T_z can be calculated as:

$$T_{x,i+1/2,j,k} = \frac{Q_{x,i+1/2,j,k}}{0.001127(M)_{i+1/2,j,k}(\Phi_{i,j,k} - \Phi_{i+1,j,k})} \tag{4-13}$$

$$T_{y,i,j+1/2,k} = \frac{Q_{y,i,j+1/2,k}}{0.001127(M)_{i,j+1/2,k}(\Phi_{i,j,k} - \Phi_{i,j+1,k})} \tag{4-14}$$

$$T_{z,i,j,k+1/2} = \frac{Q_{z,i,j,k+1/2}}{0.001127(M)_{i,j,k+1/2}(\Phi_{i,j,k} - \Phi_{i,j,k+1})} \tag{4-15}$$

As mentioned above, the purpose of scale-up for single phase flow is to preserve the gross features of flow on the simulation grid, i.e., to match the flow rates from fine-scale model to coarse-scale model. The flow rate for each grid block of fine-scale model, which is the target of study, can be simply obtained from the output of a simulation for a fine-scale model. If the potentials for each grid block of a coarse-scale model are obtained, the transmissibilities, T_x, T_y, and T_z can be calculated using Eqs. 4-13 to 4-15, which should lead to the same flow rates as in the fine-scale model. In reservoir simulation, it is possible to either input permeability for each grid block or directly input transmissibilities. Therefore, one possible approach for scale-up is to use permeability as an input in fine-scale simulation and transmissibility as an input in coarse-scale simulation in order to match the flow rates. Average pressure for each coarse-scale grid block can be obtained using pore volume average on a fine-scale gird-block pressure. The potential for coarse-scale grid block can be calculated by considering the elevation difference between two grid blocks.

In this study, only the scale-up in the vertical direction was considered, meaning only to combine the layers in vertical direction, but keep the dimensions in the horizontal direction the same in both fine scale and coarse scale. As shown in Fig. 4-2, the total flow rate for the coarse-scale grid block in x and y directions is simply the sum of the flow rates of the fine-scale grid blocks in vertical direction. In the z direction, the flow rate for coarse-scale grid block is equal to the flow rate of fine-scale grid block at the boundary of upscaled zone or layer. The potentials of coarse-scale grid block can be calculated using the following equation:

$$\Phi_{i,j,k} = \frac{\sum_{z=i}^{n} v\phi p}{\sum_{z=i}^{n} v\phi} + 0.4335 * \left(E_{i,j,k} - E_{datum}\right)\rho_f \qquad (4\text{-}16)$$

Where,

Φ = potential of grid block (i,j,k) (psi),

v = volume of fine-scale grid block (ft^3),

ϕ = porosity of fine-scale grid block (fraction),

p = pressure of fine-scale grid block (psi),

E_{datum} = elevation of reference datum (ft),

$E_{i,j,k}$ = elevation of grid block (i,j,k) (ft),

ρ_f = density of fluid in reservoir (g/cm^3),

n = number of layers upscaled.

4.2 Scale-Up for Hypothetical Reservoir Models

In this section, two hypothetical geological models were used to apply the methodology discussed in section 4.1. First, a layer-cake model without pitch-out was

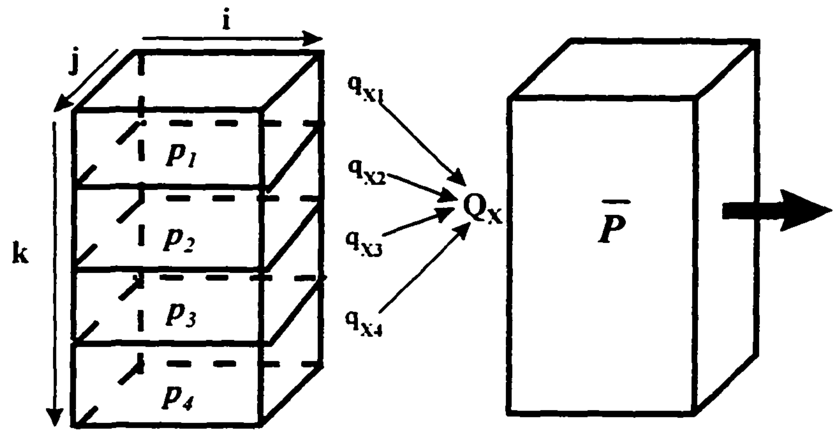

Fig. 4-2 Illustration of Upscaled Flow Rate and Pressure

considered and then pitch-out was included in the second model.

4.2.1 Description of the Hypothetical Reservoir Model

A 17-layer fine-scale hypothetical reservoir model was used to illustrate the application of scale-up described in section 4.1. The reservoir was assumed to be located at depth between 8450 to 8510 feet. The modeling area was 270x270 ft^2 with a grid system of 9x9x17 in x, y, and z directions, respectively. The porosity and permeability of the model were assumed to be randomly and normally distributed and generated using the tool for data analysis in MS Excel. The statistical properties of the model are provided in Table 4-1.

In the model, layers 6 and 12 were designed to serve as barriers between layers 5, and 7, and, 11 and 13, which have very low porosities and permeabilities, as shown in Table 4-1. The 17-layer fine-scale model was scaled up into a 5-layer coarse-scale model, (i.e., layer 1 to 5, 7 to 11, and 12 to 17 was scaled up to become layer 1, 3, and 5 in coarse-scale model, respectively). In this particular model, no pitch-out exists, meaning no zero thickness in any grid blocks.

Five wells were created, as shown in Fig. 4-3, to perform this hypothetical simulation, in which one injection well is located at the center of the model and four production wells are at the four corners of the model. Fig. 4-4 is a three dimensional view of permeability distribution of the model. The properties of reservoir fluid and several important parameters of reservoir used in the simulation are provided in Table 4-2.

Table 4 -1 Statistical Characteristics of Hypothetical Layer-Cake Model

Fine Scale (Layer)	Coarse Scale (Layer)	ϕ Mean (%)	ϕ Standard Deviation (%)	k Mean (mD)	k Standard Deviation (mD)
1 - 5	1	24.13	5.04	688.13	437.11
6	2	8.20	6.02	0.012	0.0031
7 - 11	3	18.08	3.81	96.34	65.73
12	4	7.77	7.83	0.015	0.0045
13 - 17	5	25.00	3.15	1091.97	698.39

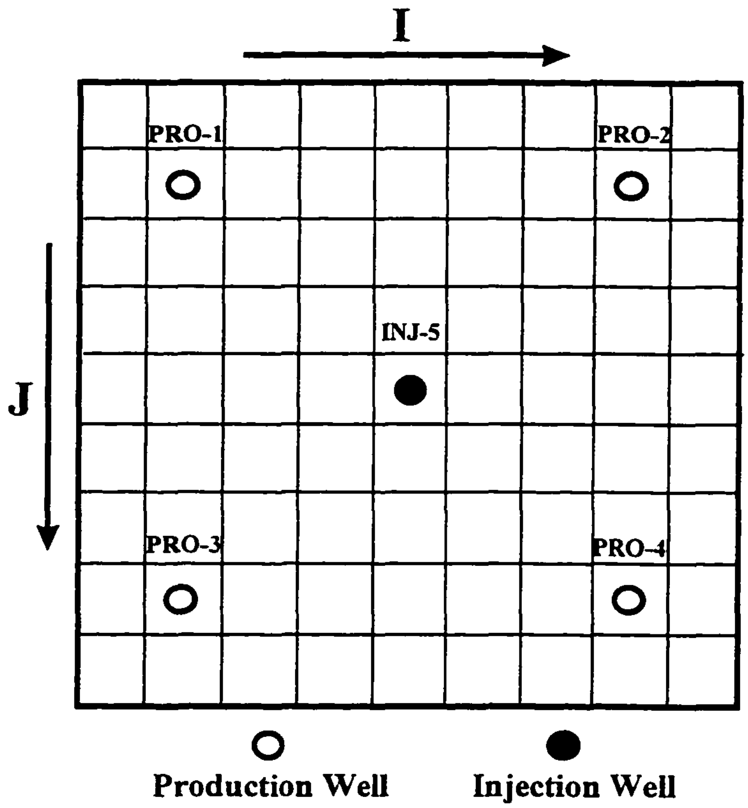

Fig. 4-3 Well Pattern Used for Hypothetical Model #1

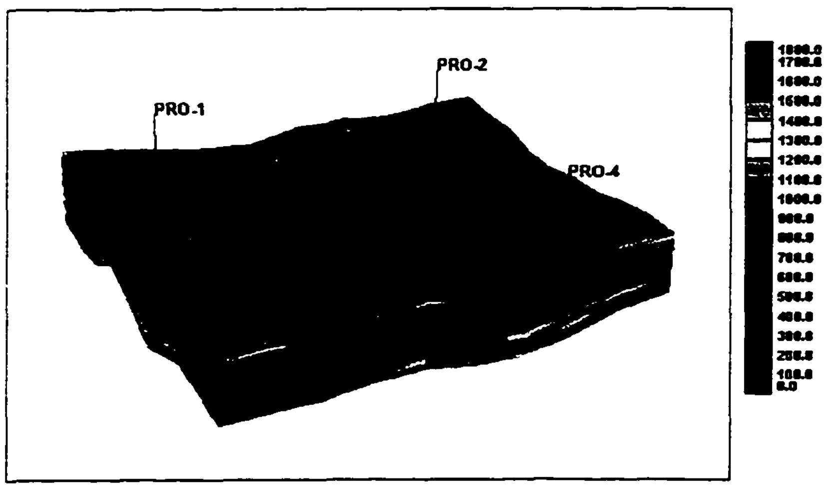

Fig.4-4 3-D View of Permeability Distribution for Model #1

Table 4-2 Properties of Reservoir Fluid and Parameters Used in the Simulation for Model #1

Parameter	Unit	Value
Water Density	gm/cc	1.0
Water Volume Factor	rb/stb	1.0
Water Viscosity	cp	1.0
Water Compressibility	psi^{-1}	$3x10^{-6}$
Pore Compressibility	psi^{-1}	$4x10^{-6}$
Reservoir Temperature	^{o}F	180
Standard Temperature	^{o}F	60
Standard Pressure	psi	14.65
P_i (at 8000 ft)	psi	2500
Q_{max} (Production Well)	STB/day	10000
P_{min}(Production Well at 8350 ft)	psi	1000
Q_{max} (Injection Well)	STB/day	2250
P_{max}(Injection Well at 8350 ft)	psi	10000

4.2.2 Test for the Validity of Transmissibility Calculation

To test the validity of the scale-up strategy, transmissibility, T_X, T_Y, and T_Z of fine-scale grid blocks were calculated using the method proposed in Section 4.1. These values were then compared with the transmissibility obtained from the simulation output as illustrated in Fig. 4-5 to Fig. 4-10. Note that all data are provided in Figs. 4-5, 4-7, and 4-9. Several negative values observed in these three plots occurred when the pressure difference between the two grid blocks was very small. When the potential was calculated, the errors were introduced. In Figs. 4-6, 4-8, and 4-10, only positive values were plotted. Most of the values follow a 45^0 line with a small percentage scattered away from this line. Overall, the plotted data in Figs 4-5 to 4-10 show that the proposed method for calculating transmissibility is valid.

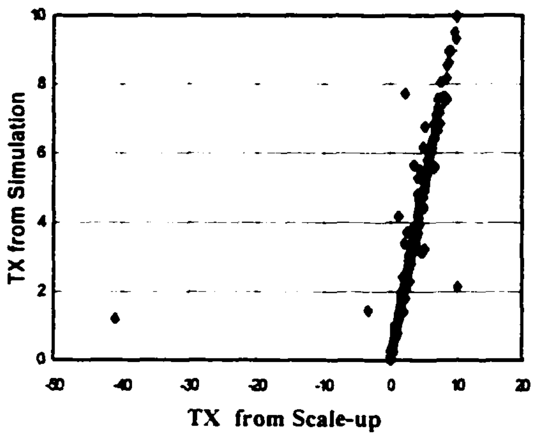

Fig. 4-5 Cross Plot of Transmissibility (T_x) Obtained from Simulation and Scale-up (Include all data)

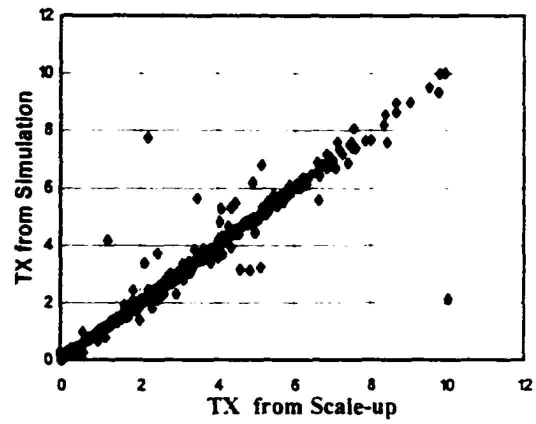

Fig. 4-6 Cross Plot of Transmissibility (T_x) Obtained from Simulation and Scale-up (Only Positive data)

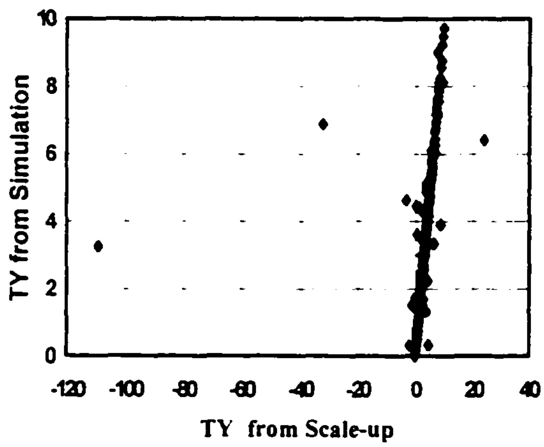

Fig. 4-7 Cross Plot of Transmissibility (T_y) Obtained from Simulation and Scale-up (Include all data)

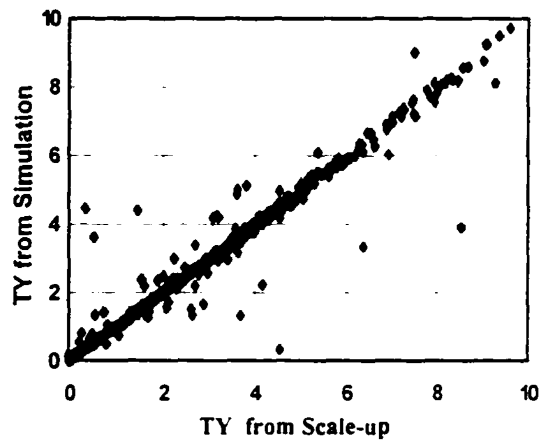

Fig. 4-8 Cross Plot of Transmissibility (T_y) Obtained from Simulation and Scale-up (Only Positive data)

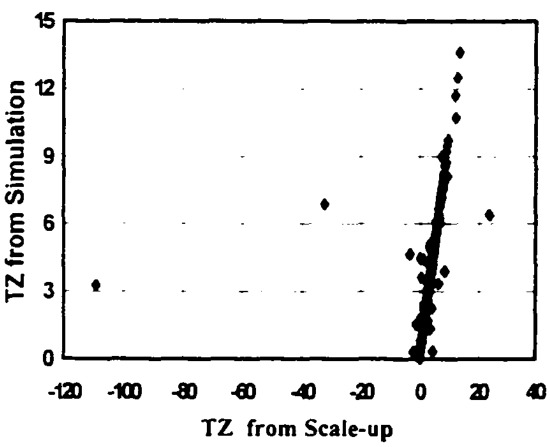

Fig. 4-9 Cross Plot of Transmissibility (T_z) Obtained from Simulation and Scale-up (Include all data)

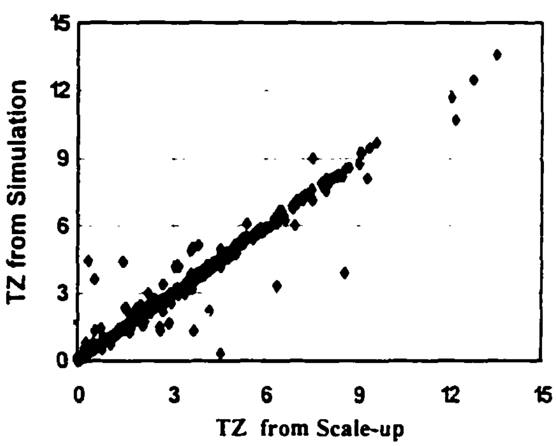

Fig. 4-10 Cross Plot of Transmissibility (T_z) Obtained from Simulation and Scale-up (Only Positive data)

4.2.3 Scale-Up for a Hypothetical Layer-Cake Reservoir Model

Scale-up was conducted by first running single-phase simulation on fine-scale model to obtain the outputs of flow rate and pressure for fine-scale grid blocks. Then the simulation was run on a coarse-scale model using the following reservoir properties: transmissibilities, pore volume, and thickness, obtained from scale-up calculation. Simulation on fine-scale model was run for ten days until stabilized production and injection rates were obtained.

Scale-up was conducted using a FORTRAN program developed in this study. A flow chart of the program is provided in Fig. 4-11. The FORTRAN program and the definitions of the parameters used are provided in Appendix.

In the calculation, a pore-volume average method was used to calculate the average pressure and porosity for each coarse grid block. Negative values of T_X, T_Y, or T_Z can occur when production rates and potential gradient between two grid blocks have different directions. The potential gradient in x or y directions may sometimes have a zero value. The program automatically checks for these problems during the calculation. When detected, the transmissibility T_x, T_y, or T_z are calculated using Eqs. 4-1 to 4-3. The average permeability K_x, and K_y for each coarse grid block were calculated from permeability of fine-scale grid blocks using thickness averaging method, and K_Z using harmonic averaging method. In Eqs. 4-1 to 4-3 , the average permeability of two half adjacent coarse grid blocks in x, y, and z directions were calculated using Eqs. 4-4 to 4-6, respectively. Flow rates and pressure in x, y, and z directions for fine-scale were obtained from an output map file. Transmissibility, thickness, and pore volume for coarse-scale model were calculated and input into the coarse-scale simulation model.

Fig. 4-11 Flow Chart of the Program for Scale-up Without Pinch-out

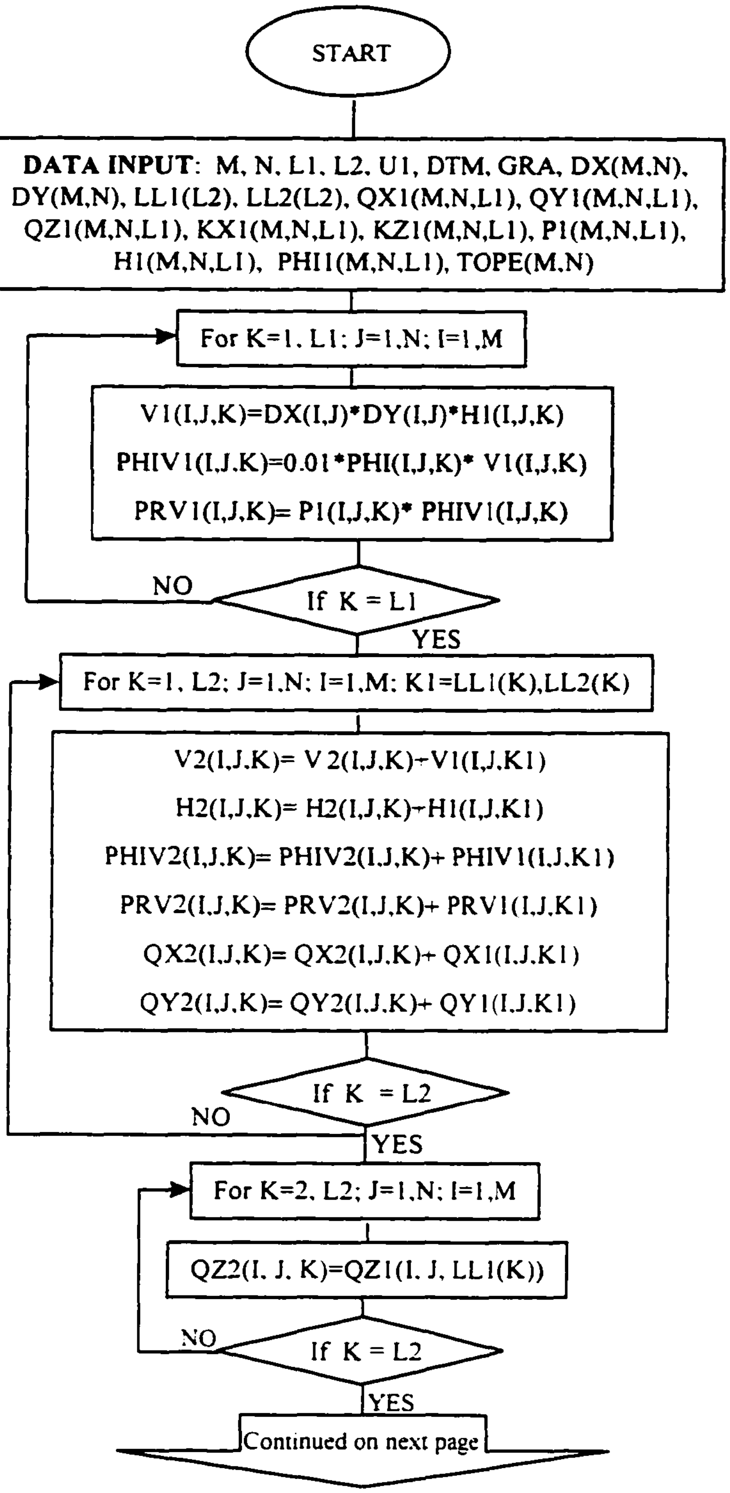

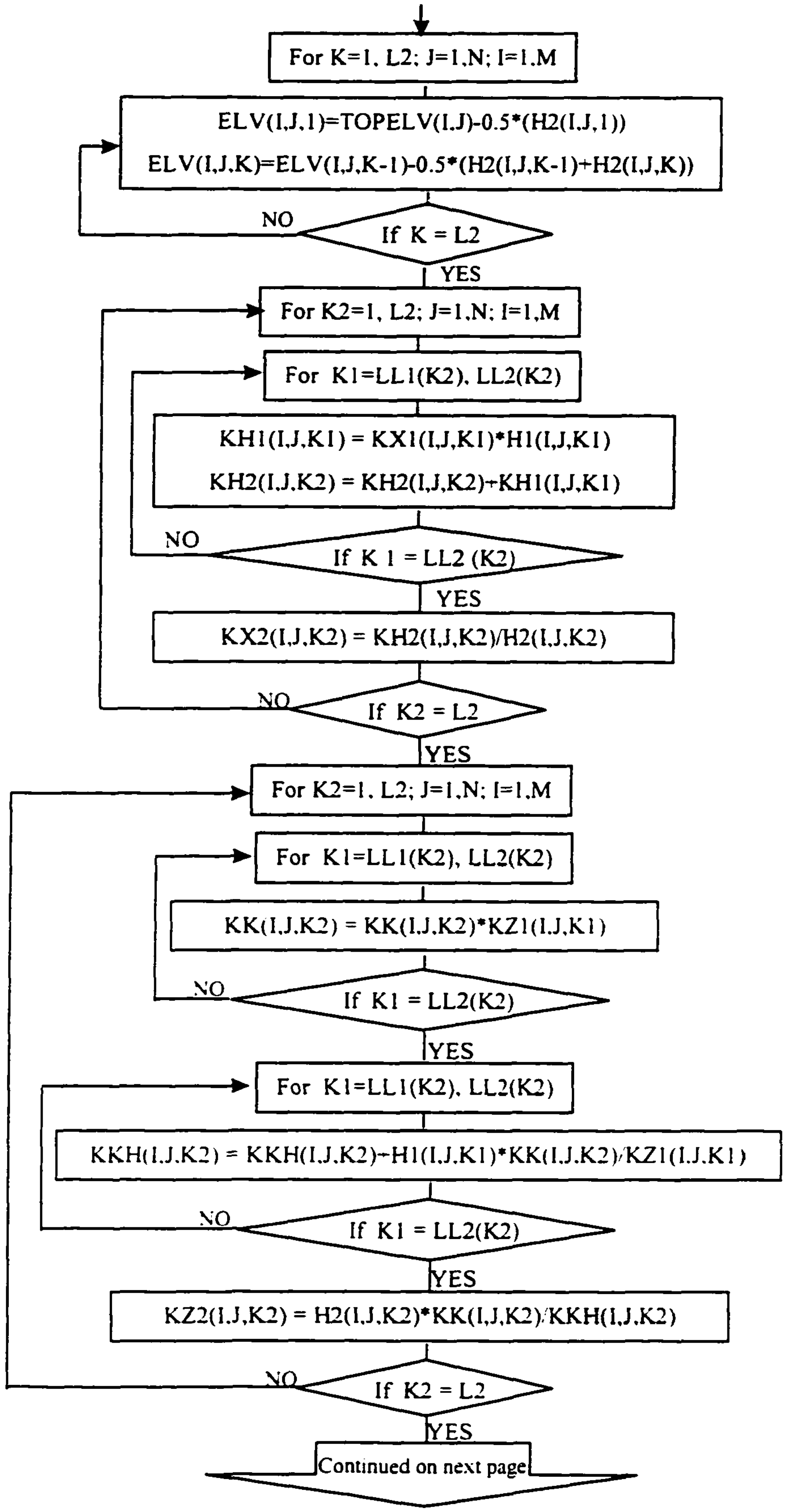
For K=1, L2; J=1,N; I=1,M
ELV(I,J,1)=TOPELV(I,J)-0.5*(H2(I,J,1))
ELV(I,J,K)=ELV(I,J,K-1)-0.5*(H2(I,J,K-1)+H2(I,J,K))
NO
If K = L2
YES
For K2=1, L2; J=1,N; I=1,M
For K1=LL1(K2), LL2(K2)
KH1(I,J,K1) = KX1(I,J,K1)*H1(I,J,K1)
KH2(I,J,K2) = KH2(I,J,K2)+KH1(I,J,K1)
NO
If K 1 = LL2 (K2)
YES
KX2(I,J,K2) = KH2(I,J,K2)/H2(I,J,K2)
NO
If K2 = L2
YES
For K2=1, L2; J=1,N; I=1,M
For K1=LL1(K2), LL2(K2)
KK(I,J,K2) = KK(I,J,K2)*KZ1(I,J,K1)
NO
If K1 = LL2(K2)
YES
For K1=LL1(K2), LL2(K2)
KKH(I,J,K2) = KKH(I,J,K2)+H1(I,J,K1)*KK(I,J,K2)/KZ1(I,J,K1)
NO
If K1 = LL2(K2)
YES
KZ2(I,J,K2) = H2(I,J,K2)*KK(I,J,K2)/KKH(I,J,K2)
NO
If K2 = L2
YES
Continued on next page

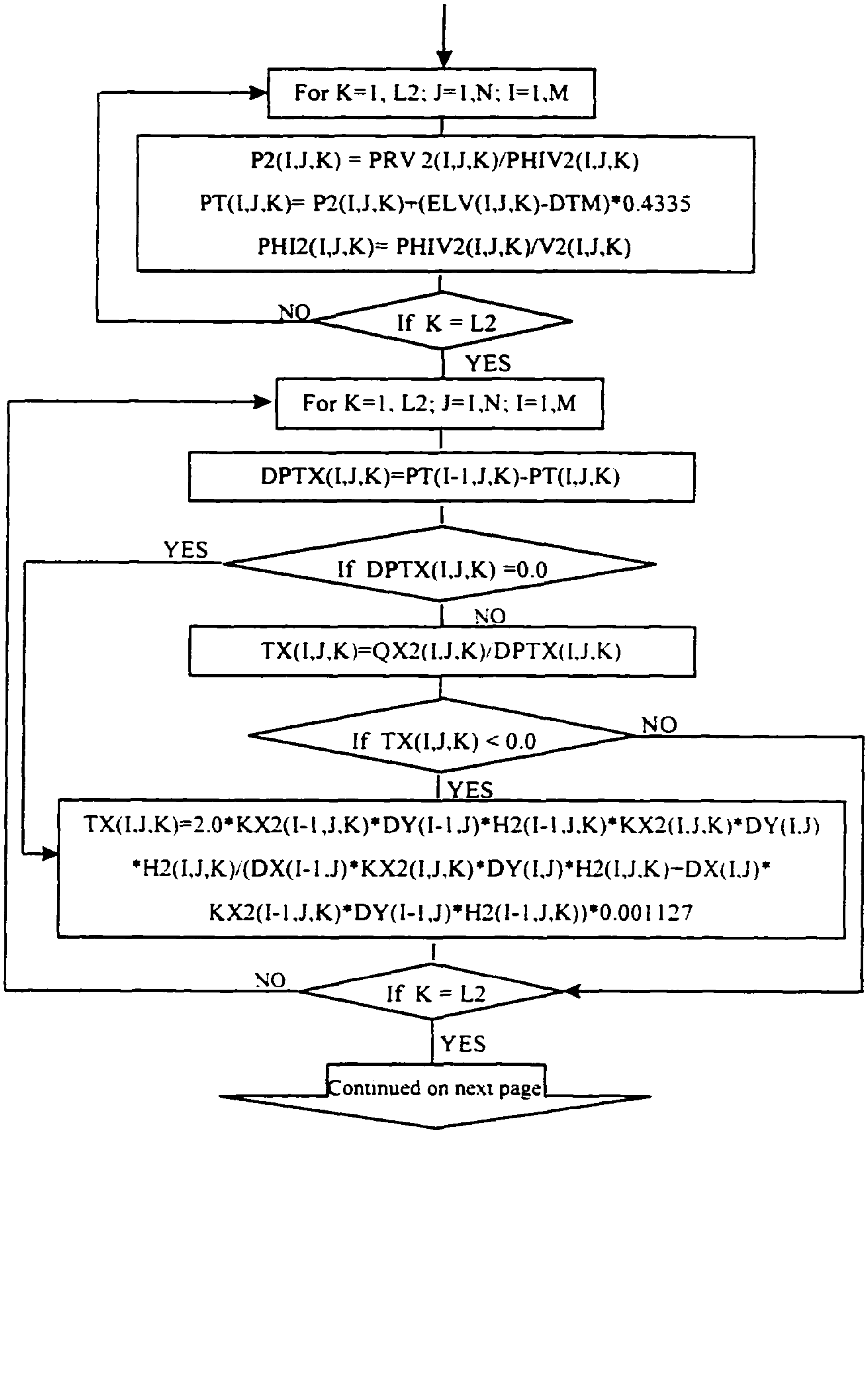

For K=1, L2; J=1,N; I=1,M
P2(I,J,K) = PRV 2(I,J,K)/PHIV2(I,J,K)
PT(I,J,K)= P2(I,J,K)+(ELV(I,J,K)-DTM)*0.4335
PHI2(I,J,K)= PHIV2(I,J,K)/V2(I,J,K)
NO
If K = L2
YES
For K=1, L2; J=1,N; I=1,M
DPTX(I,J,K)=PT(I-1,J,K)-PT(I,J,K)
YES
If DPTX(I,J,K) =0.0
NO
TX(I,J,K)=QX2(I,J,K)/DPTX(I,J,K)
If TX(I,J,K) < 0.0
NO
YES
TX(I,J,K)=2.0*KX2(I-1,J,K)*DY(I-1,J)*H2(I-1,J,K)*KX2(I,J,K)*DY(I,J)
*H2(I,J,K)/(DX(I-1,J)*KX2(I,J,K)*DY(I,J)*H2(I,J,K)+DX(I,J)*
KX2(I-1,J,K)*DY(I-1,J)*H2(I-1,J,K))*0.001127
NO
If K = L2
YES
Continued on next page

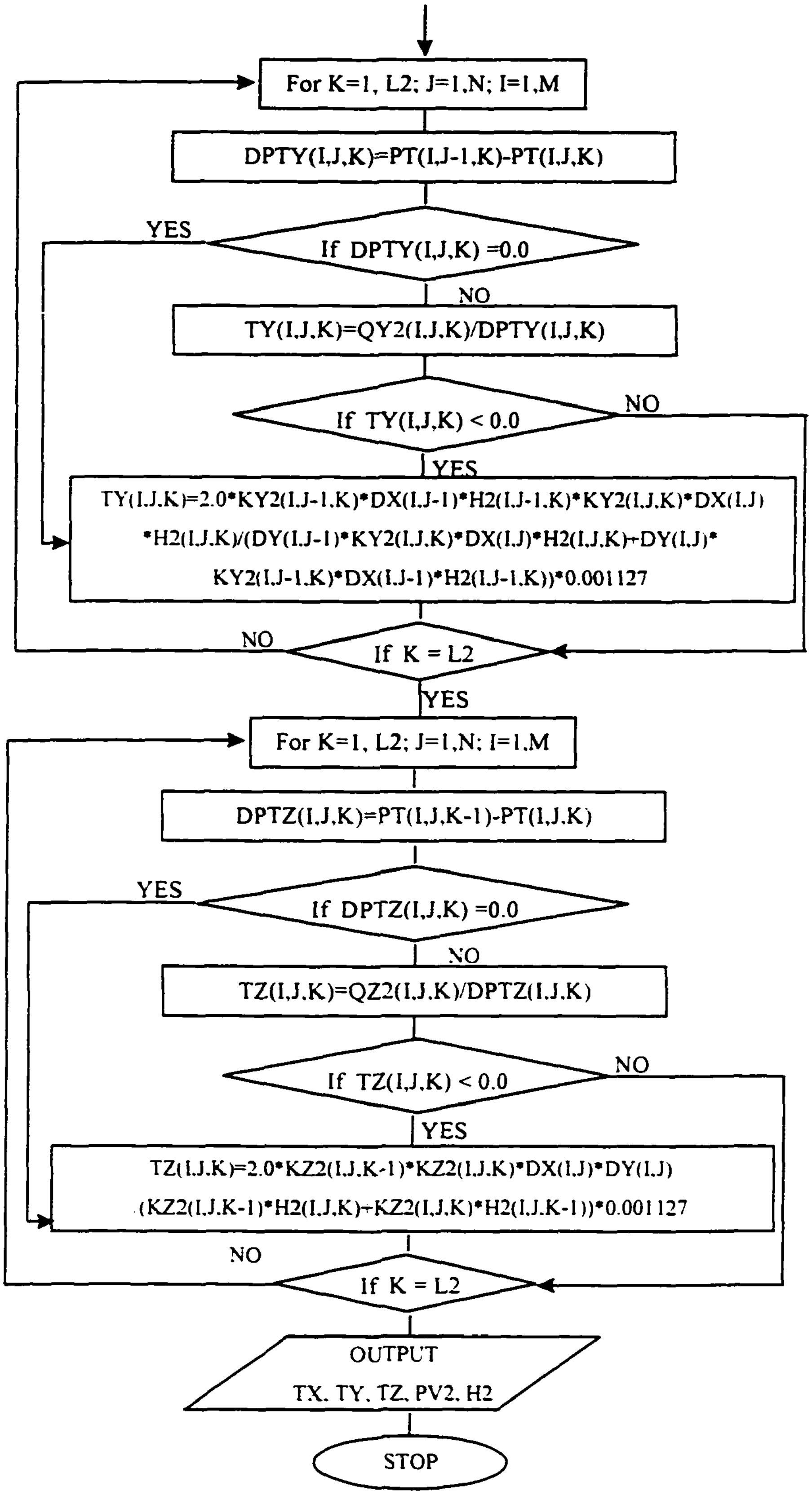

For K=1, L2; J=1,N; I=1,M
DPTY(I,J,K)=PT(I,J-1,K)-PT(I,J,K)
YES
If DPTY(I,J,K) =0.0
NO
TY(I,J,K)=QY2(I,J,K)/DPTY(I,J,K)
If TY(I,J,K) < 0.0
NO
YES
TY(I,J,K)=2.0*KY2(I,J-1,K)*DX(I,J-1)*H2(I,J-1,K)*KY2(I,J,K)*DX(I,J)
*H2(I,J,K)/(DY(I,J-1)*KY2(I,J,K)*DX(I,J)*H2(I,J,K)+DY(I,J)*
KY2(I,J-1,K)*DX(I,J-1)*H2(I,J-1,K))*0.001127
NO
If K = L2
YES
For K=1, L2; J=1,N; I=1,M
DPTZ(I,J,K)=PT(I,J,K-1)-PT(I,J,K)
YES
If DPTZ(I,J,K) =0.0
NO
TZ(I,J,K)=QZ2(I,J,K)/DPTZ(I,J,K)
If TZ(I,J,K) < 0.0
NO
YES
TZ(I,J,K)=2.0*KZ2(I,J,K-1)*KZ2(I,J,K)*DX(I,J)*DY(I,J)
(KZ2(I,J,K-1)*H2(I,J,K)+KZ2(I,J,K)*H2(I,J,K-1))*0.001127
NO
If K = L2
OUTPUT
TX, TY, TZ, PV2, H2
STOP

Simulation results, including production rate, cumulative production, injection rate, cumulative injection, and pressure, for both reservoir and individual wells were used to evaluate the results of scale-up. Figs. 4-12 to 4-14 present the scale-up results of water production rate, cumulative water production, and pressure for the reservoir. Injection rate and cumulative injection from fine-scale and coarse-scale simulation are completely consistent and were therefore not presented. Figs. 4-15 to Fig. 4-29 show the scale-up results of water production rate, cumulative water production and injection rate, cumulative water production and injection, and average wellblock pressure for well #1 to Well #5. It can be observed that:

1. The production of the reservoir went through both depletion and displacement processes in only one day period, because the volume of the reservoir is very small and the permeability of the reservoir is relatively high.
2. Water production obtained better match than reservoir and wellblock pressure. This is because, for the scale-up process proposed in this study, water production rate was the target forced to match. Reservoir and wellblock pressure were, therefore, the parameters to match for the evaluation of scale-up quality.

Analyzing the scale-up procedure and results, the difference of results between fine-scale and coarse-scale simulation could be caused by the error introduced during calculation of transmissibility. However, the main error was probably caused due to the use of scale-up of transmissibility for linear flow to the whole reservoir area. The radial flow around wellbore was not considered. It may not have been correctly upscaled by this simple process. Therefore, scale-up of radial flow around wellbore area was considered in the next section to improve the match.

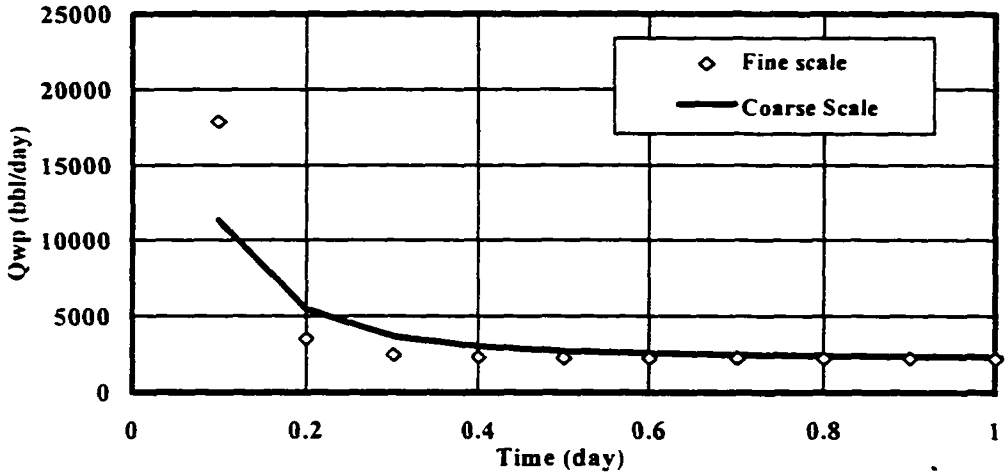

Fig. 4-12 Water Production Rate of Model #1 Without PI Scale-up

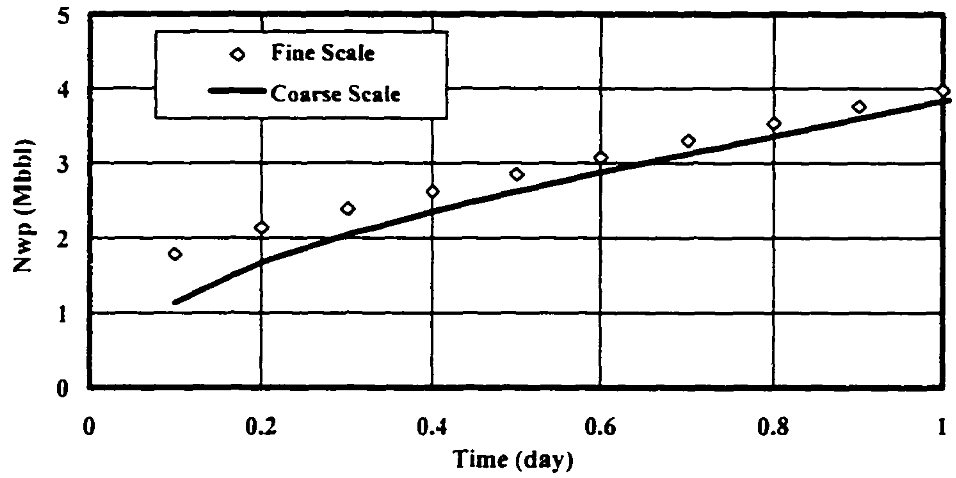

Fig. 4-13 Cum. Water Production of Model #1 Without PI Scale-up

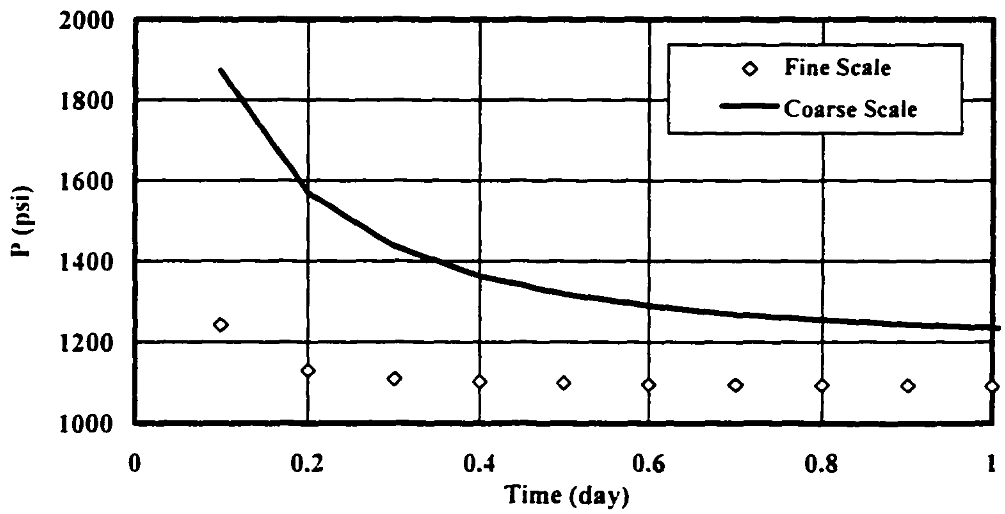

Fig. 4-14 Reservoir Pressure of Model #1 Without PI Scale-up

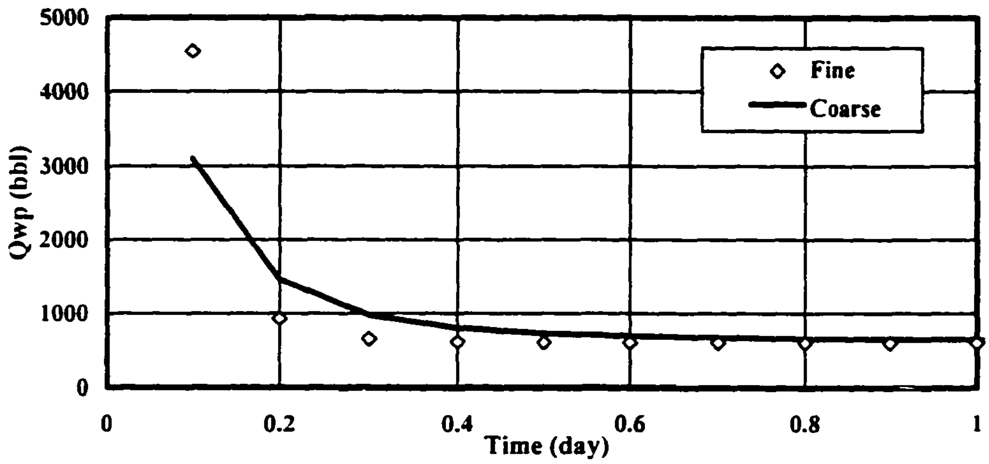

Fig. 4-15 Water Production Rate for Well #1 of Model #1 Without PI Scale-up

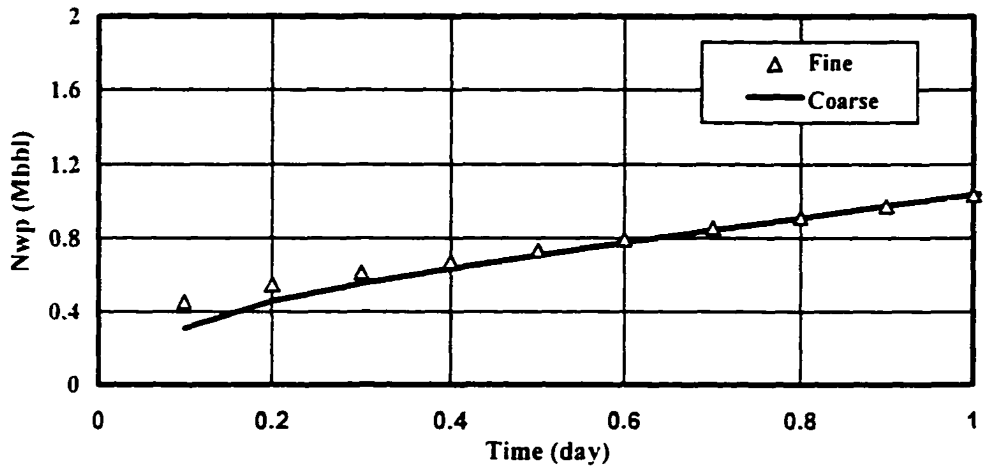

Fig. 4-16 Cum. Water Production for Well #1 of Model #1 Without PI Scale-up

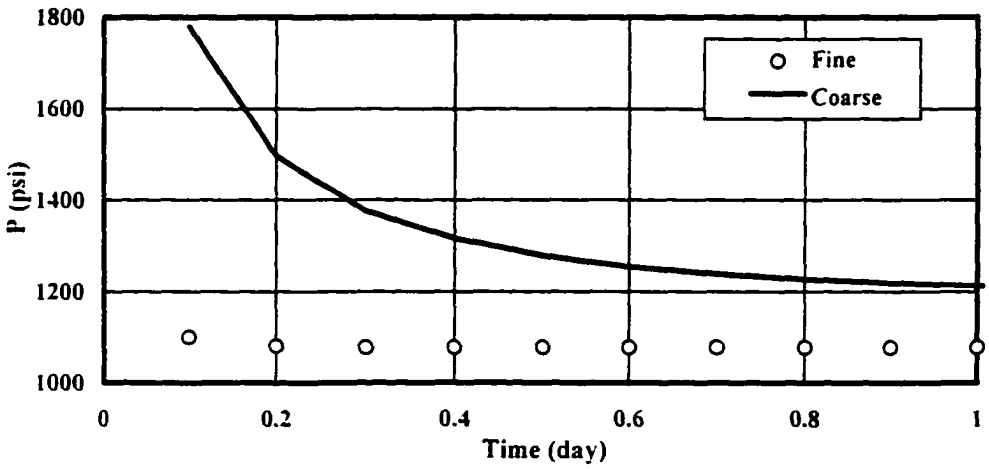

Fig. 4-17 Well Block Pressure for Well #1 of Model #1 Without PI Scale-up

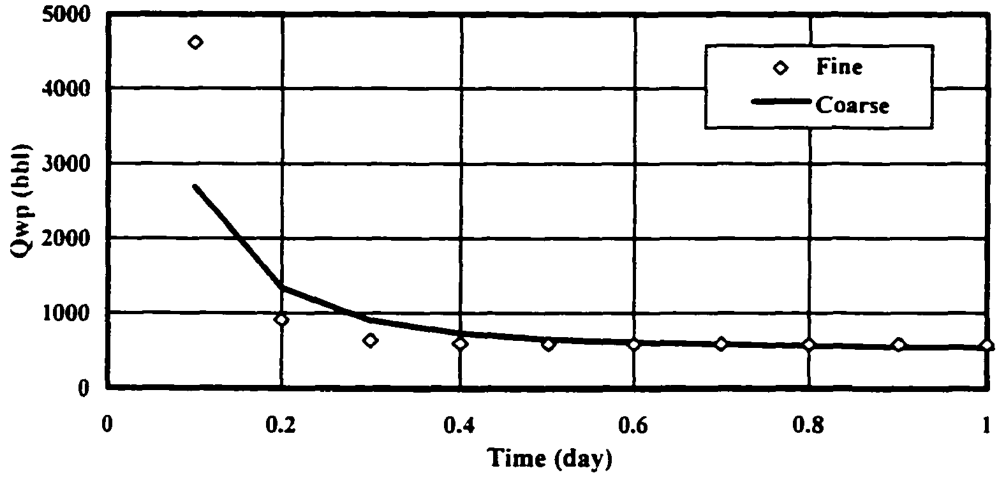

Fig. 4-18 Water Production Rate for Well #2 of Model #1 Without PI Scale-up

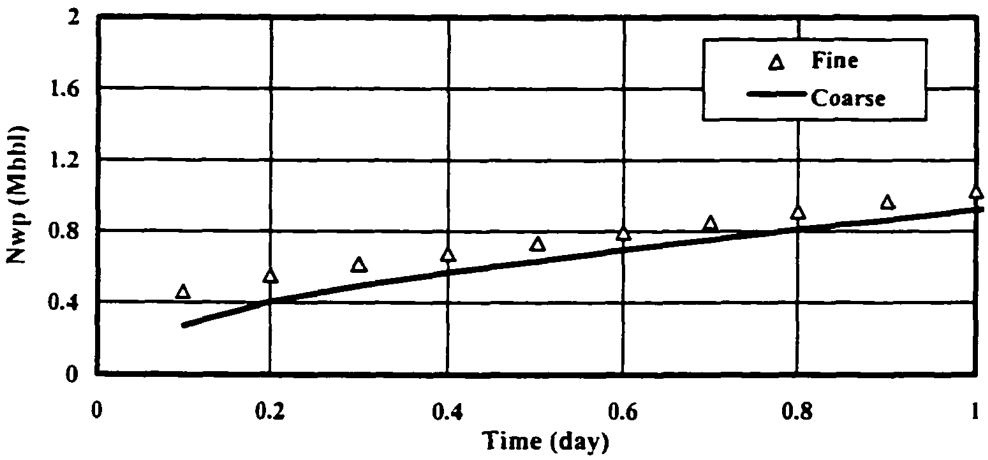

Fig. 4-19 Cum. Water Production for Well #2 of Model #1 Without PI Scale-up

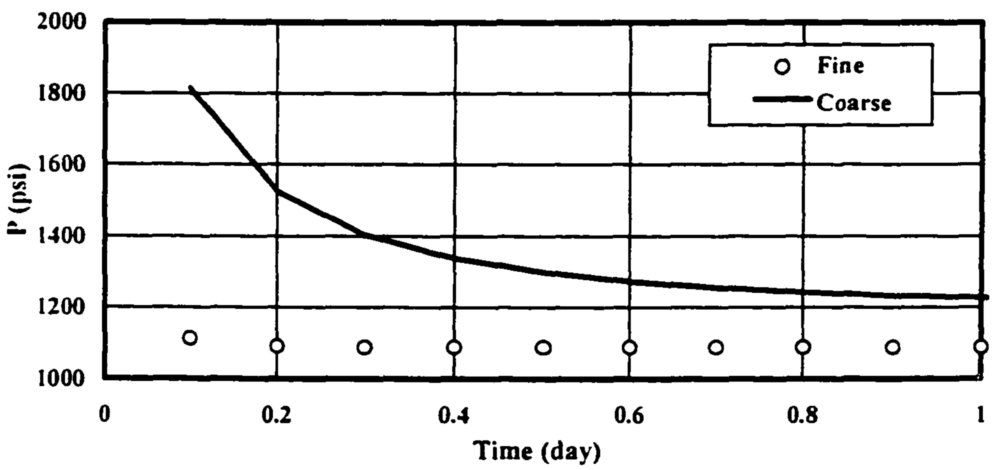

Fig. 4-20 Well Block Pressure for Well #2 of Model #1 Without PI Scale-up

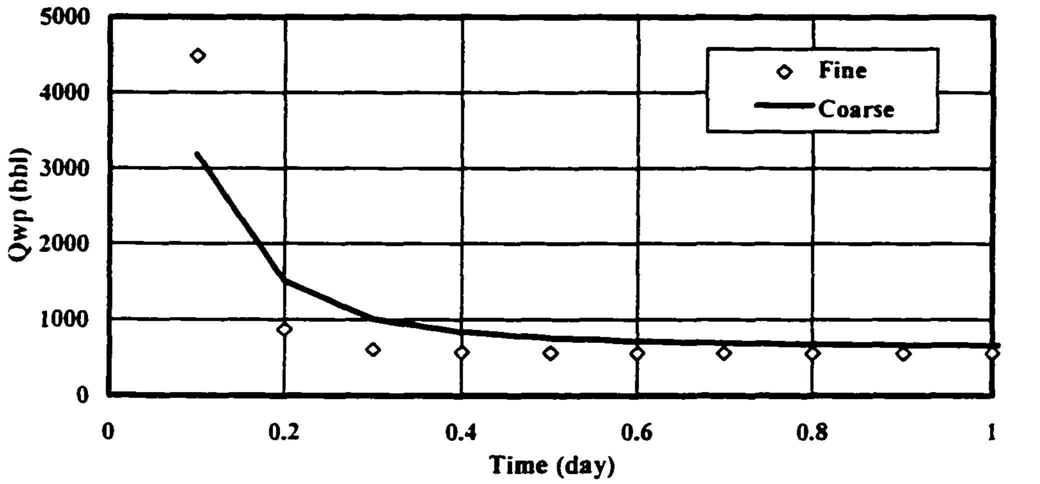

Fig. 4-21 Water Production Rate for Well #3 of Model #1 Without PI Scale-up

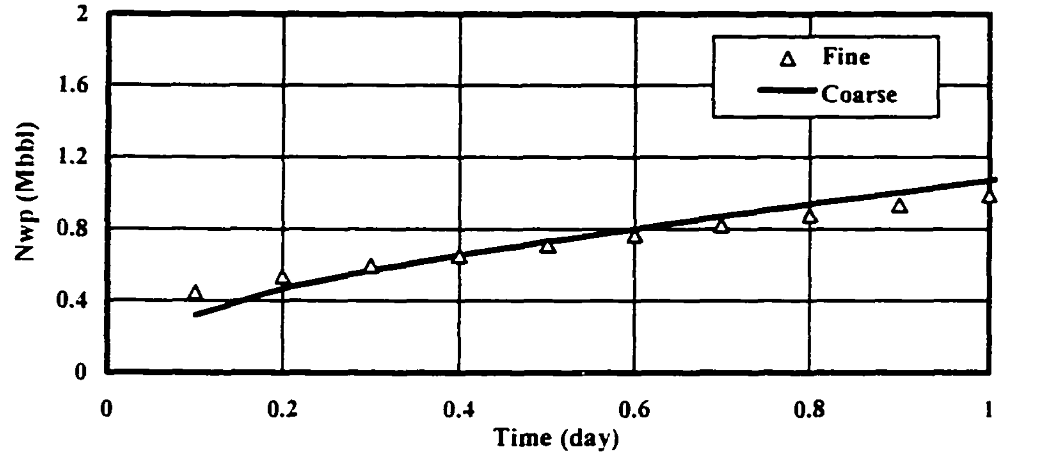

Fig. 4-22 Cum. Water Production for Well #3 of Model #1 Without PI Scale-up

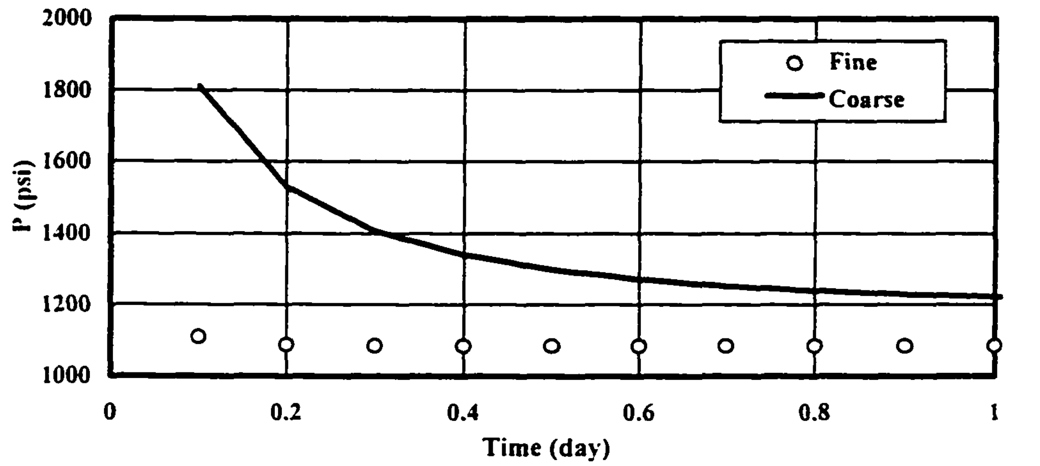

Fig. 4-23 Well Block Pressure for Well #3 of Model #1 Without PI Scale-up

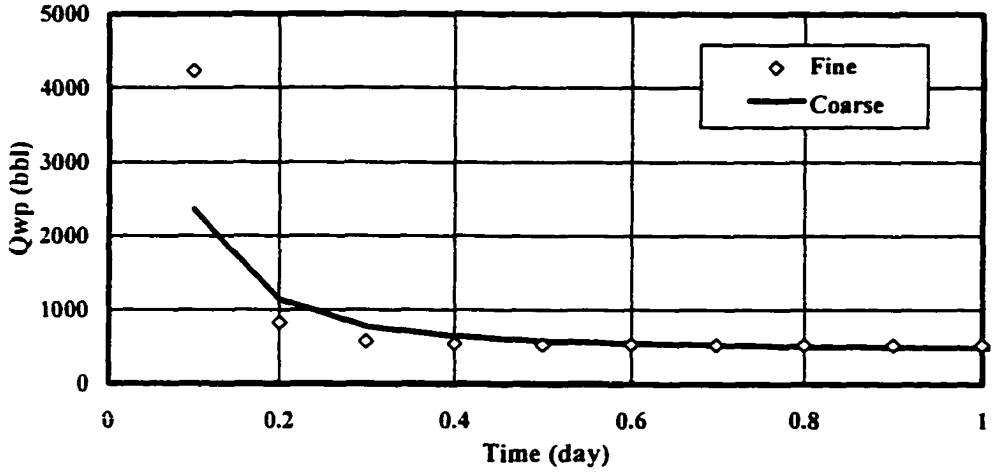

Fig. 4-24 Water Production Rate for Well #4 of Model #1 Without PI Scale-up

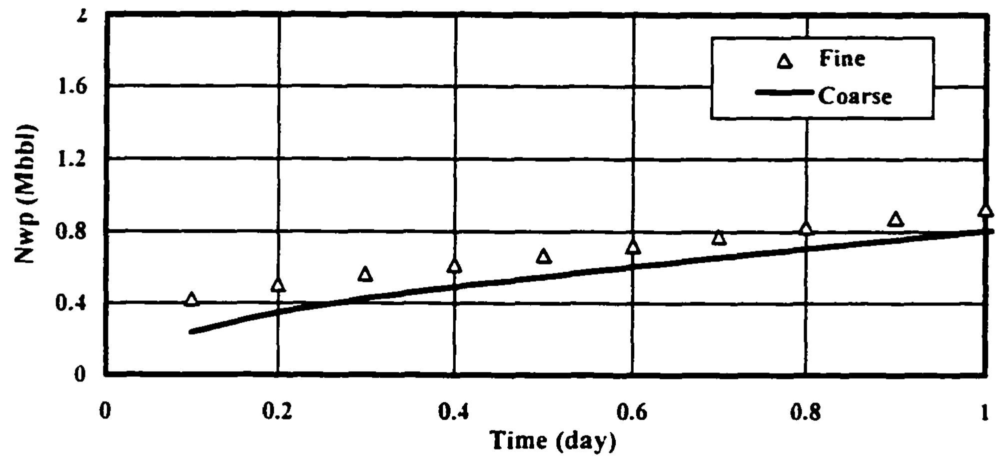

Fig. 4-25 Cum. Water Production for Well #4 of Model #1 Without PI Scale-up

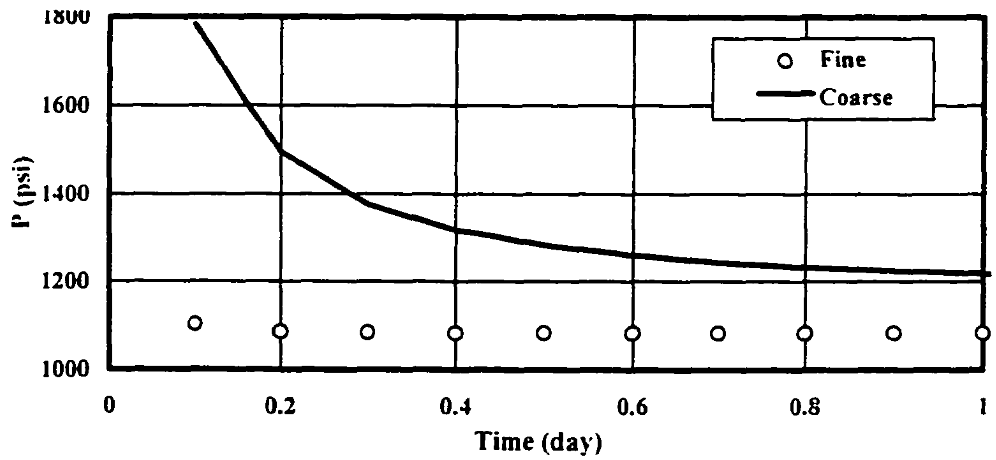

Fig. 4-26 Well Block Pressure for Well #4 of Model #1 Without PI Scale-up

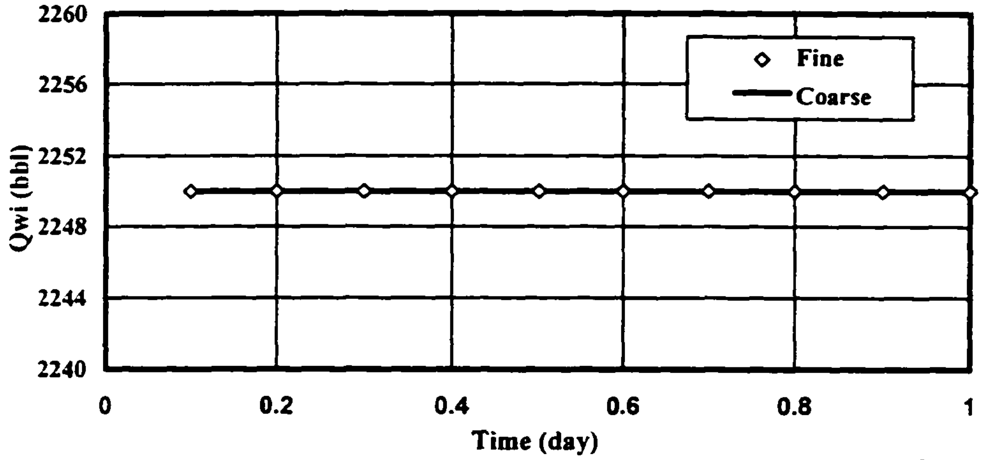

Fig. 4-27 Water Injection Rate for Well #5 of Model #1 Without PI Scale-up

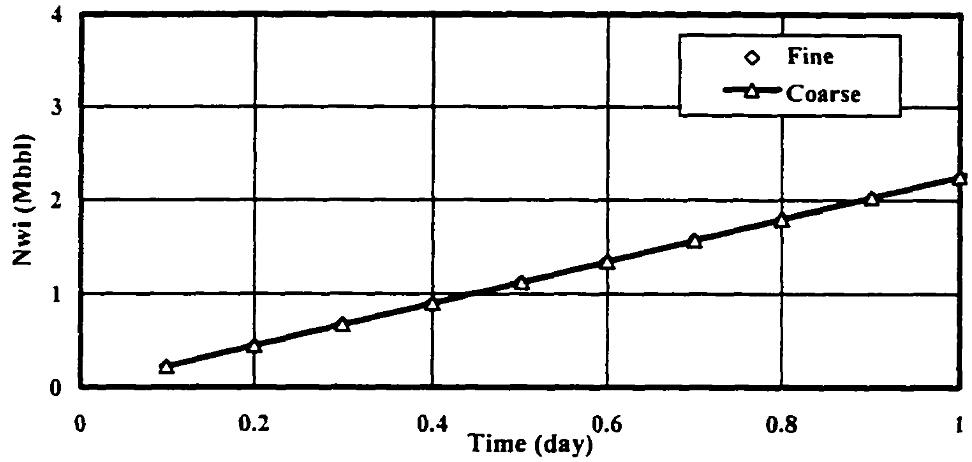

Fig. 4-28 Cum. Water Injection for Well #5 of Model #1 Without PI Scale-up

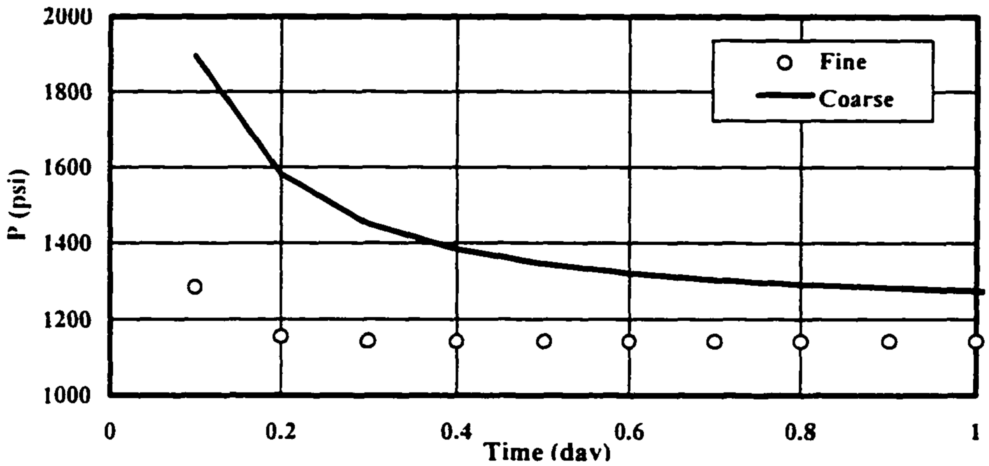

Fig. 4-29 Well Block Pressure for Well #5 of Model #1 Without PI Scale-up

4.3 Scale-up for Radial Flow Around the Wellbore

In Chapter II, the previous studies on the scale-up around wellbore were reviewed. The analytical method proposed by Soeriawinata (1996) calculates effective permeability for a coarse-scale wellblock from fine-scale permeability. This method divides the wellblock into many sectors or slices so that the grid block includes some irregular shapes. This method can scale up wellblock permeability without running a reservoir simulation. However, as using arithmetic, harmonic, or geometric methods to calculate average permeability of coarse-scale grid blocks for linear flow, the values obtained are difficult to accept, because of the complex configuration of fluid flow in formation. Still, the results are considered to be a closer approximation to the real reservoir condition than that obtained just using the grid block value alone. The concept proposed by Ding (1995) directly relates the well flow rate, which is one of the targets to match, to the parameter used in reservoir simulation. The fluid flow within reservoir is very complex at microscale. However, the flow at macroscale is of most concern to us, i.e., the flow rate of 'in' and 'out'. Ding's method also scales up transmissibility, and can therefore be easily combined with the scale-up of linear flow conducted previously.

In reservoir simulation, either the well injectivity index or the productivity index is required as an input for the simulator in order to reflect the extent of formation damage around the wellbore and the dimension of reservoir and wells. When wellblock and wellbore pressures are known, the flow rate of well can be determined by productivity index. Well injectivity index is dimensionless and can be expressed by the following equation (Landmark, 1996):

$$WI = \frac{2\pi}{Ln\left(\frac{r_b}{r_w}\right) + s} \tag{4-17}$$

where:

WI = well injectivity index (dimensionless),

r_b = equivalent radius (Peaceman) of wellblock (ft),

r_w = wellbore radius (ft),

s = skin factor.

The productivity index is related to the well injectivity index by the following equation:

$$PI = WI.\frac{0.001127\sum_{i=1}^{L}\left[\frac{khk_{rw}}{\mu_w B_w}\right]_i}{gf} \tag{4-18}$$

where:

PI = productivity index (STB/day-psi),

k = permeability of production layer (mD),

h = thickness of production layer (ft),

k_{rw} = relative permeability of water,

μ_w = viscosity of reservoir water (cp),

B_w = volume factor of reservoir water (rb/STB),

gf = geometry factor= $\frac{ln(r_e / r_w)}{ln(r_b / r_w)}$,

r_e = drainage radius (ft),

L = total layer number.

In reservoir simulation, either the well productivity or the injectivity index can be used as input. If the skin factor can be estimated, then the WI can be calculated using Eq. 4-17 and used as input. The simulator will calculate PI for the well using Eq. 4-18. If PI can be estimated by measuring the well flow rate, wellblock pressure, and wellbore pressure, then PI can be directly input into the simulation model. In this study, WI for each well in the fine-scale model was assumed to be 10 for the hypothetical model. For the simulation of coarse-scale model, Eq. 4-18, indicates that the upscaled permeability will effect the calculation of PI, so WI or PI must be considered in scale-up.

Upscaled WI cannot be simply calculated, because the upscaled skin factor is usually unknown. It is possible to calculate the upscaled PI from its definition as follows:

$$PI = \frac{Q_t}{p_g - p_b} \tag{4-19}$$

where:

Q_t = total flow rate of well (STB/day),

p_g = average wellblock pressure (psi),

p_b = bottom hole pressure (psi).

Recalling Eqs. 4-13 to 4-15 for the calculation of upscaled transmissibility of coarse grid blocks, the PI in Eq. 4-19 is, in fact, the transmissibility of wellblock to wellbore. To obtain PI in Eq. 4-19, Q_t can be obtained by simply summing the flow rate in each layer of the wellbore in the fine-scale model to represent the total flow rate of the well. P_g can be obtained using pressure values from fine-scale model and pore volume average method. Fortunately, the simulator outputs these values in the well report, as well as values for P_b. Therefore, upscaled PI for each well can be calculated using Eq. 4-19 and data from simulation report.

In VIP (Landmark, 1996) simulator, only the PI value for each well is required as an input parameter. The program will distribute the PI values for each layer internally based on the permeability and thickness of each layer. Calculated PI for both production wells and injection well in model #1 are listed in Table 4-3. The results of a simulation on the coarse-scale model using the upscaled PI in Table 4-3 are provided in Figs. 4-30 to 4-47 for both reservoir and individual wells. It was observed that significant improvements were obtained after considering the scale-up near the wellbore area. Excellent matches were obtained in all of the plots. Scale-up near wellbore is important in the overall scale-up process, so scale-up around wellbore will be included for all of the models in this study when scale-up is conducted.

Table 4-3 Well Injectivity and Productivity Index Used in the Fine-Scale and Coarse-Scale Simulations for Model #1

Well	WI Fine Scale	PI Coarse Scale
PRO-1	10	227.19
PRO-2	10	217.89
PRO-3	10	262.97
PRO-4	10	250.23
INJ-5	10	254.22

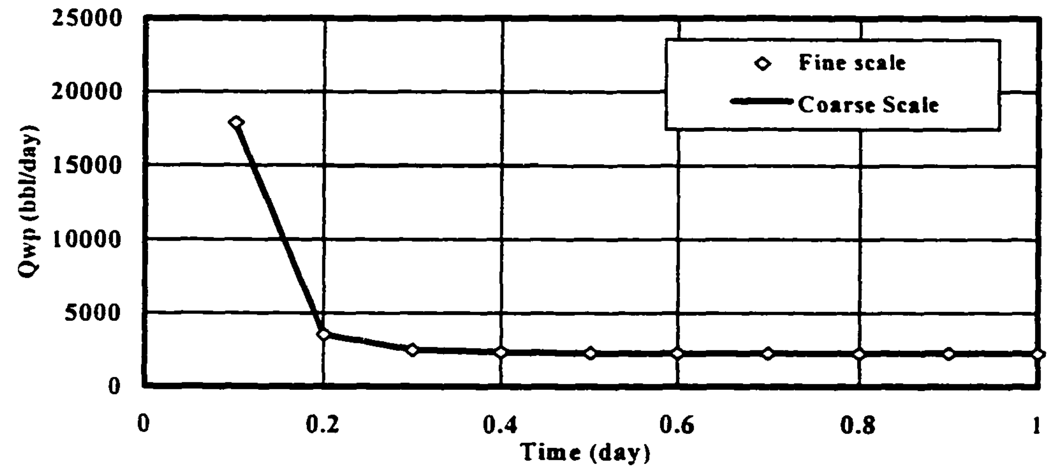

Fig. 4-30 Water Production Rate of Model #1 With PI Scale-up

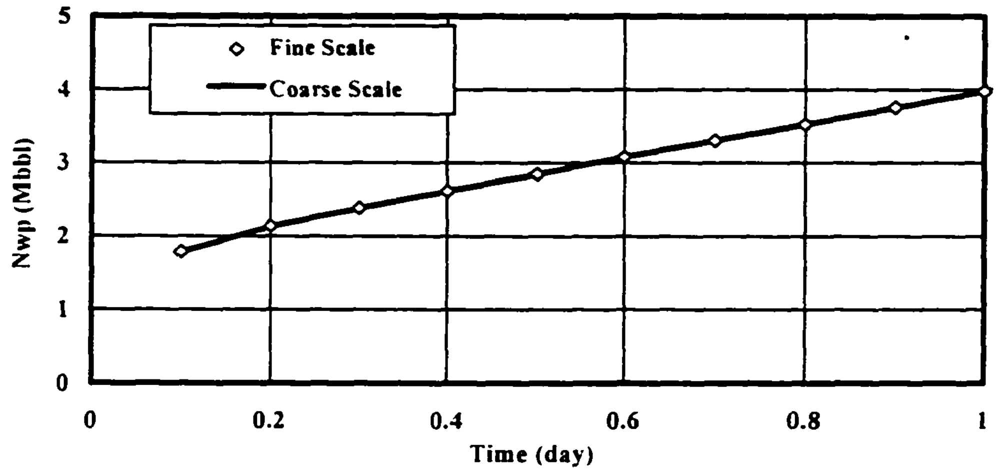

Fig. 4-31 Cum. Water Production of Model #1 With PI Scale-up

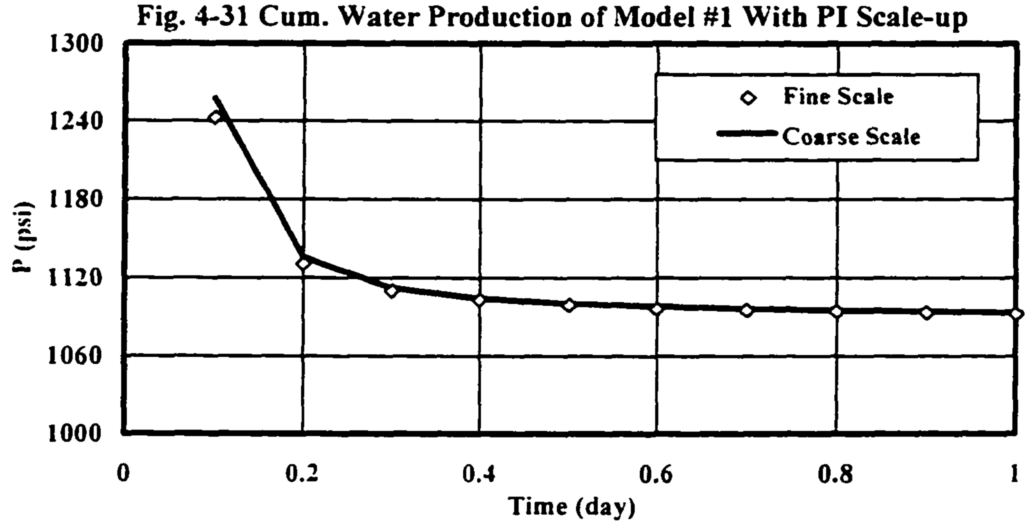

Fig. 4-32 Reservoir Pressure of Model #1 With PI Scale-up

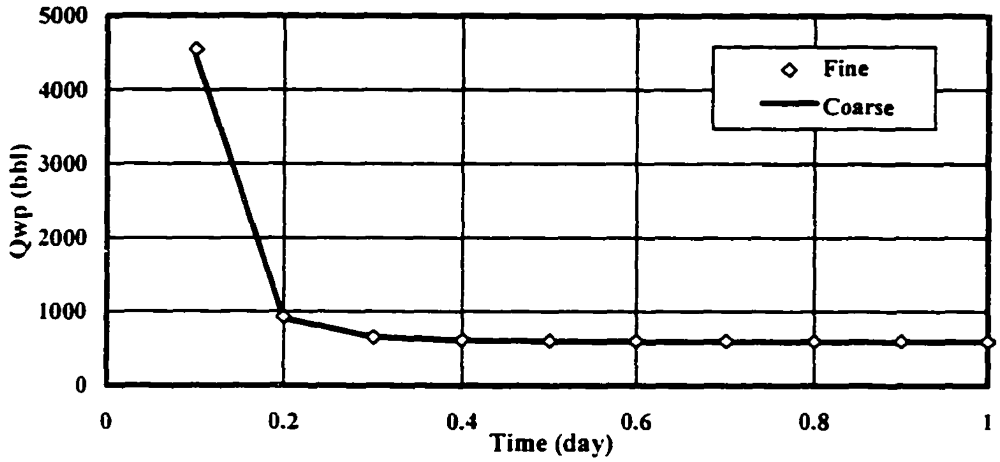

Fig. 4-33 Water Production Rate for Well #1 of Model #1 With PI Scale-up

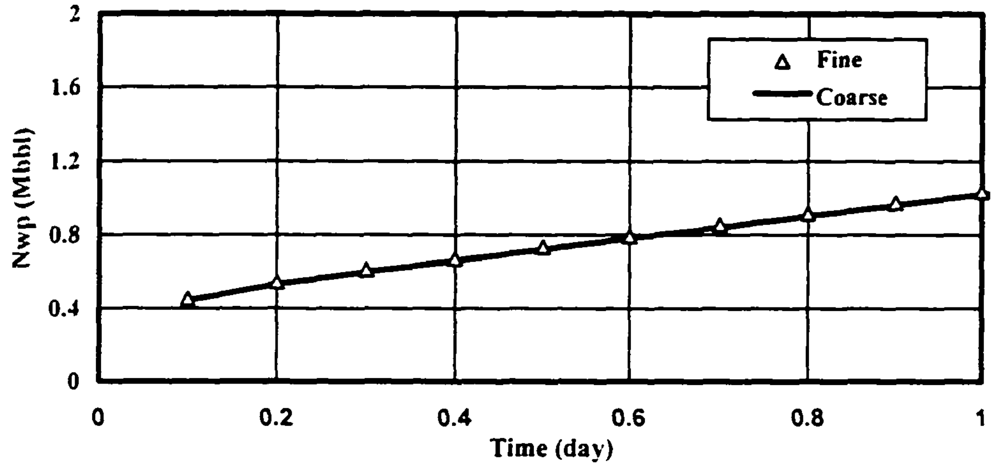

Fig. 4-34 Cum. Water Production for Well #1 of Model #1 With PI Scale-up

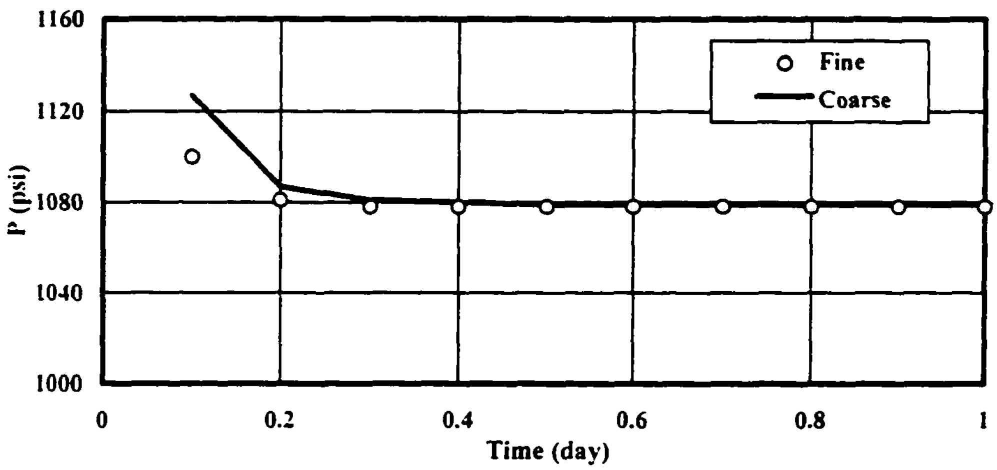

Fig. 4-35 Well Block Pressure for Well #1 of Model #1 With PI Scale-up

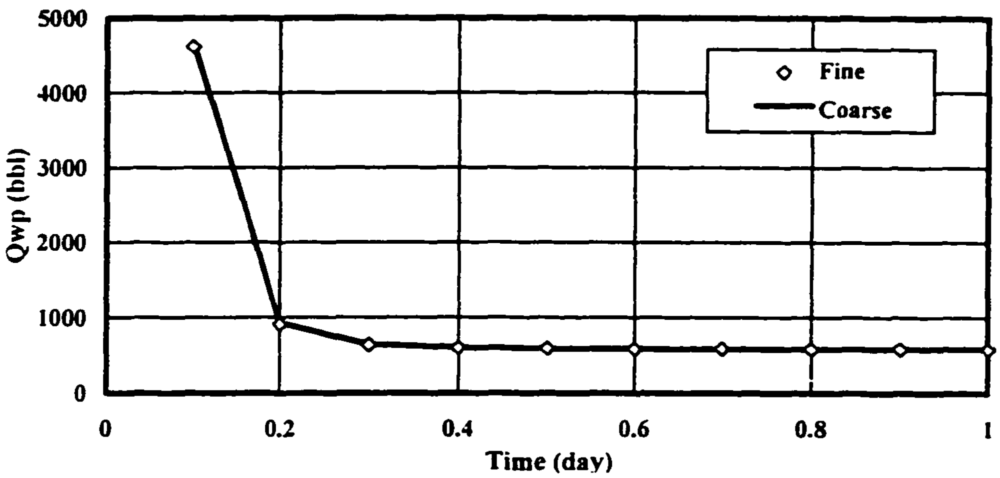

Fig. 4-36 Water Production Rate for Well #2 of Model #1 With PI Scale-up

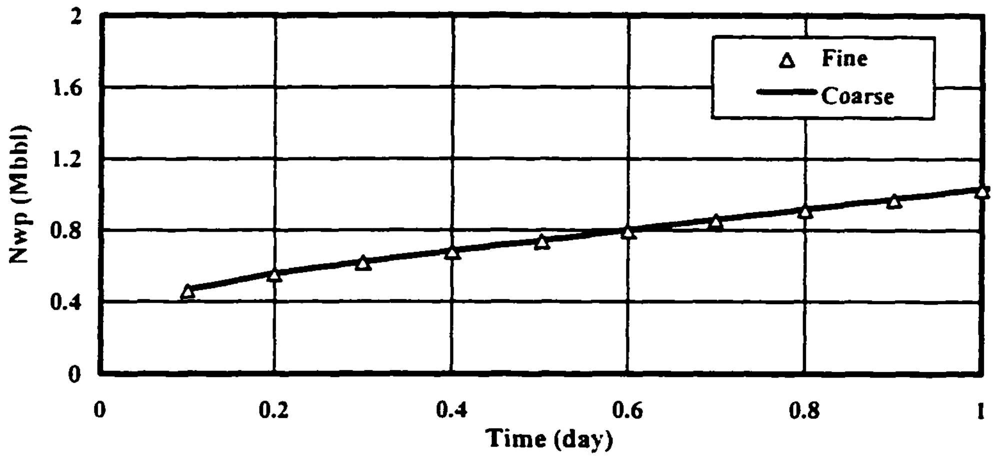

Fig. 4-37 Cum. Water Production for Well #2 of Model #1 With PI Scale-up

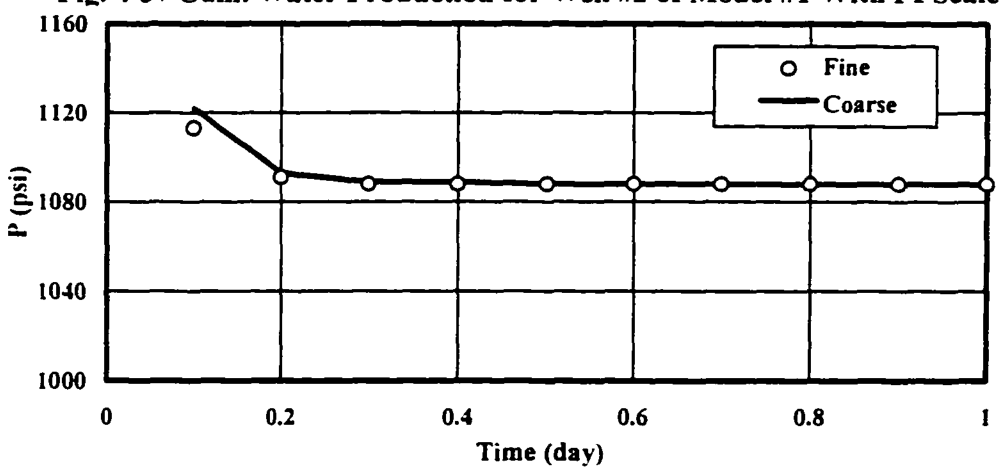

Fig. 4-38 Well Block Pressure for Well #2 of Model #1 With PI Scale-up

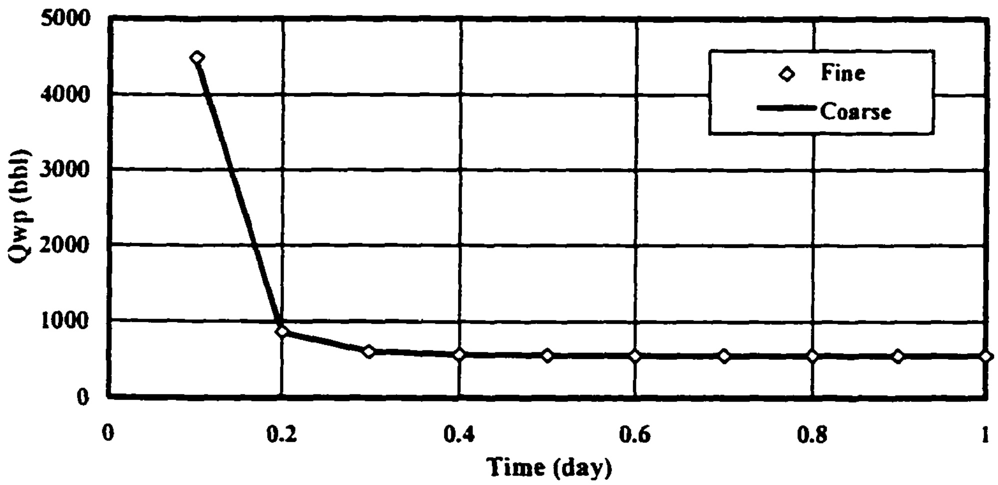

Fig. 4-39 Water Production Rate for Well #3 of Model #1 With PI Scale-up

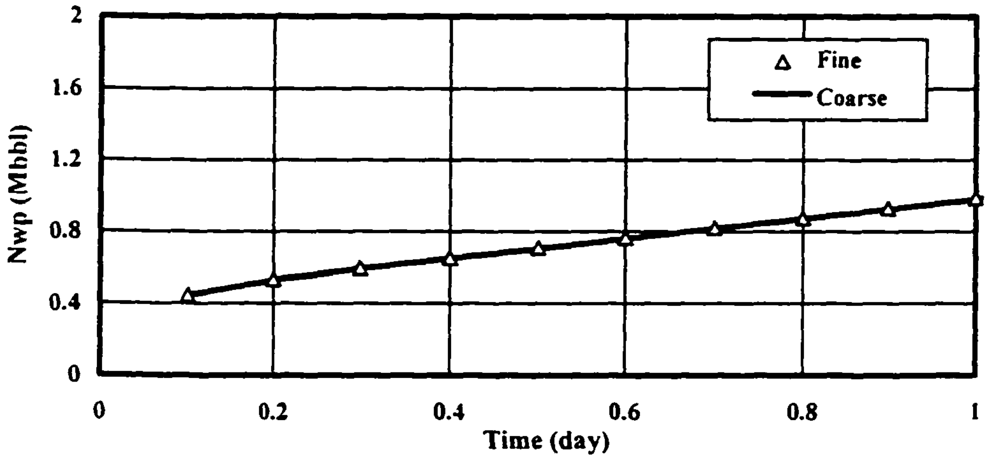

Fig. 4-40 Cum. Water Production for Well #3 of Model #1 With PI Scale-up

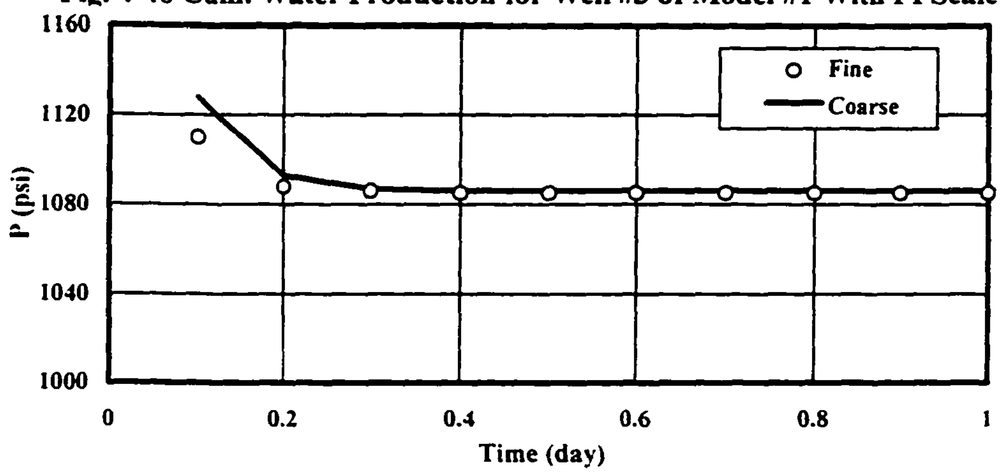

Fig. 4-41 Well Block Pressure for Well #3 of Model #1 With PI Scale-up

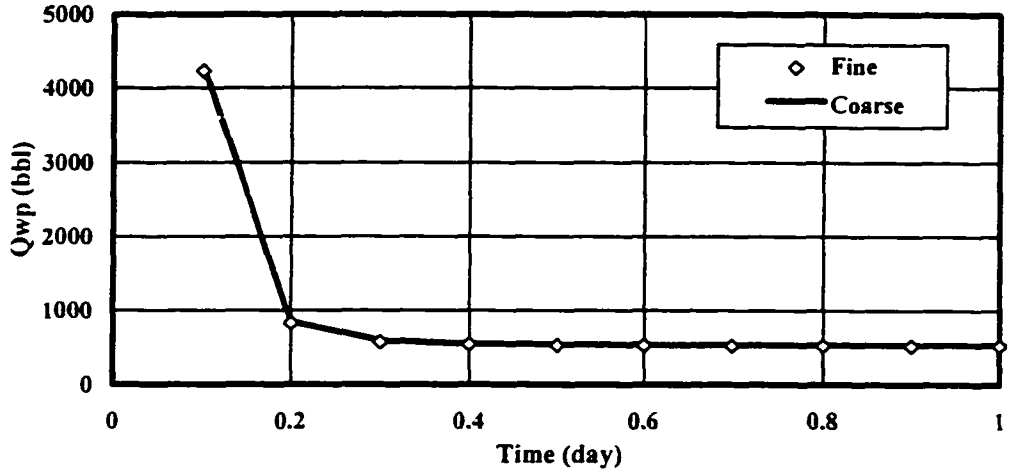

Fig. 4-42 Water Production Rate for Well #4 of Model #1 With PI Scale-up

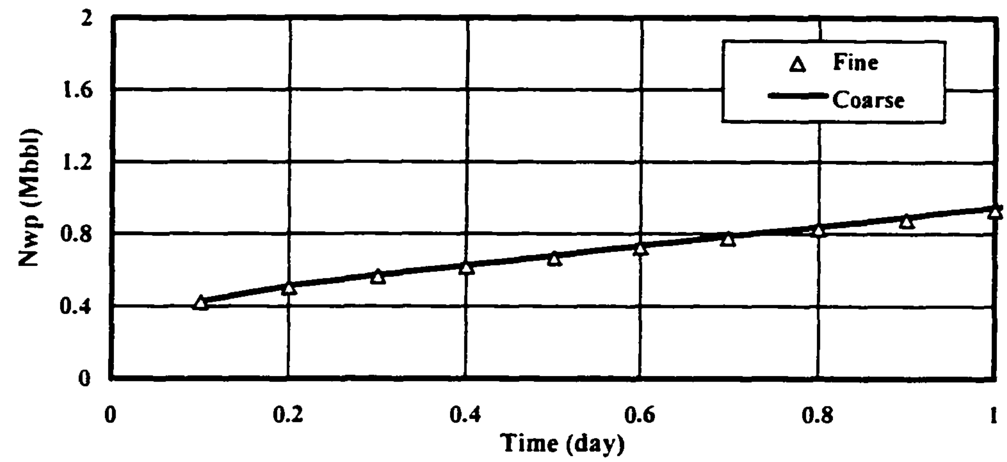

Fig. 4-43 Cum. Water Production for Well #4 of Model #1 With PI Scale-up

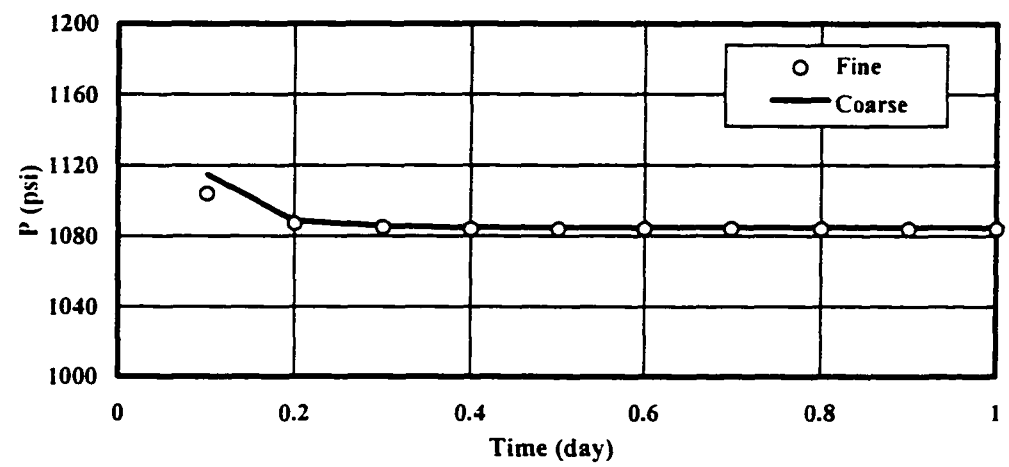

Fig. 4-44 Well Block Pressure for Well #4 of Model #1 With PI Scale-up

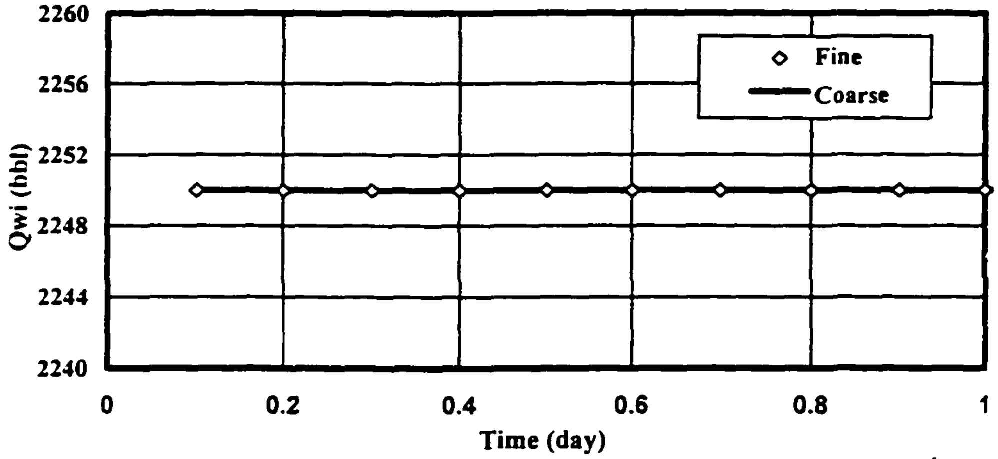

Fig. 4-45 Water Injection Rate for Well #5 of Model #1 With PI Scale-up

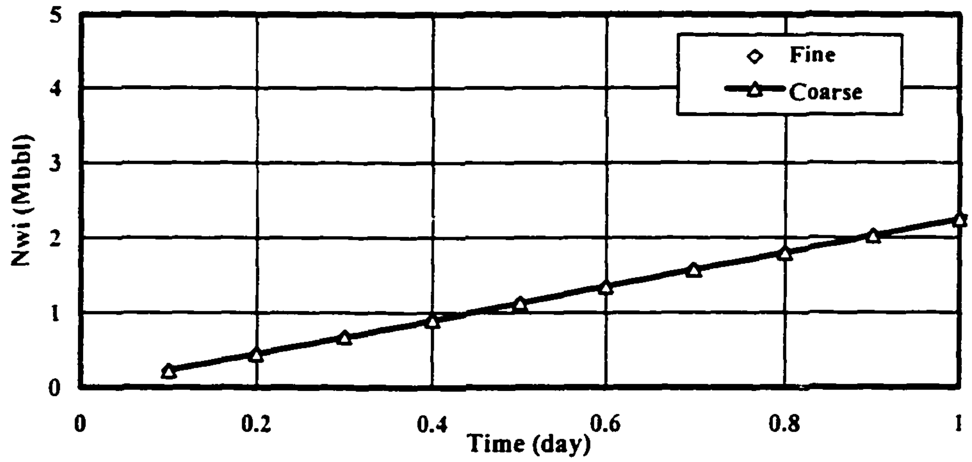

Fig. 4-46 Cum. Water Injection for Well #5 of Model #1 With PI Scale-up

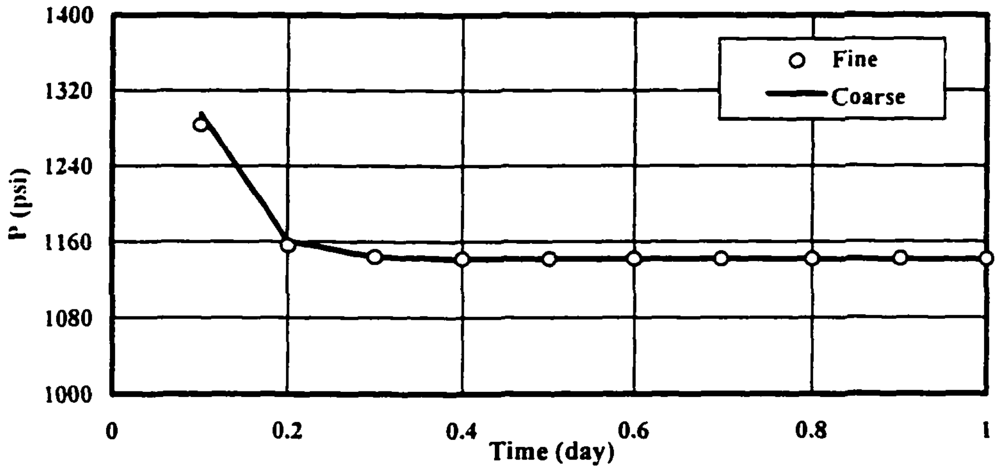

Fig. 4-47 Well Block Pressure for Well #5 of Model #1 With PI Scale-up

4.4 Scale-up for a Hypothetical Reservoir Model with Pinch-Out

In section 4.2, scale-up for a hypothetical layer-cake reservoir without pinch-out was studied and illustrated. Due to the complexity of many depositional environments, the distribution of channels, lithofacies, or flow units may not be continuous over reservoir volume studied, especially in a fine-scale model. The scale-up process described in section 4.2 is inadequate when pinch-out exists in the reservoir. Therefore, in this section, pinch-out was considered when scale-up is conducted.

4.4.1 Transmissibility for a Reservoir with Pinch-out

In a reservoir simulator, the 3-D continuity equation is solved from left to right in the x direction, from back to front in the y direction, and from top to bottom in the z direction. The transmissibility defined in a simulator for a specified grid-block are applicable to the left, back, and top faces of the grid block in x, y, and z directions, respectively. Therefore, for a reservoir with no flow boundary condition, the horizontal transmissibility, T_x and T_y are zero for grid blocks at boundaries identified with arrows in Fig. 4-48. The vertical transmissibility T_z for the grid blocks on the top layer are zero, if no pinch-out exists in this layer. When pinch-out exists in the top layer, as shown in Fig. 4-49, the vertical transmissibility for the grid blocks are zero at the top of the layer that is pinched out. Fig. 4-49 is a cross-sectional illustration of pinch-out in a geological model, with 9 columns in the x direction and 9 layers in the z direction. Pinch-outs occur in layers 3, 4, 7, and 9 in the vertical direction, and in columns 1, 2, 4, 5 and 9 in the x direction. In column 1, the grid blocks (1, 4), and (1,7) are pinched out. In this illustration, layers 3 and 5, 6 and 8, are connected to each other geologically. In the

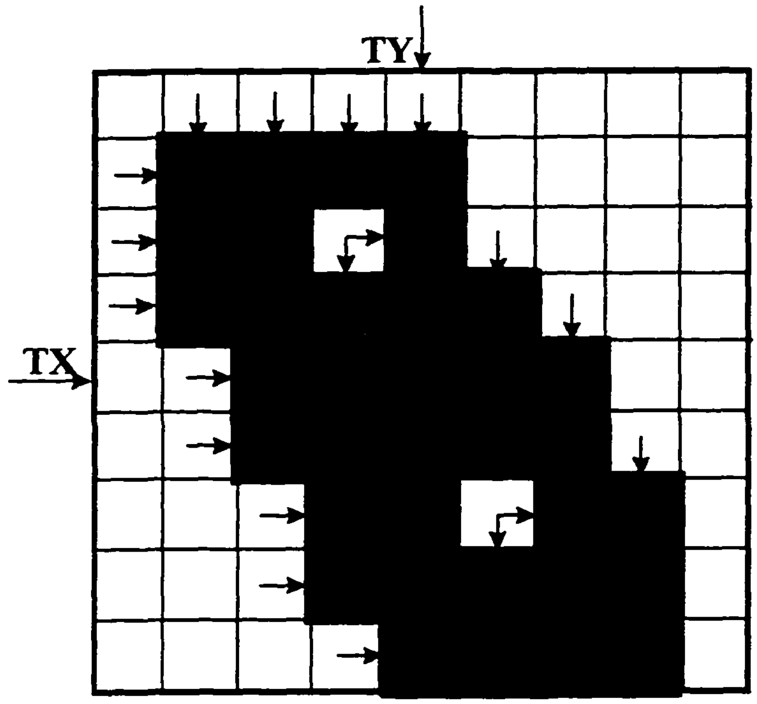

Fig. 4-48 Illustration for the Horizontal View of Pinch-Out

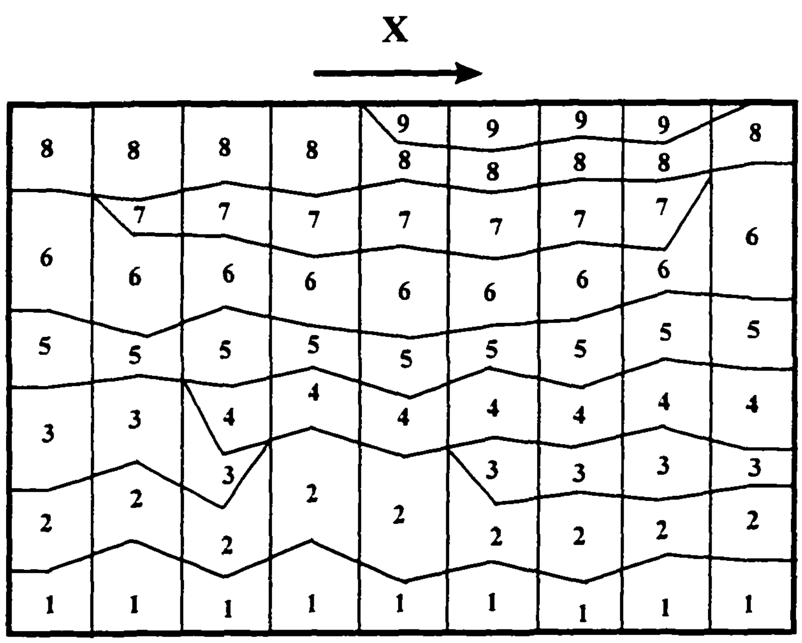

Fig. 4-49 Illustration for the Cross-Sectional View of Pinch-Out

mathematical model, when the thickness of the grid block is zero, the simulator will automatically assign a vertical transmissibility of zero to the grid block next to the grid block with zero thickness. Therefore, by default, there will be no flow between layers 3 and 5, 6 and 8 in Column 1. If a conventional transmissibility is used in the simulator, an incorrect simulation of fluid flow in the reservoir will occur. To resolve this problem, special considerations are needed for systems with pinch-out when reservoir simulation is conducted.

4.4.2 Simulation for Model with Pinch-out

It was assumed that pitch-out exists in the fine-scale model used in section 4.2 from layers 1 to 12 by setting the thickness of the pinch-out grid blocks as zero. Fig. 4-50 is the three dimensional description of permeability for the pinch-out model used in this study. Pinch-out can be observed on top of the model around well #2 and #5, where the top grid blocks were pinched out and lower permeability with blue color for the grid blocks of next layer was presented.

To simulate the pinch-out, a pinch-out option is available in VIP, which automatically detects the pinch-out between two grid blocks and connects two grid blocks with non-zero transmissibility when simulation is conducted. When this option is used, corner-point geometry system of grid block must also be used.

Two areas of concerns indicated that the pinch-out option unsuitable for this study. First, after running the simulation on fine-scale model and obtaining the flow rate and pressure for each grid block, it was found that the flow rates in the z direction

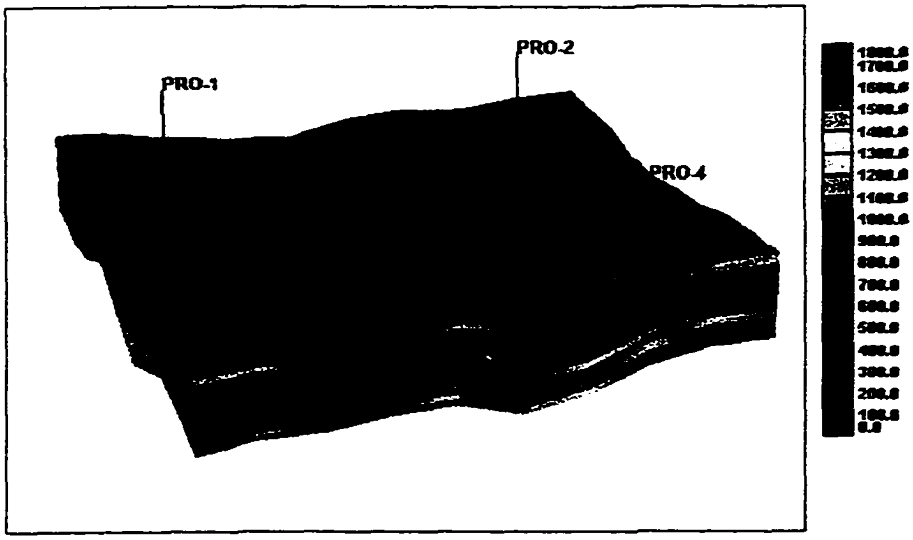

Fig. 4-50 3-D View for Permeability Distribution of Model #2 With Pinch-out

between two grid blocks, which should have opposite directions, but same values, were incorrect. They were non-zero in negative direction, but zero in positive direction, which means the simulator could not simulate the pinch-out correctly. Second, when the corner-geometry option is used in VIP, the transmissibility option can not be used, i.e., grid-block permeability must be used as input.

Because of these two constraints, it is inappropriate to use the pinch-out option in VIP for this study. A unique characteristic of the pinch-out grid blocks is that there is no horizontal flow, but a direct vertical communication. To reproduce this scenario, it can be assumed that there exists a very thin layer between two grid blocks having pinch-out grid, such that it would not cause significant error in simulation results. Fig. 4-50 is an illustration for the geological model described in Fig. 4-49, in which the bold lines represent the thin pinch-out grid blocks. It was assumed that the horizontal permeability of these thin layers is zero, so that no horizontal flow occurs in these grid blocks. A high vertical permeability was used to produce the flow rates in vertical direction between the two grid blocks, between which pinch-out exists, to be essentially the same, as in a reservoir with pinch-out. The pore volume of such thin grid blocks should be very small in order to reduce any error in the calculation of reservoir volume. The limitation of material balance in simulation will limit this assumption to some extent, because the pore volumes of these thin grid blocks cannot be so small that a violation in simulation will occur. In this study, the value used for the pinch-out grid blocks were 9999 mD for vertical permeability, 0.01 ft for thickness, and 5% for porosity.

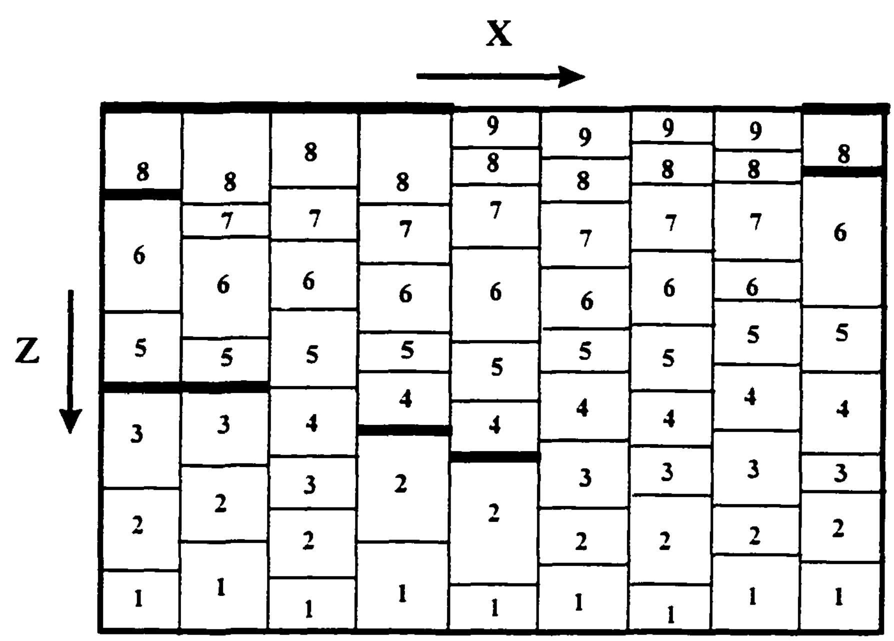

Fig. 4-51 Illustration of Pinch-Out In Mathematical Model

In comparing the pore volume of the real pinch-out model with the pseudo-pinch-out model, an error of 0.4% in pore volume resulted due to this assumption. The common tolerance for pore volume calculation in reservoir simulation is about 5%, so this assumption is reasonable.

4.4.3 Special Considerations for Pinch-out and Results of Scale-up

When pinch-out is used in the model, the process described in section 4.2.3 for scale-up on a reservoir model without pinch-out must be modified. The following special considerations are required:

1. The assumed thin grid blocks must not be included in the calculation of average permeability for coarse grid blocks.
2. When pinch-out exists between two coarse-scale grid blocks in the x or y direction, the transmissibility T_X or T_Y for this pinch-out grid block must be set to be zero.
3. The reservoir volume and pore volume for fine-scale and coarse-scale models, respectively, should be the same, so that the simulation results for fine scale and coarse scale can be compared. Therefore, the thin layers should be accounted for when porosity and thickness for coarse-scale model are calculated.

After taking the above factors into consideration, scale-up was conducted on the pinch-out model. The results are shown in Figs. 4-52 to 4-69 for the reservoir and the five individual wells, respectively. In these figures, both results with PI scale-up and without PI scale-up are displayed. The values of well injectivity index, WI, used for input in fine-scale model and upscaled productivity index PI used for coarse-scale model are listed in Table 4-4.

Table 4-4 Well Injectivity and Productivity Index Used for the Fine-Scale and Coarse-Scale Simulations for Model #2

Well	WI Fine Scale	PI Coarse Scale
PRO-1	10	313.32
PRO-1	10	170.61
PRO-1	10	177.37
PRO-1	10	220.82
INJ-5	10	200.11

It was observed in plots 4-52 to 4-69:

1. As in model #1, significant improvements were obtained after PI scale-up was considered for both water production and reservoir pressure. PI scale-up was shown again to be a very important component of the overall scale-up procedure.
2. As for model #1, water production predictions matched better than reservoir pressure without PI scale-up. After PI scale-up, successful matches were obtained in all the plots.

In summary, scale-up was conducted on two hypothetical models. A successful scale-up result was obtained. The scale-up methodology presented in this chapter was then applied to Gypsy models and are described in Chapter V.

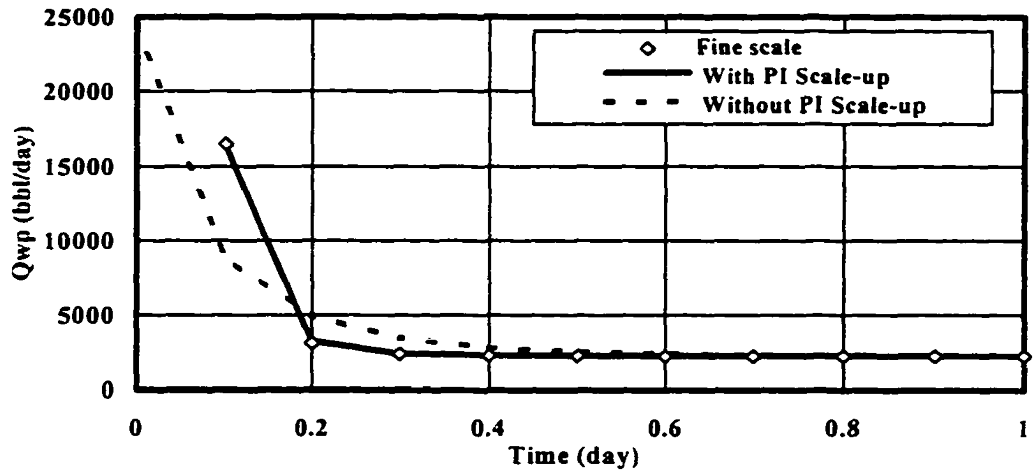

Fig. 4-52 Water Production Rate of Model #2

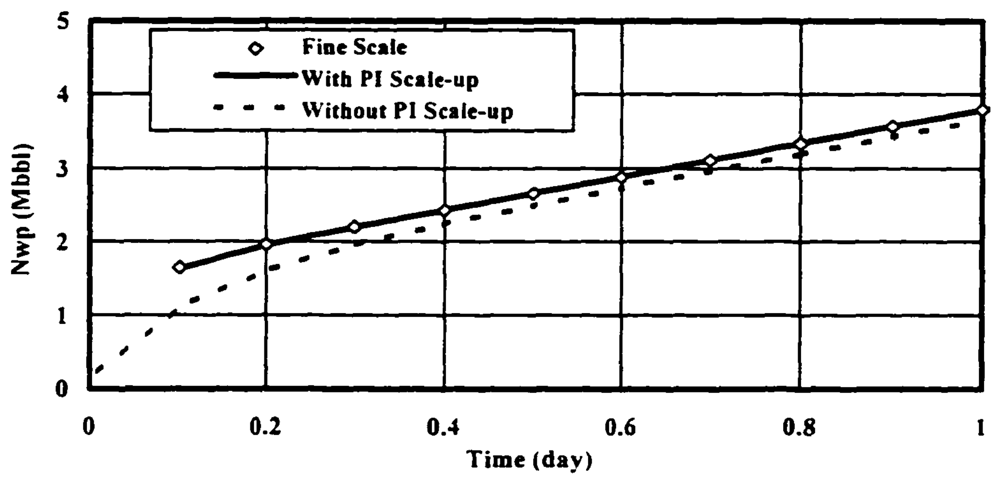

Fig. 4-53 Cum. Water Production of Model #2

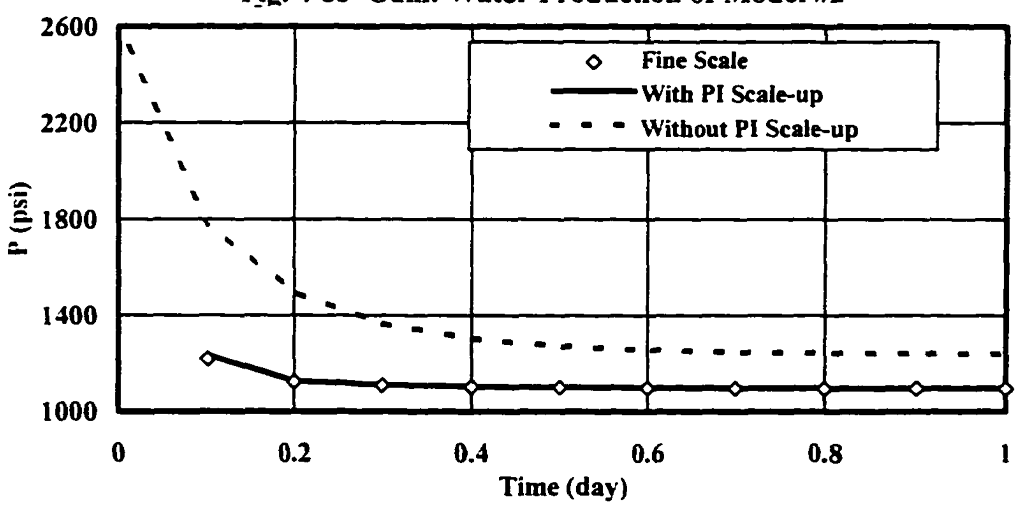

Fig. 4-54 Reservoir Pressure of Model #2

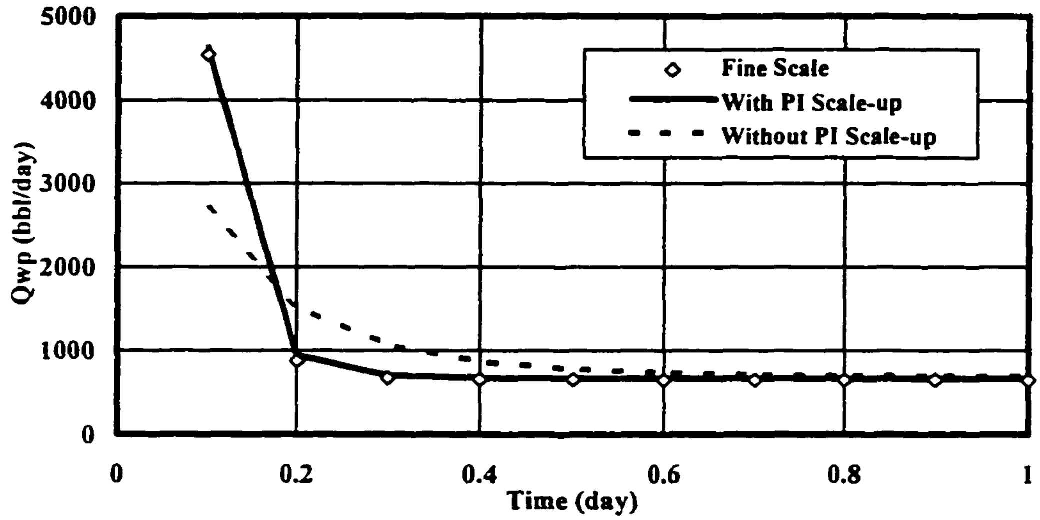

Fig. 4-55 Water Production Rate for Well #1 of Model #2

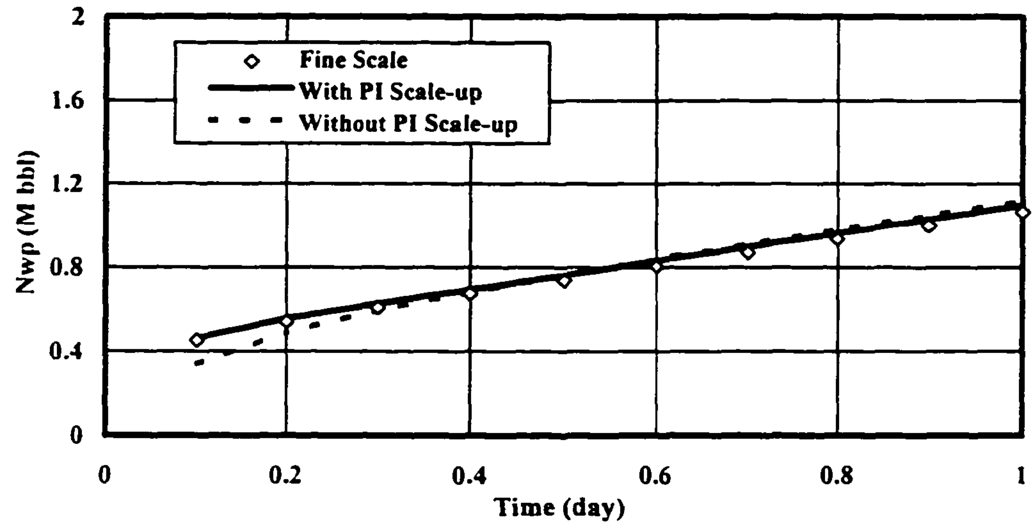

Fig. 4-56 Cum. Water Production for Well #1 of Model #2

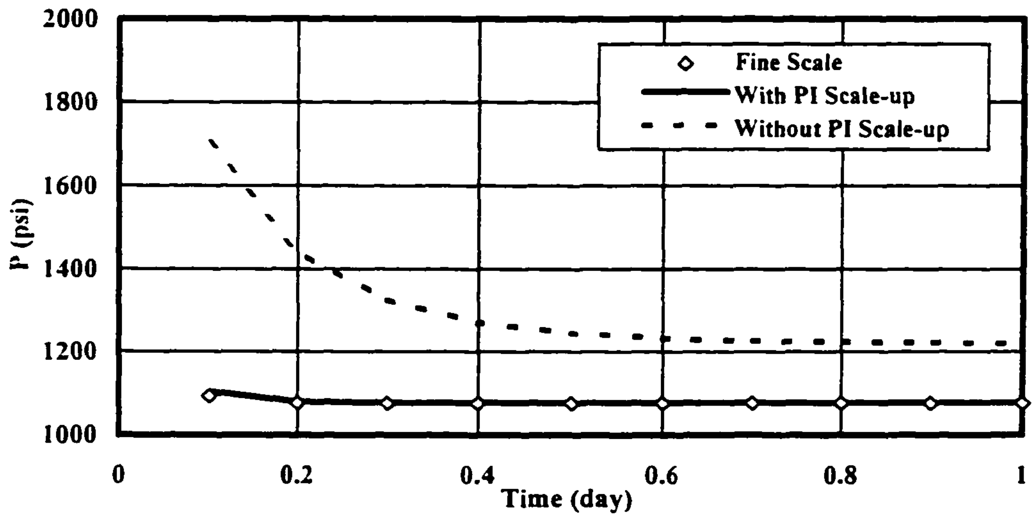

Fig. 4-57 Well Block Pressure for Well #1 of Model #2

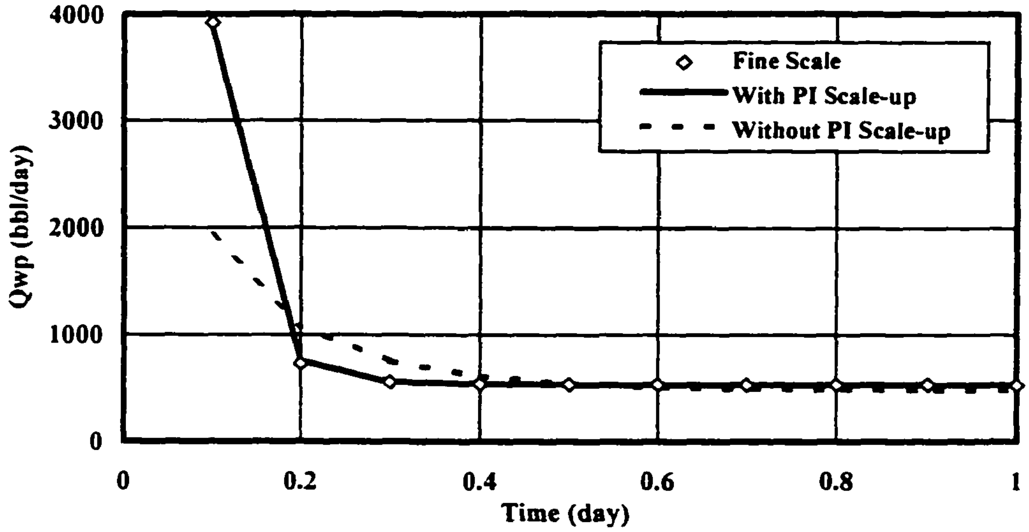

Fig. 4-58 Water Production Rate for Well #2 of Model #2

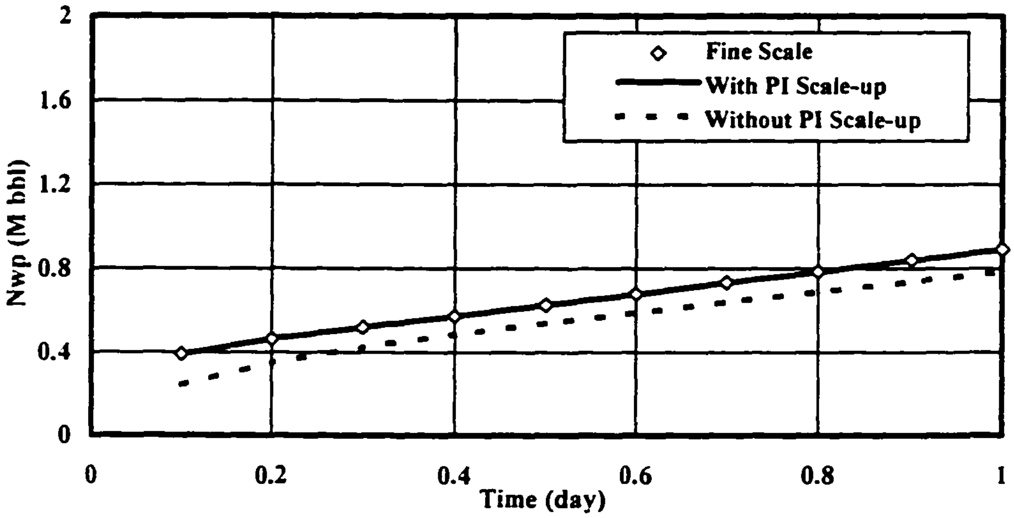

Fig. 4-59 Cum. Water Production for Well #2 of Model #2

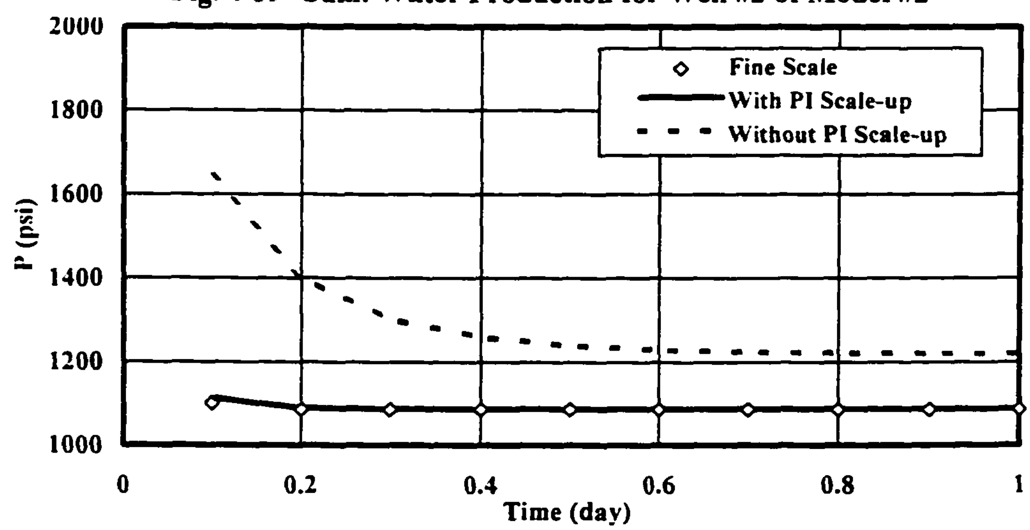

Fig. 4-60 Well Block Pressure for Well #2 of Model #2

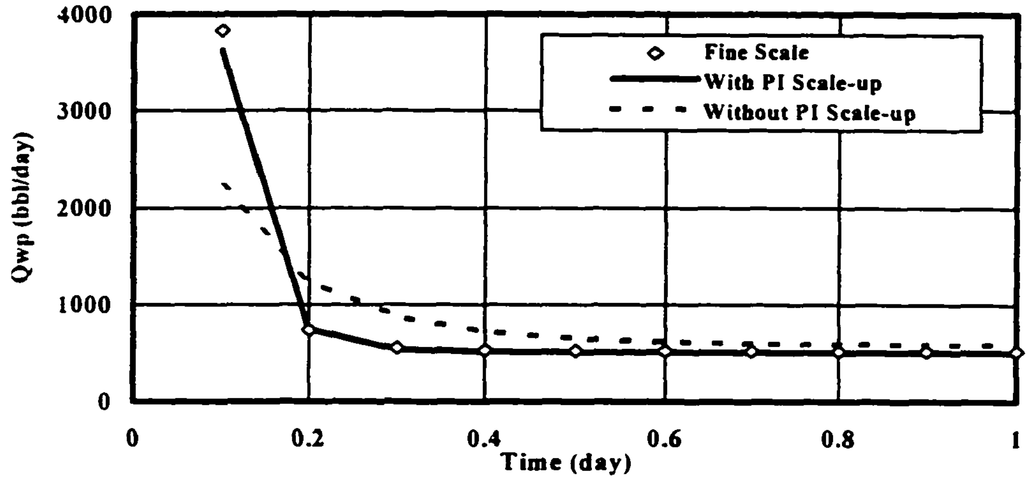

Fig. 4-61 Water Production Rate for Well #3 of Model #2

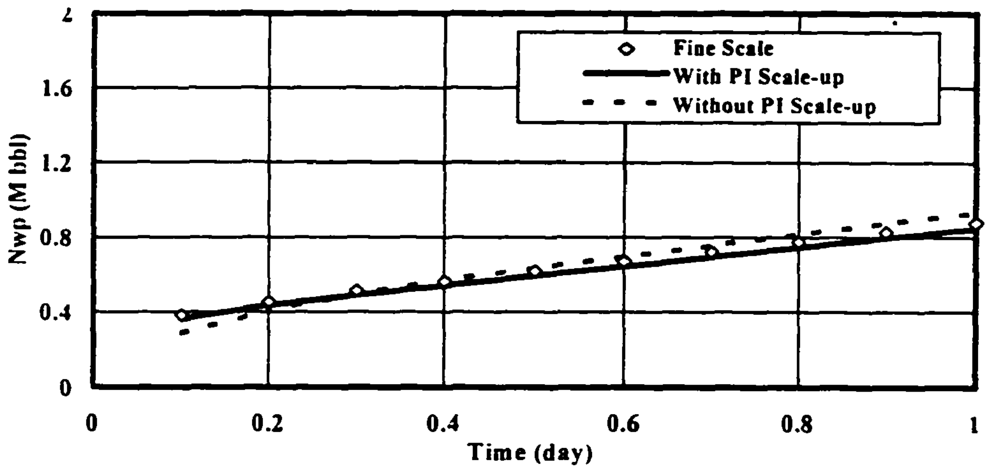

Fig. 4-62 Cum. Water Production for Well #3 of Model #2

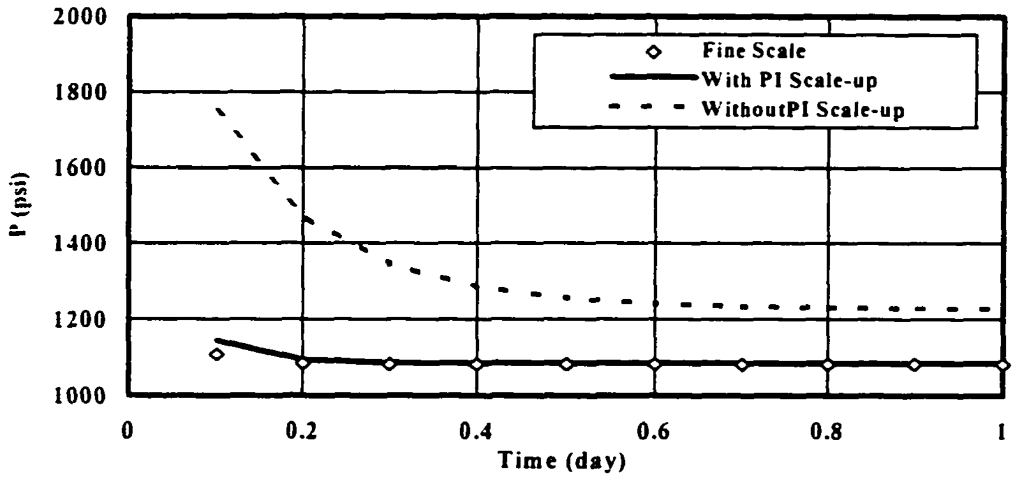

Fig. 4-63 Well Block Pressure for Well #3 of Model #2

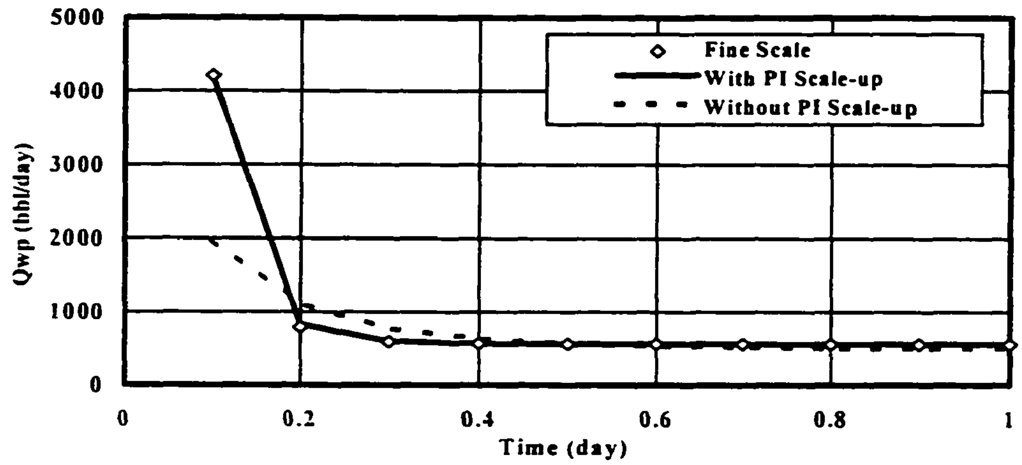

Fig. 4-64 Water Production Rate for Well #4 of Model #2

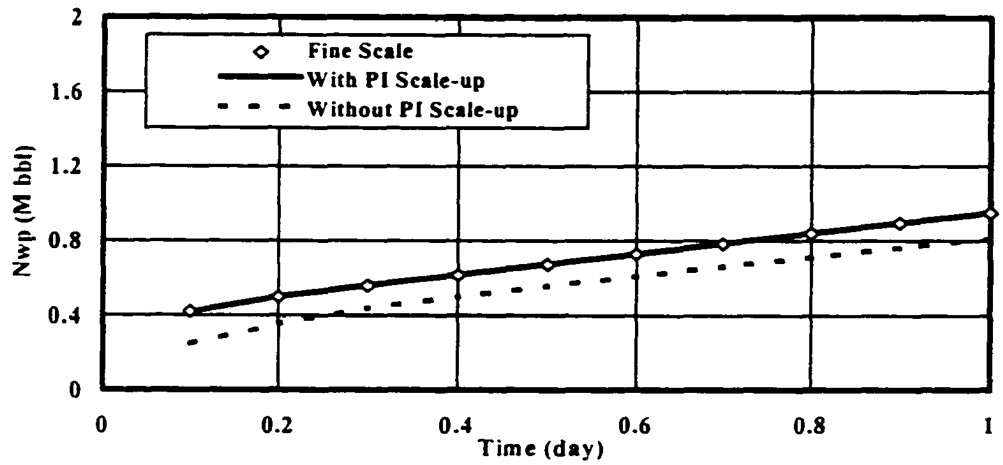

Fig. 4-65 Cum. Water Production for Well #4 of Model #2

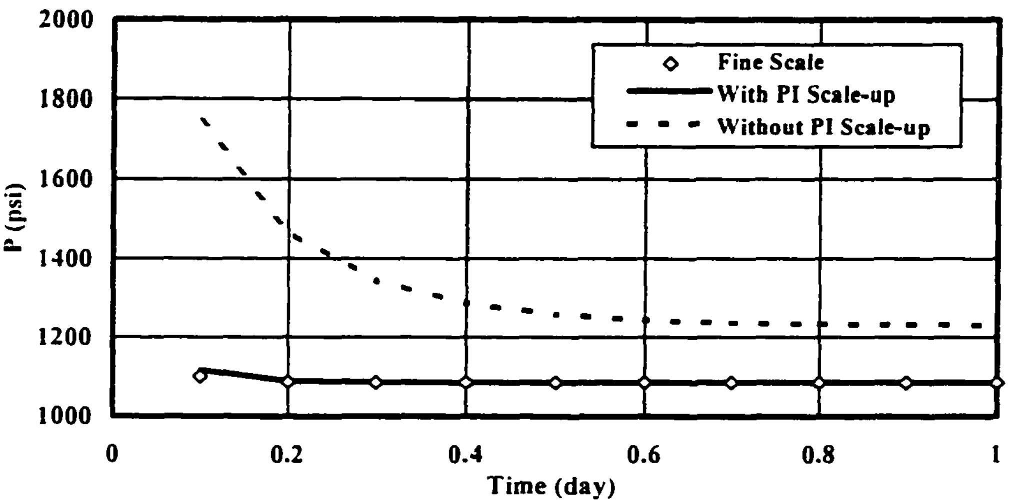

Fig. 4-66 Well Block Pressure for Well #4 of Model #2

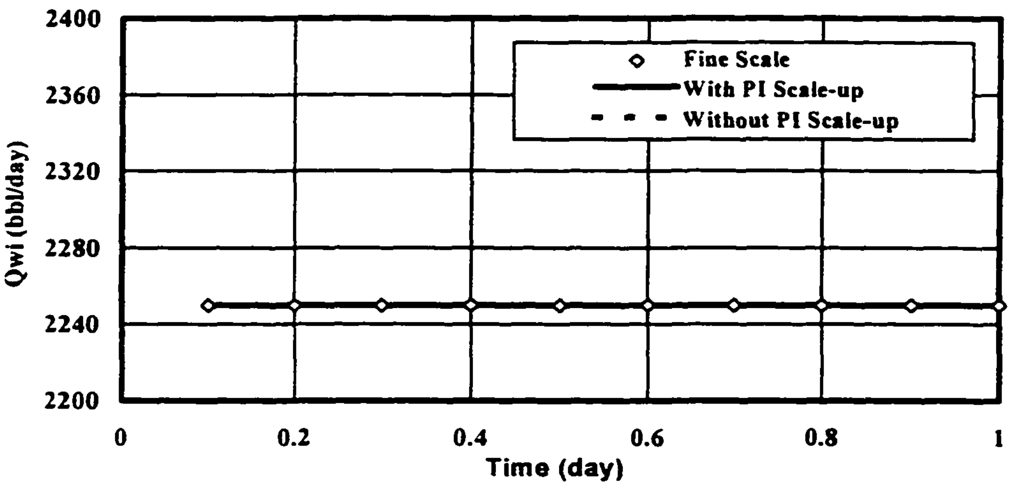

Fig. 4-67 Water Injection Rate for Well #5 of Model #2

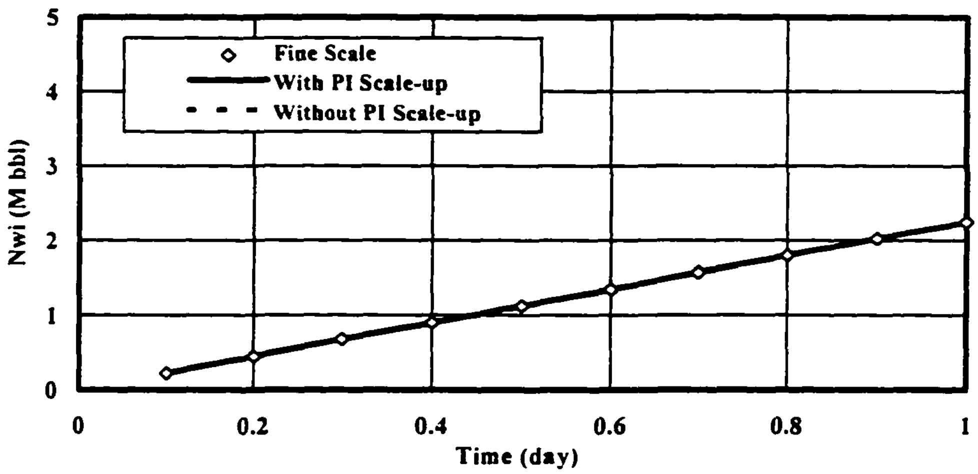

Fig. 4-68 Cum. Water Production for Well #5 of Model #2

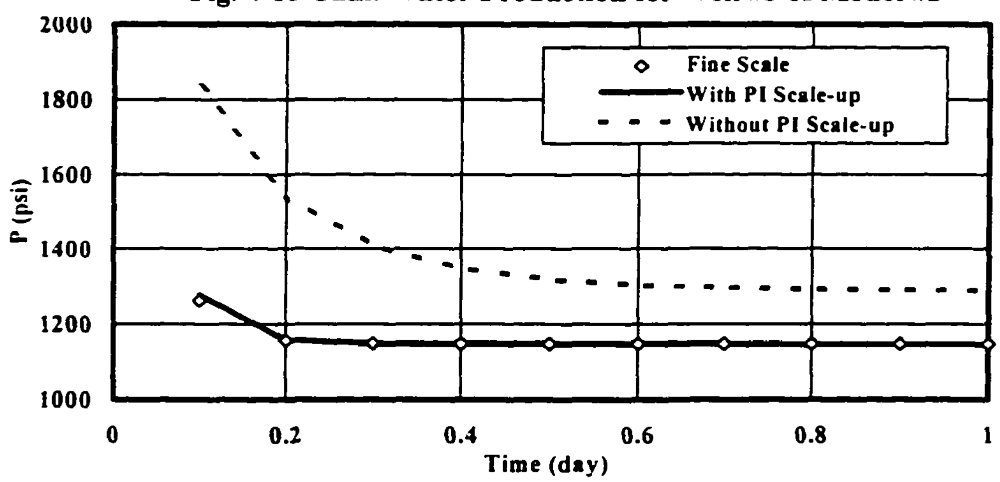

Fig. 4-69 Well Block Pressure for Well #5 of Model #2

CHAPTER V

SCALE-UP ON GYPSY FORMATION

In Chapter IV, the scale-up strategies were introduced, illustrated and validated for two hypothetical models. Successful scale-up results were obtained after a PI scale-up technique was applied. In this chapter, the scale-up strategies were applied to the three Gypsy models developed in Chapter III to study the effects of geological modeling on scale-up.

5.1 Fine-Scale Gypsy Models

Three coarse-scale geological models were developed and described in Chapter III. To perform the scale-up, fine-scale Gypsy models were developed based on three coarse-scale models presented in Chapter III. Fine-scale models were obtained by dividing each permeable layer in the coarse-scale model into layers with one foot thickness. The layers in the fine-scale model are parallel to the bottom surface of the coarse-scale layer. The six shale layers, representing impermeable layers, were kept intact in all three models. This leads to a total of 125 layers in the channel model, 198 layers in the lithofacies model, and 136 layers in the flow unit model. The properties of the models, including permeability and porosity, were determined using the deterministic method based on the available data in the previously identified 22 drilled wells.

To efficiently perform the scale-up, instead of modeling the entire volume of the reservoir, only the area where detailed information was available was simulated, as shown in Fig. 5-1. The grid system that was simulated was 23 by 29 grid blocks in the x and y directions. A 3-D view of the permeability distribution for the three fine-scale models used in scale-up are presented in Figs. 5-2 to 5-4.

The top of the Gypsy formation was initially located at the surface with an average elevation of about 885 ft, which was obtained by averaging the elevations of 22 wells. To perform the simulation, Gypsy formation was assumed to be moved vertically 9500 ft down. The elevation of the new surface of the model was assumed to be zero.

Similar to model #1 and #2, a five-spot well pattern was used in the simulation as shown in Fig. 5-1. All five wells were assumed fully perforated in all of the permeable layers. For the production wells, a maximum production of 10,000 STB/day and a minimum bottom hole pressure of 1,000 psi at elevation of -8,500 feet were assumed. For the injection well, a maximum injection rate of 2,250 STB/day and maximum bottom hole pressure of 10,000 psi at elevation of -8,500 feet were assumed.

The process simulated was single-phase water flow. Reservoir fluid properties were the same values used for the hypothetical models in Chapter IV. No-flow boundary condition was assumed. Reservoir was assumed in equilibrium condition with an initial pressure 2500 psi at a elevation of -8,000 feet.

To simulate pinch-out in various models, the technique presented and used for model #2 in Chapter IV was used, producing an error of 0.39% in reservoir pore volume in channel model, 0.53% in lithofacies model, and 0.35% in flow unit model.

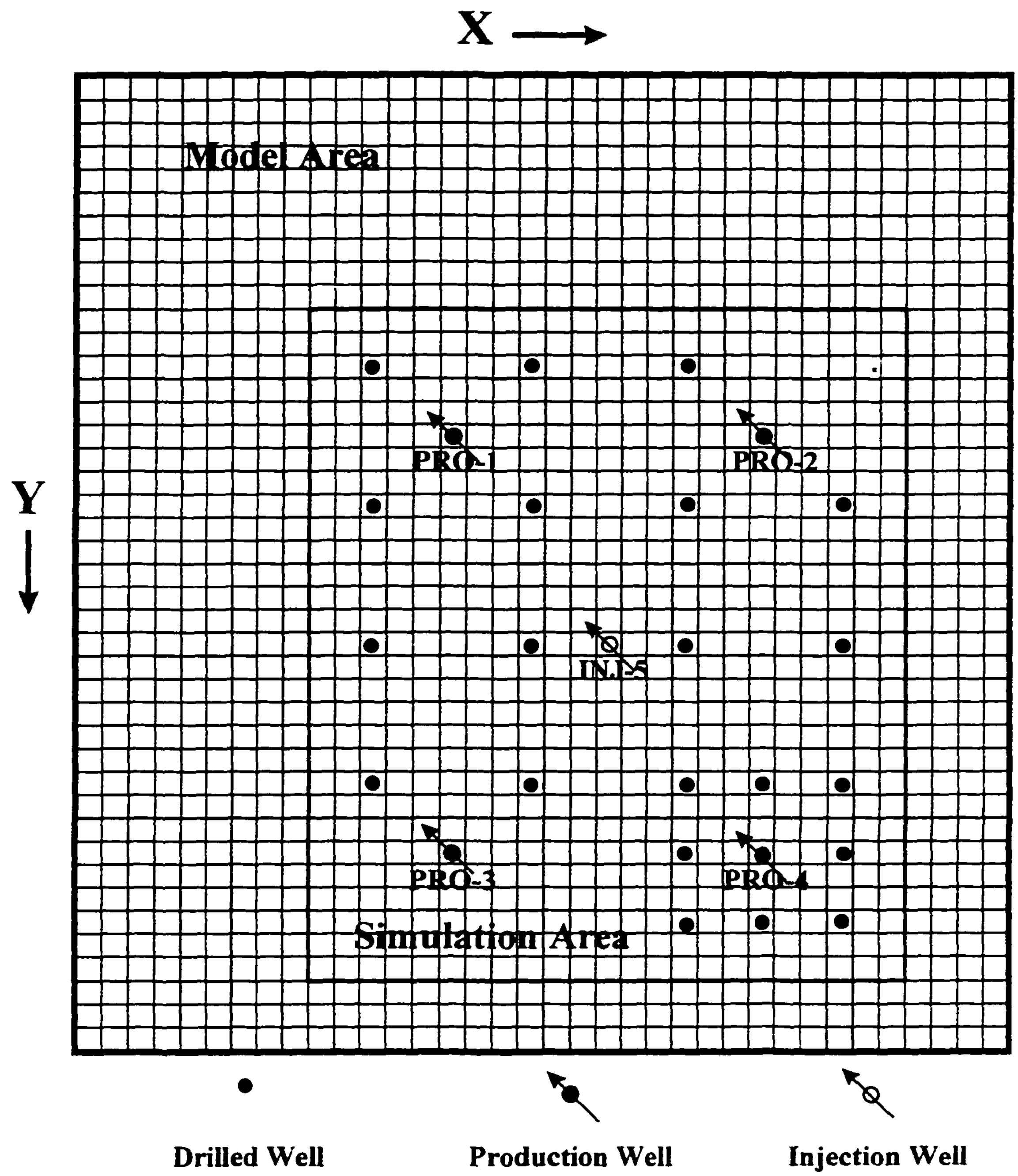

Fig. 5-1 Illustration of Geological Modeling and Simulation Area

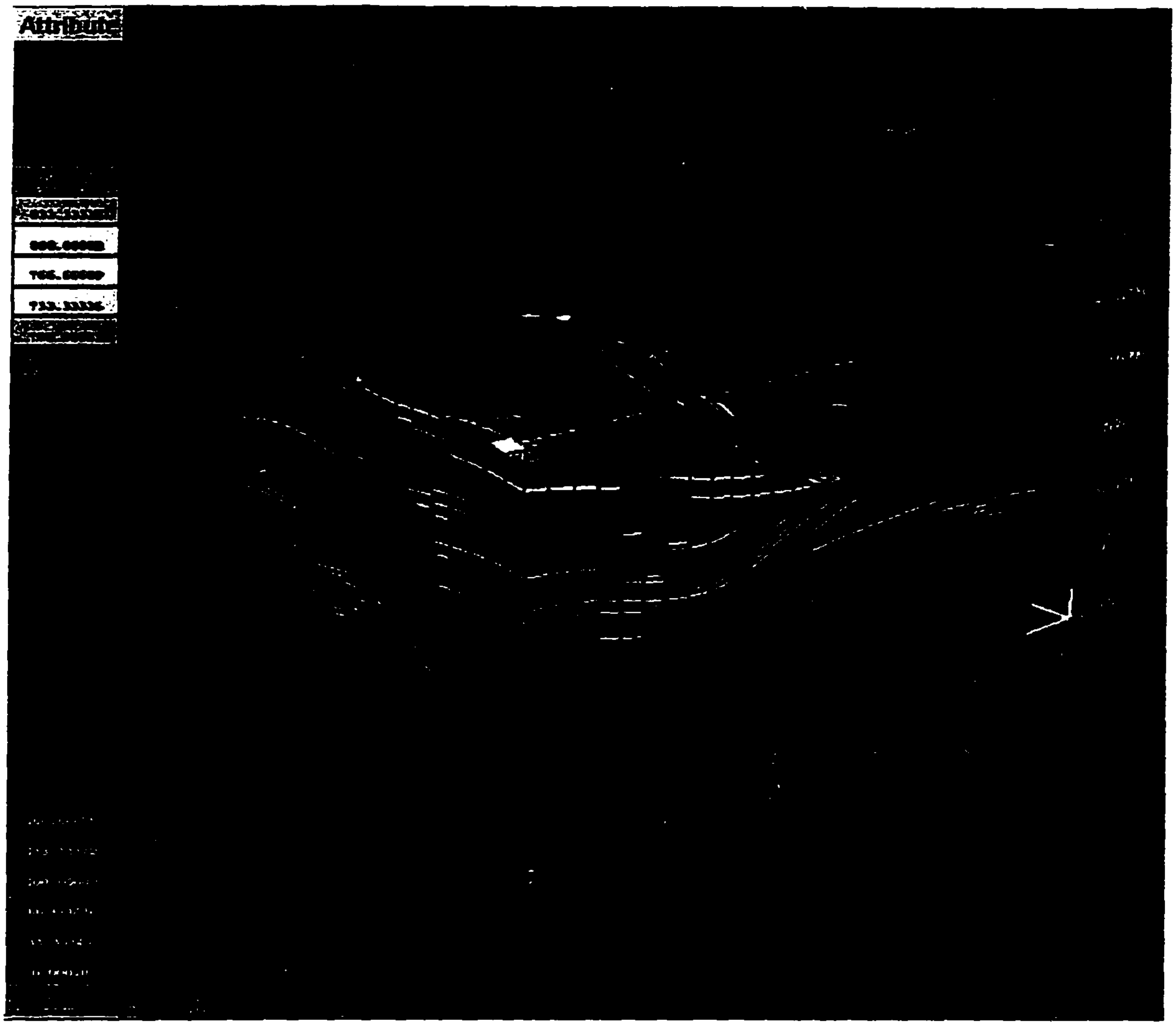

Fig. 5-2 3-D View of Permeability Distribution of

Fine-Scale Channel Model

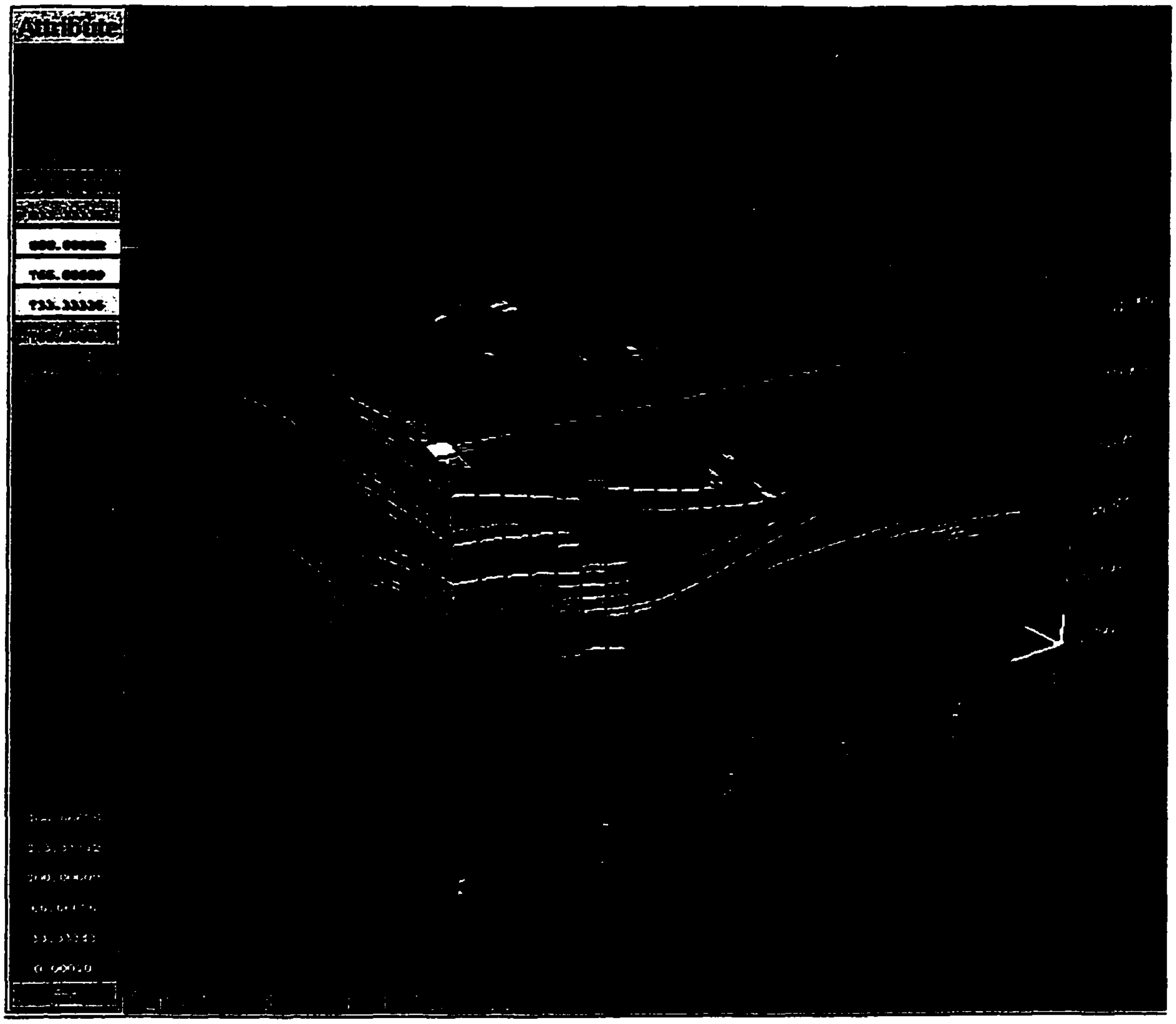

Fig. 5-3 3-D View of Permeability Distribution of Fine-Scale Lithofacies Model

Fig. 5-4 3-D View of Permeability Distribution of Fine-Scale Flow Unit Model

These errors were considered to be small enough to have negligible effect on the simulation results.

Simulation was run for 10 days of flow until a stabilized condition was obtained. As in model #1 and model #2, pressure and flowrate in three dimensions for fine-scale model were produced in an output map file. Transmissibility, thickness, and pore volume were calculated using the program developed in Chapter IV. Because of the complex structure of the model, in fine-scale model, some layers are present only in a few grid blocks. This could cause errors in the calculation of pore volume when 0.01 ft thickness was assumed for the pinch-out grid blocks. To reduce this error, layers that only occurred in a few grid blocks that had similar reservoir properties were combined to form one layer. The combination of these layers also served to reduce the computational time mainly because the memory of the available computer could not handle so many layers, especially in the lithofacies model. Table 5-1 is a summary of the three models.

Table 5-1 Summary of the Three Gypsy Models

Model	Channel	Lithofacies	Flowunit
Layers of Initial Fine-Scale Model	125	198	136
Layers of Combined Fine-Scale Model	98	107	87
Layers of Coarse-Scale Model (1)	13	28	16
Layers of Coarse-Scale Model (2)	13	13	13
Actual Pore Volume of the Model(MRB)	1001.50	906.78	967.24
Pore Volume with Pinch-out Thin Layers (MRB)	1005.37	911.57	970.63
Error Caused by Thin Layers (%)	0.39	0.53	0.35

5.2 Scale-up of the Three Gypsy Models

To compare the scale-up results, the three models were all scaled up to 13-layer coarse-scale channel model. To study the effects of layering on scale-up, the lithofacies model and flowunit model were also scaled up to 28-layer and 16-layer coarse-scale models. Scale-up was first conducted without PI scale-up using 10 as an input for the well injectivity index in all five wells for both fine-scale models and coarse-scale model. PI scale-up was then conducted. Table 5-2 shows the scaled productivity indices used for the three models. Figs. 5-5 to 5-58 illustrate the scale-up results for the three models, including the results with and without PI scale-up.

Table 5-2 Scaled Productivity Index for the Three Gypsy Models

Well	PI Channel Model	PI Lithofacies Model	PI Flowunit Model
PRO-1	272.70	229.32	346.89
PRO-2	339.15	260.23	296.18
PRO-3	124.02	123.46	151.12
PRO-4	264.17	322.05	333.19
INJ-5	190.36	189.38	181.84

The characteristics of the simulation results for the three geological models can be summarized as follows:

1. Due to the limited volume of the reservoir and its high permeability, equilibrium condition for production and injection was obtained in only five days.
2. Production initially experienced depletion process for the first 2 to 3 days and then went through a process of displacement, in which total water production rate for the reservoir was equal to the water injection rate.
3. Without PI scale-up, both production rate and pressure are significantly different between fine scale and coarse scale at the beginning. Production rate tends to matched after three days. Pressure stabilized at a constant pressure difference after about five day's production period.
4. After considering PI scale-up, satisfactory matches were obtained between fine scale and coarse scale for both water production and pressure. At the resolution of the plots, the difference between fine scale and coarse scale for scale-up with PI scale-up is not apparent. In fact, there exist small differences in the set of results. The differences will be discussed in next section using relative errors.

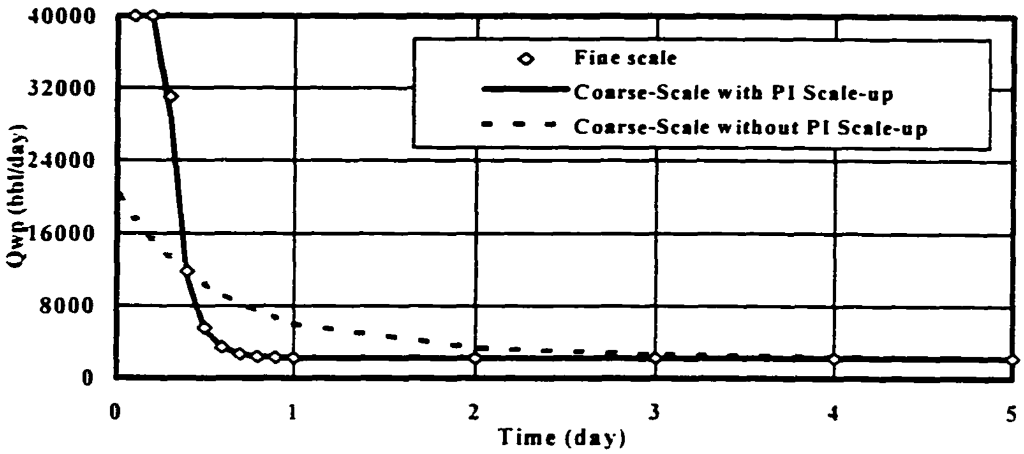

Fig. 5-5 Water Production Rate of Channel Model

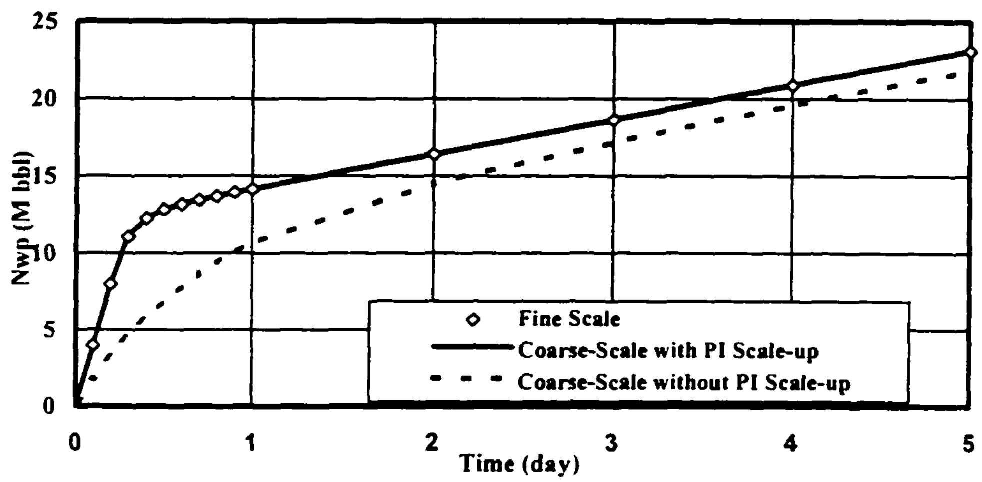

Fig. 5-6 Cum. Water Production of Channel Model

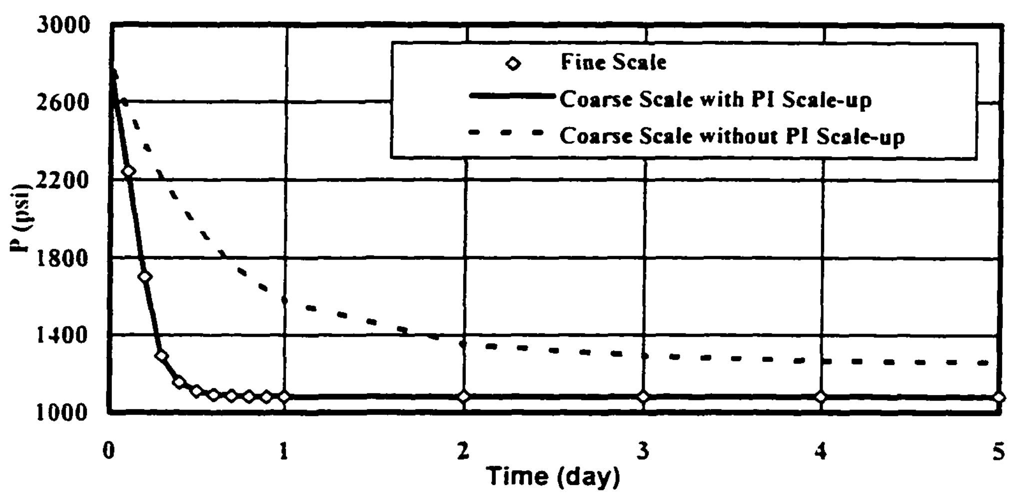

Fig. 5-7 Average Reservoir Pressure of Channel Model

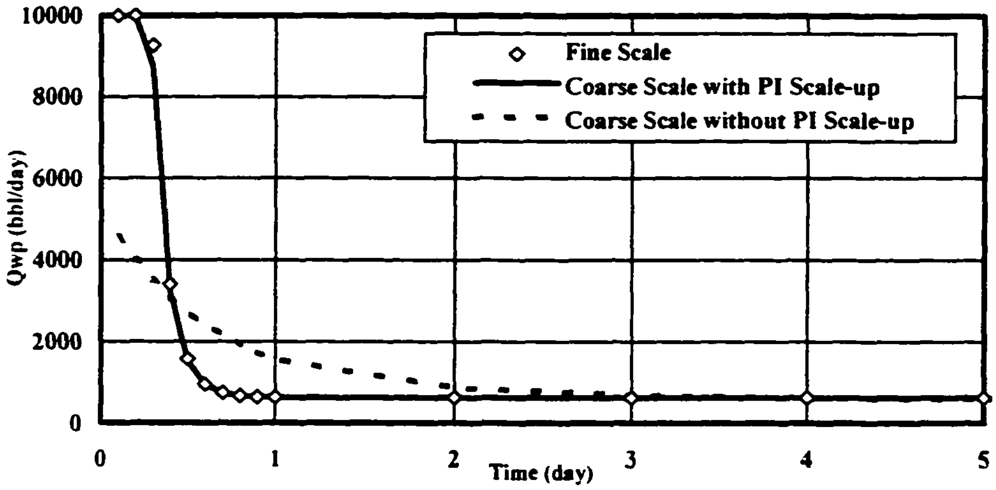

Fig. 5-8 Water Production Rate for Well #1 of Channel Model

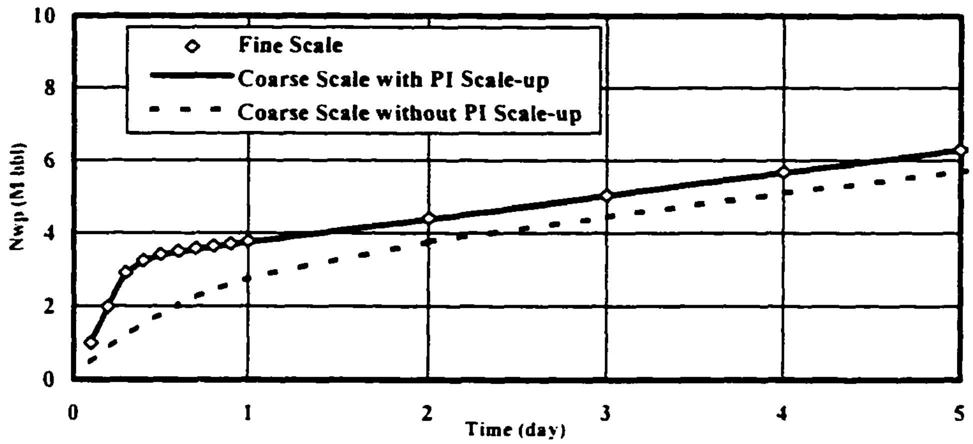

Fig. 5-9 Cum. Water Production for Well #1 of Channel Model

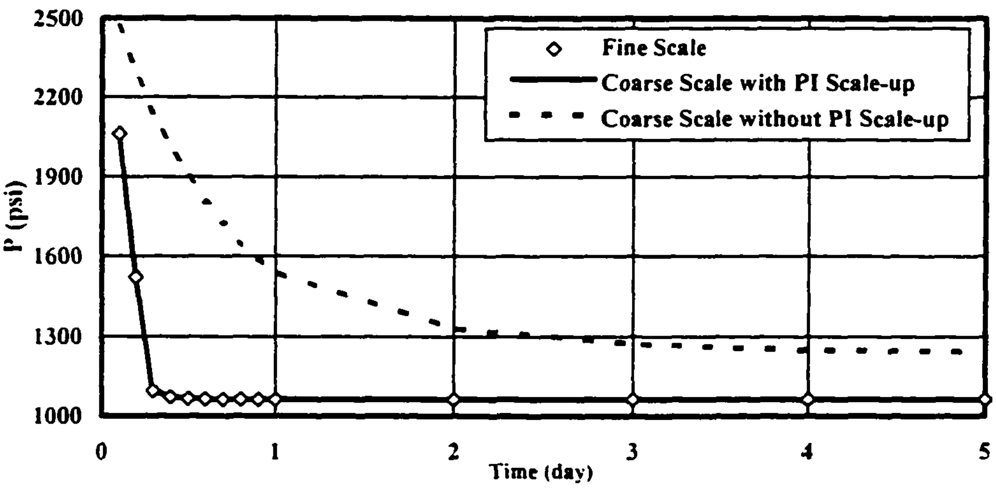

Fig. 5-10 Well Block Pressure for Well #1 of Channel Model

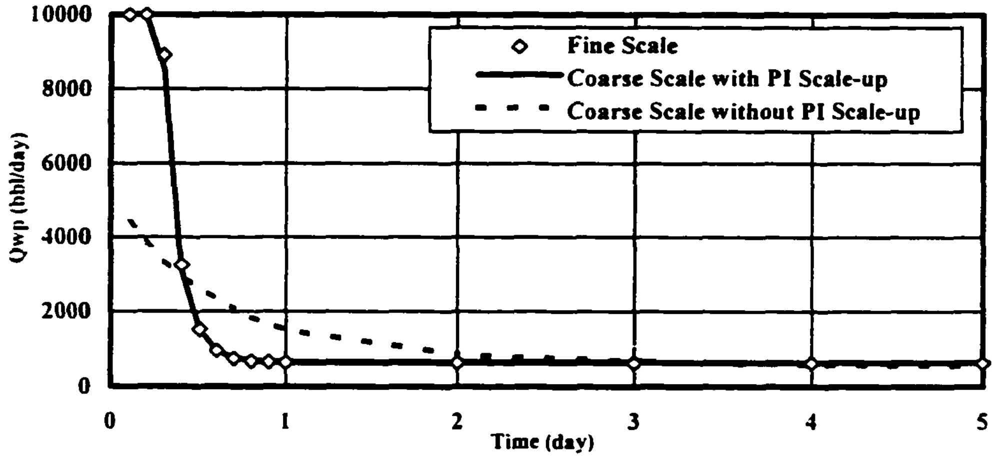

Fig. 5-11 Water Production Rate for Well #2 of Channel Model

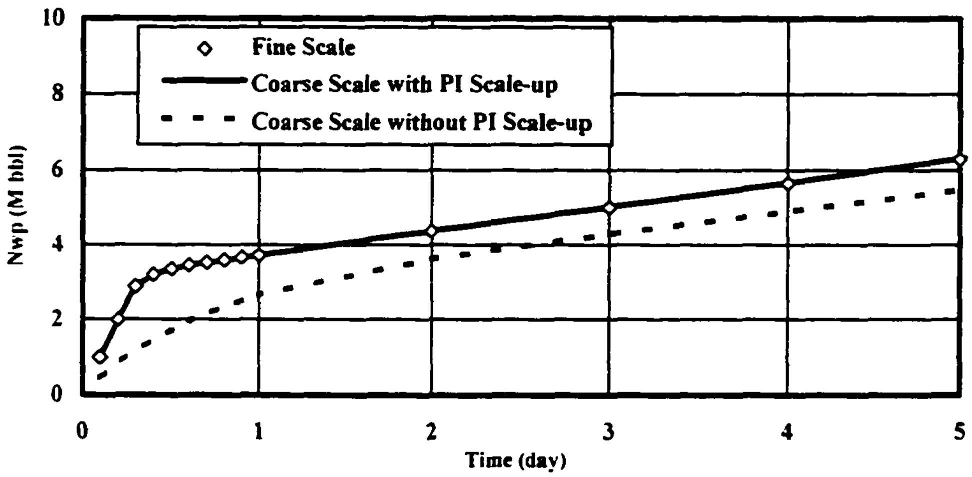

Fig. 5-12 Cum. Water Production for Well #2 of Channel Model

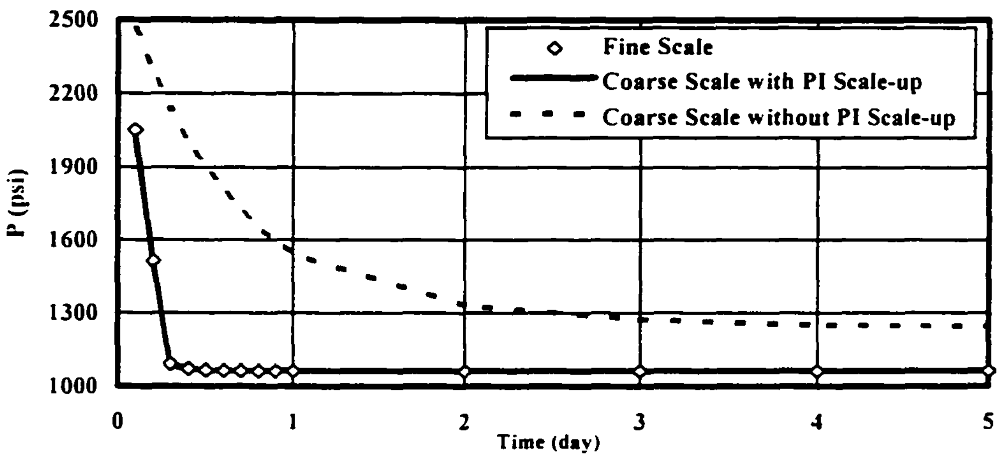

Fig. 5-13 Well Block Pressure for Well #2 of Channel Model

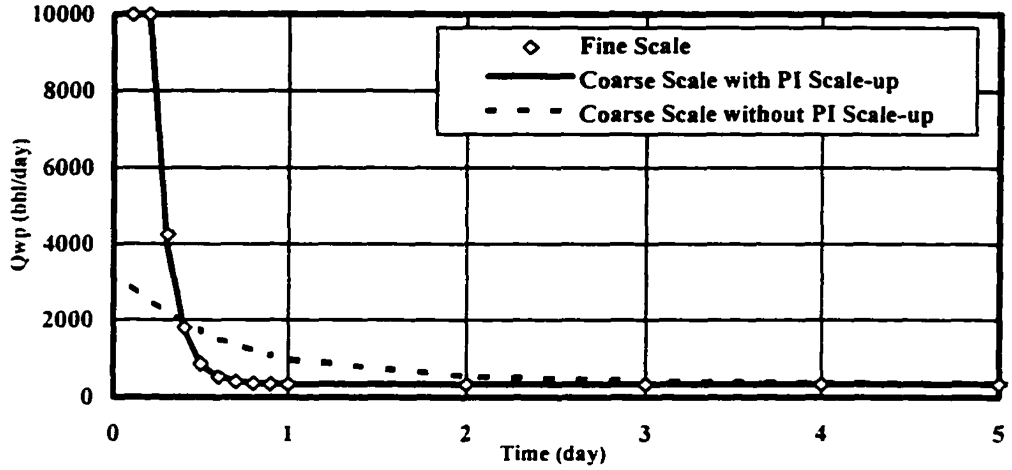

Fig. 5-14 Water Production Rate for Well #3 of Channel Model

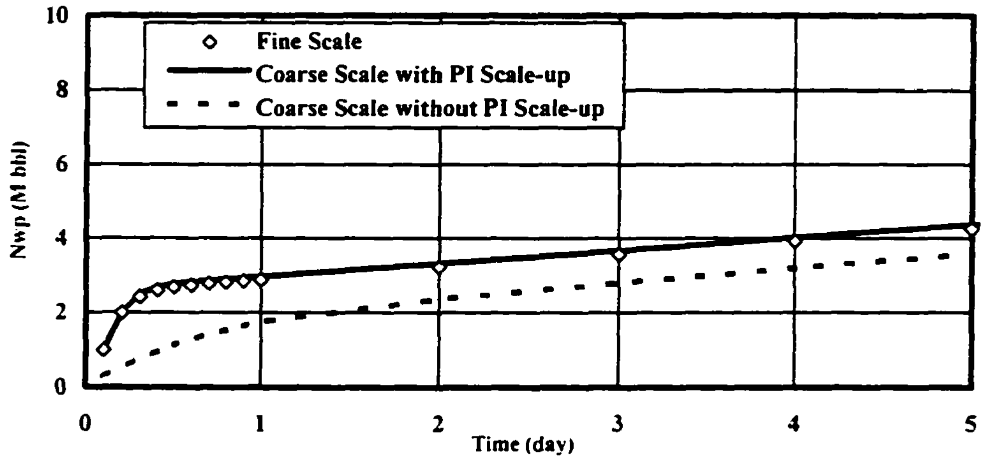

Fig. 5-15 Cum. Water Production for Well #3 of Channel Model

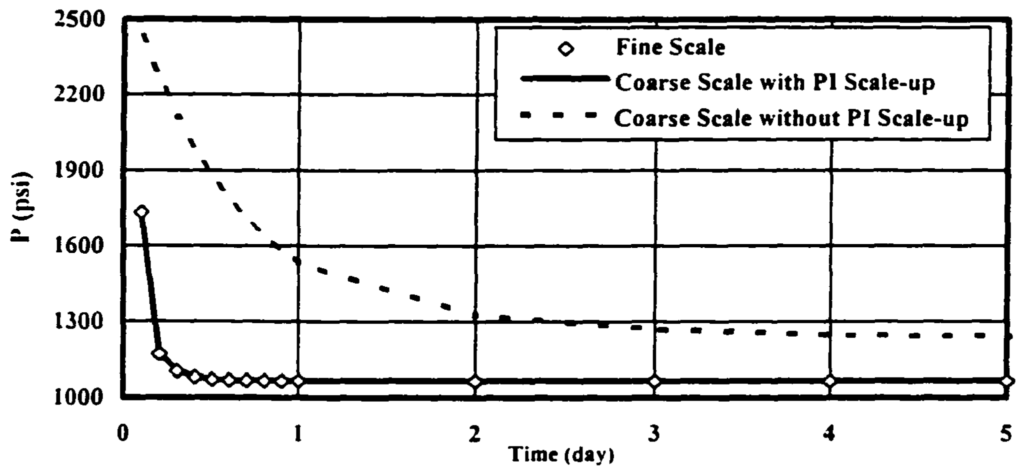

Fig. 5-16 Well Block Pressure for Well #3 of Channel Model

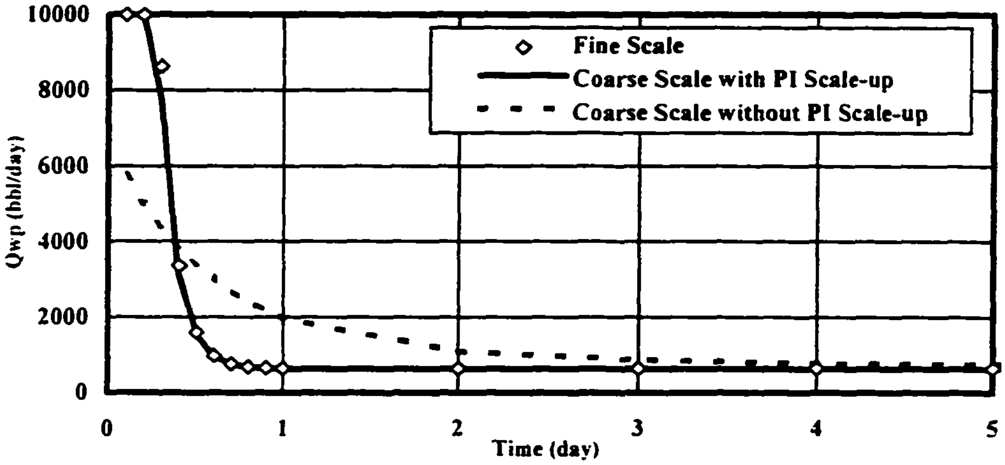

Fig. 5-17 Water Production Rate for Well #4 of Channel Model

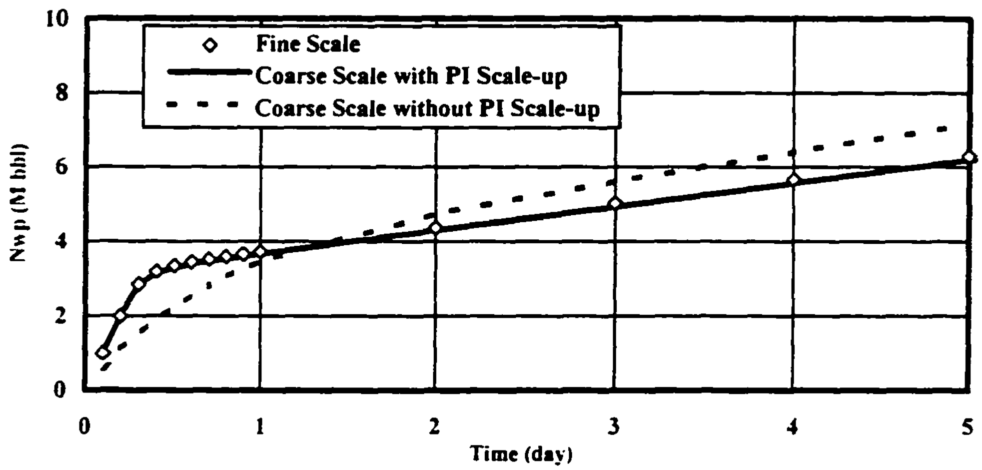

Fig. 5-18 Cum. Water Production for Well #4 of Channel Model

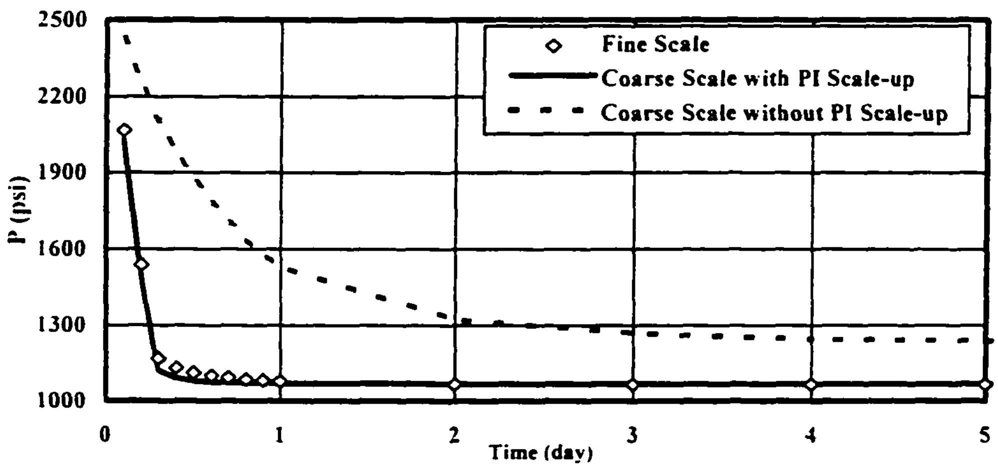

Fig. 5-19 Well Block Pressure for Well #4 of Channel Model

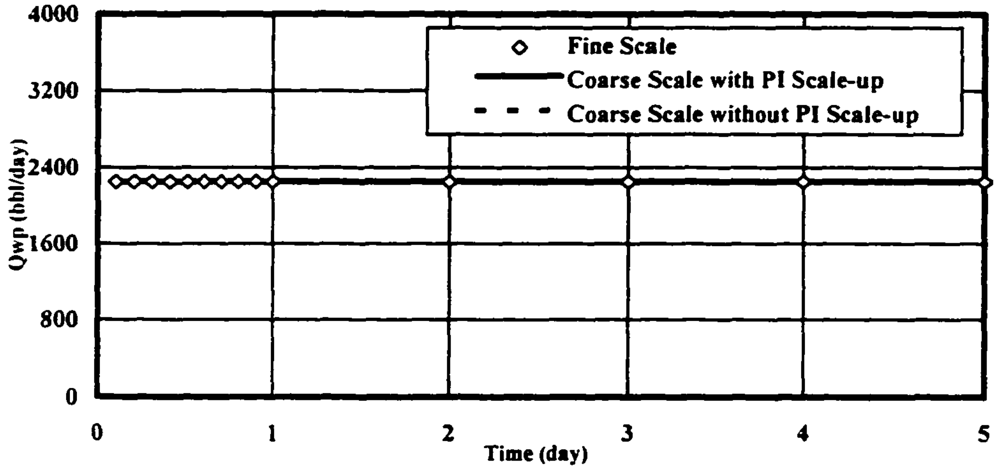

Fig. 5-20 Water Injection Rate for Well #5 of Channel Model

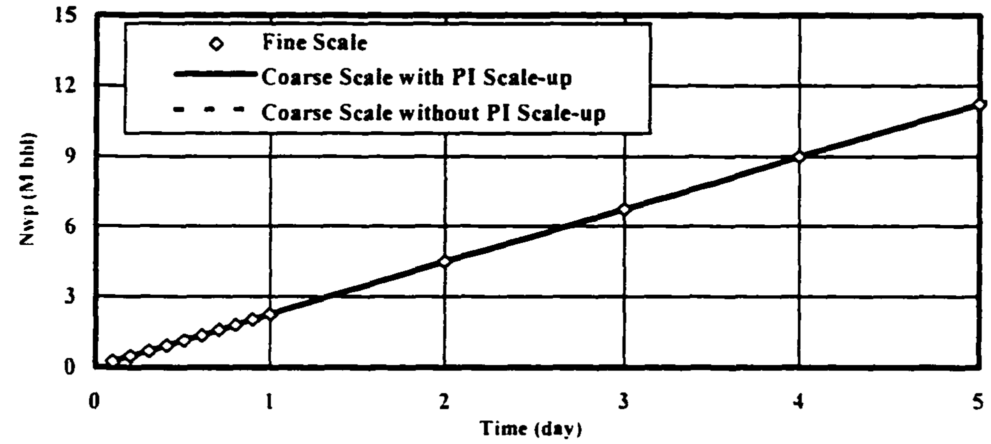

Fig. 5-21 Cum. Water Injection for Well #5 of Channel Model

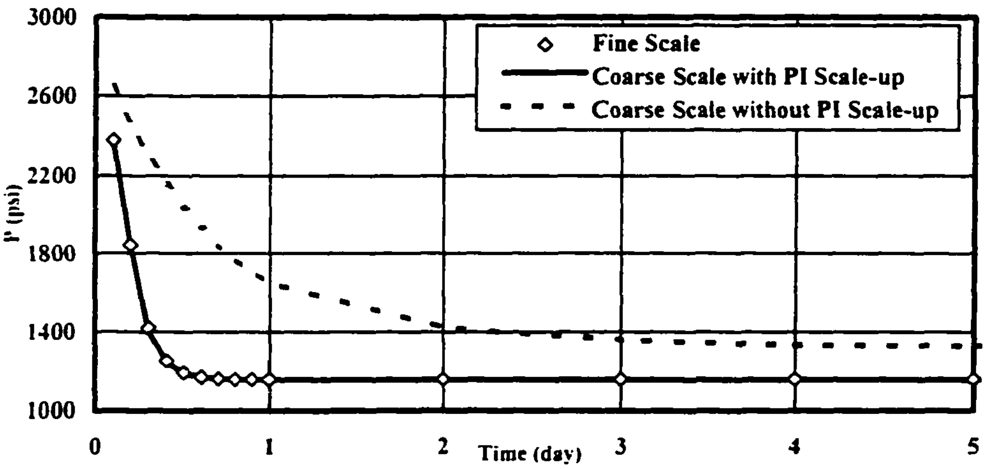

Fig. 5-22 Well Block Pressure for Well #5 of Channel Model

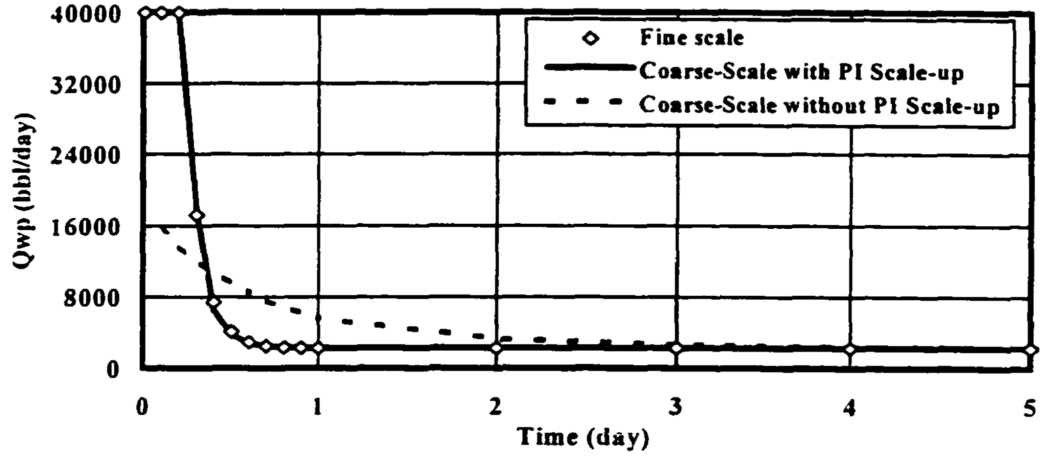

Fig. 5-23 Water Production Rate of Lithofacies Model

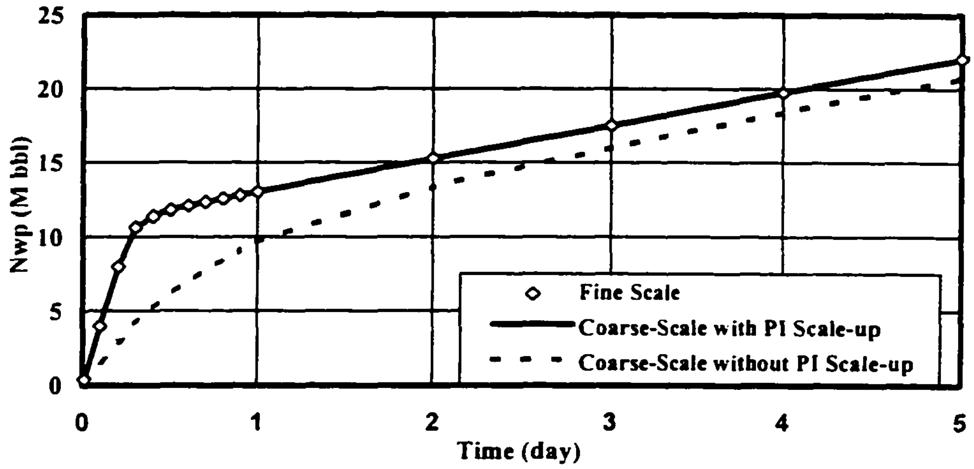

Fig. 5-24 Cum. Water Production of Lithofacies Model

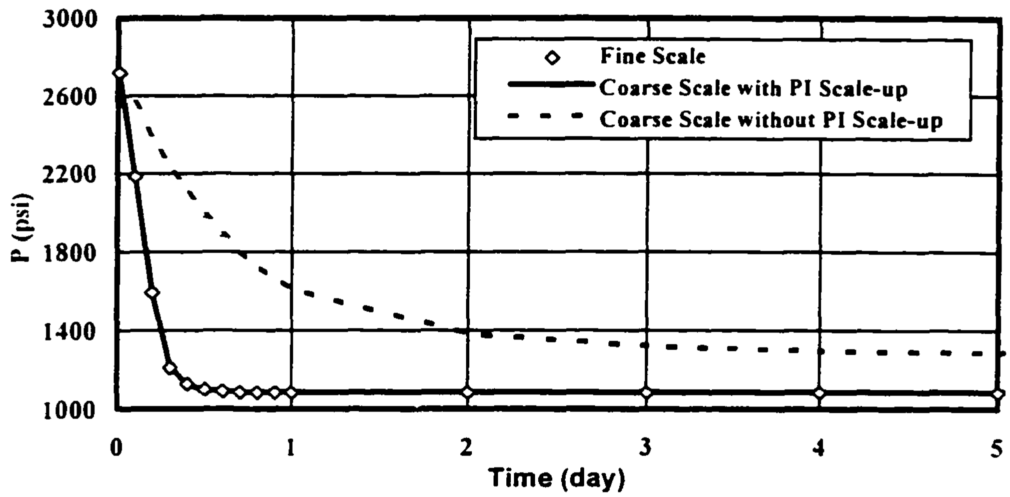

Fig. 5-25 Average Reservoir Pressure of Lithofacies Model

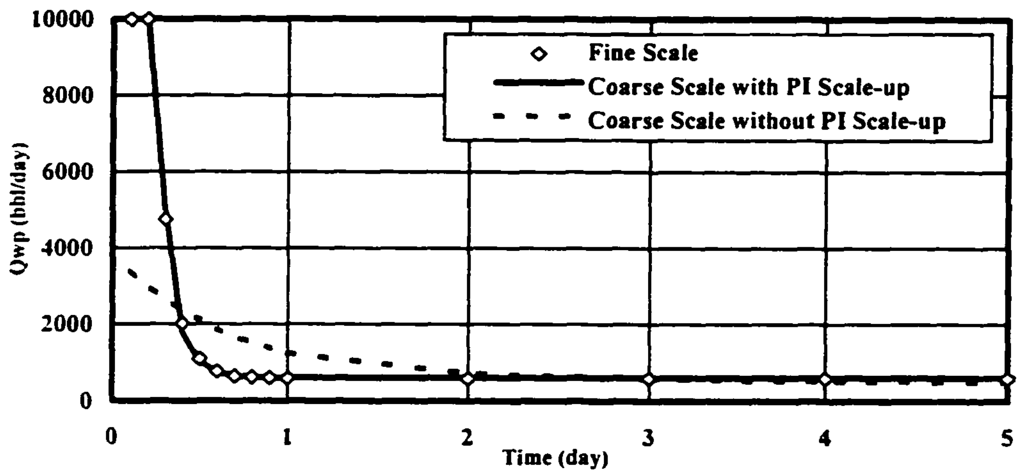

Fig. 5-26 Water Production Rate for Well #1 of Lithofacies Model

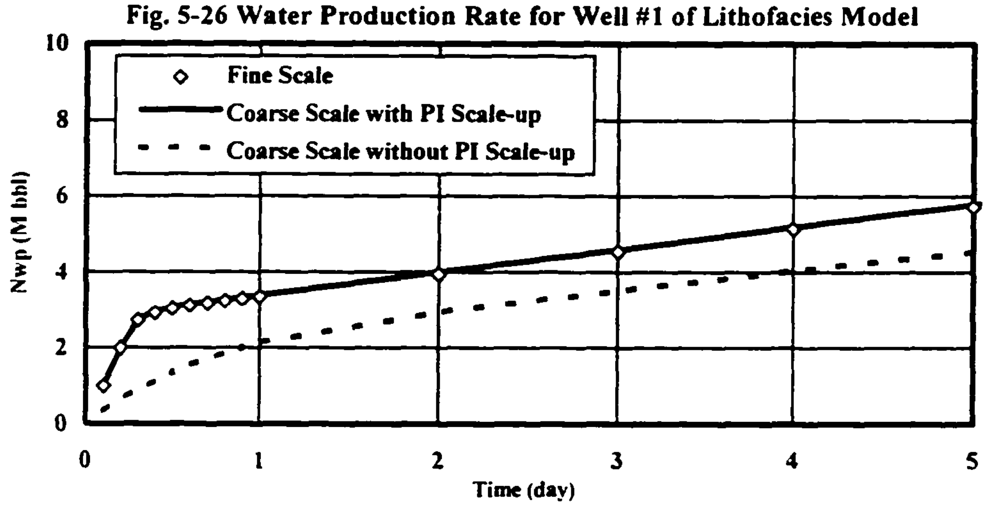

Fig. 5-27 Cum. Water Production for Well #1 of Lithofacies Model

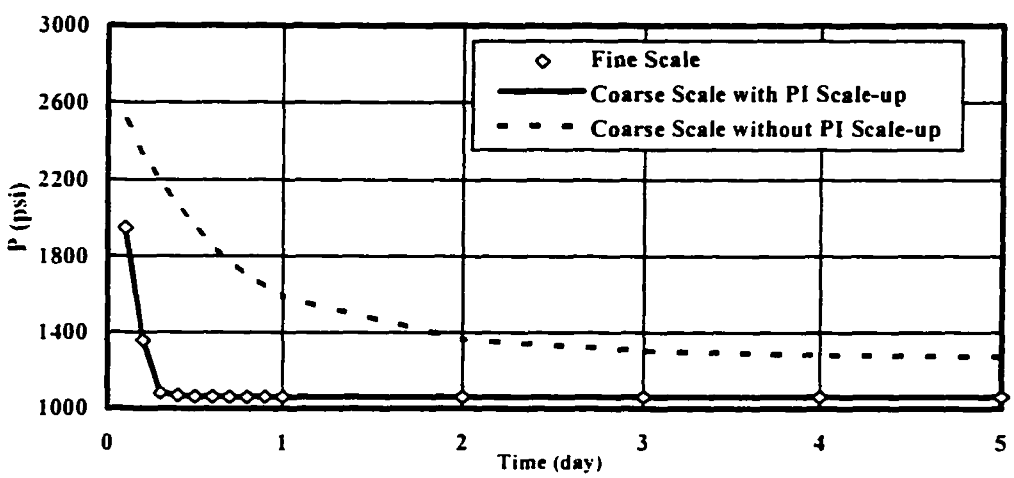

Fig. 5-28 Well Block Pressure for Well #1 of Lithofacies Model

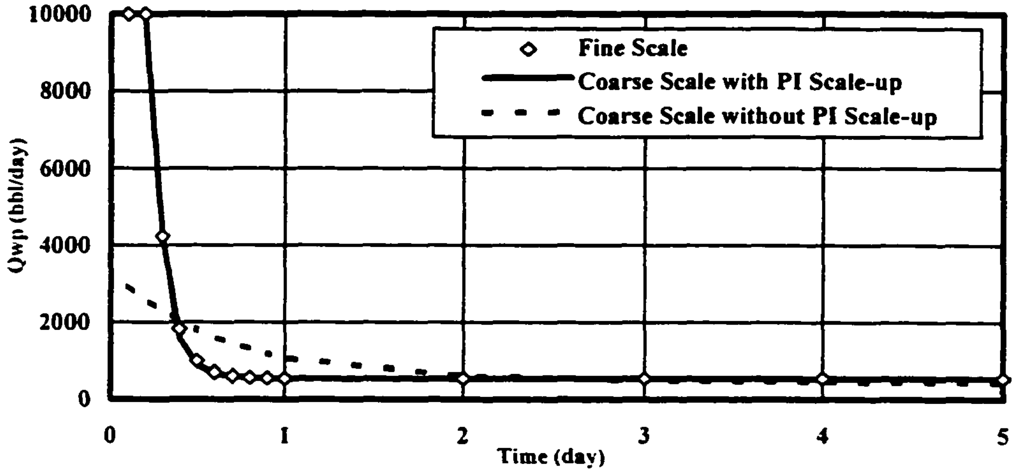

Fig. 5-29 Water Production Rate for Well #2 of Lithofacies Model

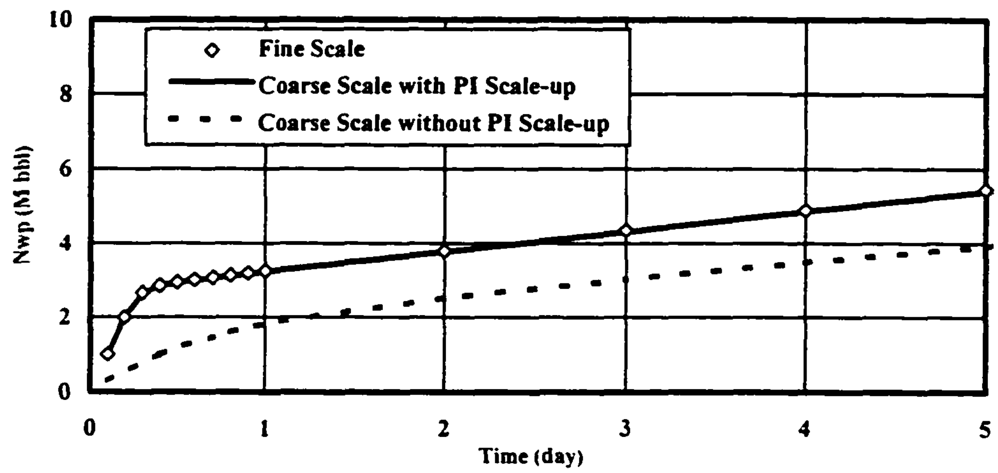

Fig. 5-30 Cum. Water Production for Well #2 of Lithofacies Model

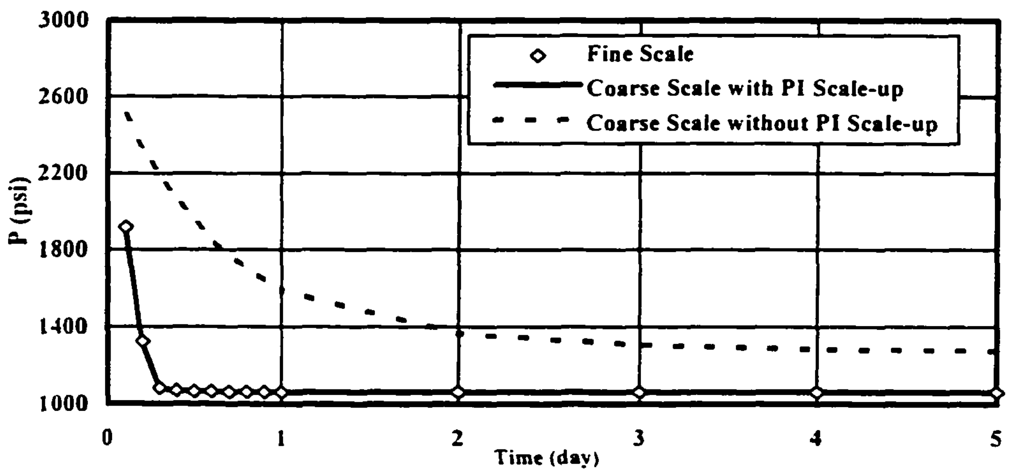

Fig. 5-31 Well Block Pressure for Well #2 of Lithofacies Model

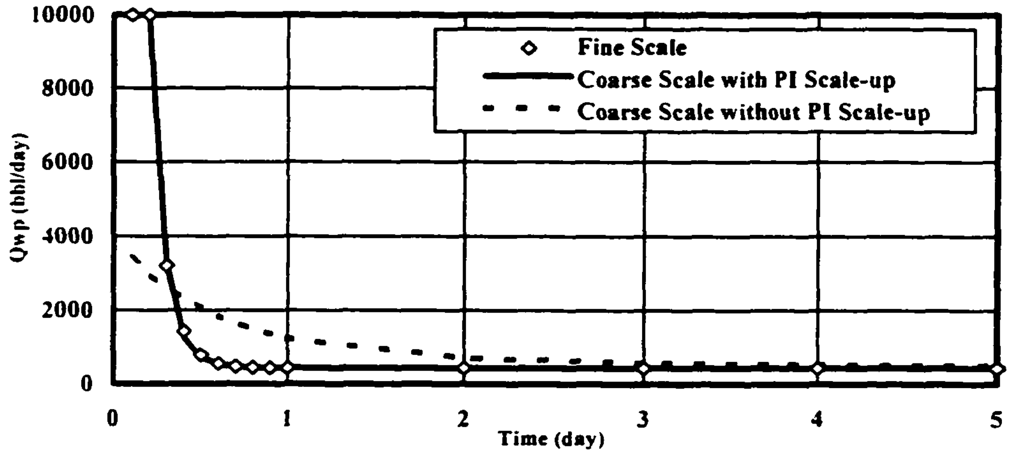

Fig. 5-32 Water Production Rate for Well #3 of Lithofacies Model

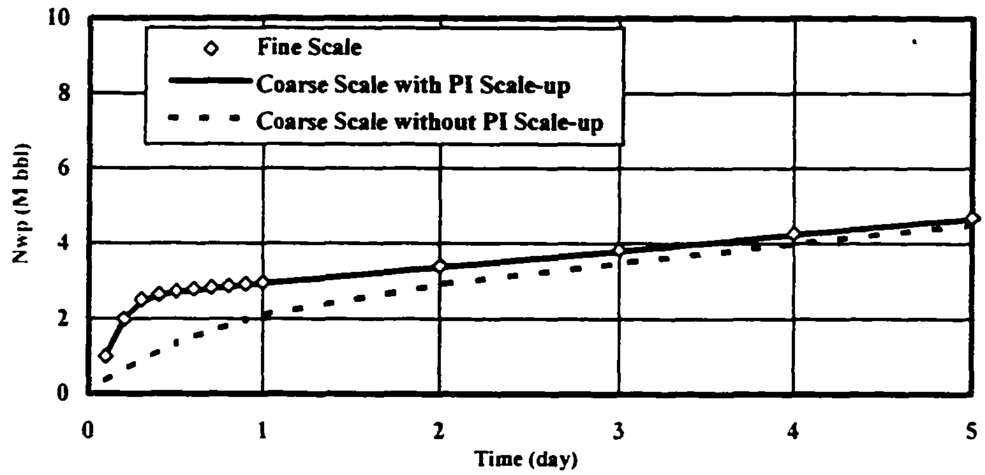

Fig. 5-33 Cum. Water Production for Well #3 of Lithofacies Model

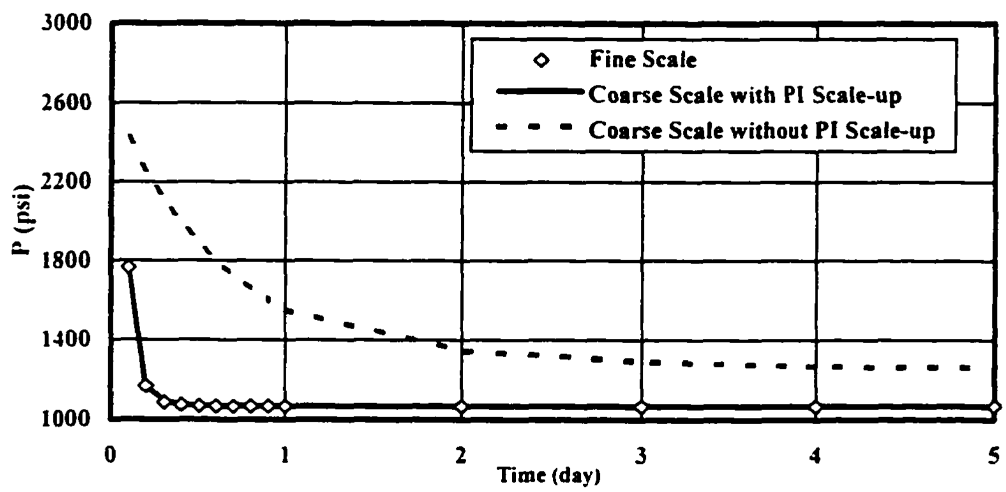

Fig. 5-34 Well Block Pressure for Well #3 of Lithofacies Model

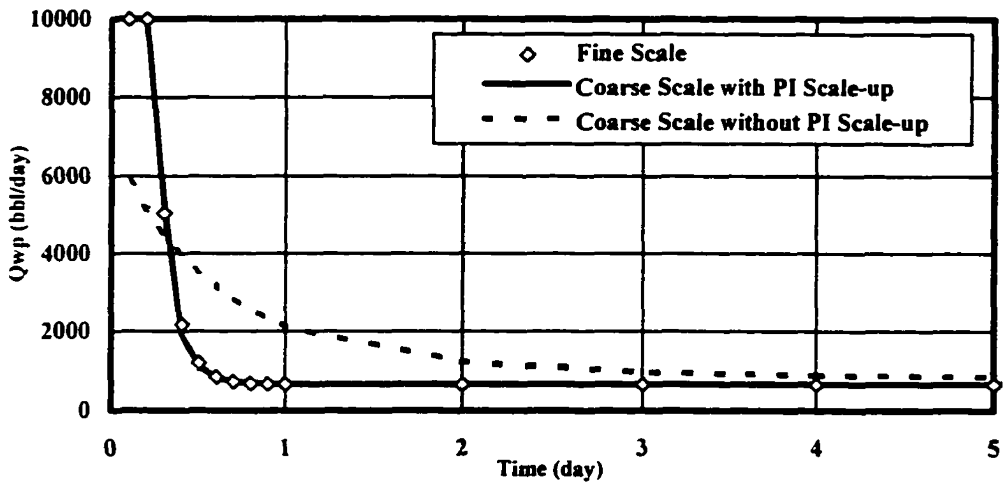

Fig. 5-35 Water Production Rate for Well #4 of Lithofacies Model

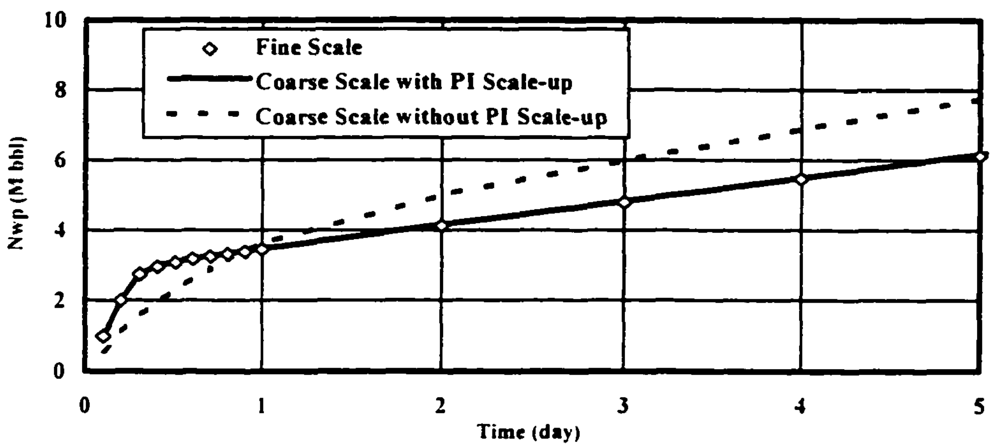

Fig. 5-36 Cum. Water Production for Well #4 of Lithofacies Model

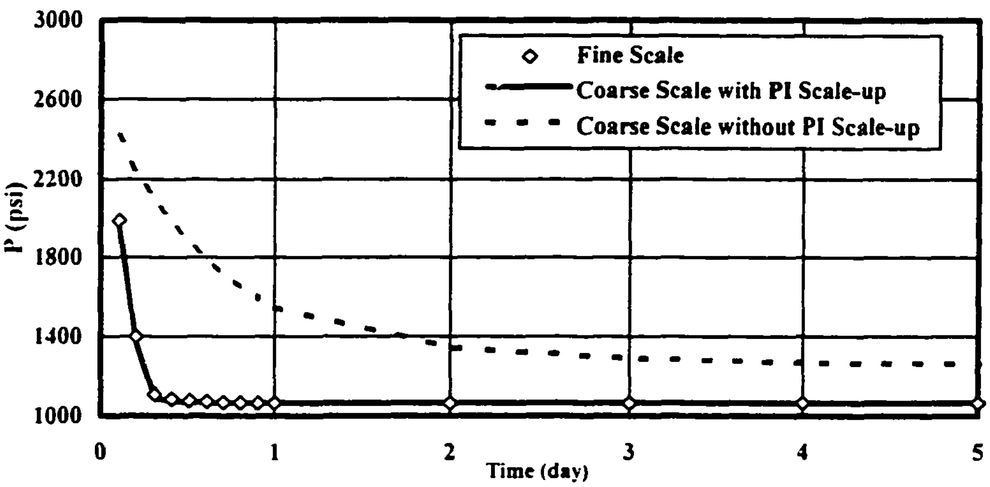

Fig. 5-37 Well Block Pressure for Well #4 of Lithofacies Model

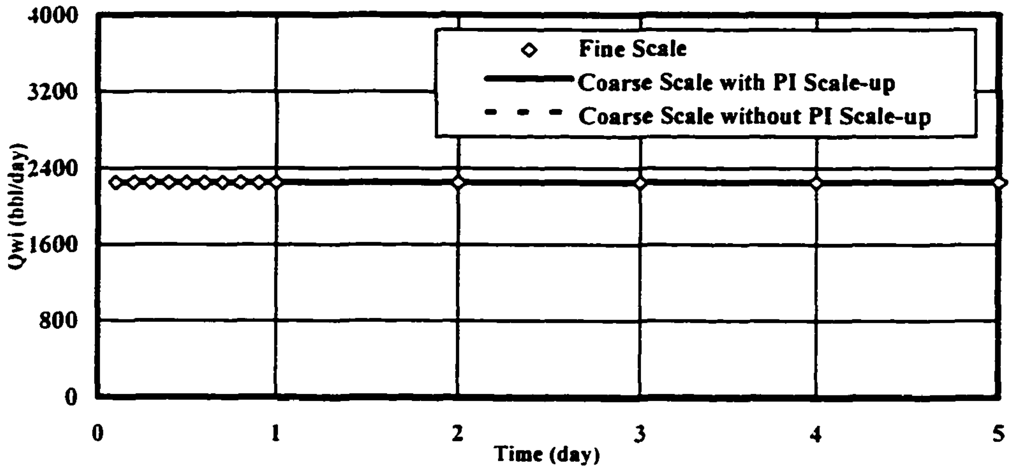

Fig. 5-38 Water Injection Rate for Well #5 of Lithofacies Model

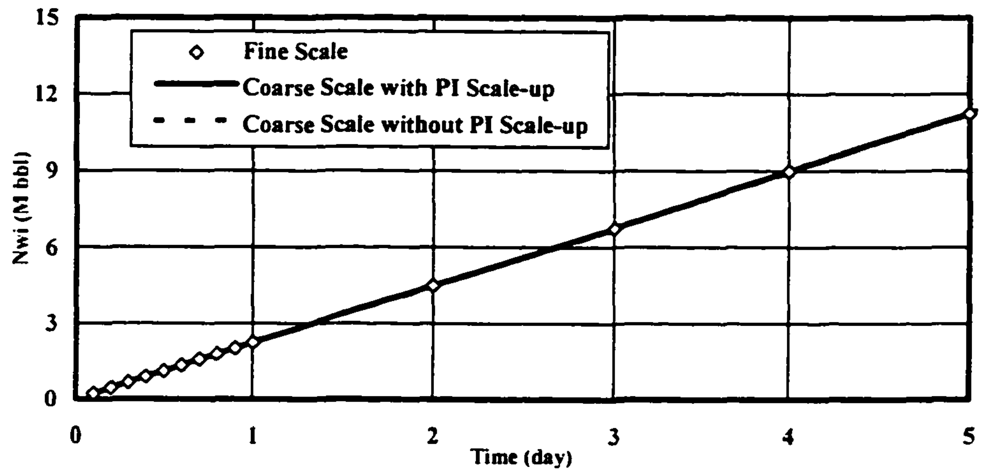

Fig. 5-39 Cum. Water Injection for Well #5 of Lithofacies Model

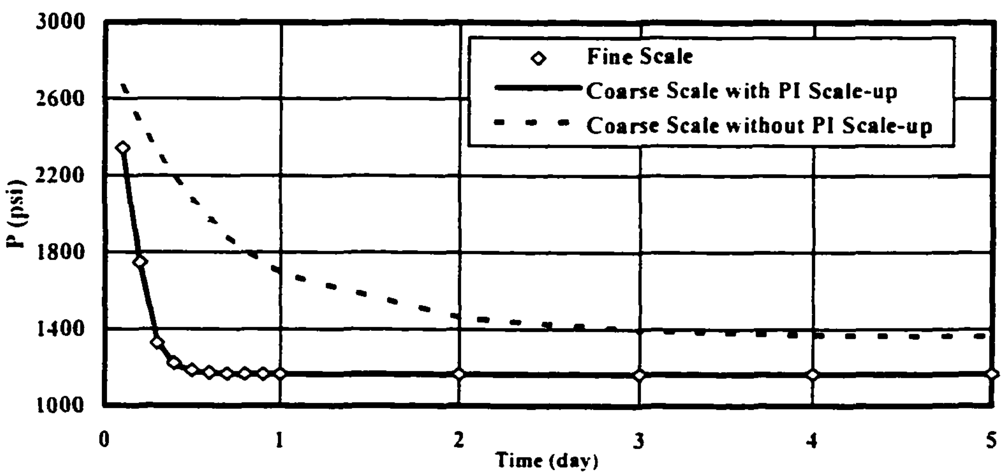

Fig. 5-40 Well Block Pressure for Well #5 of Lithofacies Model

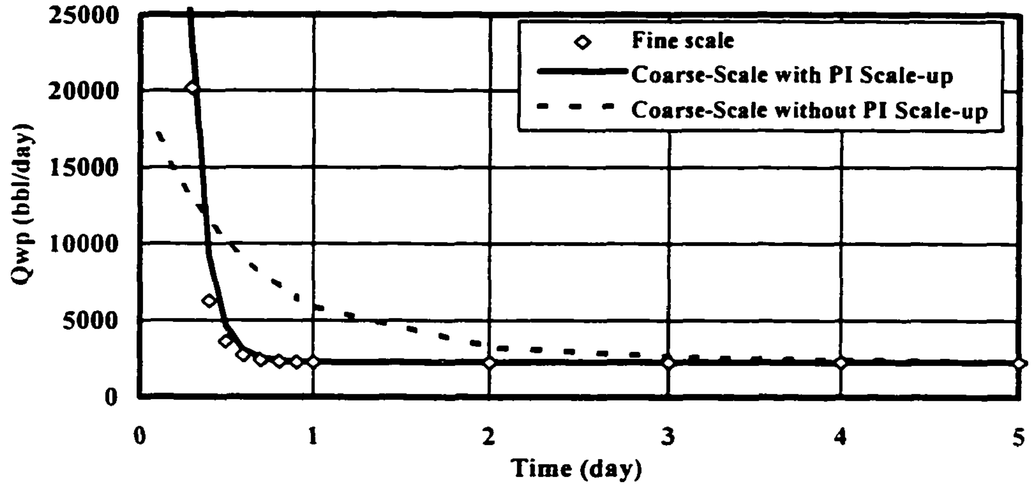

Fig. 5-41 Water Production Rate of Flow Unit Model

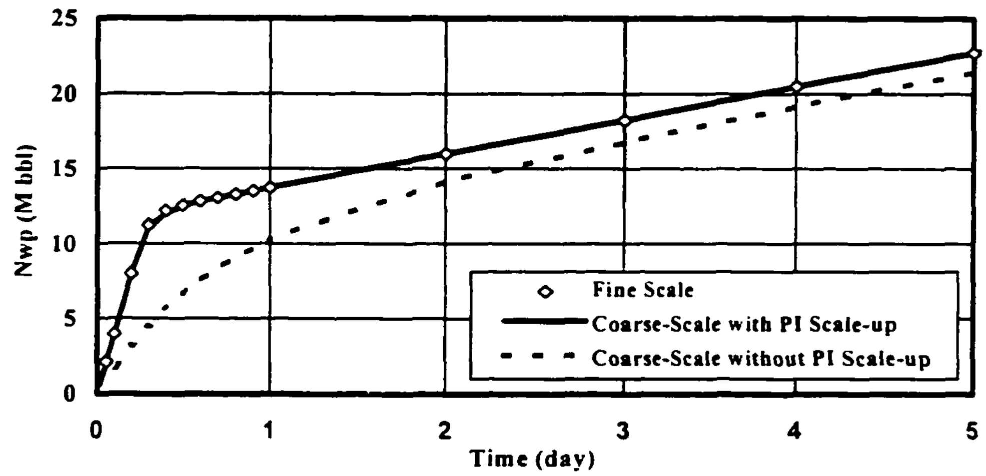

Fig. 5-42 Cum. Water Production of Flow Unit Model

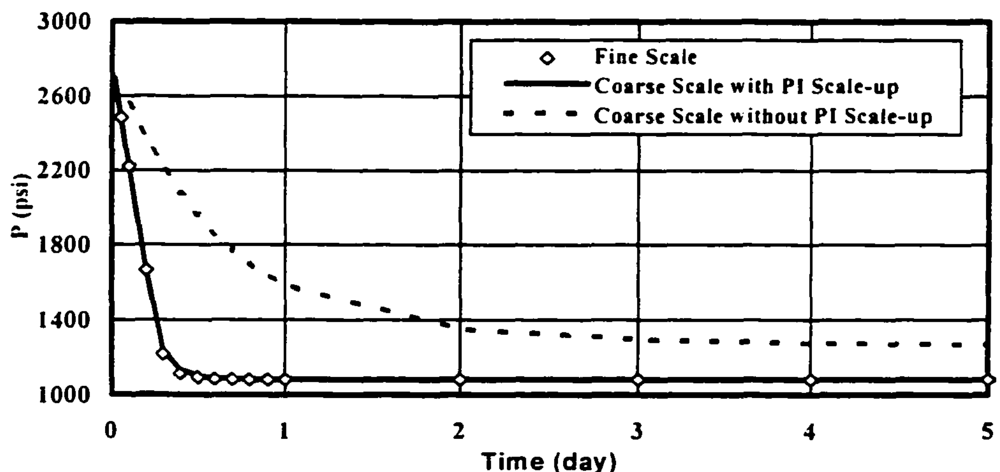

Fig. 5-43 Average Reservoir Pressure of Flow Unit Model

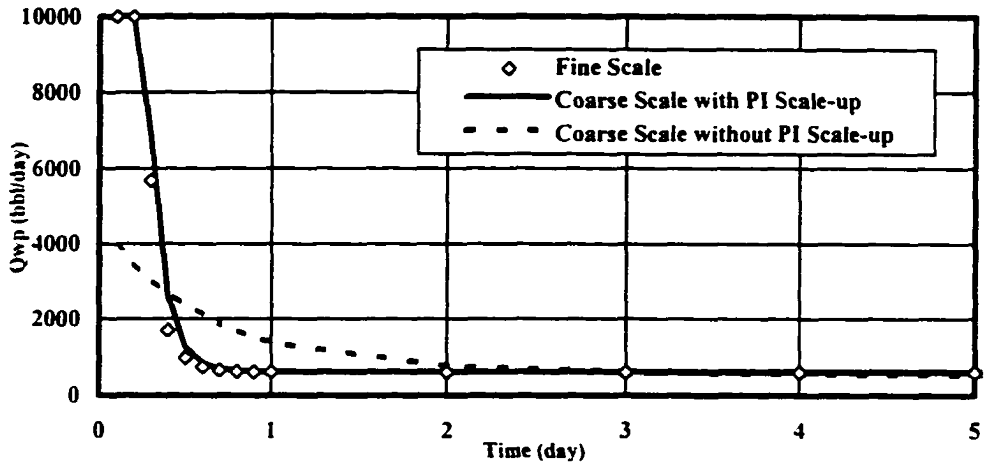

Fig. 5-44 Water Production Rate for Well #1 of Flow Unit Model

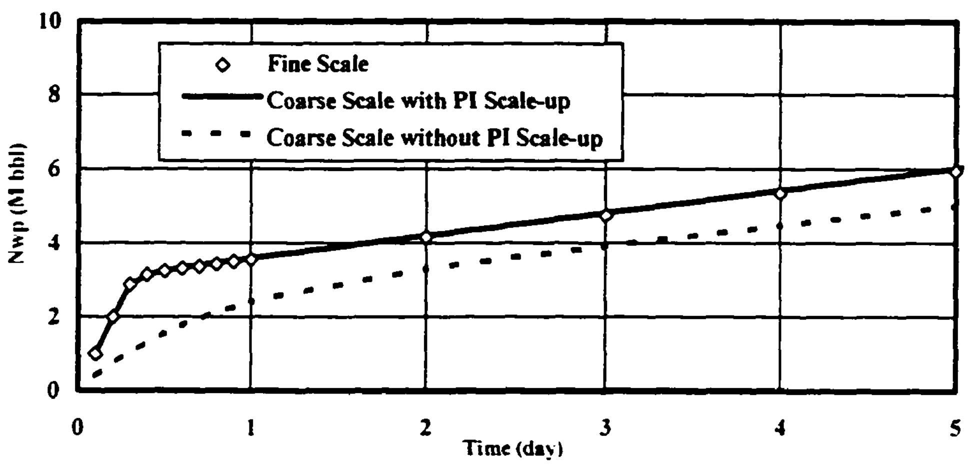

Fig. 45 Cum. Water Production for Well #1 of Flow Unit Model

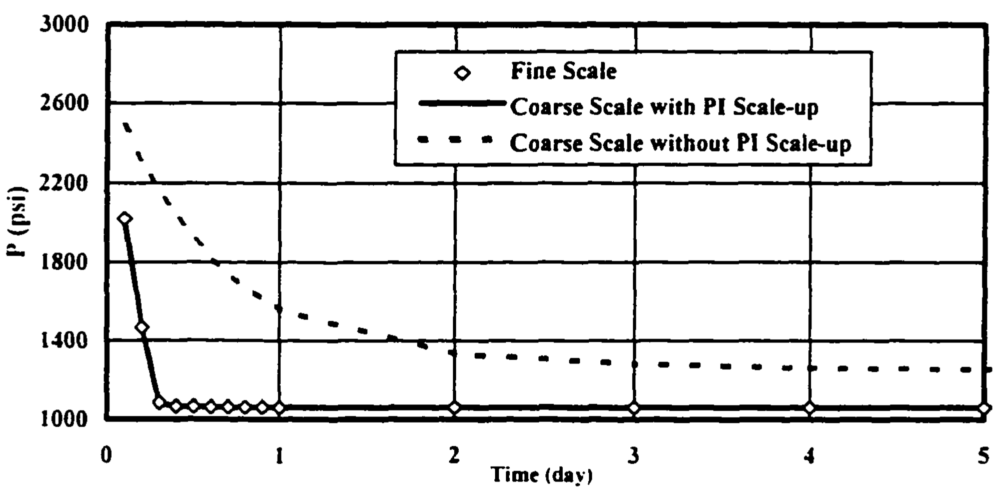

Fig. 5-46 Well Block Pressure for Well #1 of Flow Unit Model

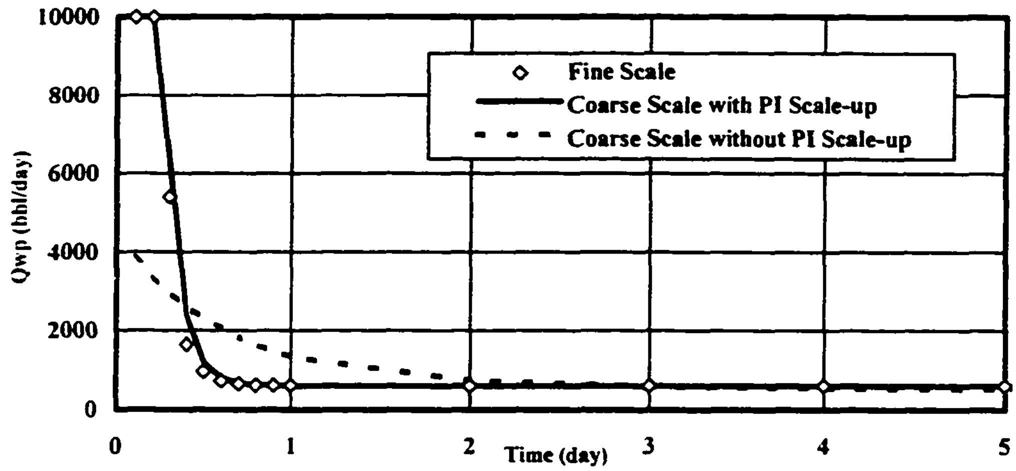

Fig. 5-47 Water Production Rate for Well #2 of Flow Unit Model

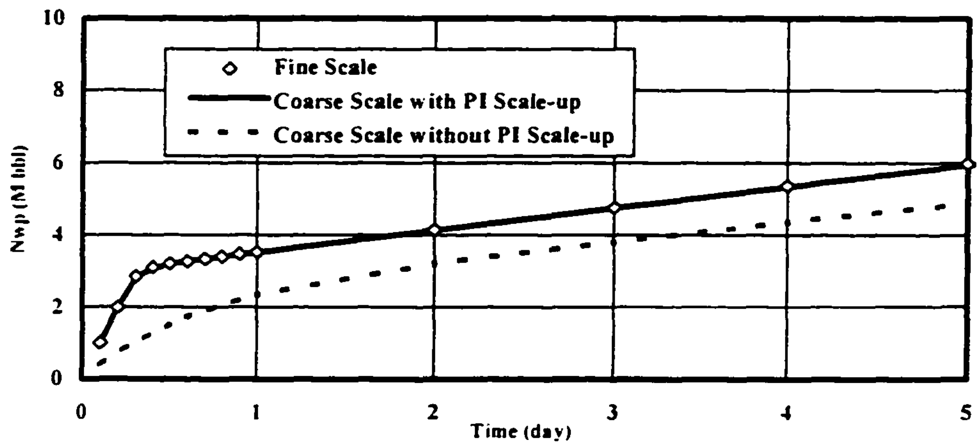

Fig. 5-48 Cum. Water Production for Well #2 of Flow Unit Model

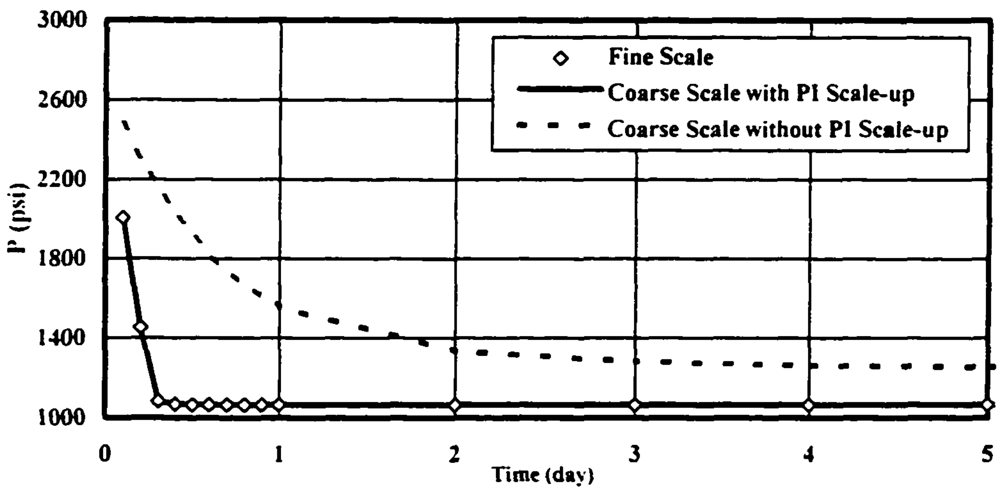

Fig. 5-49 Well Block Pressure for Well #2 of Flow Unit Model

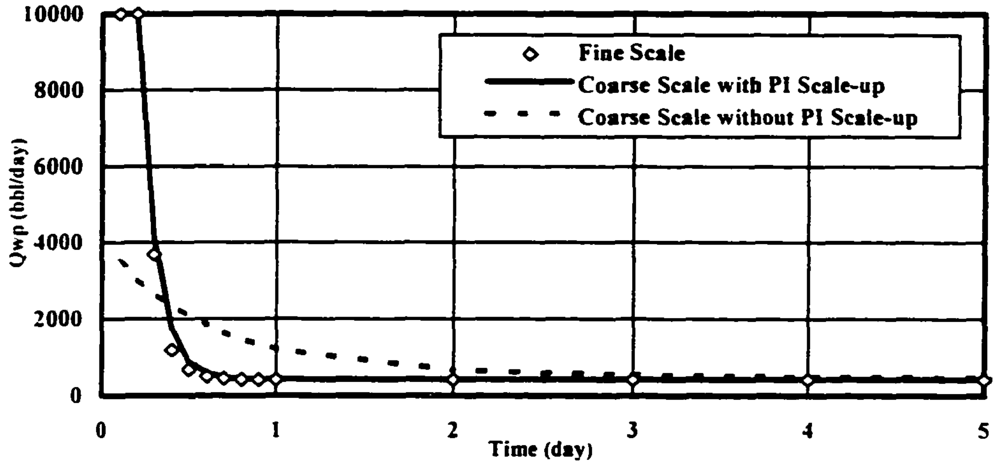

Fig. 5-50 Water Production Rate for Well #3 of Flow Unit Model

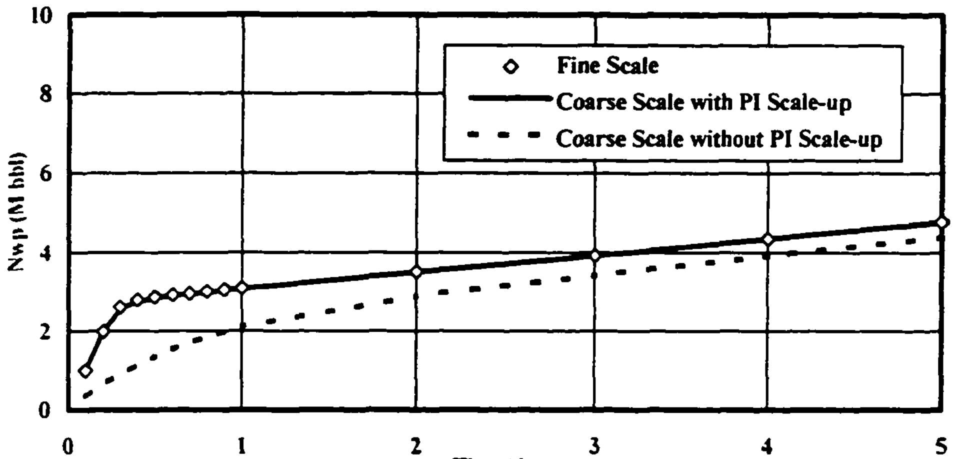

Fig. 5-51 Cum. Water Production for Well #3 of Flow Unit Model

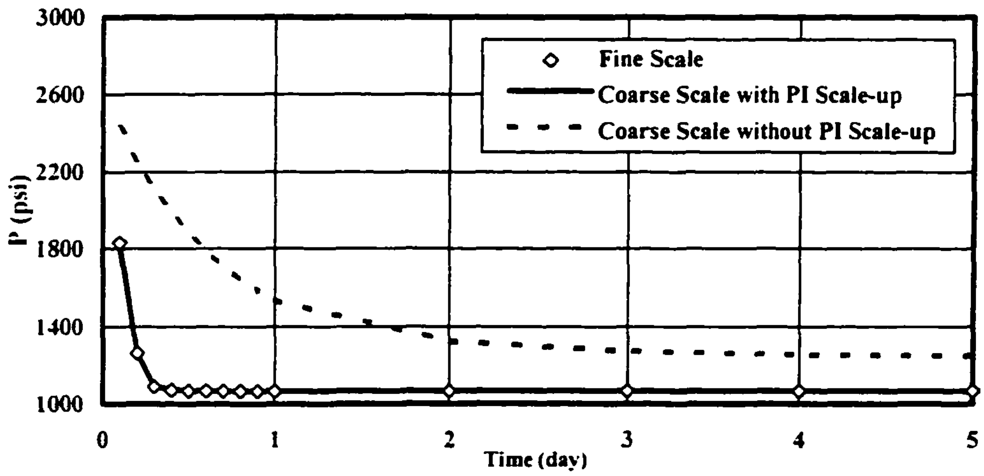

Fig. 5-52 Well Block Pressure for Well #3 of Flow Unit Model

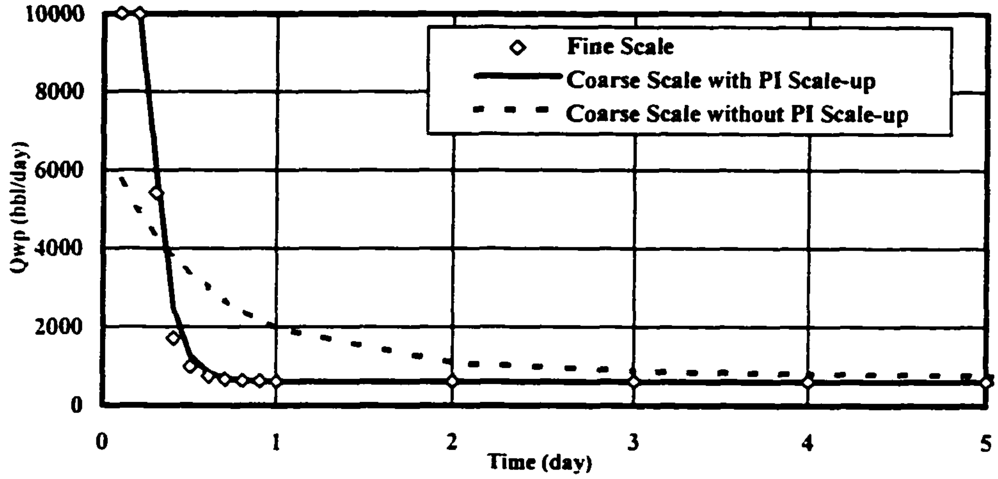

Fig. 5-53 Water Production Rate for Well #4 of Flow Unit Model

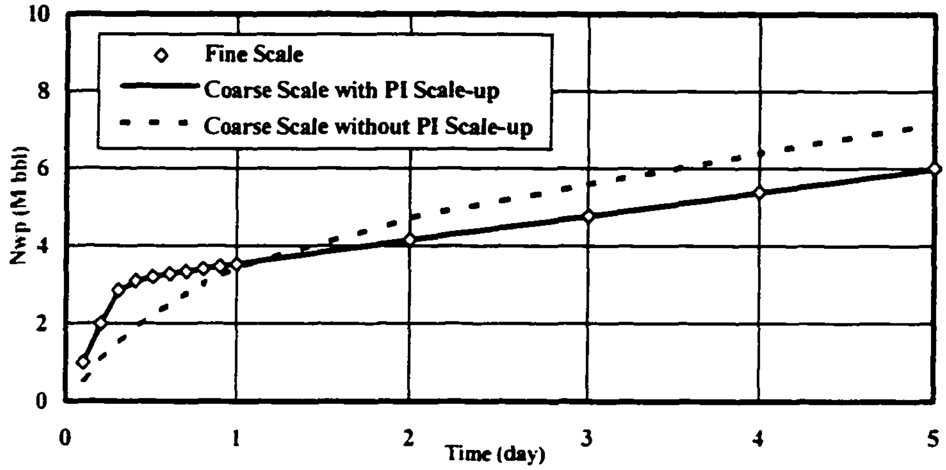

Fig. 5-54 Cum. Water Production for Well #4 of Flow Unit Model

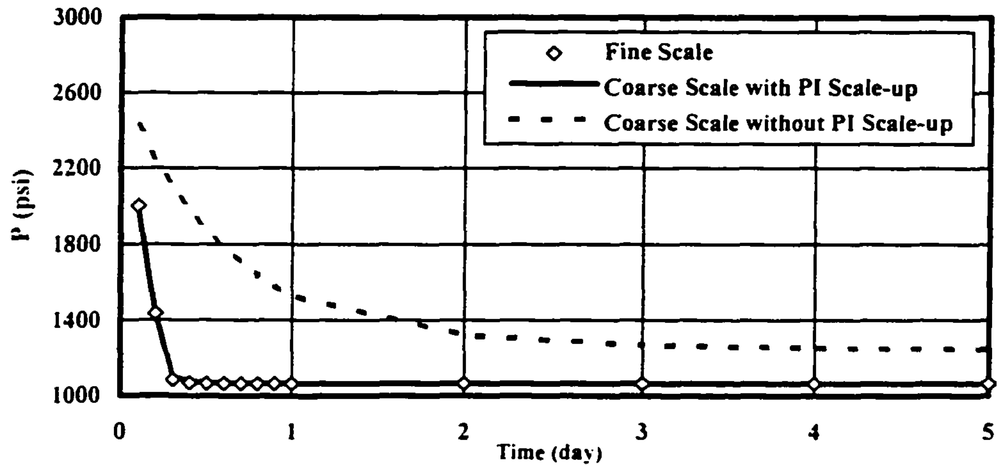

Fig. 5-55 Well Block Pressure for Well #4 of Flow Unit Model

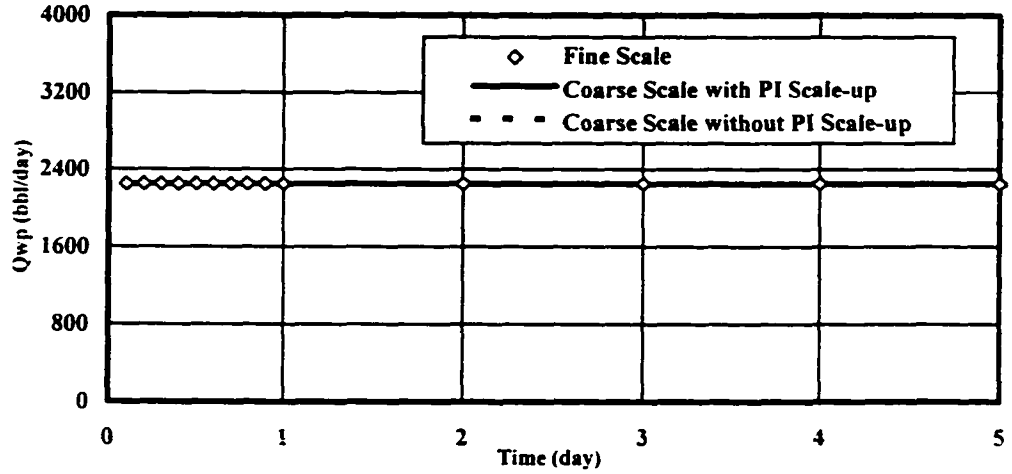

Fig. 5-56 Water Injection Rate for Well #5 of Flow Unit Model

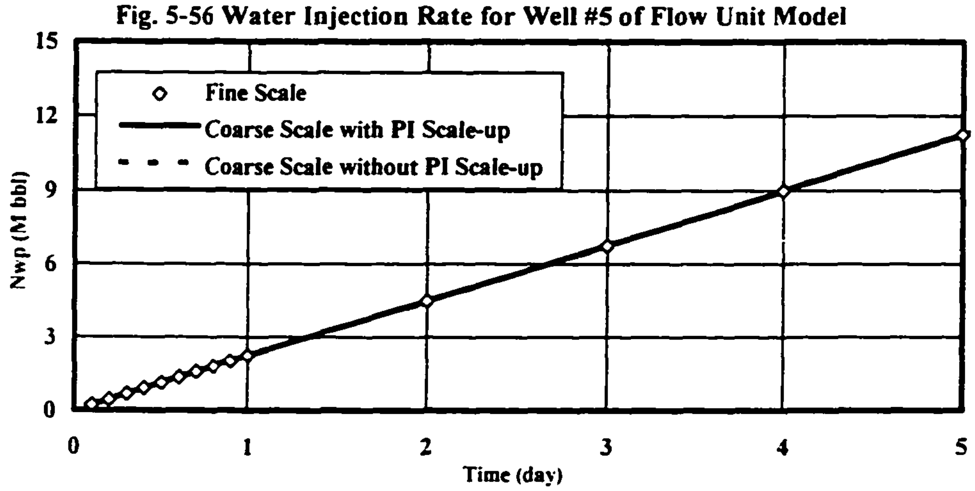

Fig. 5-57 Cum. Water Injection for Well #5 of Flow Unit Model

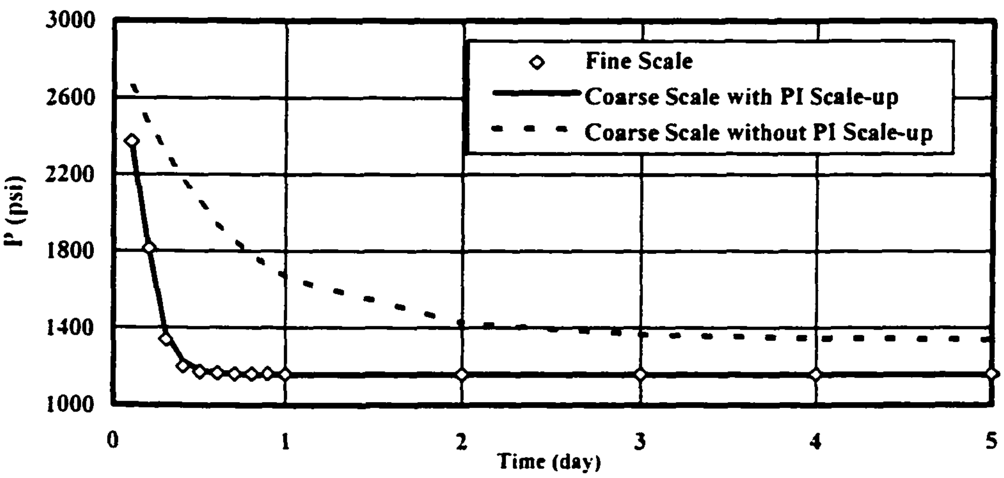

Fig. 5-58 Well Block Pressure for Well #5 of Flow Unit Model

5.3 Effects of Geological Modeling on Scale-up

The scale-up results for three Gypsy models were discussed and provided in section 5.2. In this section, the results are compared and evaluated using relative error method.

The relative error defined and used in this study is as follows:

$$\delta = \frac{V_C - V_F}{V_F} \tag{5-1}$$

where:

δ = relative error.

V_C = value obtained from coarse scale.

V_F = value obtained from fine scale.

Figs. 5-59 to 5-64 show the comparisons of water production rate. cumulative water production. and reservoir pressure for fine scale and coarse scale of the three models with and without PI scale-up. In order to study the effects of geological modeling on scale-up. the comparisons of 28-layer and 13-layer coarse-scale lithofacies models. and 16-layer and 13-layer coarse-scale flowunit models are also presented in Figs. 5-91 to 5-102.

Figs. 5-59 to 5-61 show the comparison of water production rate. cumulative water production. and reservoir pressure without PI scale-up for three 13-layer upscaled models. It can be observed that without PI scale-up, the error caused by scale-up is unacceptably large. Therefore. it must be emphasized that the scale-up of productivity index is very important in scale-up. Without PI scale-up, the three models produced comparable results.

Figs. 5-62 to 5-64 show the comparison of water production rate, cumulative water production, and reservoir pressure for three models with PI scale-up for three 13-layer models. Significant improvements were obtained after considering PI scale-up. The largest error for water production, which occurred in flowunit model, is 47%. Other errors calculated were 6.7% for cumulative production, and 2.1% for reservoir pressure, which are much lower than the errors in Figs. 5-59 to 5-61. The lithofacies and channel models obtained comparable results, while the flowunit model produced the worst scale-up result in the three models.

The scale-up results for four production wells without PI scale-up were provided in Figs. 5-65 to 5-76. When PI scale-up was not performed, the lithofacies model obtained better matches in wells #1 and #2 for water production rate, and the channel model obtained better matches in wells #3 and 4. The largest error calculated is 300%, which occurred in well #4. For cumulative water production, the flowunit model obtained better matches in wells #1, #2 and #3, but the channel model obtained a better match in well #4. The largest error for cumulative production was -73% which occurred in well #3. For wellblock pressure, all three models produced similar matches in four production wells. The largest error for wellblock pressure was 103%, which occurred in well #1.

The scale-up results with PI scale-up for four production wells are shown in Figs. 5-77 to 5-88. Significant improvements were obtained in all four wells and shown in all three plots. For water production rate, the channel model obtained the best match in all four wells, while the flowunit model gave the worst. The largest error for water production rate was 55% in well #1. For cumulative water production, the lithofacies model obtained the best match and the flowunit model again obtained the worst. The largest error was only 9% in well #1. Wellblock pressure again obtained similar matches in all four wells. The largest error for wellblock pressure was only 4% in well #4.

The water injection rate and cumulative water injection were exactly the same for fine scale and coarse scale in all three models, so only the results of wellblock pressure are shown in Figs. 5-89 to 5-90. Without PI scale-up, the channel model obtained the best match, with the largest error at 80%. With PI scale-up, the lithofacies model obtained the best match. The largest error was only 2.2% in the flowunit model.

Figs. 5-91 to 5-96 show the scale-up results for 28-layer and 13-layer lithofacies models with and without PI scale-up. Without PI scale-up, two models produced basically the same matches in water production rate. The 13-layer model obtained better matches in cumulative production and reservoir pressure than the 28-layer model. With PI scale-up, the 28-layer model produced a better result in water production, but the 13-layer model produced better results in cumulative water production and reservoir pressure.

Figs. 5-97 to 5-102 show the results for two flowunit models. Without PI scale-up, the 13-layer model produced better results than the 16-layer model in water production rate, cumulative water production, and reservoir pressure. With PI scale-up, the 13-layer model still produced significantly better results than the 16-layer model in all plots.

Based on the scale-up results on three geological models presented in Figs. 5-5 to 5-102, and the discussion above, the following statements can be made:

1. When scale-up of transmissibility is conducted, PI scale-up must be included. Without PI scale-up, the results are unacceptable, especially at onset of the production. The highest relative error produced without PI scale-up was up to 230% in water production rate.
2. Strategies of geological modeling have significant effects on scale-up. With PI scale-up, the channel model and the lithofacies model produced comparable matches. However, the flowunit model produced the worst matches in both water production and reservoir pressure. This is not consistent with expectations that the lithofacies model should produce the best match, and the channel model produce the worst.
3. When analyzing the process of geological modeling, the lithofacies unit is the smallest and most homogenous unit obtainable. However, when the lithofacies unit was divided into many layers to develop the fine-scale model, many grid blocks in the same layer in fine-scale model did not connect to each other horizontally. Therefore, no horizontal flow occurred between these grid blocks in the mathematical model. In real reservoir condition, even though these grid blocks do not connect to other grid blocks in the same layer, horizontal flow would still exist in these grid blocks, i.e., between the grid blocks belonging to different lithofacies unit. Therefore, a finer-scale model does not necessarily produce more accurate results.

There is a limit to the degree of fine-scale that the model should have as good as possible horizontal communication. If too fine a scale is used, the model may lead to wrong simulation results, because the flow configuration was changed due to the limitation of mathematical strategies in simulator.

4. In the lithofacies model, the 28-layer model did not improve the scale-up results beyond that of the 13-layer model. The same is true for the flowunit model, i.e., the 16-layer model did not show better results than the 13-layer model, in fact, the accuracy decreased. This indicates that between two flow barriers, having more homogeneous lithofacies units or flow units as the targets for scale-up may not improve modeling results, probably due to a 'horizontal pinch-out' effect. Therefore, in reservoir simulation and scale-up, optimizing results occurs when the individual layer is as homogeneous as possible and the horizontal distribution of each layer is as wide as possible.

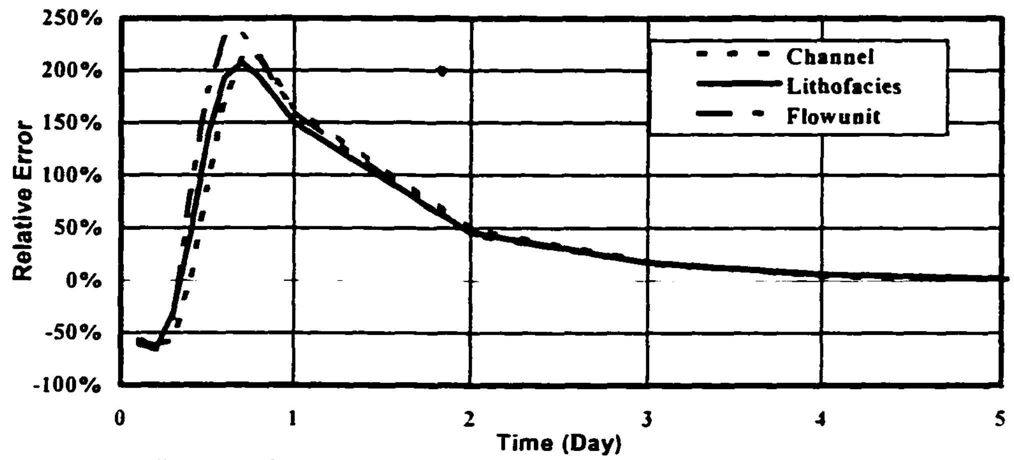

Fig. 5-59 Relative Errors of Water Production Rate for Different Models Without PI Scale-up

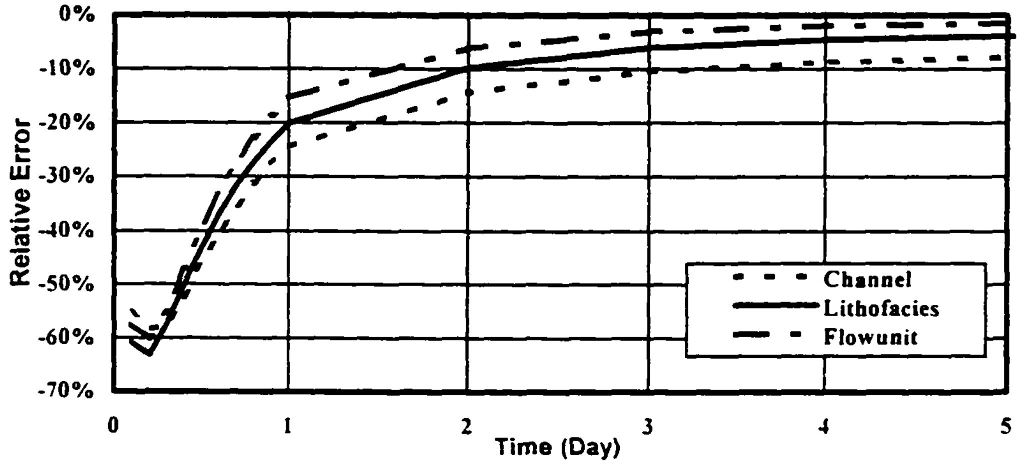

Fig. 5-60 Relative Errors of Cum. Water Production Rate for Different Models Without PI Scale-up

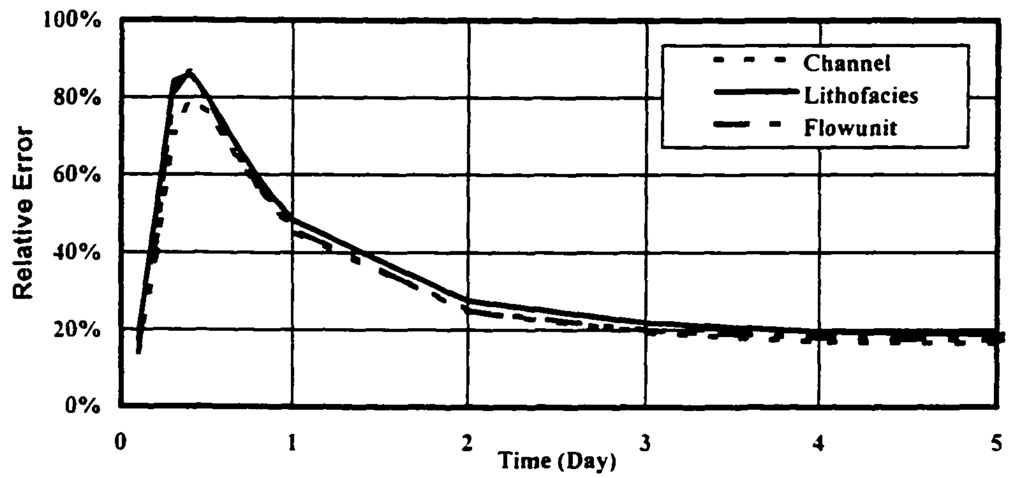

Fig. 5-61 Relative Errors of Reservoir Pressure for Different Models Without PI Scale-up

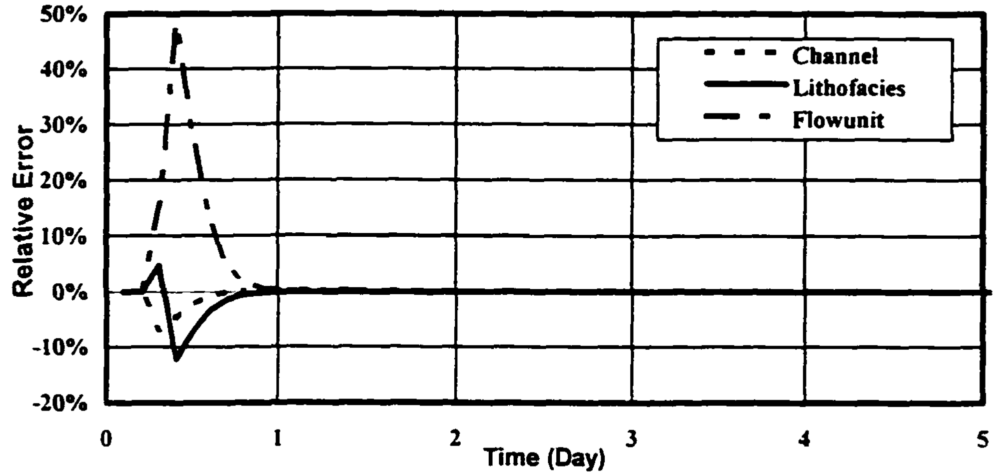

Fig. 5-62 Relative Errors of Water Production Rate for Different Models With PI Scale-up

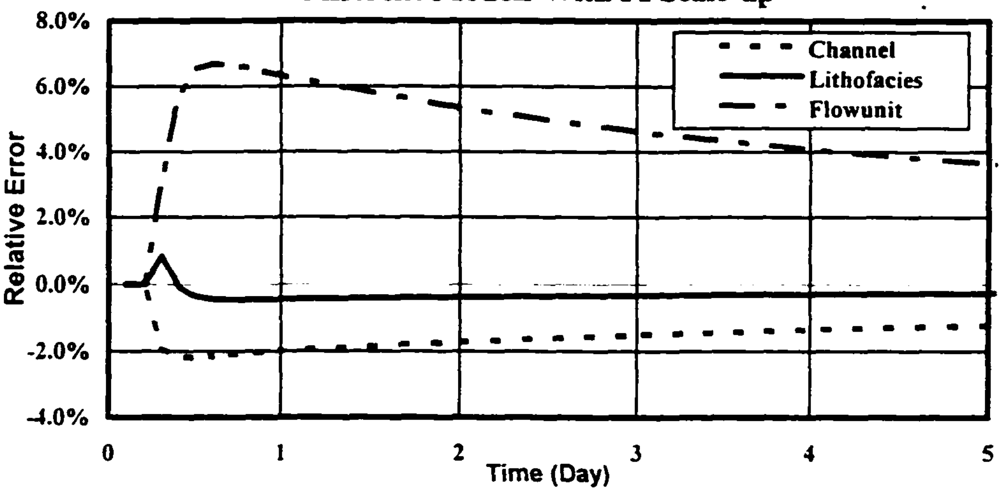

Fig. 5-63 Relative Errors of Cum. Water Production Rate for Different Models With PI Scale-up

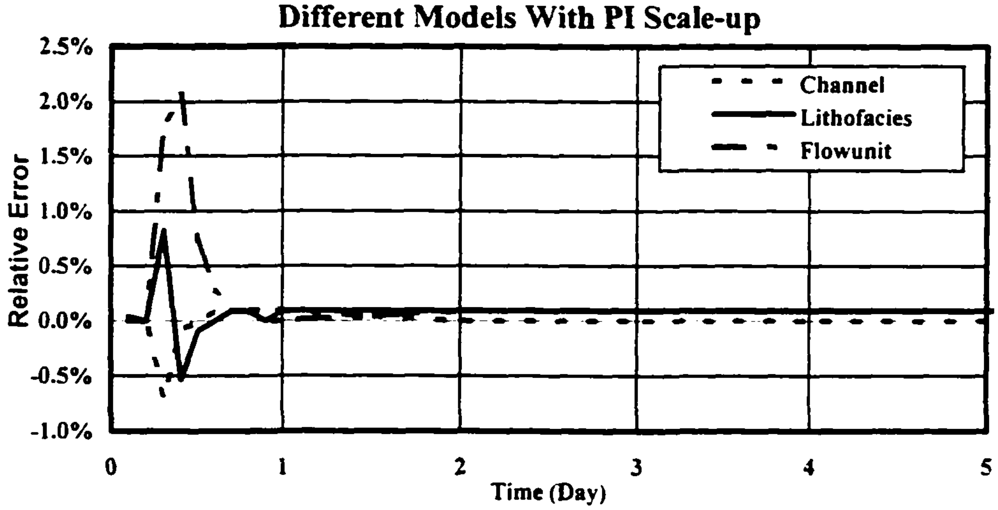

Fig. 5-64 Relative Errors of Reservoir Pressure for Different Models With PI Scale-up

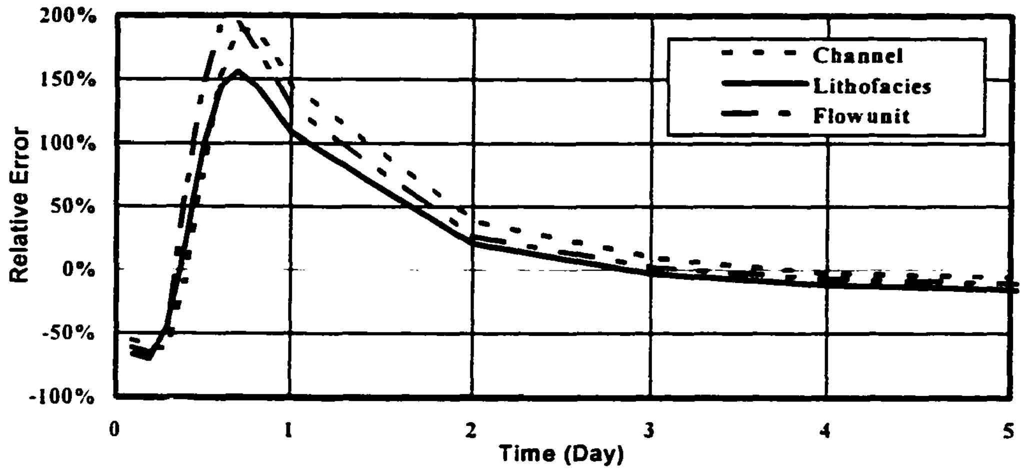

Fig. 5-65 Relative Errors of Water Production Rate Without PI Scale-up for Well #1 in Three Different Models

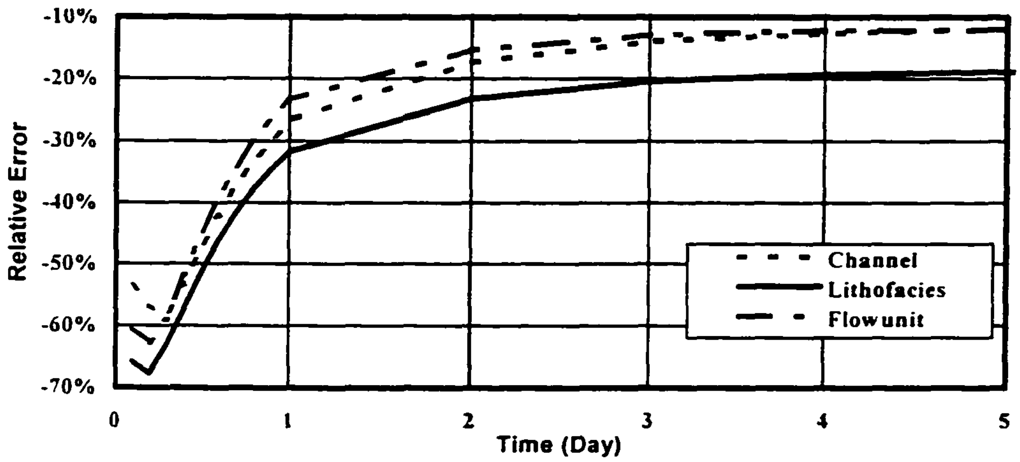

Fig. 5-66 Relative Errors of Cum. Water Production Without PI Scale-up for Well #1 in Three Different Models

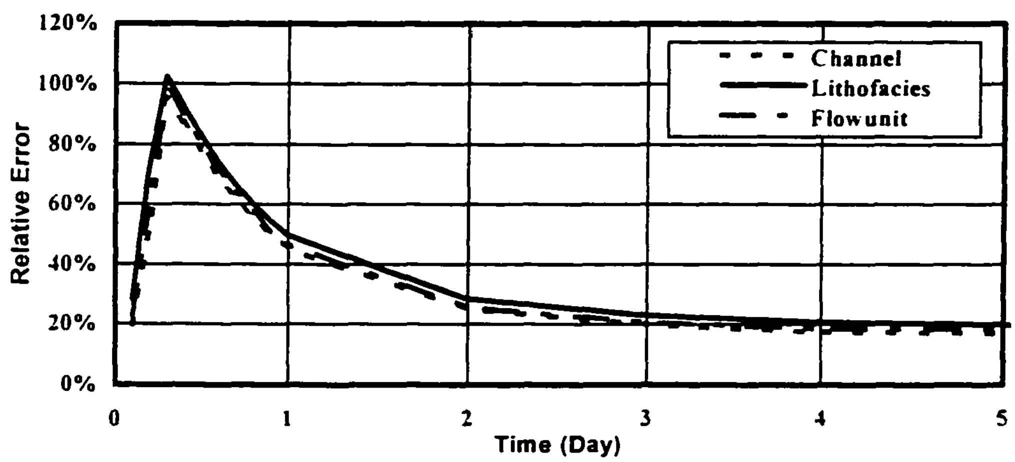

Fig. 5-67 Relative Errors of Average Wellblock Pressure Without PI Scale-up for Well #1 in Three Different Models

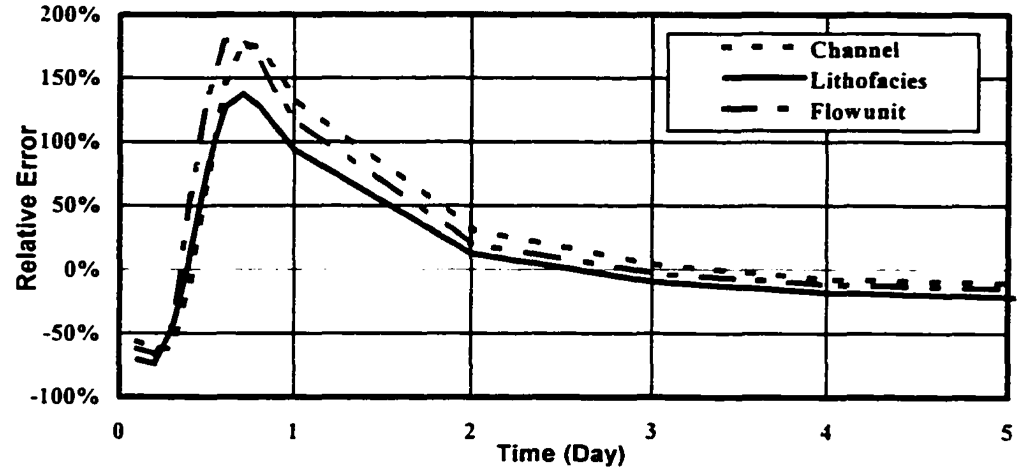

Fig. 5-68 Relative Errors of Water Production Rate Without PI Scale-up for Well #2 in Three Different Models

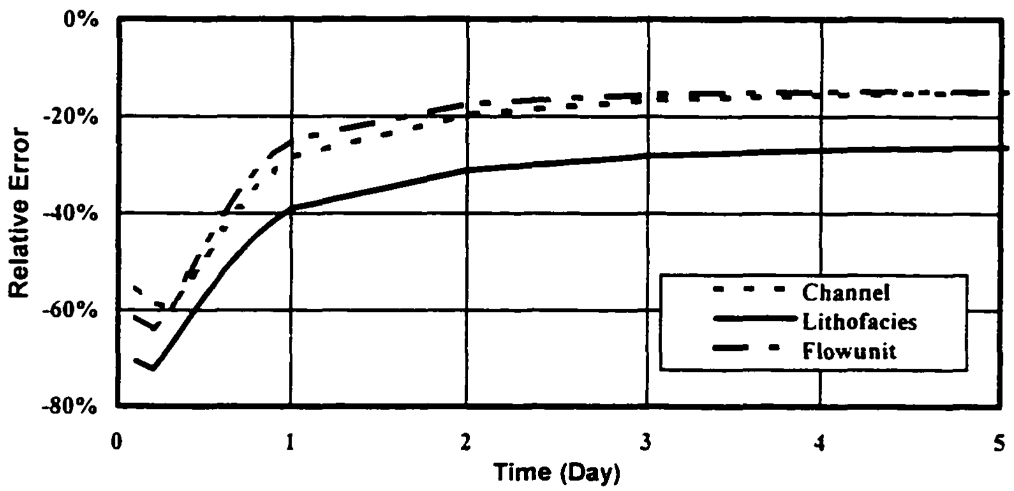

Fig. 5-69 Relative Errors of Cum. Water Production Without PI Scale-up for Well #2 in Three Different Models

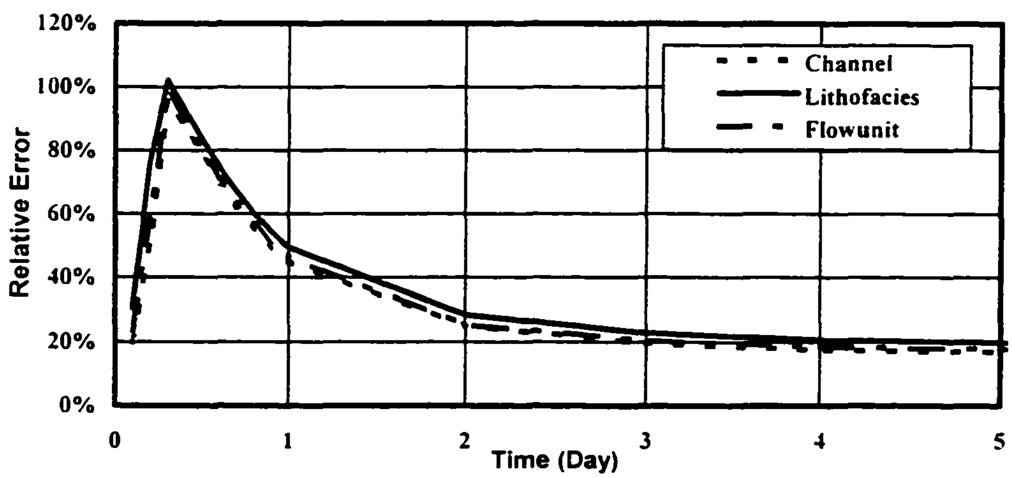

Fig. 5-70 Relative Errors of Average Wellblock Pressure Without PI Scale-up for Well #2 in Three Different Models

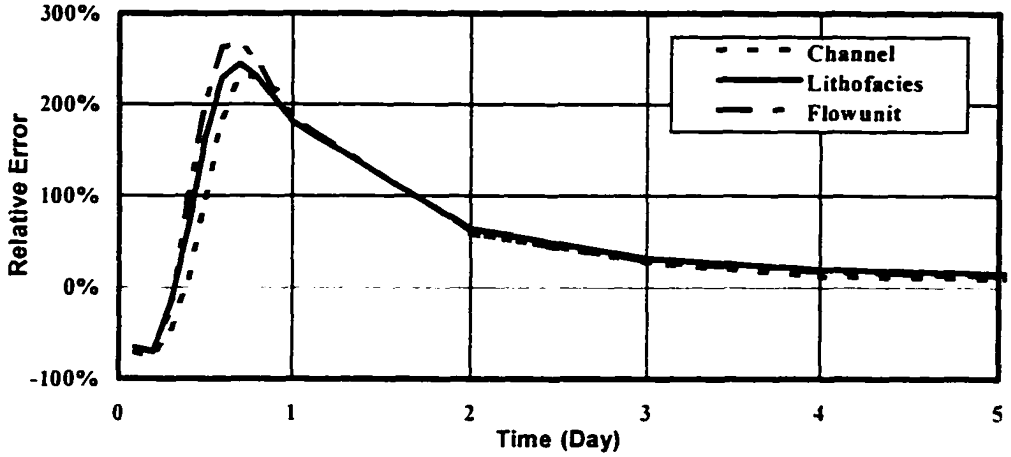

Fig. 5-71 Relative Errors of Water Production Rate Without PI Scale-up for Well #3 in Three Different Models

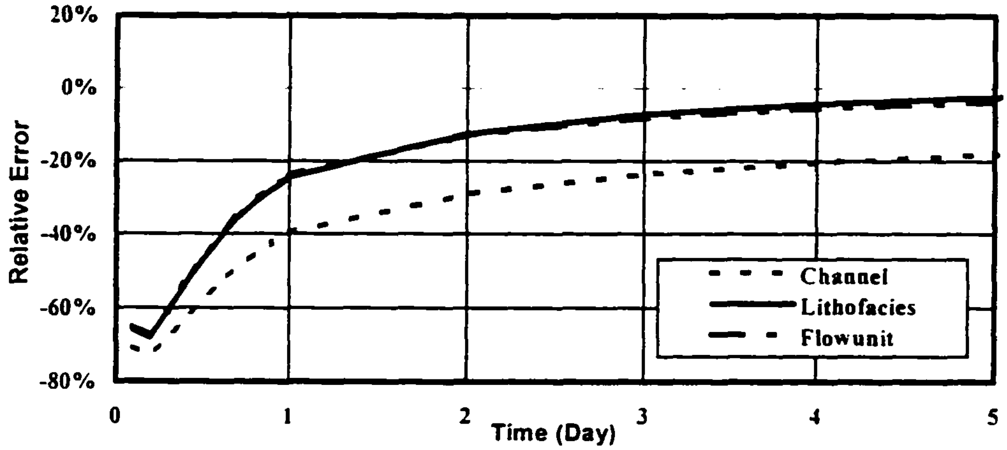

Fig. 5-72 Relative Errors of Cum. Water Production Without PI Scale-up for Well #3 in Three Different Models

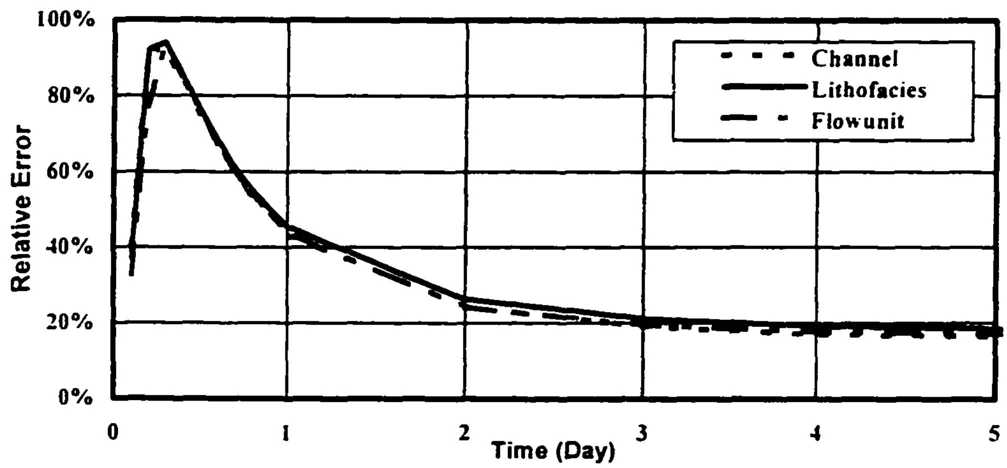

Fig. 5-73 Relative Errors of Average Wellblock Pressure Without PI Scale-up for Well #3 in Three Different Models

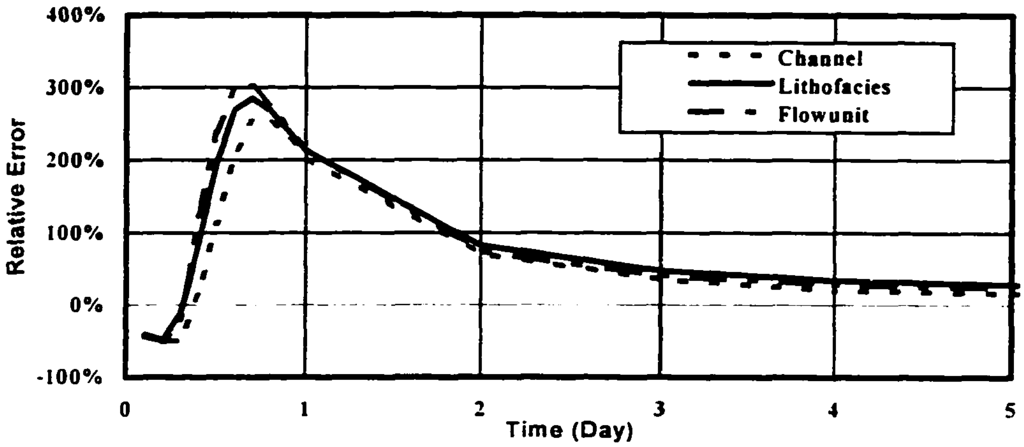

Fig. 5-74 Relative Errors of Water Production Rate Without PI Scale-up for Well #4 in Three Different Models

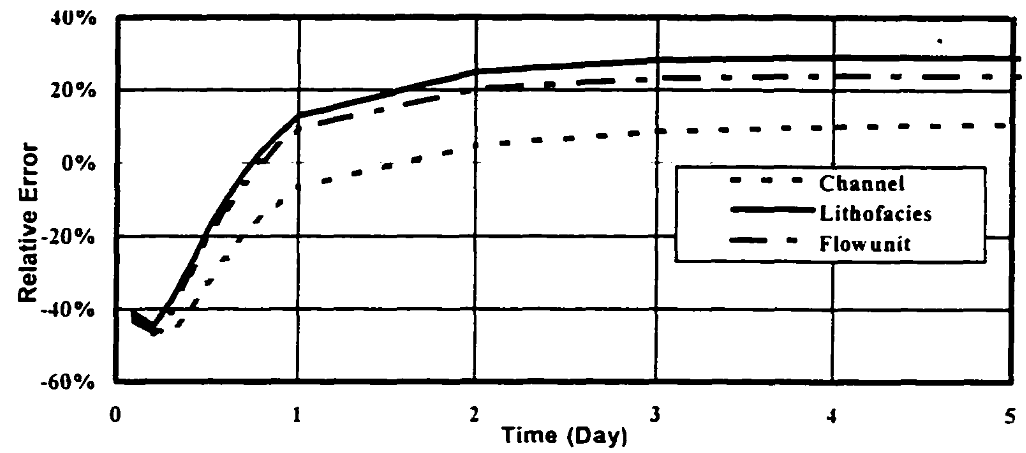

Fig. 5-75 Relative Errors of Cum. Water Production Without PI Scale-up for Well #4 in Three Different Models

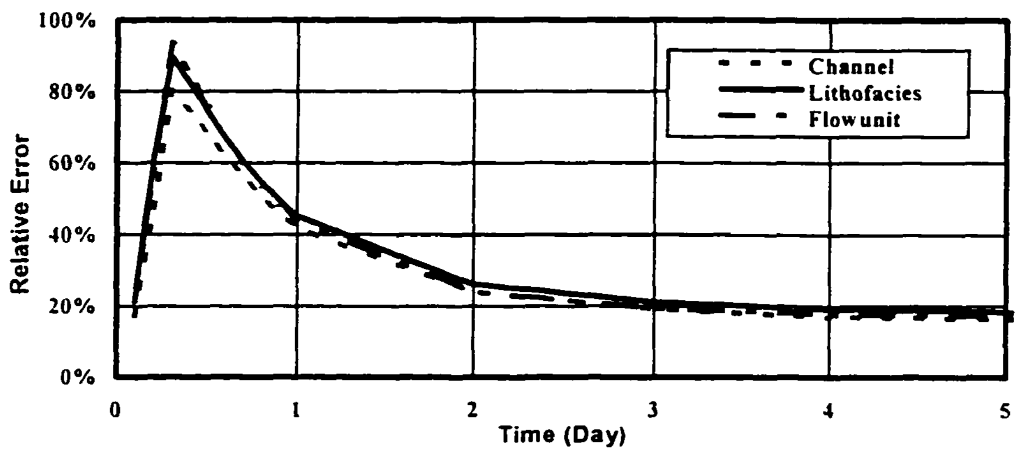

Fig. 5-76 Relative Errors of Average Wellblock Pressure Without PI Scale-up for Well #4 in Three Different Models

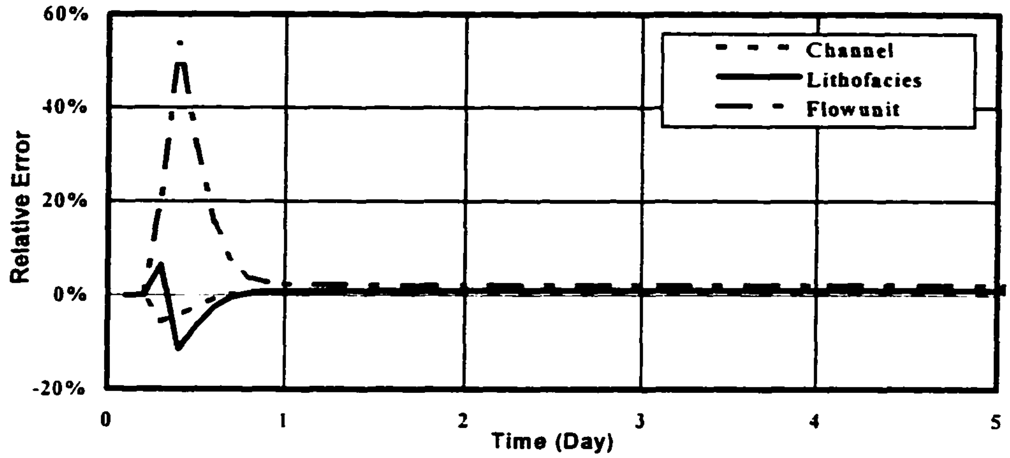

Fig. 5-77 Relative Errors of Water Production Rate With PI Scale-up for Well #1 in Three Different Models

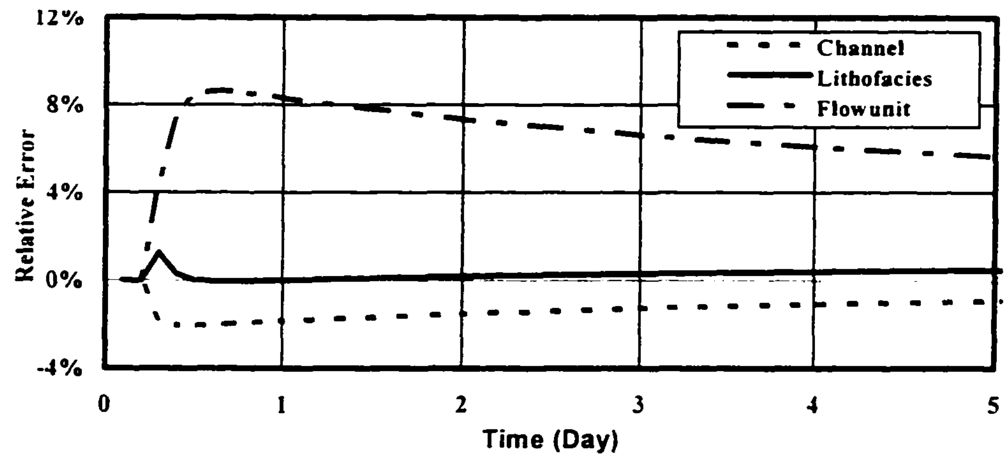

Fig. 5-78 Relative Errors of Cum. Water Production With PI Scale-up for Well #1 in Three Different Models

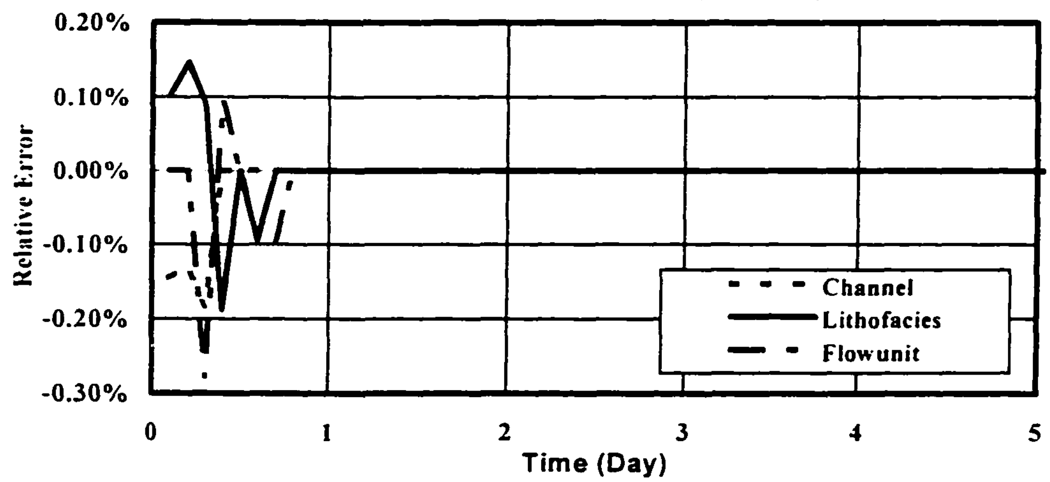

Fig. 5-79 Relative Errors of Average Wellblock Pressure With PI Scale-up for Well #1 in Three Different Models

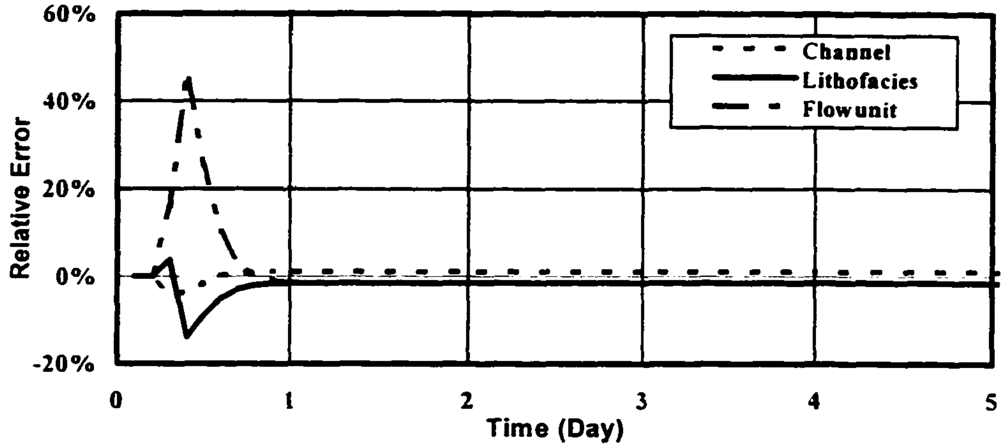

Fig. 5-80 Relative Errors of Water Production Rate With PI Scale-up for Well #2 in Three Different Models

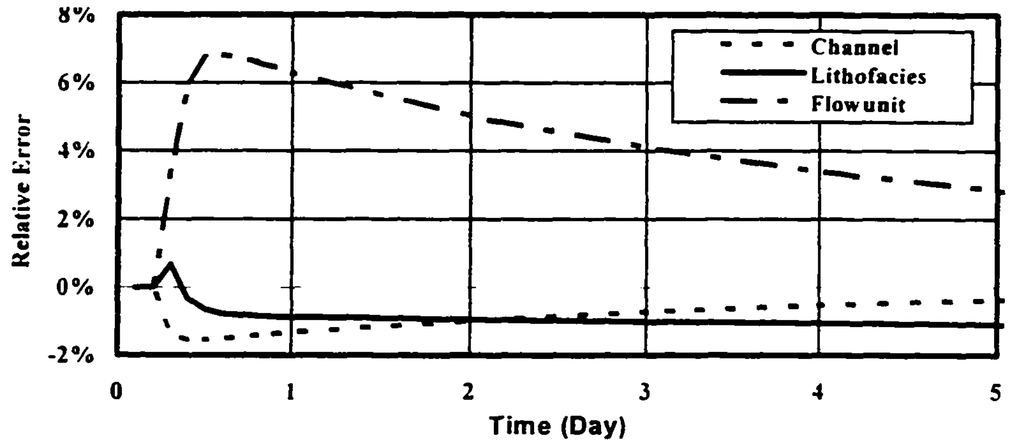

Fig. 5-81 Relative Errors of Cum. Water Production With PI Scale-up for Well #2 in Three Different Models

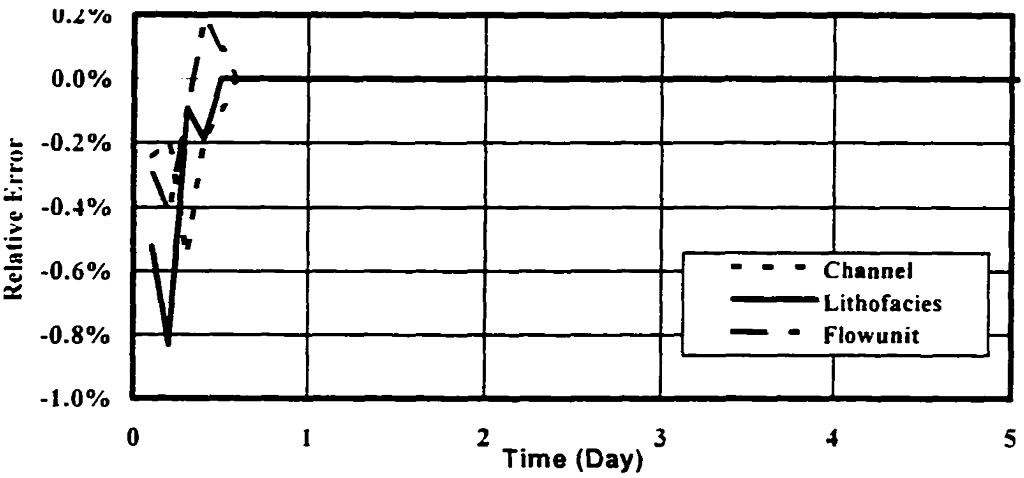

Fig. 5-82 Relative Errors of Average Wellblock Pressure With PI Scale-up for Well #2 in Three Different Models

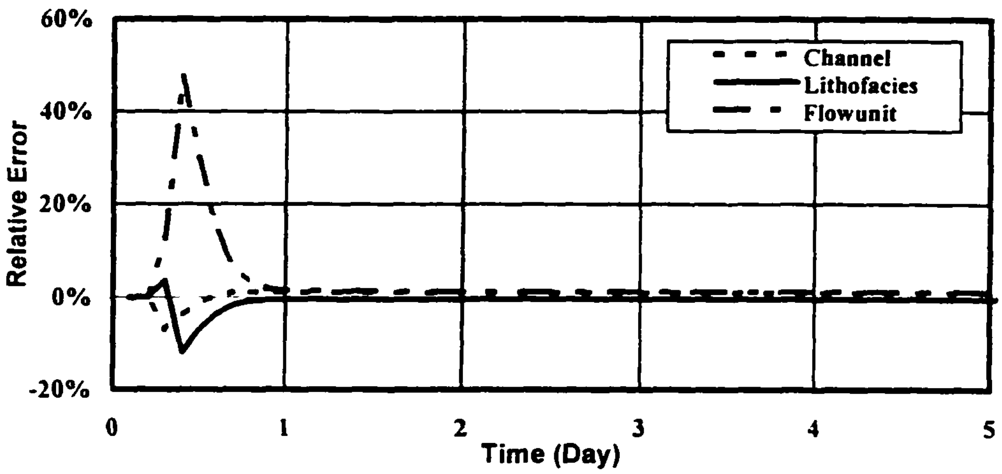

Fig. 5-83 Relative Errors of Water Production Rate With PI Scale-up for Well #3 in Three Different Models

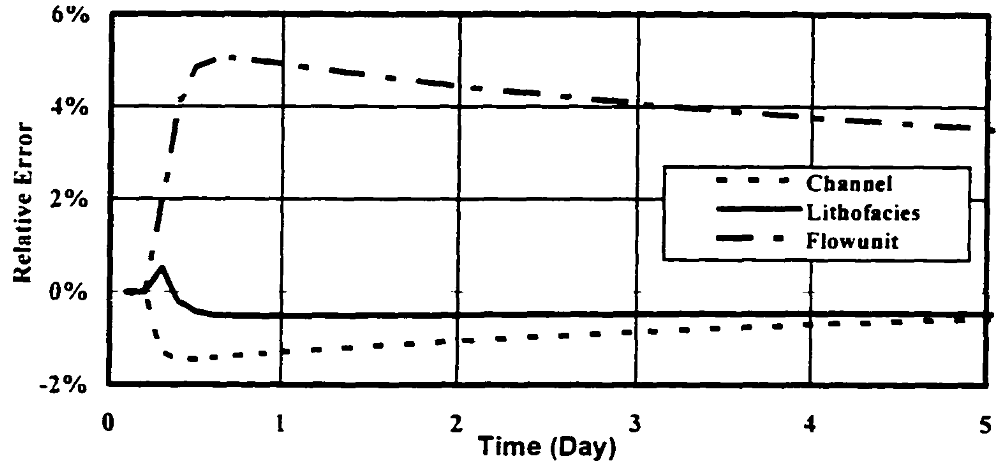

Fig. 5-84 Relative Errors of Cum. Water Production With PI Scale-up for Well #3 in Three Different Models

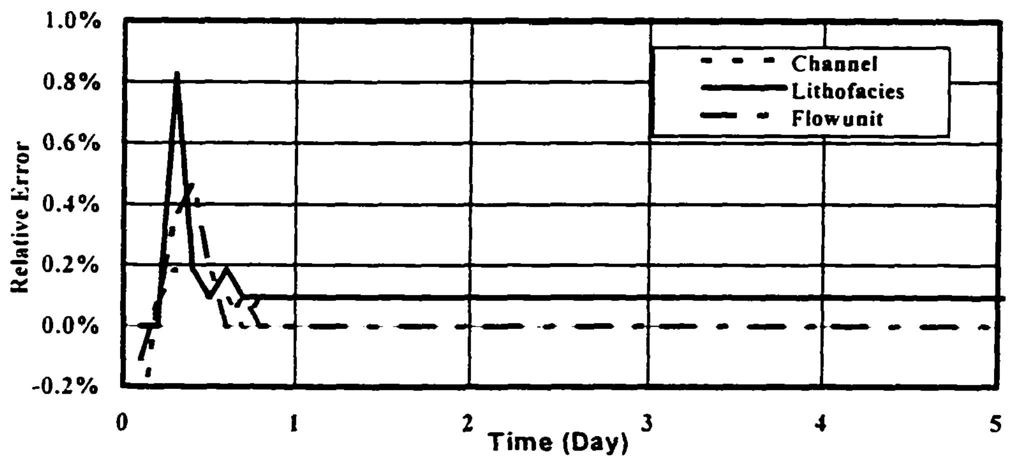

Fig. 5-85 Relative Errors of Average Wellblock Pressure With PI Scale-up for Well #3 in Three Different Models

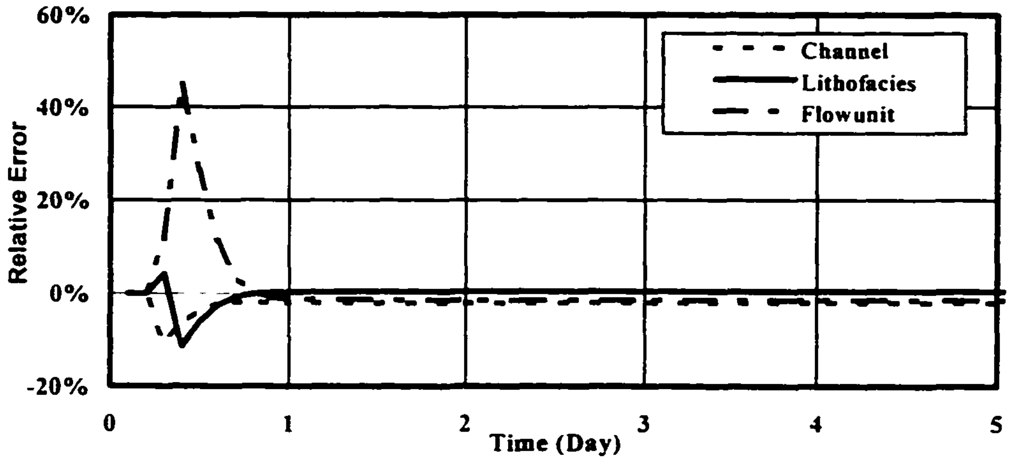

Fig. 5-86 Relative Errors of Water Production Rate With PI Scale-up for Well #4 in Three Different Models

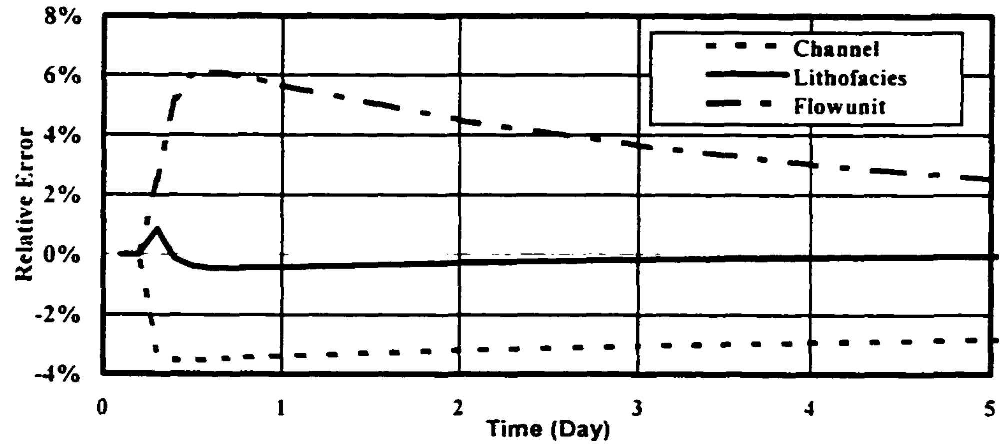

Fig. 5-87 Relative Errors of Cum. Water Production With PI Scale-up for Well #4 in Three Different Models

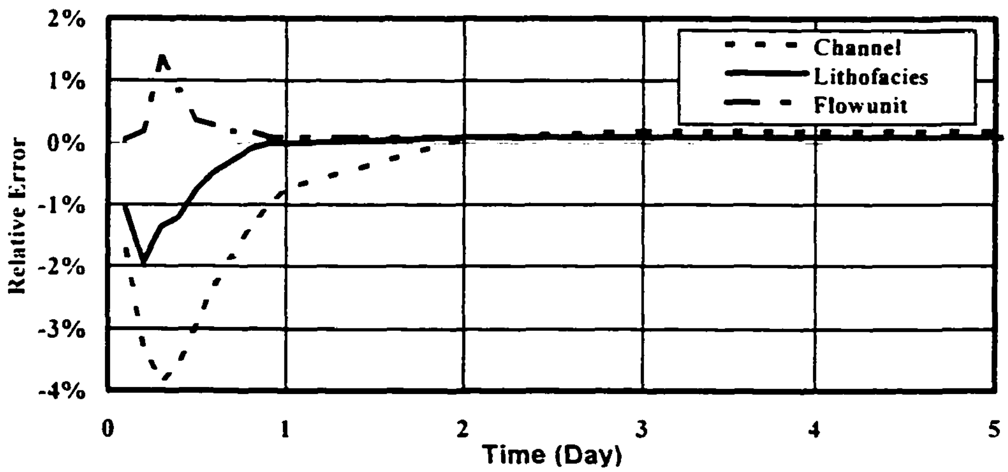

Fig. 5-88 Relative Errors of Average Wellblock Pressure With PI Scale-up for Well #4 in Three Different Models

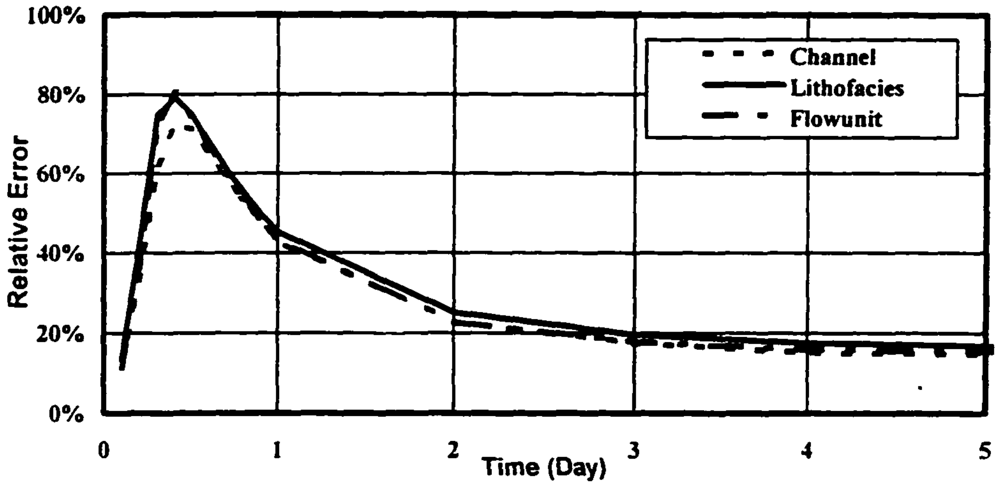

Fig. 5-89 Relative Errors of Wellblock Pressure Without PI Scale-up for Well #5 in Three Different Models

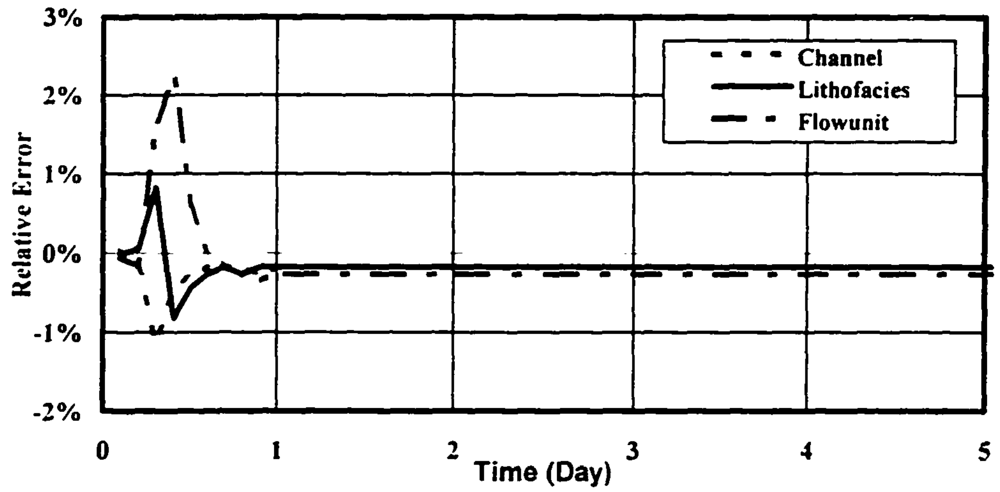

Fig. 5-90 Relative Errors of Wellblock Pressure With PI Scale-up for Well #5 in Three Different Models

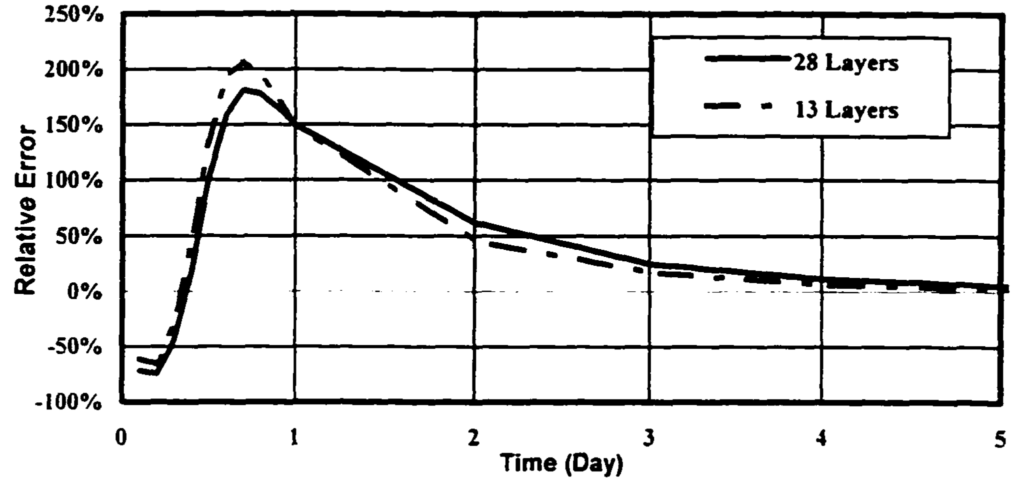

Fig. 5-91 Relative Errors of Water Production Rate Without PI Scale-up for Lithofacies Models

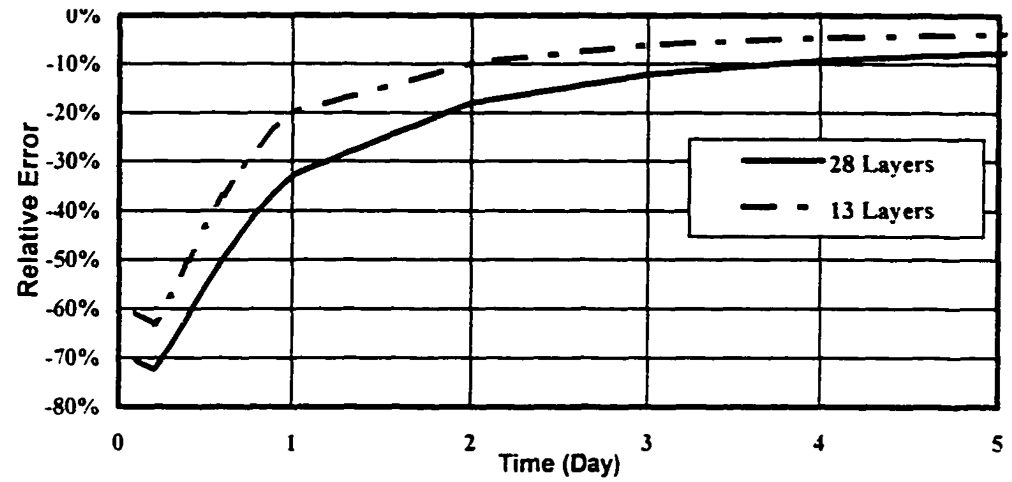

Fig. 5-92 Relative Errors of Cum. Water Production Without PI Scale-up for Lithofacies Models

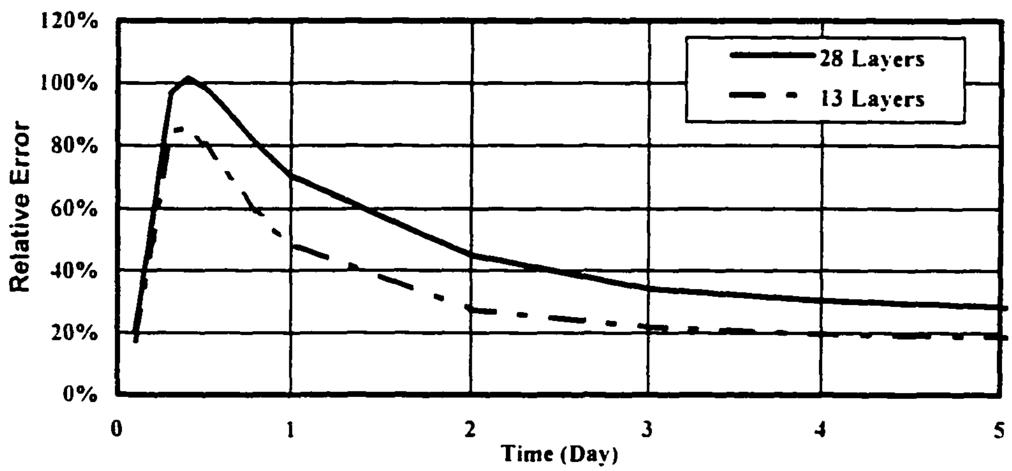

Fig. 5-93 Relative Errors of Average Reservoir Pressure Without PI Scale-up for Lithofacies Models

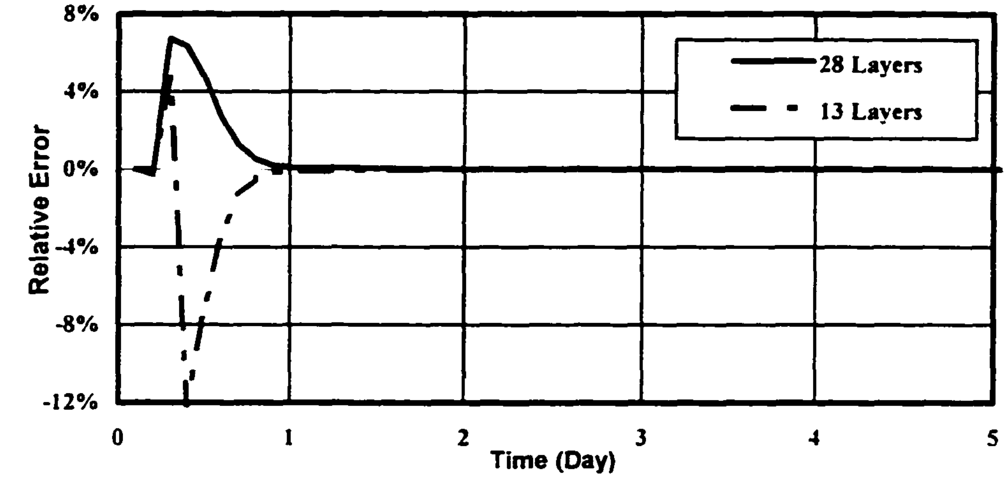

Fig. 5-94 Relative Errors of Water Production Rate With PI Scale-up for Lithofacies Models

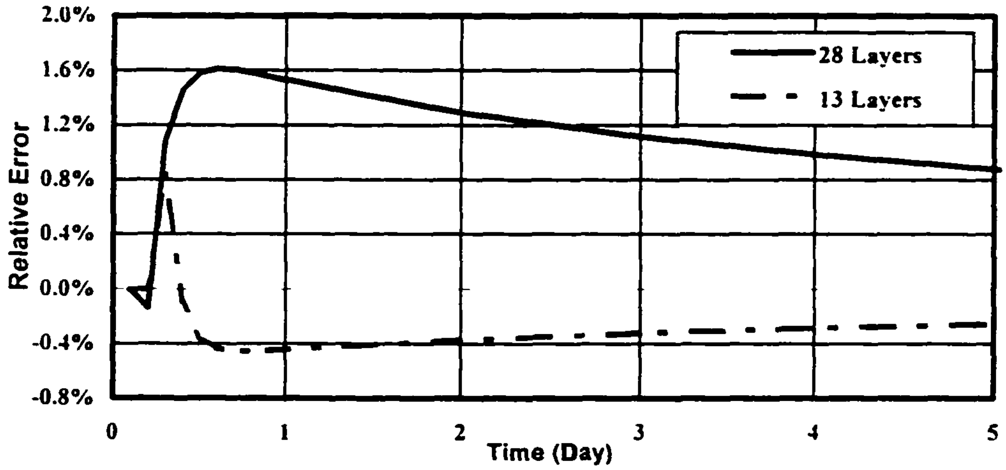

Fig. 5-95 Relative Errors of Cum. Water Production With PI Scale-up for Lithofacies Models

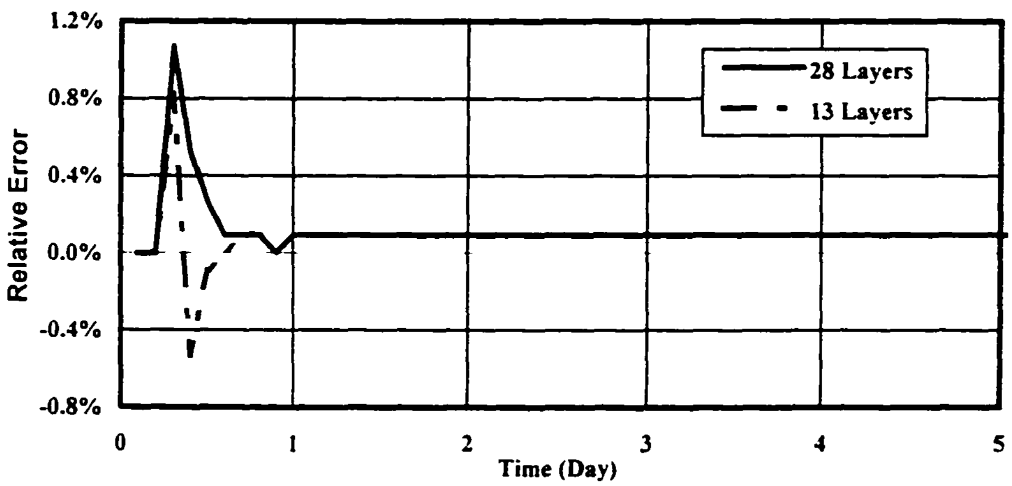

Fig. 5-96 Relative Errors of Average Reservoir Pressure With PI Scale-up for Lithofacies Models

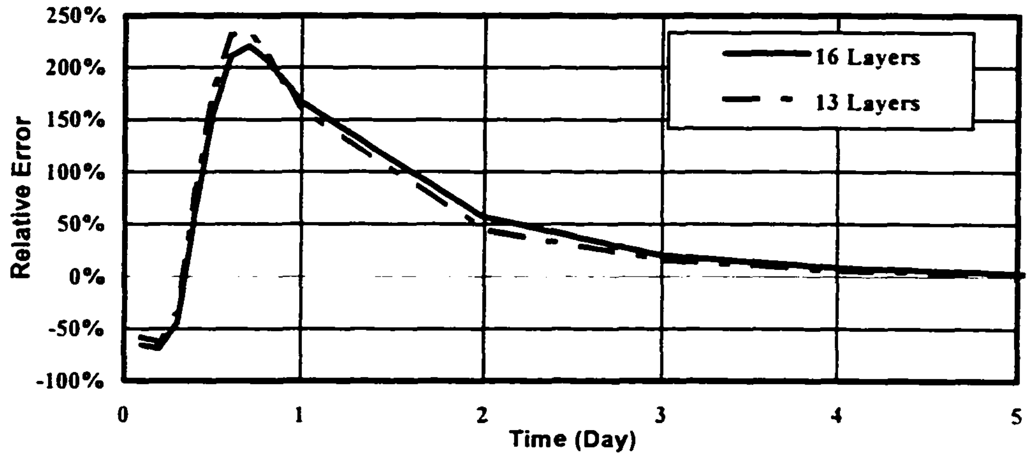

Fig. 5-97 Relative Errors of Water Production Rate Without PI Scale-up for Flowunit Models

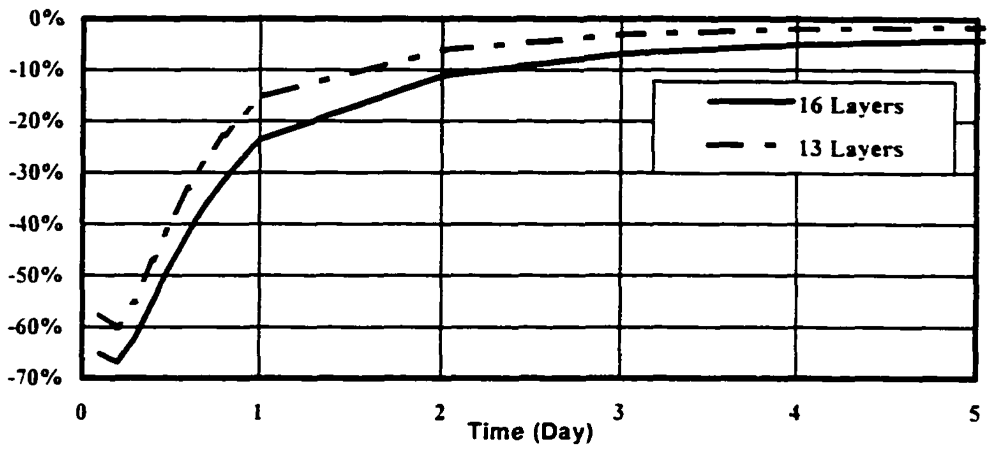

Fig. 5-98 Relative Errors of Cum. Water Production Without PI Scale-up for Flowunit Models

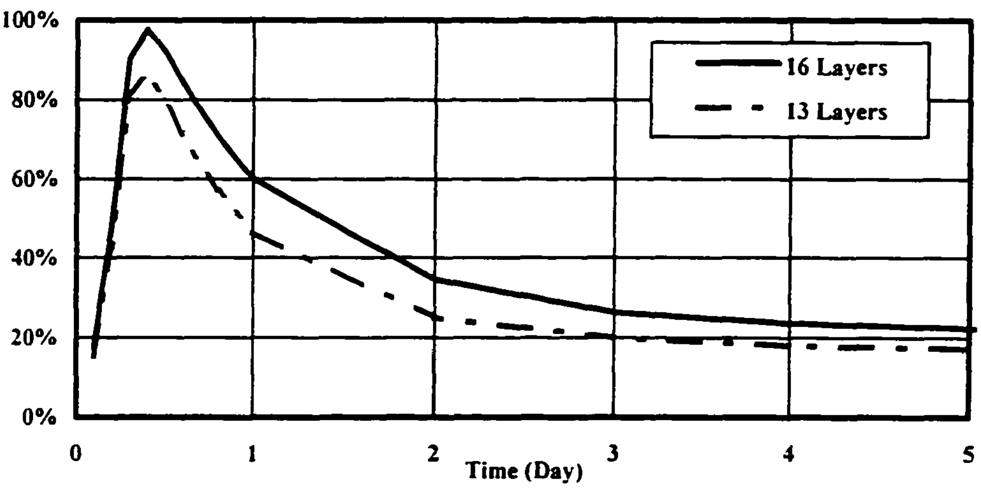

Fig. 5-99 Relative Errors of Average Reservoir Pressure Without PI Scale-up for Flowunit Models

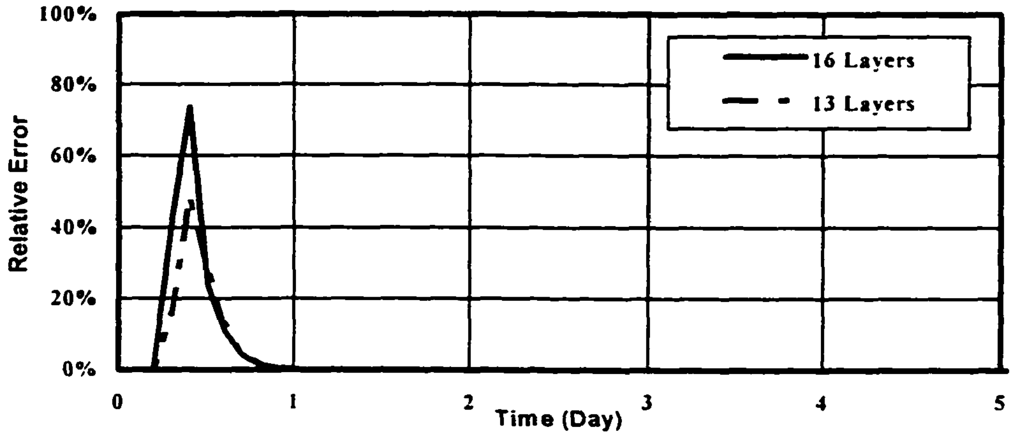

Fig. 5-100 Relative Errors of Water Production Rate With PI Scale-up for Flowunit Models

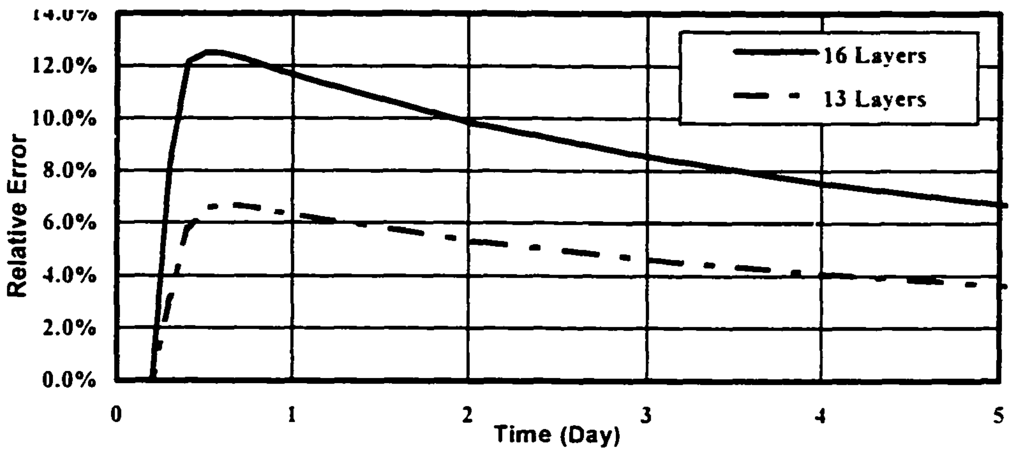

Fig. 5-101 Relative Errors of Cum. Water Production With PI Scale-up for Flowunit Models

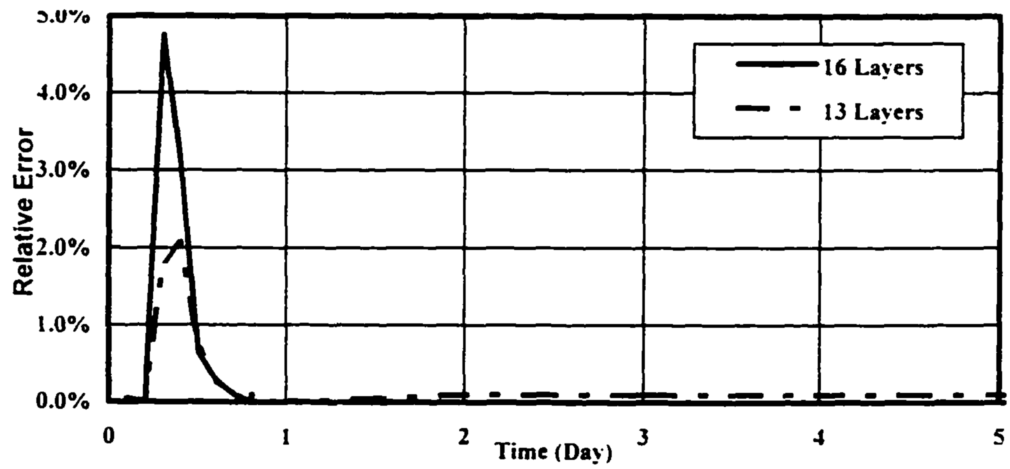

Fig. 5-102 Relative Errors of Average Reservoir Pressure With PI Scale-up for Flowunit Models

CHAPTER VI

EFFECTS OF WELL LOCATION AND BOUNDARY CONDITION ON QUALITY OF SCALE-UP

In this chapter, flow in the Gypsy channel model was simulated for different boundary conditions and different production-injection scenarios. Scale-up techniques, including PI scale-up, were then applied to study the effects of boundary condition, well location, and production and injection scenario on the quality of performance match with the scaled-up model. The purpose of such studies was to define the scope of reservoir flow for which the proposed scaling methods are valid.

6.1 Effects of Well Location on Scale-up

Nine wells were designed and used to study the effects of well location on scale-up. Two production-injection scenarios were studied. Scenario #1, as shown in Fig. 6-1, is a nine-spot corner-drive production-injection scenario. Scenario #2, as shown in Fig. 6-2, is a line-drive production-injection scenario. The initial conditions for reservoir, well production, and injection controls are the same as used for three Gypsy models in Chapter V. A well injectivity index of 10 was used in the fine scale simulation, which is the same as used in previous models. The scaled productivity indices used for the nine wells in the two production-injection scenarios are listed in Table 6-1 and 6-2.

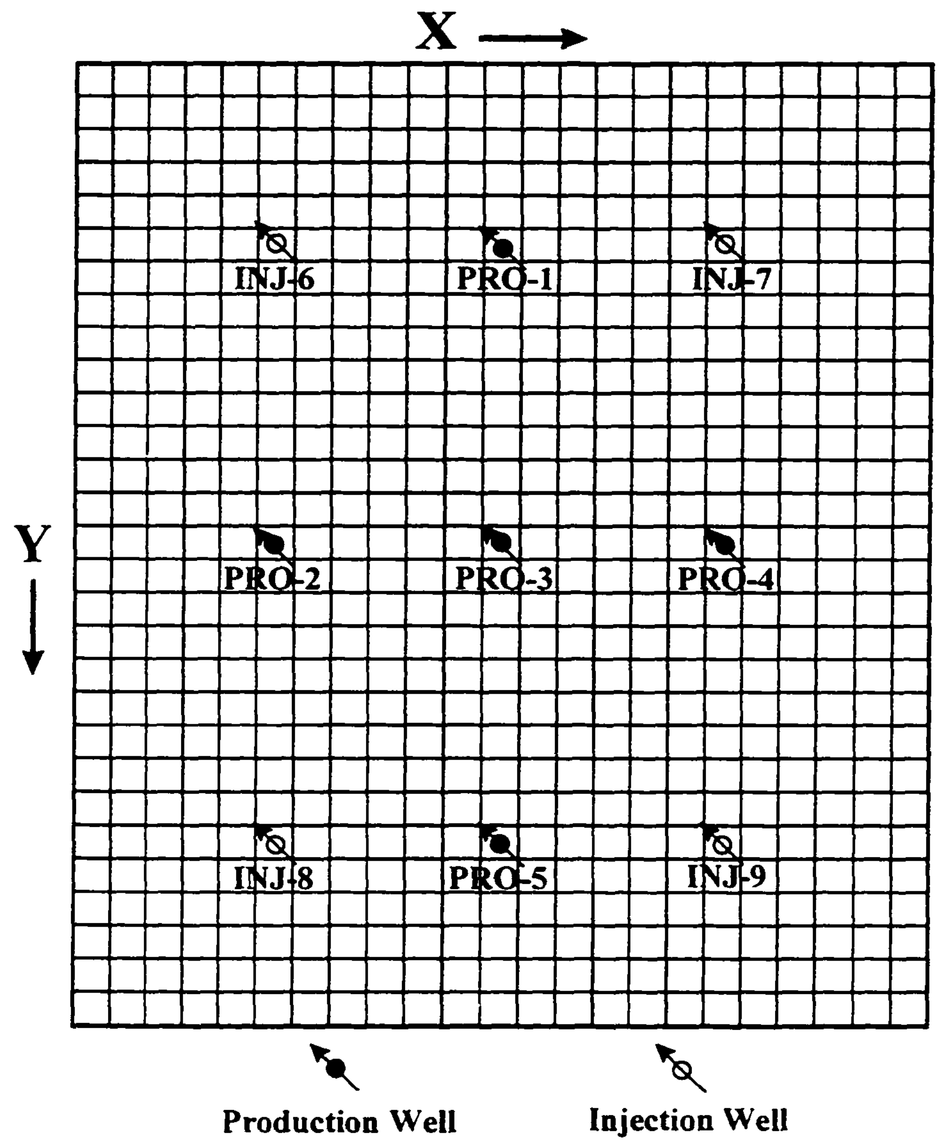

Fig. 6-1 Illustration of Nine-Spot Drive Well Pattern

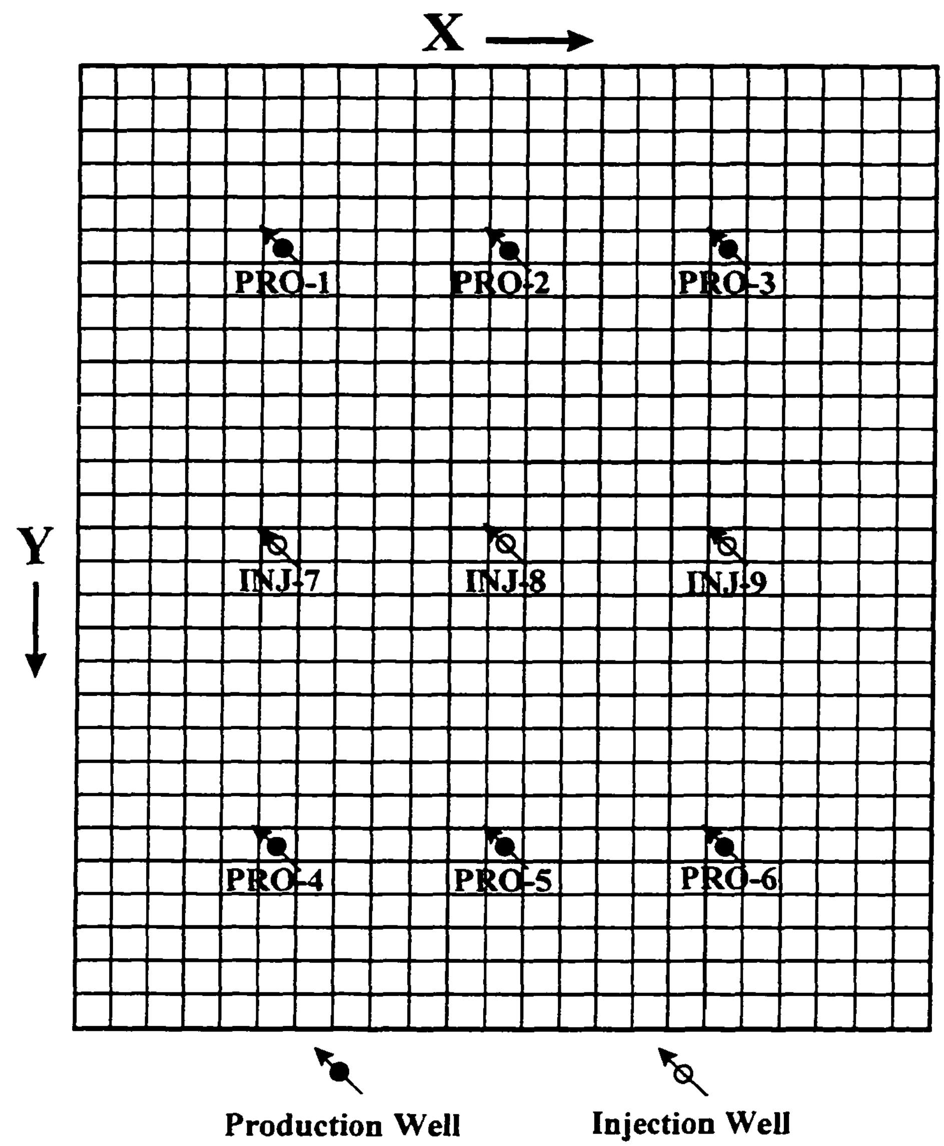

Fig. 6-2 Illustration of Line-Drive Well Pattern

Table 6-1 Scaled Productivity Index Used for Nine-Spot Drive Scenario

Well	PI
PRO-1	358.82
PRO-2	179.62
PRO-3	191.95
PRO-4	199.10
PRO-5	208.21
INJ-6	258.71
INJ-7	277.13
INJ-8	101.19
INJ-9	235.00

Table 6-2 Scaled Productivity Index Used for Line-drive Scenario

Well	PI
PRO-1	282.60
PRO-2	412.73
PRO-3	291.94
PRO-4	113.90
PRO-5	216.47
PRO-6	274.78
INJ-7	180.15
INJ-8	190.33
INJ-9	190.08

A comparison of results for the three different production-injection scenarios are presented in Figs. 6-3 to 6-5. In the plots, the results for five-spot scenario are from the simulation for channel model in Chapter V.

From the plots, the following observations were made:

1. Quality of performance prediction for scaled-up models is affected by the production-injection scenarios. Significant differences in scale-up results for line-drive, nine-spot drive, and fine-spot drive exist with and without PI scale-up processes.
2. The line-drive scenario produced the best results in three production-injection scenarios. The nine-spot scenario produced the worst matches. This is probably because in line-drive scenario, the overall flow configuration of fluid in reservoir is more linear than with the nine-spot drive scenario. The nine-spot scenario has more radial flow and that may cause the larger error, because the scale-up of transmissibility is only suitable for linear flow, even though PI scale-up was conducted to reduce this effect.
3. When comparing the five-spot and nine-spot drive scenarios, the five-spot drive obtained a better match than the nine-spot drive, because more wells cause more radial flow in reservoir, and subsequently may cause the larger error in scale-up. PI scale-up significantly reduced this error in both water production and reservoir pressure, but did not completely fix the problem with the method used.

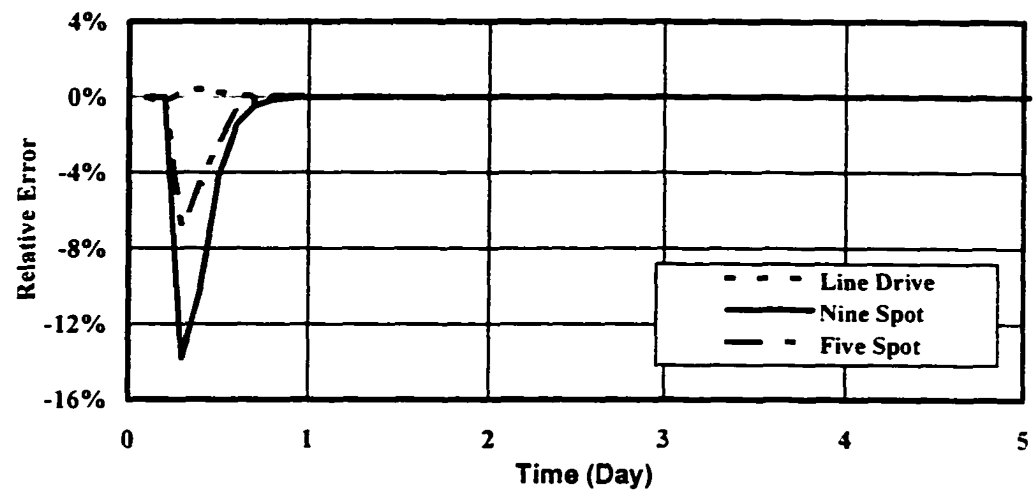

Fig. 6-3 Relative Errors of Water Production Rate for Different Production Scenarios

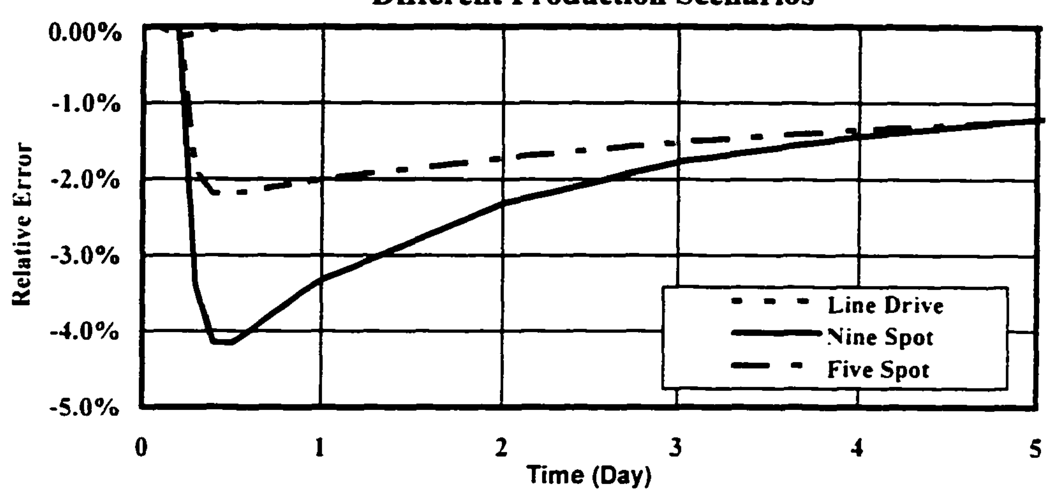

Fig. 6-4 Relative Errors of Cum. Water Production for Different Production Scenarios

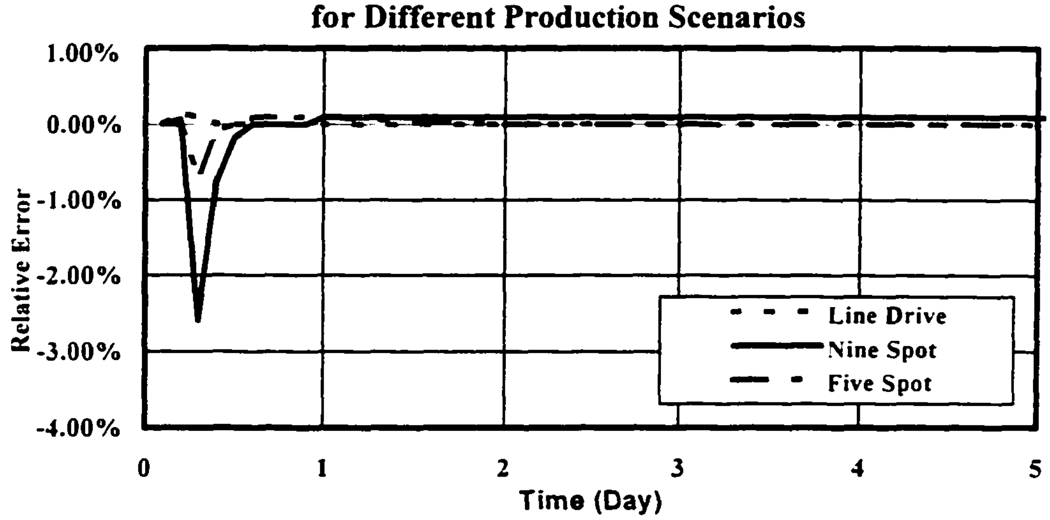

Fig. 6-5 Relative Errors of Reservoir Pressure for Different Production Scenarios

6.2 Effects of Boundary Condition on Scale-up

Three different boundary conditions were used and simulated in order to study the effects of boundary conditions on the results of scale-up. The channel model was again used as the reservoir model. To reduce the effects of other reservoir conditions on scale-up, the line drive scenario used in section 6.1 was used as the only production-injection scenario, because it showed the best scale-up results in earlier study.

The first boundary condition studied was an edge-water drive, where the reservoir was assumed to be surrounded by a very large aquifer that provided constant pressure at the reservoir boundary. No bottom water was used in this particular model. To simulate a constant pressure around the reservoir, the equivalent diameter of the edge-water aquifer should be about 10 times that of the equivalent diameter of the reservoir (Craft and Hawkins, 1989) One more line of grid-blocks with a size of 3,280 feet was added to the reservoir model in both X and Y directions, as shown in Fig. 6-6. This lead to a ratio of 8.8 of equivalent diameter of edge water area to the equivalent diameter of reservoir.

The second boundary condition studied was bottom-water drive, where the reservoir was assumed to have a very large bottom water with constant pressure. No water was used at the edge of the reservoir. An additional grid with a size of 3,280 feet was added to the reservoir model in the z directions, as shown in Fig. 6-7.

The third boundary condition studied was a no-flow boundary condition, in which the reservoir was sealed on all directions. The result was the same as for the line-drive scenario in Chapter V.

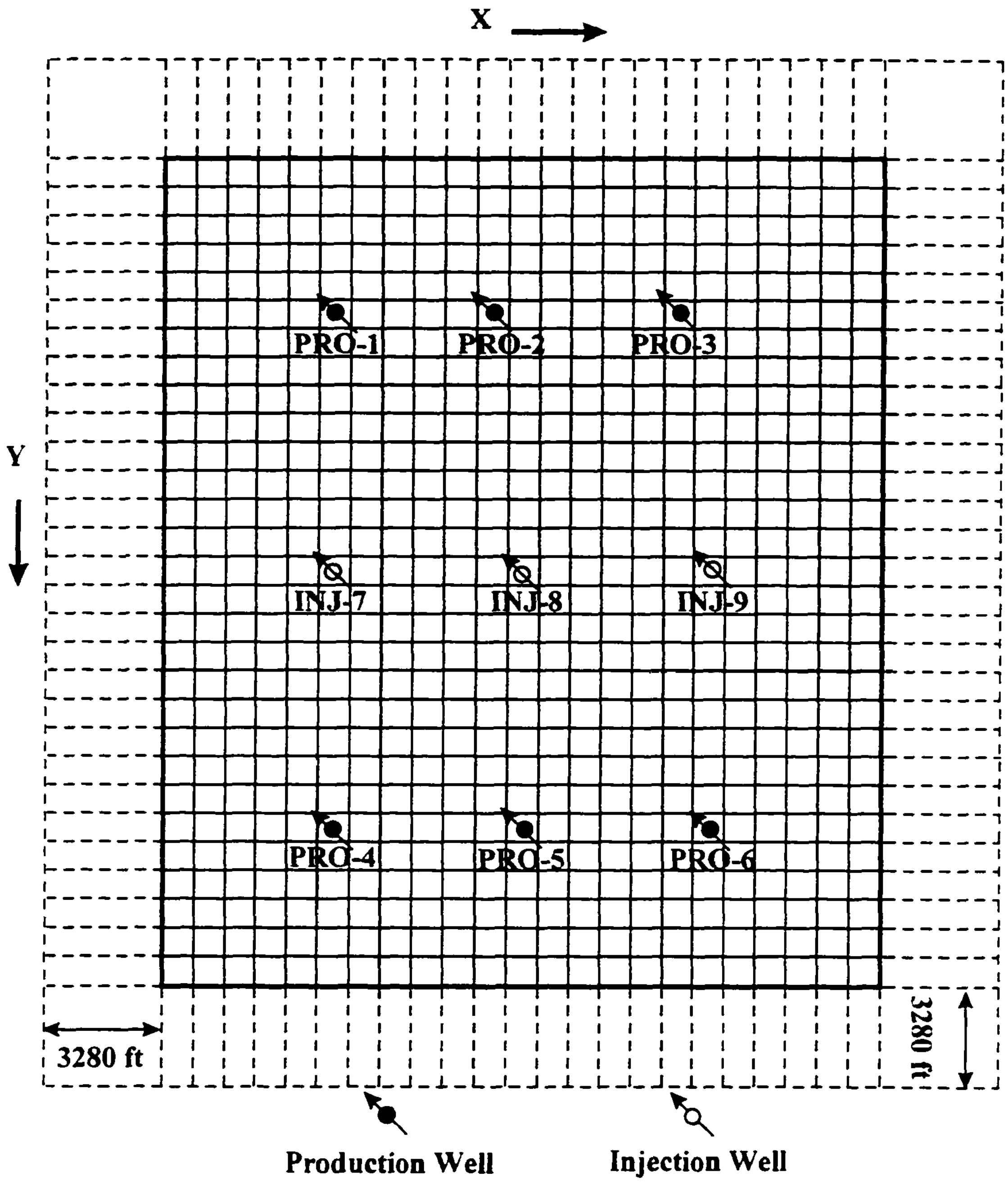

Fig. 6-6 Illustration of Reservoir Model and Well Pattern Used for Edge-Water Drive Scenario

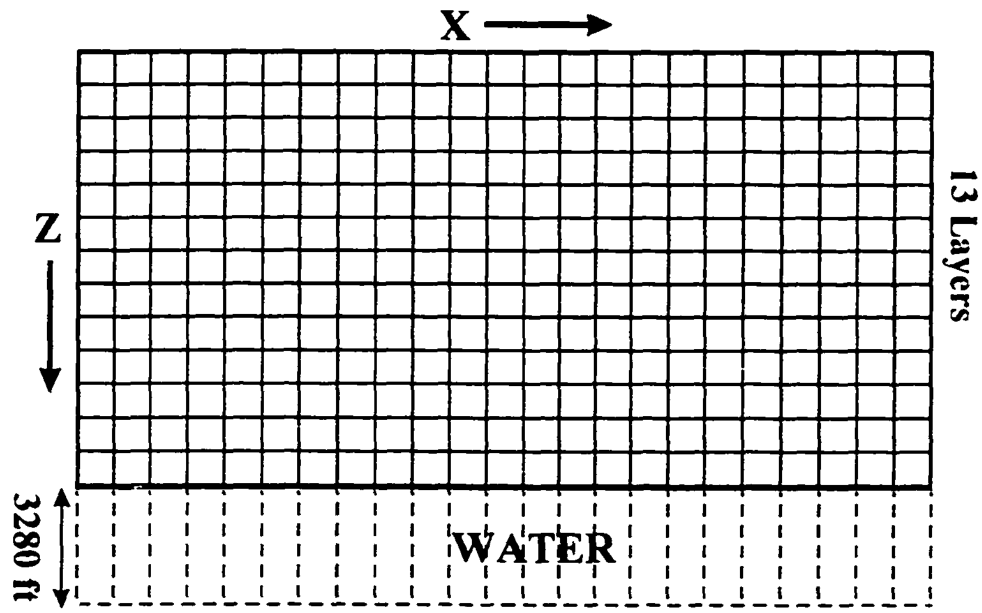

Fig. 6-7 Illustration of Reservoir Model Used for Bottom-Water Drive

Table 6-3 Scaled Productivity Index Used for Different Boundary Conditions

Well	Bottom Water	Edge Water	No Flow
PRO-1	249.91	261.08	282.60
PRO-2	324.80	329.38	412.73
PRO-3	254.44	286.69	291.94
PRO-4	103.52	106.51	113.90
PRO-5	190.23	201.01	216.47
PRO-6	224.50	241.40	274.78
INJ-7	237.10	180.15	180.15
INJ-8	207.92	207.92	190.33
INJ-9	207.62	190.08	190.08

Scale-up was conducted with PI scale-up. The productivity index values used in PI scale-up are listed in Table 6-3. The scale-up results for these different boundary conditions are presented in Figs. 6-11 to 6-13. It was observed that the no-flow boundary condition provided better results than flow-boundary conditions in water production. The bottom-water boundary condition resulted in the largest error in water production. The reservoir pressures of fine and coarse scales for edge-water drive prediction were almost completely matched.

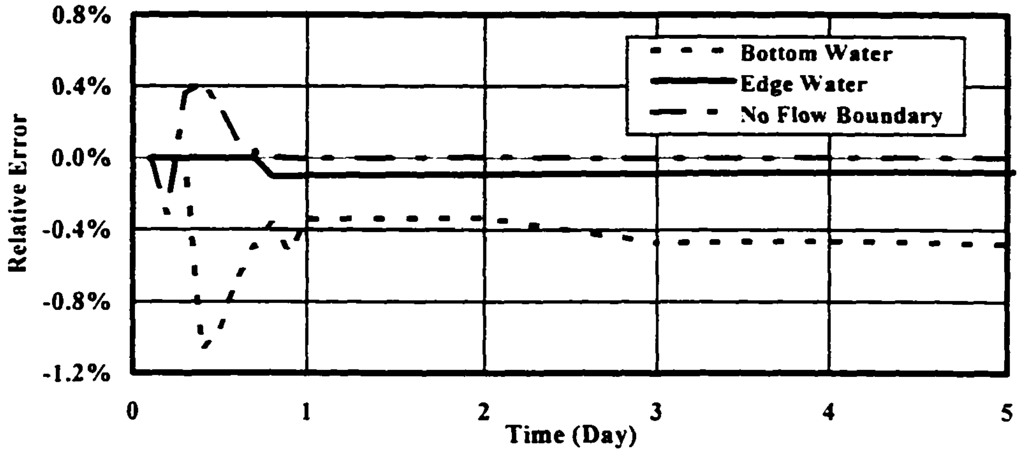

Fig. 6-8 Relative Errors of Water Production Rate for Different Boundary Conditions

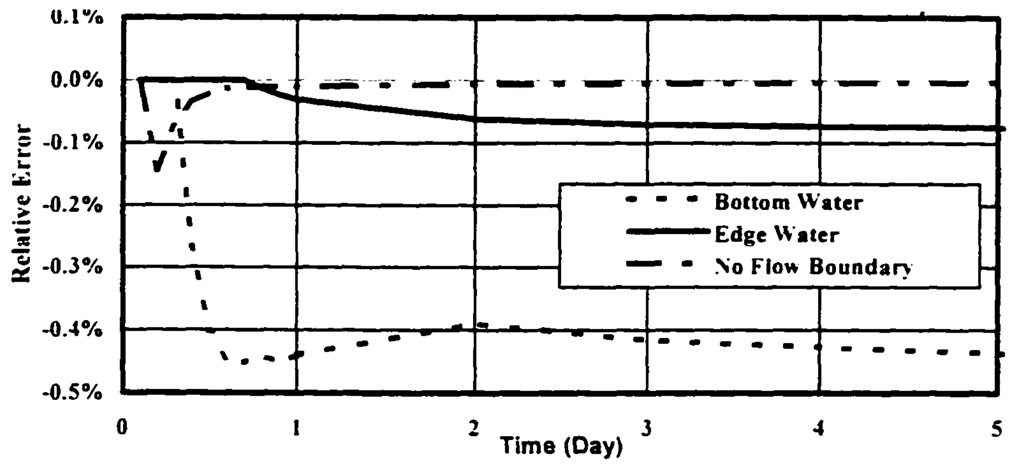

Fig. 6-9 Relative Errors of Cum. Water Production for Different Boundary Conditions

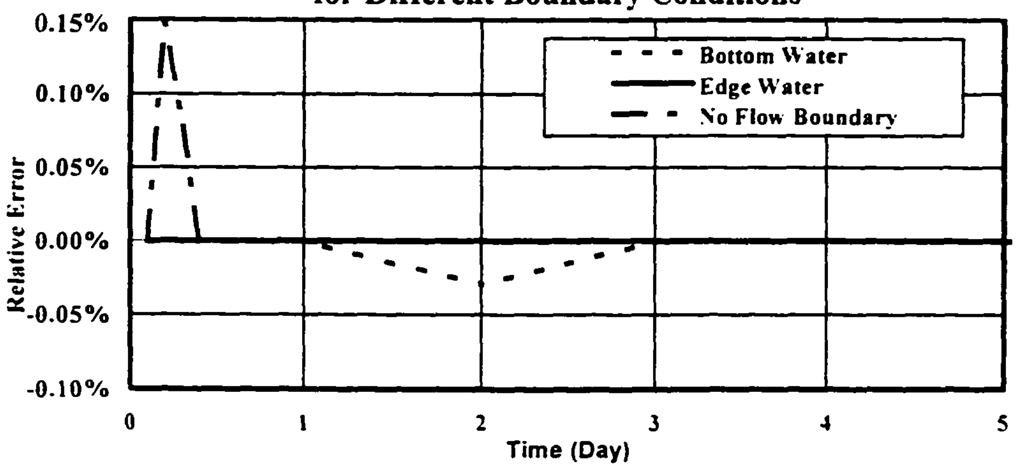

Fig. 6-10 Relative Errors of Reservoir Pressure for Different Boundary Conditions

CHAPTER VII

CONCLUSIONS AND RECOMMENDATIONS

Different strategies of geological modeling were applied as discussed in Chapter III, and three models for Gypsy formation were developed. The methodology for scale-up of transmissibility was described and illustrated in Chapter IV. Two hypothetical models were used to illustrate the application of scale-up, in which both no pinch-out and pinch-out alternatives were considered. Scale-up was conducted for the Gypsy channel, lithofacies, and flowunit models to study the effects of geological modeling processes on scale-up and performance predictions. To study the effects of well location and boundary condition on scale-up, three different production-injection scenarios and three different boundary conditions were considered for the Gypsy channel model and scale-up processes were conducted.

7.1 Conclusions

Based on the studies conducted in Chapter III to Chapter VI, the following conclusions are obtained:

1. The transmissibility scale-up is only suitable for linear flow. For radial flow around the wellbore, a scale-up on productivity index must be conducted in order to obtain accurate results. The results indicated that scale-up of the productivity index (PI) is very important in the overall scale-up process. Significant improvements were obtained after conducting PI scale-up.

2. The scale-up method utilized in this study results in significant differences at earlier time (transient). However, exact method used does not affect the long-term performance.
3. In scale-up process, special considerations must be given to the pinch-out existing in the model. Otherwise, incorrect simulation results occur in the fine-scale simulation. This, in turn, results in incorrect scale-up results.
4. Based on the heterogeneity analysis, the Gypsy formation was not accurately characterized using the deterministic method, because the standard deviations obtained in all three models were lower than the standard deviation obtained from core analysis. The lithofacies model provided a better description than the channel and flow unit models.
5. When the deterministic method was used to determine the distribution of reservoir properties, the search radius, R, has a significant effect on the resulting heterogeneity of the geological model. The extent of heterogeneity decreased with increasing values of R.

7.2 Limitations and Scope of Validity of the Proposed Scaling Process

In Chapter 6, the validity of the proposed strategy to various reservoir systems was studied. Based on this study, the following observations are made:

1. Strategies of geological modeling produce significant effects on scale-up. Obvious differences in scale-up results occurred between the three Gypsy models. Based on

the scale-up results obtained from this study, the channel model and the lithofacies model produce similar results, but flow unit model provides inferior results.

2. Three production scenarios were used to study the effects of well location on scale-up. Based on the study, the well location in the production-injection scenario has significant effect on scale-up. Comparing the scale-up results for nine-spot drive, line-drive, and five-spot drive, the line-drive scenario produced the best matches for both water production and reservoir pressure. This may be attributed to the effects of dominant linear flow in the line-drive scenario. Even though PI scale-up was conducted to reduce the error caused in radial flow, radial flow effects in nine-spot drive and fine-spot drive could not be satisfactorily reduced.

3. The effects of boundary conditions on scale-up were studied. Comparing the scale-up results obtained in this study, no-flow boundary condition obtained a better result compared to reservoir with a flow boundary condition. When flow boundary condition is applied in scale-up, edge-water drive produced better results than the bottom-water drive.

7.3 Recommendations for Future Studies

The effects of geological modeling, well location, production-injection scenario, and boundary condition on scale-up have been studied and evaluated in this study. However, there are several areas that should be further studied. The following areas are recommended:

1. This study focused on the geological modeling using the deterministic method. In Chapter III, the Gypsy models were not accurately described because the standard

deviations obtained from modeling for both porosity and permeability were much lower than these obtained from core analysis. Geostatistical method should be applied to generate geological models to compare the scale-up results with the results obtained using deterministic method.

2. In this study, the problem of pinch-out in vertical direction was solved and evaluated. However, fluid flow in the horizontal direction, when pinch-out exists, can also cause incorrect simulation of flow.. Lithofacies model was expected to be the best model for scale-up. However, it did not show much better results than channel model in this study. This may be caused by the discontinuity of grid block or 'horizontal pinch-out effects' in fine-scale lithofacies model. Therefore, the effect of horizontal continuity of reservoir on scale-up should be conducted

3. The methodology proposed in this study for scale-up produced successful scale-up results. However, the scale-up was conducted outside of the simulator, i.e., fine-scale simulation was run first. Data for flow rate and pressure for fine-scale grid blocks were obtained from an output map file. This process is cumbersome. A possible approach for streamlining the process is to incorporate the methodology into the simulator, or to develop an external program which is invoked by the simulator.

NOMENCLATURE

B	formation volume factor (rb/stb)
B_w	volume factor of reservoir water (rb/stb)
E_{datum}	elevation of reference datum (ft)
$E_{i,j,k}$	elevation of grid block (i,j,k) (ft)
FZI	flow zone indicator
gf	geometry factor
h	thickness of grid block (ft)
h	thickness of production layer (ft)
k	permeability of production layer (mD)
K	permeability (μm^2)
k_{layer}	permeability for the layer (mD)
k_r	relative permeability of fluid
k_{sector}	permeability for the sector (mD)
k_{rw}	relative permeability of water
k_x	average permeability of the two half grid blocks (mD)
k_y	average permeability of the two half grid blocks (mD)
k_z	average permeabilities of the two half grid blocks (mD)
L	total number of layer
M	mobility of the fluid
n	number of layer upscaled
n	total number of well values used
n_{sector}	total number of sector
$n_{bsector}$	total number of block in a sector
Nwi	cumulative water injection rate (Mbbl)
Nwp	cumulative water production (Mbbl)
P	pressure (psi)

p	pressure of fine-scale grid block (psi)
P_f	wellblock pressure of fine grid (psi)
P_c	wellblock pressure of coarse grid (psi)
P_w	wellbore pressure (psi)
p_g	average pressure of wellblock (psi)
p_b	bottom hole pressure (psi)
$p_{i,j}$	wellblock pressure (psi)
PI	productivity index (STB/day-psi)
PI_c	productivity index of coarse grid (STB/day/psi)
PI_f	productivity index of fine gird (STB/day/psi)
Δp_x	pressure difference between two grid blocks in x direction
Δp_y	pressure difference between two grid blocks in y direction
$q_{i-1/2,j}$	flux between two grid blocks
Q	flow rate (STB/day)
Q_t	total flow rate of well (STB/day)
Qwi	water injection rate (STB/day)
Qwp	water production rate (STB/day)
Q_x	flow rate in x directions (STB/day)
Q_y	flow rate y directions (STB/day)
Q_z	flow rate z directions (STB/day)
r	distance between well and the interpolated point
r_b	equivalent radius (Peaceman) of the gridblock containing the well (ft)
r_{fi}	farthest point from i-th block to the well (ft)
r_{ni}	nearest point from i-th block to the well (ft)
r_w	wellbore radius (ft)
r_e	drainage radius (ft)
R	search radius
RQI	reservoir quality index
s	skin factor (dimensionless)

T_b	transmissibility between well to wellblock (ft. mD)
T_x	transmissibility in x direction (ft. mD)
T^{xx}	normal transmissibility between two grid blocks (ft. mD)
T^{yy}	transverse transmissibility between two grid blocks (ft. mD)
T_y	transmissibility in y direction (ft. mD)
T_z	transmissibility in z direction (ft. mD)
v	volume of fine-scale grid block (ft^3)
V	final cell value in deterministic equation
V_C	value obtained from coarse scale
V_F	value obtained from fine scale
W	weighting function in deterministic equation
WI	well injectivity index (dimensionless)
w_{sector}	weighting coefficient of the i-th sector
x	dimension of grid block in x direction (ft)
x	power factor
Δx	length of grid block in x direction (ft)
y	dimension of grid block in y direction (ft)
Δy	length of grid block in y direction (ft)
z	dimension of grid block in z direction (ft)
Z	well value
Δz	length of grid block in z direction (ft)
ϕ	porosity (fraction)
Φ	potential of grid block (psi)
μ	viscosity (cp)
ρ_f	density of fluid in reservoir (g/ cm^3)
μ_w	viscosity of reservoir water (cp)
δ	relative error

REFERENCES

Aasum, Y., Kasap, E. and Kelkar, M. (1993): "Analytical Upscaling of Small-Scale Permeability Using a Full Tensor," SPE 25913 presented at the SPE Rocky Mountain Regional/Low Permeability Reservoir Symposium, Denver, CO, April 12-14.

Amaefule, J.O., Altunbay, M., Tiab, D., Kersey, D.G. and Keelan, D.K (1993): "Enhanced Reservoir Description: Using Core and Log Data to Identify Hydraulic (Flow) Units and Predict Permeability in Uncored Intervals/Wells," paper SPE 26436 presented at the 1993 SPE Annual Technical Conference and Exhibition, Houston, TX, October 3-6.

Begg, S.H., Carter, R.R. and Dranfield, P. (1989): "Assigning Effective Values to Simulator Gridblock Parameters for Heterogeneous Reservoirs," *SPERE*, November, p. 455-463.

Begg, S.H. and King, P.R. (1985): "Modeling the Effects of Shales on Reservoir Performance: Calculation of Effective Vertical Permeability," SPE 13529 Presented at the 1985 Reservoir Simulation Symposium held in Dallas, TX, Feb. 10-13.

Cardwell, Jr. W. T. and Parsons, R. L. (1945): "Average Permeabilities of Heterogeneous Oil Sands," *Trans.*, AIME, 160, p. 34-42.

Christie, M. A. (1996): "Upscaling for Reservoir Simulation," *JPT*, November, p. 1004-1010.

Christie, M. A., Mansfield, M., King, P. R. Barker, J.K. and Culverwell, I. D. (1995): "A Renormalization Based Upscaling Technique for WAG Floods in Heterogeneous Reservoirs," SPE 29127 presented at the 13th SPE Symposium on Reservoir Simulation, San Antonio, TX, February 12-15.

Collins, R. E. (1961): *Flow of Fluids Through Porous materials*, PennWell Publishing Company, Tulsa, Oklahoma.

Collins, T. M. (1996): "Methodology for Constructing High Resolution Three Dimensional Reservoir Characterization Models for Petroleum and Environmental Applications," Master's Thesis, University of Oklahoma, Norman.

Craft B.C., Hawkins, M.F. and Terry, R.E. (1989): *Applied Petroleum Reservoir Engineering*, Prentice Hall, Englewood Cliffs, NJ.

Ding, Y. (1995): "Scaling-up in the Vicinity of Wells in Heterogeneous Field," SPE 29137 presented at the 13th SPE Symposium on Reservoir Simulation, San Antonio, TX. Feb. 12-15.

Doyle, J.D. and Sweet, M.L. (1992): "Geological Characterization of the IRD GYPSY Study Sites," BP Exploration Internal Report No. H092072, June.

Doyle, J.D., O'Meara Jr., D.J., and Witterholt, E.J. (1992): "The "Gypsy" Field Research Program in Integrated Reservoir," SPE 24710 Presented at the 67th Annual Technical Conference and Exhibition of the Society of Petroleum Engineers held in Washington, DC, Oct. 4-7.

Dubrule, O. and Haldorsen, H.H. (1986): "Geostatistics for Permeability Estimation," *Reservoir Characterization*, Academic Press, Inc., p. 223.

Finley, R.J. and Tyler, N. (1986): "Geological Characterization of Sandstone Reservoirs," *Reservoir Characterization*, Academic Press, Inc., p. 1.

Forgotson, Jr. J.M. (1996): "Role of Reservoir Characterization in Improved Petroleum Recovery," Class Note.

Gautier, Y. and Natinger, B. (1994): "Preferential Flow-Paths Detection for Heterogeneous Reservoirs Using a New Renormalization Technique," Topic C: Scale Change Procedure, 1994 European Conference on the Mathematics of Oil Recovery, Røros, Norway, June, 7-10.

GeoGraphix, Inc. (1994), *GES User's Guide*, November.

Haldorsen, H. H. (1986): "Simulator Parameter Assignment and the Problem of Scale in Reservoir Engineering," *Reservoir Characterization*, Academic Press, Inc., p. 293-340.

Harris, D.G. and Hewitt, C.H. (1977): "Synergism in Reservoir Management - The Geological Perspective," *JPT*, July, p. 761-770.

Hearn, C.L., Ebanks, W.J., and Ranganathan, V. (1984): "Geological Factors Influencing Reservoir Performance of the Hartzog Draw Field, Wyoming," *JPT*, August, p. 1335-1344.

Hearn, C.L., Hobson, J.P. and Fowler, M.L. (1986): "Reservoir Characterization for Simulation, Hartzog Draw Field, Wyoming," *Reservoir Characterization*, Academic Press, Inc., p. 341.

King, M.J. (1993): "Application and Analysis of Tensor Permeability to Cross-Bedded Reservoir," *Proc.*, Seventh European IOR Symposium, Moscow.

King, P.R. (1989): "The Use of Renormalization for Calculating Effective Permeability," *Transport in Porous Media*, 4, 37-58.

King, P.R., Muggeridge, A.H., and Price, W.G. (1993): "Renormalization Calculations of Immiscible Flow," *Transport in Porous Media*, 12, p. 237-260.

King, P.R. and Williams, J.K. (1994): "Upscaling Permeability: Mathematics of Renormalization," 1994 European Conference on the Mathematics of Oil Recovery, Røros, Norway, June, 7-10.

Kyte, J. R. and Berry D. W. (1975): "New Pseudo Functions to Control Numerical Dispersion," *SPEJ*, August, p.269-276.

Landmark Graphics Corporation (1995): *Stratigraphic Geocellular Modeling Reference Guide*, December.

Landmark Graphics Corporation (1996): *VIP-Executive Reference Manual*, March.

Lasseter, T. J., Waggoner, J. R. and Lake, L. W. (1986): "Reservoir Heterogeneity and Their Influence on Ultimate Recovery," *Reservoir Characterization I*, Academic Press, Inc., p. 544-556.

Peaceman, D.W. (1996): "Effective Transmissibilities of a Gridblock by Upscaling - Why Use Renormalization," SPE 36722 presented at the 1996 SPE Annual Technical Conference and Exhibition, Denver, CO, Oct. 6-9.

Pickup, G.E. and Sorbie, K.S. (1994): "Development and Application of a New Two-Phase Scaleup Method Based on Tensor Permeability," SPE 28586 presented at the SPE 69th Annual Technical Conference and Exhibition, New Orleans, LA, Sept. 25-28.

Pickup, G.E., Jensen, J.L, Ringrose, P.S. and Sorbie, K.S. (1992) :" A Method for Calculating Permeability Tensors Using Perturbed Boundary Conditions," *Proc.*, Third European Conference on the Mathematics of Oil Recovery, p. 225.

Rodriguez, A. (1988): "Facies Modeling and the Flow Units Concept as a Sedimentological Tool in Reservoir Description," SPE 18154 Presented at the 63dr Annual Technical Conference and Exhibition of the Society of Petroleum Engineers held in Houston, TX, Oct. 2-5.

Scuta, M.S. (1997): "Flow Units and Upscaling of a Complex Carbonate Reservoir Using a 3-D Geological Model," SPE paper presented at the SPE Annual Technical Conference and Exhibition held in San Antonio, TX, Oct. 5-8.

Slatt, R.M. and Hopkins, G.L. (1988): "Scales of Geological Reservoir Description for Engineering Applications: North Sea Oilfield Example," SPE 18136 presented at the 1988 SPE Annual Technical Conference and Exhibition, Houston, TX, Oct. 2-5.

Soeriawinata, J., and Kelkar, M. (1996): "Permeability Upscaling for Near-Wellbore Heterogeneities," SPE 36518 presented at the 1996 SPE Annual Technical Conference and Exhibition, Denver, CO, Oct. 6-9.

Testerman, J.D. (1962): "A Statistical Reservoir-Zonation Technique," *JPT*, August. p. 889-893.

Ti. G., Ogbe, D.O., Munly, W. and Hatzignatiou, D.G. (1995): "Use of Flow Unit as a Tool for Reservoir Description: A Case Study," *SPE Formation Evaluation*. June, p. 122-128.

Weber, K.L. and Geuns, L.C. (1990): "Framework for Constructing Clastic Reservoir Simulation Models," *JPT*. October.

Willhite, G.P (1986): *Water Flooding*, SPE Textbook Series Vol. 3, p. 270.

White, C.D. and Horne, R.N. (1987): "Computing Absolute Transmissibility in the Presence of Fine-Scale Heterogeneity," SPE 16011 Presented at the North SPE Symposium on Reservoir Simulation held in San Antonio, TX. Feb. 1-4.

APPENDIX

A.1 FORTRAN PROGRAM FOR TRANSMISSIBILITY SCALE-UP

```
C  PROGRAM FOR TRANSMISSIBILITY SCALE-UP
   PARAMETER (M=23,N=29,L1=99,L2=14,VKZ=9999.0,VDZ=0.01,NW=9)
   REAL  KX1(M,N,L1),KX2(M,N,L2),KH1(M,N,L1),KH2(M,N,L2),
   1        KK(M,N,L2),KKH(M,N,L2),KZ1(M,N,L1),KZ2(M,N,L2),
   1        MD(NW)
   INTEGER  WX(NW),WY(NW)
   DIMENSION QX1(M,N,L1),QX2(M,N,L2),QY1(M,N,L1),
   1      QY2(M,N,L2),QZ1(M,N,L1),QZ2(M,N,L2),
   1      P1(M,N,L1),P2(M,N,L2),PT(M,N,L2),
   1      DPTX(M,N,L2),DPTY(M,N,L2),DPTZ(M,N,L2),
   1      H1(M,N,L1),H2(M,N,L2),H3(M,N,L2),
   1      PRV1(M,N,L1),PRV2(M,N,L2),
   1      V1(M,N,L1),V2(M,N,L2),
   1      PHI1(M,N,L1),PHI2(M,N,L2),
   1      PHIV1(M,N,L1),PHIV2(M,N,L2),
   1      TX(M,N,L2),TY(M,N,L2),TZ(M,N,L2),
   1      LL1(L2),LL2(L2),HT(NW),ELV(M,N,L2),TOPE(M,N),
   1      DX(M,N),DY(M,N)
C  READING DATA
   OPEN (1,FILE='c:\wei\program\bottom\input\qx.prn')
   READ (1,*) (((QX1(I,J,K),I=1,M),J=1,N),K=1,L1)
   CLOSE (1)
   OPEN (2,FILE='c:\wei\program\bottom\input\qy.prn')
   READ (2,*) (((QY1(I,J,K),I=1,M),J=1,N),K=1,L1)
   CLOSE (2)
   OPEN (3,FILE='c:\wei\program\bottom\input\qz.prn')
   READ (3,*) (((QZ1(I,J,K),I=1,M),J=1,N),K=1,L1)
   CLOSE (3)
   OPEN (4,FILE='c:\wei\program\bottom\input\p.prn')
   READ (4,*) (((P1(I,J,K),I=1,M),J=1,N),K=1,L1)
   CLOSE (4)
   OPEN (4,FILE='c:\wei\program\bottom\input\dx.out')
   READ (4,*) ((DX(I,J),I=1,M),J=1,N)
   CLOSE (4)
   OPEN (4,FILE='c:\wei\program\bottom\input\dy.out')
   READ (4,*) ((DY(I,J),I=1,M),J=1,N)
   CLOSE (4)
   OPEN (5,FILE='c:\wei\program\bottom\input\dz.out')
   READ (5,*) (((H1(I,J,K),I=1,M),J=1,N),K=1,L1)
   CLOSE (5)
   OPEN (6,FILE='c:\wei\program\bottom\input\phi.out')
   READ (6,*) (((PHI1(I,J,K),I=1,M),J=1,N),K=1,L1)
   CLOSE (6)
   OPEN (7,FILE='c:\wei\program\bottom\input\topelv.prn')
   READ (7,*) ((TOPE(I,J),I=1,M),J=1,N)
```

```
      CLOSE (7)
      OPEN (8,FILE='c:\wei\program\bottom\input\data.prn')
      READ (8,*) (LL1(I),LL2(I),I=1,L2),UW,GRA,DTM,
     1(WX(I),WY(I),I=1,NW)
      CLOSE (8)
      OPEN (9,FILE='c:\wei\program\bottom\input\kx.out')
      READ (9,*) (((KX1(I,J,K),I=1,M),J=1,N),K=1,L1)
      CLOSE (9)
      OPEN (10,FILE='c:\wei\program\bottom\input\kz.out')
      READ (10,*) (((KZ1(I,J,K),I=1,M),J=1,N),K=1,L1)
      CLOSE (10)
C     CALCULATION OF V1,PHIV1,PRV1
      DO 1 K=1,L1
      DO 2 J=1,N
      DO 3 I=1,M
      V1(I,J,K)=DX(I,J)*DY(I,J)*H1(I,J,K)
      PHIV1(I,J,K)=PHI1(I,J,K)*0.01*V1(I,J,K)
      PRV1(I,J,K)=P1(I,J,K)*PHIV1(I,J,K)
    3 CONTINUE
    2 CONTINUE
    1 CONTINUE
C     CALCULATION OF PRV2,H2,V2,PHIV2,QX2,QY2
      DO 4 K2=1,L2
      DO 5 J=1,N
      DO 6 I=1,M
      PRV2(I,J,K2)=0.0
      H2(I,J,K2)=0.0
      H3(I,J,K2)=0.0
      V2(I,J,K2)=0.0
      PHIV2(I,J,K2)=0.0
      QX2(I,J,K2)=0.0
      QY2(I,J,K2)=0.0
      DO 7 K1=LL1(K2),LL2(K2)
      PRV2(I,J,K2)=PRV2(I,J,K2)+PRV1(I,J,K1)
      H2(I,J,K2)=H2(I,J,K2)+H1(I,J,K1)
      IF (KZ1(I,J,K1) .NE. VKZ .AND. H1(I,J,K1) .NE. VDZ)
     1H3(I,J,K2)=H3(I,J,K2)+H1(I,J,K1)
      V2(I,J,K2)=V2(I,J,K2)+V1(I,J,K1)
      PHIV2(I,J,K2)=PHIV2(I,J,K2)+PHIV1(I,J,K1)
      QX2(I,J,K2)=QX2(I,J,K2)+QX1(I,J,K1)
      QY2(I,J,K2)=QY2(I,J,K2)+QY1(I,J,K1)
    7 CONTINUE
    6 CONTINUE
    5 CONTINUE
    4 CONTINUE
C     CALCULATION OF QZ2
      DO 8 K=2,L2
      DO 9 J=1,N
      DO 10 I=1,M
      QZ2(I,J,K)=QZ1(I,J,LL1(K))
   10 CONTINUE
    9 CONTINUE
    8 CONTINUE
```

```
C  CALCULATION OF ELEVATION
   DO 12 K=1,L2
   DO 13 J=1,N
   DO 14 I=1,M
   IF (K .EQ. 1) ELV(I,J,1)=TOPE(I,J)-0.5*(H2(I,J,1))
   IF (K .GT. 1) ELV(I,J,K)=ELV(I,J,K-1)
  1-0.5*(H2(I,J,K-1)+H2(I,J,K))
14 CONTINUE
13 CONTINUE
12 CONTINUE
C  CALCULATION OF KH2,KX2
   DO 15 K2=1,L2
   DO 16 J=1,N
   DO 17 I=1,M
   KH2(I,J,K2)=0.0
   DO 18 K1=LL1(K2),LL2(K2)
   IF (KZ1(I,J,K1) .NE. VKZ .AND. H1(I,J,K1) .NE. VDZ) THEN
   KH1(I,J,K1)=KX1(I,J,K1)*H1(I,J,K1)
   KH2(I,J,K2)=KH2(I,J,K2)+KH1(I,J,K1)
   ELSE
   END IF
18 CONTINUE
   IF (H3(I,J,K2) .NE. 0.0) KX2(I,J,K2)=KH2(I,J,K2)/H3(I,J,K2)
   IF (H3(I,J,K2) .EQ. 0.0) KX2(I,J,K2)=0.0
17 CONTINUE
16 CONTINUE
15 CONTINUE
C  CALCULATION OF KZ2
   DO 19 K2=1,L2
   DO 20 J=1,N
   DO 21 I=1,M
   KK(I,J,K2)=1.0
   DO 22 K1=LL1(K2),LL2(K2)
   IF (KZ1(I,J,K1) .NE. VKZ .AND. H1(I,J,K1) .NE. VDZ)
  1KK(I,J,K2)=KK(I,J,K2)*KZ1(I,J,K1)
22 CONTINUE
   KKH(I,J,K2)=0.0
   DO 23 K1=LL1(K2),LL2(K2)
   IF (KZ1(I,J,K1) .NE. VKZ .AND. H1(I,J,K1) .NE. VDZ)
  1KKH(I,J,K2)=KKH(I,J,K2)+H1(I,J,K1)*KK(I,J,K2)/KZ1(I,J,K1)
23 CONTINUE
   IF (H3(I,J,K2) .NE. 0.0) THEN
   KZ2(I,J,K2)=H3(I,J,K2)*KK(I,J,K2)/KKH(I,J,K2)
   ELSE
   KZ2(I,J,K2)=VKZ
   END IF
21 CONTINUE
20 CONTINUE
19 CONTINUE
C  CALCULATIONS OF P2, PHI2
   DO 24 K=1,L2
   DO 25 J=1,N
   DO 26 I=1,M
```

```
      P2(I,J,K)=PRV2(I,J,K)/PHIV2(I,J,K)
      PT(I,J,K)=P2(I,J,K)+(ELV(I,J,K)-DTM)*0.4335
      PHI2(I,J,K)=PHIV2(I,J,K)/V2(I,J,K)
   26 CONTINUE
   25 CONTINUE
   24 CONTINUE
C  CALCULATIONS OF TX
      DO 27 K=1,L2
      DO 28 J=1,N
      DO 29 I=2,M
      IF (H3(I-1,J,K) .EQ. 0.0 .OR. H3(I,J,K) .EQ. 0.0) THEN
      TX(I,J,K)=0.0
      ELSE
      DPTX(I,J,K)=PT(I-1,J,K)-PT(I,J,K)
      IF (DPTX(I,J,K) .NE. 0.0) THEN
      TX(I,J,K)=QX2(I,J,K)/DPTX(I,J,K)
      ELSE
C  HARMONIC AVERAGE METHOD WITH DIFFERENT DX & DY
      TX(I,J,K)=2.0*KX2(I-1,J,K)*DY(I-1,J)*H2(I-1,J,K)*
     1KX2(I,J,K)*DY(I,J)*H2(I,J,K)/
     1(DX(I-1,J)*KX2(I,J,K)*DY(I,J)*H2(I,J,K)+
     1DX(I,J)*KX2(I-1,J,K)*DY(I-1,J)*H2(I-1,J,K))*0.001127
      END IF
      IF (TX(I,J,K) .LT. 0.0)
     1TX(I,J,K)=2.0*KX2(I-1,J,K)*DY(I-1,J)*H2(I-1,J,K)*
     1KX2(I,J,K)*DY(I,J)*H2(I,J,K)/
     1(DX(I-1,J)*KX2(I,J,K)*DY(I,J)*H2(I,J,K)+
     1DX(I,J)*KX2(I-1,J,K)*DY(I-1,J)*H2(I-1,J,K))*0.001127
      END IF
   29 CONTINUE
   28 CONTINUE
   27 CONTINUE
C  CALCULATIONS OF TY
      DO 30 K=1,L2
      DO 31 I=1,M
      DO 32 J=2,N
      IF (H3(I,J-1,K) .EQ. 0.0 .OR. H3(I,J,K) .EQ. 0.0) THEN
      TY(I,J,K)=0.0
      ELSE
      DPTY(I,J,K)=PT(I,J-1,K)-PT(I,J,K)
      IF (DPTY(I,J,K) .NE. 0.0) THEN
      TY(I,J,K)=QY2(I,J,K)/DPTY(I,J,K)
      ELSE
C  HARMONIC AVERAGE METHOD WITH DIFFERENT DX & DY
      TY(I,J,K)=2.0*KX2(I,J-1,K)*DX(I,J-1)*H2(I,J-1,K)*
     1KX2(I,J,K)*DX(I,J)*H2(I,J,K)/
     1(DY(I,J-1)*KX2(I,J,K)*DX(I,J)*H2(I,J,K)+
     1DY(I,J)*KX2(I,J-1,K)*DX(I,J-1)*H2(I,J-1,K))*0.001127
      END IF
      IF (TY(I,J,K) .LT. 0.0)
     1TY(I,J,K)=2.0*KX2(I,J-1,K)*DX(I,J-1)*H2(I,J-1,K)*
     1KX2(I,J,K)*DX(I,J)*H2(I,J,K)/
     1(DY(I,J-1)*KX2(I,J,K)*DX(I,J)*H2(I,J,K)+
```

```
     1DY(I,J)*KX2(I,J-1,K)*DX(I,J-1)*H2(I,J-1,K))*0.001127
      END IF
 32   CONTINUE
 31   CONTINUE
 30   CONTINUE
C     CALCULATIONS OF TZ
      DO 33 J=1,N
      DO 34 I=1,M
      DO 35 K=2,L2
      DPTZ(I,J,K)=(PT(I,J,K-1)-PT(I,J,K))
      IF (DPTZ(I,J,K) .NE. 0.0) THEN
      TZ(I,J,K)=QZ2(I,J,K)/DPTZ(I,J,K)
      ELSE
C     HARMONIC AVERAGE METHOD WITH DIFFERENT DX & DY
      TZ(I,J,K)=2.0*KZ2(I,J,K-1)*KZ2(I,J,K)*DX(I,J)*DY(I,J)
     1/(KZ2(I,J,K-1)*H2(I,J,K)+KZ2(I,J,K)*H2(I,J,K-1))*0.001127
      ENDIF
      IF (TZ(I,J,K) .LE. 0.0)
     1TZ(I,J,K)=2.0*KZ2(I,J,K-1)*KZ2(I,J,K)*DX(I,J)*DY(I,J)
     1/(KZ2(I,J,K-1)*H2(I,J,K)+KZ2(I,J,K)*H2(I,J,K-1))*0.001127
 35   CONTINUE
 34   CONTINUE
 33   CONTINUE
      DO 36 K=1,NW
      HT(K)=0.0
      DO 37 J=1,L2
      HT(K)=HT(K)+H2(WX(K),WY(K),J)
 37   CONTINUE
      MD(K)=-TOPE(WX(K),WY(K))+HT(K)/2.0
 36   CONTINUE
C     WRITING OUTPUT
      OPEN (11,FILE='c:\wei\program\bottom\output\tx.out')
      WRITE (11,300) ((((TX(I,J,K)),I=1,M),J=1,N),K=1,L2)
      CLOSE (11)
      OPEN (12,FILE='c:\wei\program\bottom\output\ty.out')
      WRITE (12,300) ((((TY(I,J,K)),I=1,M),J=1,N),K=1,L2)
      CLOSE (12)
      OPEN (13,FILE='c:\wei\program\bottom\output\tz.out')
      WRITE (13,300) ((((TZ(I,J,K)),I=1,M),J=1,N),K=1,L2)
      CLOSE (13)
      OPEN (14,FILE='c:\wei\program\bottom\output\pv.out')
      WRITE (14,200) (((PHIV2(I,J,K),I=1,M),J=1,N),K=1,L2)
      CLOSE (14)
      OPEN (23,FILE='c:\wei\program\bottom\output\h.out')
      WRITE (23,200) ((((H2(I,J,K)),I=1,M),J=1,N),K=1,L2)
      CLOSE (23)
      OPEN (30,FILE='c:\wei\program\bottom\output\mdepth.out')
      WRITE (30,200) (MD(I),I=1,NW)
      CLOSE (30)
100   FORMAT (1X,4F20.4)
200   FORMAT (1X,4F20.6)
300   FORMAT (1X,4F20.8)
      STOP
      END
```

A.2 DEFINITIONS OF PARAMETERS IN THE PROGRAM

DPTX potential difference between two grid block of coarse-scale model in x direction (psi)

DPTY potential difference between two grid block of coarse-scale model in y direction (psi)

DPTZ potential difference between two grid block of coarse-scale model in z direction (psi)

DTM reference elevation (ft)

DX dimension of grid block in x direction (ft)

DY dimension of grid block in y direction (ft)

ELV elevation at the center of the grid block (ft)

GRA gravity of water (gm/cc)

H1 thickness of grid block for fine-scale model (ft)

H2 thickness of coarse-scale gird-block including the pinch-out grid thickness (ft)

H3 thickness of coarse-scale gird-block excluding the pinch-out grid thickness (ft)

HT total thickness of formation at wellbore (ft)

I gird number in x direction for fine-scale model

J gird number in y direction for fine-scale model

KH1 KX1*H1 for fine-scale model

KH2 KX2*H2 for coarse scale-model

KX1 permeability of fine-scale gird block in x direction (mD)

KX2 permeability of coarse-scale gird block in x direction (mD)

KY1 permeability of fine-scale gird block in y direction (mD)

KY2 permeability of coarse-scale gird block in y direction (mD)

KZ1 permeability of fine-scale gird block in z direction (mD)

KZ2 permeability of coarse-scale gird block in z direction (mD)

L1 total grid number in z direction for fine-scale model

L2	total grid number in z direction for coarse-scale model
LL1	layer number in fine-scale model for the layers at the top boundary of coarse-scale model
LL2	layer number in fine-scale model for the layers at the bottom boundary of coarse-scale model
M	total grid number in x direction for coarse-scale model
MD	mid-depth of formation at wellbore (ft)
N	total grid number in y direction for coarse-scale model
NW	total well number in simulation
P1	pressure of grid block for fine-scale model (psi)
P2	pressure of grid block for coarse-scale model (psi)
PHI1	porosity of grid block for fine-scale model (%)
PHI2	porosity of grid block for coarse-scale model (%)
PHIV1	pore volume of fine-scale grid block (ft^3)
PHIV2	pore volume of coarse-scale grid block (ft^3)
PRV1	PHIV1*P1 for fine-scale grid block (ft^3)
PRV2	PHIV2*P2 for coarse-scale grid block (ft^3)
PT	potential of coarse-scale gird block (psi)
QX1	flow rate of gird block in x direction of fine-scale model (STB/day)
QY1	flow rate of gird block in y direction of fine-scale model (STB/day)
QZ1	flow rate of gird block in z direction of fine-scale model (STB/day)
QX2	flow rate of gird block in x direction of coarse-scale model (STB/day)
QY2	flow rate of gird block in y direction of coarse-scale model (STB/day)
QZ2	flow rate of gird block in z direction of coarse-scale model (STB/day)
TOPE	elevation at top of the model (ft)
TX	transmissibility of coarse-scale model in x direction (STB-cp/day-psi)
TY	transmissibility of coarse-scale model in y direction (STB-cp/day-psi)
TZ	transmissibility of coarse-scale model in z direction (STB-cp/day-psi)
UW	viscosity of water (cp)

V1	volume of gird block for fine-scale model (ft^3)
V2	pore volume of coarse-scale grid block (ft^3)
VDZ	thickness of pinch-out grid block (ft)
VKZ	vertical permeability of pinch-out grid block (mD)
WX	well location in x direction (grid block)
WY	well location in y direction (grid block)

IMAGE EVALUATION TEST TARGET (QA-3)

150mm

6"

APPLIED IMAGE . Inc
1653 East Main Street
Rochester, NY 14609 USA
Phone: 716/482-0300
Fax: 716/288-5989